U.PORTO
FEUP FACULDADE DE ENGENHARIA
UNIVERSIDADE DO PORTO

ARTIFICIAL INTELLIGENCE FOR AN ENHANCED AS-IS BIM ENERGY ANALYSIS

Enabling an efficient energy retrofit through the automation of the scan-to-BIM process

LUÍS PEDRO NEVES SANHUDO

A thesis submitted in partial fulfilment of the requirements for the degree of

DOCTOR OF PHILOSOPHY IN CIVIL ENGINEERING

Supervised by: Prof. Dr. João Pedro da Silva Poças Martins

Co-supervised by: Prof. Dr. Nuno Manuel Monteiro Ramos

JULY 2021

DOUTORAMENTO EM ENGENHARIA CIVIL

DEPARTAMENTO DE ENGENHARIA CIVIL

Tel. +351-22-508 1901

Fax +351-22-508 1446

✉ prodec@fe.up.pt

Editado por

FACULDADE DE ENGENHARIA DA UNIVERSIDADE DO PORTO

Rua Dr. Roberto Frias

4200-465 PORTO

Portugal

Tel. +351-22-508 1400

Fax +351-22-508 1440

✉ feup@fe.up.pt

http://www.fe.up.pt

Aos meus Pais, Irmã e Fabiana

Research is the study of failure. More precisely, research is the study of obtaining new knowledge through failure. A bad researcher fails 100% of the time, while a good one fails only 99% of the time.

Károly Zsolnai-Fehér

ACKNOWLEDGEMENTS

Durante os últimos quatro anos, várias pessoas marcaram o longo percurso que foi o meu Doutoramento, dando o seu contributo, direta ou indiretamente, para a finalização deste trabalho. Assim, apesar de dedicar os próximos parágrafos a quem teve uma especial influência neste longo caminho, gostava de agradecer a todos os que deixaram para trás a mais pequena das marcas.

Ao meu orientador, o Professor Doutor João Pedro Poças Martins, pelo investimento, apoio, disponibilidade, orientação e amizade que demonstrou ao longo deste trabalho. Obrigado por me permitir escolher temas científicos que me fascinam, dar a liberdade de os explorar de forma independente e saber quando impor algumas regras, que também são precisas.

Ao meu coorientador, o Professor Doutor Nuno Manuel Monteiro Ramos, pelo incentivo e pelos conhecimentos transmitidos.

Ao Professor Doutor Jaime dos Santos Cardoso, pelos conhecimentos transmitidos e por me apoiar na transição entre a Engenharia Civil e os desenvolvimentos de Inteligência Artificial.

Aos meus amigos, em especial ao Bernardo, Rita, Vítor, Rui e Andreia, pela amizade e pela necessária dose diária de distração.

À minha irmã e ao Sérgio, pelos anos de apoio e motivação. E ao Guilherme, pela sua alegria.

À Fabiana, pelo amor e pela paciência. Por todos os altos e por me tirar dos baixos. Pelo conforto, pelo carinho, pela aventura e pela companhia ao olhar o futuro comigo.

Aos meus pais, pelo amor, pela dedicação, por me porem sempre à frente, por me darem tudo o que tenho e o que sou.

Este trabalho foi financiado por: Bolsa de Doutoramento SFRH/BD/129652/2017, financiada por fundos nacionais através da FCT. Financiamento Base – UIDB/04708/2020 e Financiamento programático – UIDP/04708/2020 da Unidade de Investigação CONSTRUCT – Instituto de I&D em Estruturas e Construções – financiada por fundos nacionais através da FCT/MCTES (PIDDAC).

ABSTRACT

In the last few years, energy retrofit of the existing building stock has quickly positioned itself centre stage of research and application, with several European directives and countries' legislations focusing the topic in pursuit of sustainability and economic goals. Similarly, as a prominent topic within the Architecture, Engineering and Construction industry, Building Information Modelling (BIM) has risen in importance in scientific and practical communities, morphing itself from a futuristic scholar concept into a vital core piece of the industry. With an increasing overlap of both areas, researchers and practitioners focused the As-Is BIM Energy Analysis (AIBEA) of a building as an answer to the slow progress of retrofitting the existing building stock, enabling the quick analysis of a building's energy consumption and the exhaustive comparison of constructive solutions to increase its efficiency. However, several obstacles still hinder the overall productivity and accuracy of this process, with multiple scientific works denoting a growing need to swiftly and automatically acquire accurate, structured, and semantically enriched three-dimensional digital models of existing buildings.

To this end, the present thesis aims to contribute with an answer to this problem by tackling it from two perspectives: (1) the development of supporting documentation and tools for an accurate and swift AIBEA, and (2) the integration and automation of the scan-to-BIM process. To achieve this goal, the author relies on two primary technologies: laser scanning and Artificial Intelligence (AI). These are applied to accurately acquire the as-is building geometry and automate the resulting point cloud segmentation, classification, and modelling within a BIM authoring environment.

Initially, this thesis starts by reviewing the state of the art and theoretical basis on AIBEA and scan-to-BIM, exploring multiple related topics as existing legislation and supporting documentation for the AIBEA workflow; as-is building geometric and energy-related data acquisition; existing software tools and interoperability; AI; deep learning approaches to point cloud segmentation and classification; as well as automated BIM modelling and subsequent data enrichment. Afterwards, the thesis' contributions are presented and divided into five unique modules, allowing for a thorough exploration of each contribution. The modules are: (1) identification of AIBEA requirements; (2) as-is building data acquisition; (3) point cloud segmentation and classification; (4) automated BIM modelling; and (5) BIM model enrichment and exportation to energy analysis software. Together, the modules comprise a methodology for an enhanced AIBEA. This methodology is then applied in five different experiments to evaluate its performance and identify its advantages and limitations. Based on the achieved results, relevant conclusions regarding the thesis' contributions and applied technologies are retrieved. The experiments achieved successful results, justifying its continuous development in future works.

Throughout the thesis, multiple topics of further interest to the literature are expanded, promoting the research of existing scientific and industry problems, and proposing original methods for the identification of contractual requirements and quality verification parameters for the scan-to-BIM process; analysis of laser scanner parameters and its influence over the final point cloud information; optimal placement of laser scanner stations; artificial training of deep learning algorithms; and identification of construction materials through laser scanning.

KEYWORDS: Enhanced as-is BIM energy analysis; Automated scan-to-BIM; Artificial Intelligence; Point cloud segmentation and classification; Data mapping and material recognition.

RESUMO

Nos últimos anos, a reabilitação energética do edificado existente tem vindo a ocupar uma posição central na indústria da Arquitetura, Engenharia e Construção, com múltiplas diretivas europeias e legislações nacionais a focarem o tópico em busca de sustentabilidade e objetivos económicos. De forma semelhante, o *Building Information Modelling* (BIM) tem vindo a crescer em importância nas comunidades científicas e práticas do setor, evoluindo rapidamente de um conceito puramente futurista e acadêmico para uma das peças centrais da Construção. Com a crescente sobreposição entre estas duas áreas, recentes esforços focaram a Análise Energética BIM *As-Is* (AEBAI) de um edifício como solução para o lento progresso de reabilitação energética do edificiado existente, permitindo uma análise rápida do consumo energético de um edifício e a subsequente comparação exaustiva de soluções construtivas para melhoria da sua eficiência energética. Contudo, existem ainda vários obstáculos que ameaçam a produtividade e precisão desta solução, com múltiplos trabalhos científicos a evidenciarem uma crescente necessidade de adquirir, de forma rápida e automática, modelos digitais de três dimensões, estruturados e semanticamente enriquecidos, de edifícios existentes.

Neste sentido, a presente tese visa contribuir com uma solução, abordando o problema a partir de duas perspetivas: (1) desenvolvimento de documentação e ferramentas de apoio a uma AEBAI rápida e precisa; (2) integração e automatização do processo *scan-to-BIM*. Para atingir este objetivo, o autor conta com duas tecnologias-chave, nomeadamente, o *laser scanning* e a Inteligência Artificial (IA). Estas tecnologias são aplicadas para, respetivamente, adquirir com precisão a geometria *as-is* do edifício e automatizar a segmentação, classificação e modelação de nuvens de pontos em ambientes BIM.

Inicialmente, a tese começa por apresentar uma revisão do estado da arte e das bases teóricas da AEBAI e do processo *scan-to-BIM*, explorando vários tópicos relacionados como: legislação e documentação de apoio à AEBAI; aquisição de informação *as-is* geométrica e energética de um edifício; *software* e interoperabilidade existente; IA; *deep learning* para segmentação e classificação de nuvens de pontos; e modelação automática BIM e alternativas para subsequente enriquecimento com informação energética. Posteriormente, as contribuições da tese são apresentadas e divididas por cinco módulos distintos, permitindo uma ampla exploração de cada contribuição. Os módulos são: (1) identificação de requisitos para AEBAI; (2) aquisição de informação *as-is* do edifício; (3) segmentação e classificação de nuvem de pontos; (4) modelação BIM; e (5) enriquecimento do modelo BIM e exportação para software de análise energética. O conjunto destes módulos compreende uma metodologia para melhoria da AEBAI. Por fim, esta metodologia é aplicada em cinco diferentes casos de estudos, com o objetivo de avaliar o seu desempenho e identificar as suas atuais vantagens e limitações. Com base nos resultados obtidos, são retiradas conclusões relevantes sobre as contribuições da tese e das tecnologias nela aplicadas. Os casos de estudo originaram resultados positivos, justificando o contínuo desenvolvimento da metodologia proposta em trabalhos futuros

Ao longo da tese, vários tópicos de elevado impacto científico são explorados, promovendo a resposta a problemas existentes na literatura, e à proposta de metodologias originais para a identificação de requisitos contratuais e parâmetros de qualidade do processo *scan-to-BIM*; análise das propriedades do *laser scanner* e a sua influência na nuvem de pontos final; posicionamento otimizado de estações *laser scanner*; treino artificial de algoritmos *deep learning*; e identificação de materiais por *laser scanning*.

PALAVRAS-CHAVE: Análise energética BIM *as-is*; Automatização do processo *scan-to-BIM*; Inteligência artificial; Segmentação e classificação de nuvem de pontos; Mapeamento de dados e reconhecimento de materiais.

GENERAL INDEX

FIGURES INDEX

TABLES INDEX

EQUATION INDEX

SYMBOLS, ACRONYMS AND ABBREVIATIONS

2D – Two-Dimensional

3D – Three-Dimensional

3DCNN-DQN-RNN – Three-Dimensional Convolutional Neural Network, Deep Q-Network, and Residual Recurrent Neural Network

3DContextNet – Three-Dimensional Contextual Network

3DMV – Three-Dimensional Multi-View Network

3D-PointCapsNet – Three-Dimensional Point Capsule Network

3D-SIS – Three-Dimensional Semantic Instance Segmentation Network

3DSphericalCNN – Three-Dimensional Spherical Convolutional Neural Network

3DTI-Net – Three-Dimensional Transform-Invariant Network

3P-RNN – Pointwise Pyramid Pooling Recurrent Neural Network

AABB – Axis-Aligned Minimum Bounding Box

Acc – Per-Class Accuracy

A-CNN – A-CNN: Annularly Convolutional Neural Networks

AdB – AdaBoost

AEC - Architecture, Engineering and Construction

AGCN – Attention-based Graph Convolution Networks

AI – Artificial Intelligence

AIA – American Institute of Architects

AIBEA – As-Is BIM Energy Analysis

ANN – Artificial Neural Networks

API – Application Programming Interface

ArtBIM-PC – Artificial BIM Point Clouds Dataset

ASIS – Associatively Segmenting Instances and Semantics Network

ASR – Attention-based Score Refinement Network

AVOD – Aggregate View Object Detection Network

BEM – Building Energy Modelling

BIM – Building Information Modelling

BIPS – Building-Integrated Photovoltaic Systems

B-Rep – Boundary Representation

CAD – Computer Aided Design

CFD – Computational Fluid Dynamics

ClusterNet – Cluster Network

CNN – Convolutional Neural Network

CO_2 – Carbon Dioxide

COBIM – Common BIM Requirements

COMBINE – Computer Models for the Building Industry in Europe

ConvPoint – Continuous Convolutions Point Cloud Network

COVID-19 – Coronavirus Disease 2019

CRF – Conditional Random Fields

CSG – Constructive Solid Geometry

DAR-Net – Dynamic Aggregation Network

DBSCAN – Density-based Spatial Clustering of Applications with Noise

DeepGCNs – Deep Graph Convolutional Networks

DeepSets – Deep Sets Network

DensePoint – Densely Contextual Representation for Efficient Point Cloud Processing Network

DGCNN – Dynamic Graph Convolutional Neural Network

DL – Deep Learning

DPAM – Dynamic Points Agglomeration Module

DPC – Dilated Point Convolutions

DT – Decision Tree

EdgeConv – Edge Features Convolution

EIR – Exchange Information Requirements

EU – European Union

ExT – Extremely Randomized Forest

FCN – Fully Convolutional Network

FCPN – Fully Convolutional Point Network

FEUP – Faculdade de Engenharia da Universidade do Porto

Flex-Conv – Flex-Convolution Network

FPFH – Fast Point Feature Histograms

FPNN – Field Probing Neural Network

FPS – Farthest Point Sampling

Frustum PointNet – Frustum Point Cloud Network

G3DNet – Graph Three-Dimensional Network

GAC – Graph Attention Convolution

gbXML – Green Building Extensible Markup Language

GCNN – Geodesic Convolutional Neural Networks

Geo-CNN – Geometric-Induced Convolution Neural Network

GPU – Graphics Processing Unit

GrB – Gradient Boosting

Grid-GCN – Grid-Graph Convolutional Networks

GSA – General Services Administration

GUI – Graphical User Interface

GVCNN – Group-View Convolutional Neural Network

HBIM – Historic/Heritage Building Information Modelling

H-CNN – Spatial Hashing Based Convolutional Neural Network

HDR – High Dynamic Range

HGNN – Hypergraph Neural Networks

HSV – Hue-Saturation-Value

HT – Hough Transform

HVAC – Heating, Ventilation, and Air Conditioning

IBDE – Integrated Building Design Environment

ICADS – Intelligent Computer Aided Design System

ICP – Iterative Closest Point

IFC – Industry Foundation Classes

InterpCNNs – Interpolated Convolutional Neural Networks

IoT – Internet of Things

IoU – Intersection-Over-Union

JSIS3D – Joint Semantic-Instance Three-Dimensional Segmentation Network

JSNet – Joint Instance and Semantic Segmentation Network

JSON – JavaScript Object Notation

KCNet – Kernel Correlation Network

KD-Net – Deep K-Dimensional Network

KNN – K-Nearest Neighbours

KPConv – Kernel Point Convolution

KP-FCNN – Kernel Point Fully Convolutional Neural Network

LatticeNet – Permutohedral Lattices Network

LDGCNN – Linked Dynamic Graph Convolutional Neural Network

LiDAR – Light Detection and Ranging

LocalSpecGCN – Local Spectral Graph Convolution Network

LoD – Level of Detail

LOD – Level of Development

LP-3DCNN – Local Phase Three-Dimensional Convolutional Neural Network

LR – Logistic Regression

LReLU – Leaky Rectified Linear Function

LSANet – Local Spatial Aware Network

LSSHOT – Linear Straight Signature Histogram of Orientations

mAcc – Mean Accuracy Over Classes

MCCNN – Monte Carlo Convolutional Neural Network

MHBN – Multi-view Harmonized Bilinear Network

MinkowskiNet – Minkowski Convolutional Neural Network

mIoU – Mean Intersection-Over-Union

ML – Machine Learning

MLP – Multilayer Perceptron

Mo-Net – Moments Network

MoNet – Motion-based Point Cloud Prediction Network

MRF – Markov Random Fields

MV3D – Multi-View Three-Dimensional Network

MVCNN – Multi-View Convolutional Neural Network

NBS – National Building Specification

oAcc – Overall Accuracy

O-CNN – Octree-based Convolutional Neural Network

OctNet – Octree Network

OOBB – Object-Oriented Minimum Bounding Box

PATs – Point Attention Transformers

PCCN – Parametric Continuous Convolutional Neural Network

PCMat-30 – 30 Points Cloud Materials Dataset

PCNN – Point Convolutional Neural Network

Point2Sequence – Attention-based Sequence to Sequence Point Network

PointASNL – Point Adaptive Sampling Local-Nonlocal Network

PointAugment – Auto-Augmentation Point Network

PointCNN – Point Cloud Convolutional Neural Network

PointConv – Point Convolution Network

PointDAN – Point Cloud Domain Adaptation Network

PointGCN – Point Graph Convolutional Neural Network

PointGCR – Point Global Context Reasoning Network

PointGrid – Point Grid Network

PointIT – Point Instance Segmentation Network

PointNet – Deep Point Sets Network

PointNet++ – Deep Hierarchical Point Sets Network

PointPillars – Point Pillars Network

PointSeg – Point Segmentation Network

PointSIFT – Point Scale-Invariant Feature Transform Network

PointWeb – Fully-Linked Point Web Network

PS^2-Net – Point Cloud Semantic Segmentation Network

PVCNN – Point-Voxel Convolutional Neural Network

PVConv – Point-Voxel Convolution

PVNet – Pixel-Wise Voting Network

PVRNet – Point-View Relation Neural Network

PyramNet – Pyramid Attention Network

RangeNet++ – Range Image Network Plus Plus

RANSAC – Random Sample Consensus

RBF – Radial Basis Function

RCNet – Recurrent Set Encoder and Convolutional Feature Aggregator Network

RCNet-E – Recurrent Set Encoder and Convolutional Feature Aggregator Network Ensemble

RDp – Random Dropout

ReLU – Rectified Linear Unit

RF – Random Forest

RGB – Red, Green, and Blue

RGB-D – Red, Green, Blue and Depth

RGB-I – Red, Green, Blue and Intensity

RGCNN – Regularized Graph Convolutional Neural Network

RIConv – Rotation Invariant Convolutions

RNN – Recurrent Neural Network

RotationNet – Rotation Network

RS-CNN – Relation-Shape Convolutional Neural Network

RSNet – Recurrent Slice Networks

S3DIS – Stanford Three-Dimensional Indoor Scene Dataset

SASO – Semantic Association and Salient Optimization Network

ScanComplete – Three-Dimensional Scan Completion Network

SECOND – Sparsely Embedded Convolutional Detection

SEGCloud – Segmentation of Cloud Images Network

SFCNN – Spherical Fractal Convolutional Neural Networks

SGPN – Similarity Group Proposal Network

ShellNet – Shell Convolution Network

SnapNet – Snapshot Network

S-NET – Simplified Network

SO-Net – Self-Organizing Network

Sparce3D – Sparce Three Dimensional Convolutional Neural Networks

SPG – Superpoint Graph Network

Spherical CNNs – Spherical Convolutional Neural Networks

SPHNet – Spherical Harmonic Network

SpiderCNN – Spider Convolutional Neural Network

SPLATNet – Sparse Lattice Network

SqueezeNet – Squeeze Network

SqueezeSeg – Squeeze Segmentation Network

SqueezeSegV2 – Squeeze Segmentation Network Version 2

SRINet – Strictly Rotation-Invariant Network

SRN – Structural Relation Network

SSCN – Submanifold Sparse Convolutional Network

SSP+SPG – Supervized Superpoint and Superpoint Graph Network

STEP – Standard for the Exchange of Product model data

SVM – Support Vector Machines

TangentConv – Tangent Convolutions

VFE – Voxel Feature Encoding

VIKOR – *VlseKriterijumska Optimizacija I Kompromisno Resenje* (Multi-Criteria Optimization and Compromise Solution)

VoxelNet – Voxel Network

VoxNet – Voxel Network

VV-Net – Voxel Variational Autoencoder Network

XML – Extensible Markup Language

1

INTRODUCTION

This initial chapter displays a brief introduction to the studied subjects, starting with its framework and motivation (Section 1.1), followed by the thesis' objectives and methodology (Section 1.2), and finally, the thesis' structure (Section 1.3).

1.1. FRAMEWORK AND MOTIVATION

Increasing energy efficiency and reducing energy consumption are some of the leading research objectives in the Architecture, Engineering and Construction (AEC) industry [1-3]. In recent years, these goals have even been backed by international strategies, such as the European Union's (EU) 2030 Climate & Energy Framework, aiming for an increase in energy efficiency, as well as a reduction in greenhouse gas emissions [4]. Considering that buildings are responsible for approximately 40% of EU's energy consumption, the achievement of these strategies is tightly linked with the existing building stock [1], namely, its energy retrofit.

However, currently, only a slim percentage of EU's building stock is renovated each year, despite the ageing and energy inefficiency shown by a large portion of its buildings [5]. This is generally attributed to the lack of financial incentives for building renovation compared to new construction [6, 7], as well as the multiple challenges faced by AEC professionals when tackling the former [6, 8-10]. Although financial support measures are already being developed and implemented in the EU to stimulate long-term renovation strategies [11, 12], the complexity intrinsic to these projects remains, with many of the same challenges lingering unanswered. Most challenges branch from the ill or non-existent management and storage of building data across its life cycle, as well as the complexity surrounding the deterioration and ageing of the building and its associated systems. These challenges hinder the design team's ability to swiftly create suitable solutions for renovation projects, lengthening and increasing its cost [6, 8, 9].

To this end, in the last few years, this issue developed into a prominent research topic in the AEC industry, especially in what regards short-term benefits. Building Information Modelling (BIM) is often associated with this research, being indicated as an indispensable part of the solution [9, 10, 13-22]. In this solution, BIM works as a centralised database to store and examine all the building's information, subsequently supplying this data to energy analysis software, where the building model can be carefully analysed and optimised for increased energy efficiency.

In the current literature, this workflow from as-is building data to BIM and ensuing examination in energy analysis software is entitled “as-is BIM energy analysis”, from now on identified as AIBEA, and is considered a vital component in solving the slow retrofit of the existing building stock. Despite this, as several works have noted [22-27], the application of AIBEA in retrofitting projects is still limited, with the exhaustive documentation and analysis effort that must be performed to create an as-is BIM model being pointed out as the dominant reason behind its limited application.

Parallel to these developments, the scan-to-BIM process has recently risen in popularity within research and practice communities, leveraging the increased accuracy and decreased costs of new building surveying technologies to assist in developing as-is BIM models. In particular, laser scanning has shown promising results in surveying a building’s geometry, offering a quick and accurate method to obtain its point cloud. In addition to being easily visualised and understood by all project stakeholders [22, 28-30], the acquired point cloud can be imported into BIM authoring environments, acting as a detailed reference during the modelling process.

However, despite seeming a clear answer to AIBEA current deterrents, the scan-to-BIM process also presents its limitations, with the importation process, as well as the preceding point cloud treatment and subsequent modelling, remaining a mostly manual, time-consuming, labour-intensive, subjective, and error-prone process, which significantly reduces its viability [23, 27]. In this sense, several recent studies [22-24, 27-29, 31-34] identify an increasing need to develop a method to automatically and accurately acquire semantically enriched BIM models, automating the scan-to-BIM process and, thus, eliminating a significant portion of its drawbacks. Such a method would avoid the point cloud importation into the BIM authoring software, automatically extracting the building elements dimensions from the point cloud and directly modelling them in BIM.

Although some studies have, in recent weeks, presented restricted and partial solutions to this problem, a complete integrated solution is still lacking, which this thesis aims to offer. To do so, the present thesis explores another rising topic within the AEC industry: Artificial Intelligence (AI); particularly the field of Machine Learning (ML) and, even more specifically, Deep Learning (DL). This latter subset of ML methods works exceptionally well on unstructured data, a feature which the current thesis leverages to extract information from building point clouds, enabling its complete segmentation and classification into building elements, and subsequent modelling in a BIM authoring software.

It is this thesis’ hypothesis that by automating the scan-to-BIM process and integrating it in the AIBEA workflow, several of the existing drawbacks limiting the latter’s success can be overcome and, by extension, the energy retrofit of the existing building stock and its related sustainability goals can be promptly achieved. Throughout this thesis, the resulting AIBEA workflow from integrating the scan-to-BIM process and other proposed improvements is titled “enhanced AIBEA”.

1.2. Objectives and Methodology

The present thesis’ main objective entails developing and applying a methodology to improve the current AIBEA workflow, comprising the entire process from contractual agreement to BIM modelling. Through this methodology, an enhanced AIBEA workflow is achieved. Six secondary goals have been designed to accomplish this main objective, dividing the thesis into multiple milestones and simplifying its approach. Below are the secondary objectives:

- Proposal of a theoretical methodology for an enhanced AIBEA workflow, including the integration and automation of the scan-to-BIM process;
- Creation of a framework for the definition of contractual information requirements in energy-related BIM projects;
- Establishment of guidelines for an as-is building data acquisition;
- Development of an AI model for the automated segmentation and classification of point clouds into building elements;
- Development of a software tool for an automated BIM modelling and semi-automated characterisation of building elements;
- Development of an AI model for the automated characterisation of building elements.

To tackle these objectives, the methodology seen in Figure 1.1 was created and followed throughout the thesis development.

Initially, after identifying the motivation behind the current thesis, a thorough literature review of relevant past works was carried out, allowing the author to narrow the research problem and identify existing knowledge gaps. Specifically, this review allowed for the identification of AIBEA's importance to the topic, as well as its current limitations, which the author believes to be in a unique position to address.

Following the literature review, a theoretical methodology was designed and proposed to solve the identified problem [22]. This framework was grounded in the acquired knowledge during the literature review and aimed to develop an enhanced AIBEA workflow. Among other improvements, this methodology entails the integration and automation of the scan-to-BIM process in the AIBEA workflow, taking advantage of laser scanning and AI as the primary technologies to support its development. Several of the steps and tools indicated in the proposed methodology required answering open research problems, further enhancing the present work relevance.

After the methodology definition, the ensuing steps comprised the practical development of each of its five unique modules. These modules included the establishment of a framework for the definition of contractual information requirements in energy-related BIM projects [35]; the creation of guidelines to support as-is building data acquisition [29, 36]; the development of DL models to segment and classify points clouds into building elements; the development of traditional ML models to extract geometric features from the classified elements; and the development of software tools for the automated modelling and data enrichment of BIM models [33, 37].

Parallel to the above-mentioned practical developments, multiple surveys were performed to acquire the point clouds of several buildings. These point clouds were used during the training and testing of the developed AI models and were acquired following the proposed guidelines for as-is building data acquisition. The data acquired from these efforts was further augmented with point clouds stored in existing publicly available datasets and points clouds artificially generated by the author. These two last data origins were identified as required to avoid the lengthy and exhaustive process of manually mass-producing labelled building point clouds.

Finally, the methodology was tested in five different experiments to evaluate its performance and identify its advantages and limitations.

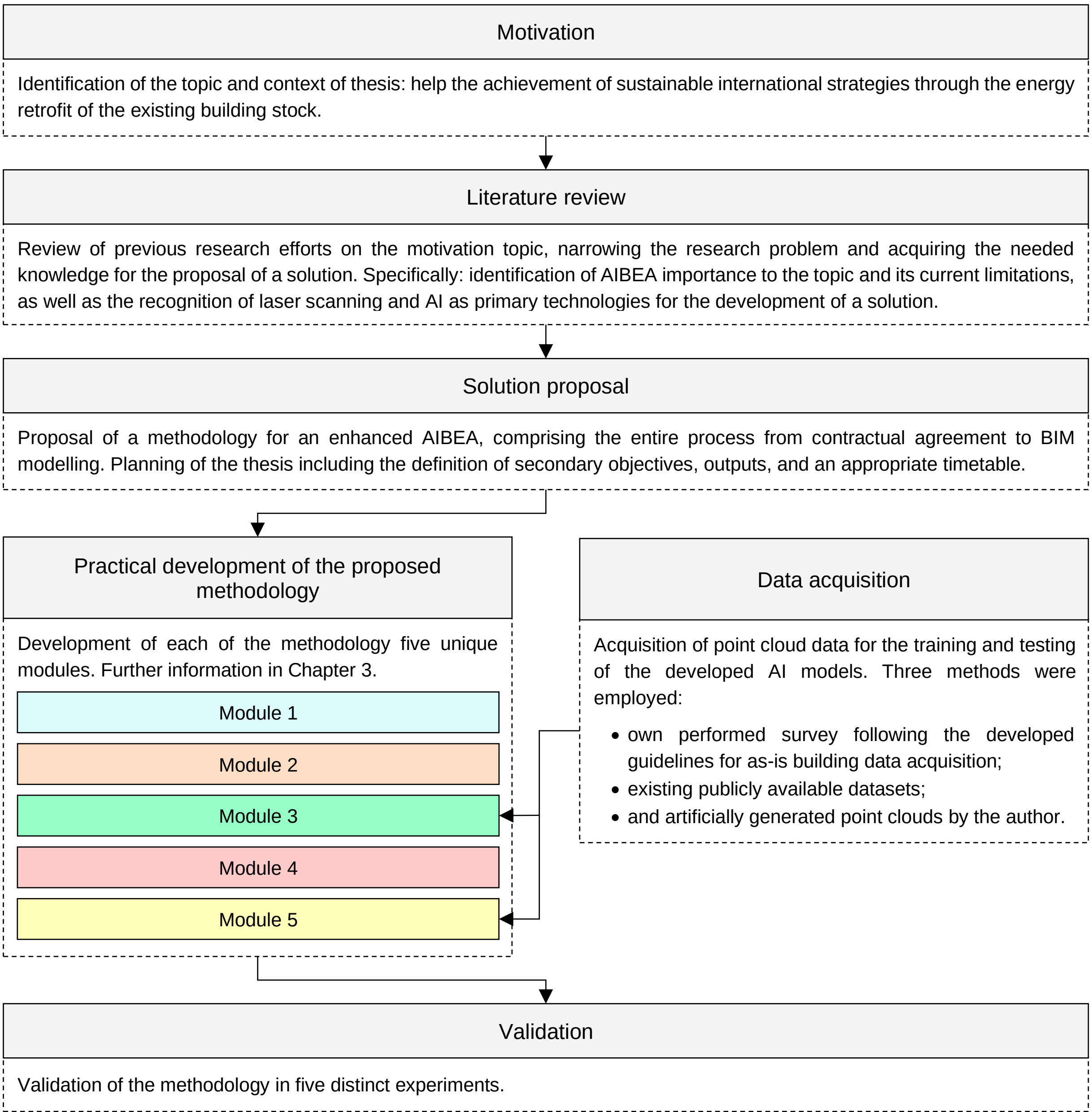

Figure 1.1 – Overview of the research methodology

1.3. Structure

The present work is divided into five unique chapters:

- Introductory in nature, Chapter 1 establishes the framework and motivation for the thesis, defines its objectives and methodology, and presents its structure;
- Chapter 2 comprises the state of the art and theoretical basis on topics relevant to the thesis. It aims to identify and contextualise the tackled problem, presenting essential concepts to understand the proposed solution. In particular, topics like existing legislation and supporting documentation for the AIBEA workflow; as-is building data acquisition; existing AIBEA-related software tools and interoperability; current approaches to point cloud segmentation; and automated modelling and enrichment of BIM models are discussed;

- Chapter 3 starts by presenting an overview of the thesis' major contributions, laying the groundwork for their improved understanding. It divides these contributions into five unique modules, which comprise the methodology for an enhanced AIBEA. The modules are: (1) identification of AIBEA requirements; (2) as-is building data acquisition; (3) point cloud segmentation and classification; (4) automated BIM modelling; and (5) BIM model enrichment and exportation to energy analysis software. Each module is thoroughly explained, with their respective purpose, workflow, intra- and inter-connections being examined;
- Chapter 4 validates the thesis' contributions through their application to five distinct experiments. The experiments are first characterised by carefully examining the chosen datasets, implementation details, and selected evaluation metrics; and then discussed through the analysis of the acquired results;
- Finally, Chapter 5 presents the thesis' main conclusions and outputs, revisiting and answering the initially proposed objectives. Additionally, topics that should be subject to future analysis and development are enumerated, indicating underdeveloped aspects of the methodology that should be further explored, and research opportunities that could be pursued with the thesis' advanced knowledge.

2

LITERATURE REVIEW

The current chapter presents the literature review on topics relevant to the thesis. It starts by introducing a larger challenge, slowly narrowing its focus to a smaller, yet essential, problem, tackled in the current thesis. It aims to expose this problem further, justifying its importance and the need for a solution.

2.1. Addressing the problem: A slow and inefficient retrofit of the existing building stock

Increasing energy efficiency and reducing energy consumption are among the leading research objectives in the AEC Industry [1-3]. In recent years, these goals have even been backed by international strategies, such as EU's 2030 Climate & Energy Framework, aiming for a 32.5% improvement in energy efficiency, as well as a 40% reduction in greenhouse gas emissions, based on 1990 levels [4]. These values are expected to be revised upwards in 2023 [4]. Considering that buildings are responsible for approximately 40% of EU's energy consumption and 36% of Carbon Dioxide (CO_2) emissions, the achievement of these strategies is tightly linked with the existing building stock [1], namely, its energy retrofit.

The energy retrofit of an existing building entails technically intervening in its energy system to enhance its energy efficiency, conservation, and savings [38]. Despite recent advances in new construction-related technology, recent studies indicate that the energy retrofit of the current building stock has not only to be considered if the above-mentioned goals are to be accomplished [39, 40] but also presents itself as one of the most efficient solutions to do so [40].

However, currently, only 0.4 to 1.2% of the building stock is renovated each year (dependent on the EU state member), despite 35% of EU's buildings being over 50 years old and 75% being considered energy inefficient [5]. This is mostly caused by the lack of financial incentives for building renovation compared to new construction, as well as the multiple challenges faced by AEC professionals when tackling energy retrofitting. Among them [6-10, 22, 38]:

- the intervention of multiple stakeholders along the different stages of the building life cycle;
- the complexity surrounding the deterioration and ageing of building systems;
- the uniqueness of each building's design and energy consumption;
- and the lack of a reliable decision-support system to identify performance-effective and cost-optimal retrofit measures.

Although financial support measures are already being developed and implemented in the EU to stimulate long-term renovation strategies [11, 12], the complexity intrinsic to these projects remains, with many of the same challenges lingering unanswered. Most of these challenges branch from the ill or non-existent management and storage of building-related data throughout its life cycle, as well as the complexity surrounding a building's energy performance assessment and enhancement. These challenges hinder the design team's ability to swiftly create suitable solutions for energy retrofit projects, lengthening and increasing its cost [6, 8, 9].

To this end, in the last few years, energy retrofitting has developed into a prominent research topic in the AEC industry, especially in what regards short-term benefits [9, 10, 13-15, 17, 18, 20]. As identified in multiple reviews [20, 41-44], this issue is often at the centre of top-ranked research clusters, with several of the most frequently cited articles relating to this topic [45, 46]. In particular, in 2016, Göçer et al. [10] identified multiple studies concerning energy retrofit methodologies, dividing them into four major groups: statistical approaches; machine learning methods; computational models; and simulation software. Table 2.1 identifies the works stated in [10], alongside recent works highlighted by the thesis' author.

Table 2.1 – Energy retrofit methodologies applied in research

Method	Articles
Statistical approach	[47-50]
Machine learning methods	[51-54]
Computational models	[55-57]
Simulation software	[58-61]

However, more recently, a new approach has been proposed by several studies [9, 10, 13-22], introducing BIM as an indispensable part of the solution. In one such study, Sanhudo et al. [22] connected the energy retrofitting inherent complexity and unanswered challenges to the exhaustive documentation and intricate analysis processes that precede the actual energy retrofit of a building, suggesting the use of BIM as a centralised database to store, organise and examine the building geometry, construction typology, and thermal properties. BIM interoperability with building energy analysis software can then be leveraged to quickly transfer the building data, streamlining multiple steps in traditional energy retrofitting projects.

This workflow from as-is building data to BIM and ensuing examination in energy analysis software is entitled "as-is BIM energy analysis" and is currently considered an essential component in solving the slow retrofit of the existing building stock. The following sections explore this workflow and its related research.

2.2. Current solution: As-is BIM energy analysis

The core idea behind AIBEA is to take advantage of BIM's interoperability with energy analysis software to swiftly evaluate and decide on energy retrofit solutions. To this end, AIBEA is described as a workflow that comprises three main steps:

1. acquiring data regarding the as-is building;
2. storing this data in the building's BIM model (which may need to be created or updated);
3. and transferring the BIM model information to energy analysis software to examine and optimise the building's energy efficiency.

In recent years, several authors have analysed the application of AIBEA under multiple scenarios, with all of the identified works showcasing an overall success. In 2016, Maggie Khaddaj and Issam Srour [19] gave an early review of this topic, identifying its potential. Given the early stages of AIBEA at this time, few examples of its application were indicated. However, just two years later, Sanhudo et al. [22] reviewed the topic by identifying numerous research efforts applying AIBEA, showcasing the topic growth. The authors indicate advantages and limitations to the workflow, proposing future works and expected trends for its improvement. Since then, this field's research has kept increasing, with multiple authors advancing the topic [28, 62-68]. For instance:

- in 2019, Rocha et al. [28] applied AIBEA to assess eight different retrofitting solutions to improve the winter thermal comfort of an existing bus station in Porto, Portugal. The authors evaluate each solution impact on building energy consumption, indicating a successful combination of BIM and energy analysis methodologies. In another work of the same year, Thais Sartori and João Luiz Calmon [63] analysed the impact of five unique energy retrofit actions on the life cycle energy consumption of two existing neighbourhood dwellings, applying *ArchiCAD* as the BIM authoring tool and *EnergyPlus* as the energy analysis software. The authors indicate a successful application of the AIBEA workflow, suggesting the further development and integration of BIM tools in the life cycle analysis of a building;
- in 2020, Wahhaj Ahmed and Muhammad Asif [65] explored AIBEA to assess the techno-economic feasibility of retrofitting existing homes in Saudi Arabia. The authors compare eight different energy retrofit solutions in two real case studies, dividing these solutions into three distinct levels of implementation cost. In the same year, Freitas et al. [67] presented a feasibility study using a combination of *Rhinoceros CAD*, *Grasshopper* and *Ladybug*, to assess building-integrated photovoltaic systems (BIPS) intended to retrofit seven existing institutional office buildings. The authors highlight the importance of integrating BIM modelling software and simulation tools, indicating aspects that could be improved in the future;
- finally, in 2021, Zhang et al. [68] proposed a novel multi-criteria decision-making framework for the optimal selection of external walls retrofit techniques. The authors apply BIM to acquire several BIM-based wall retrofitting schemes, followed by their evaluation, ranking, and selection using the fuzzy VIKOR method [69].

Throughout these studies, the authors rely on three core concepts of AIBEA: BIM; as-is BIM; and BIM energy analysis. These concepts are focused on the following sections.

2.2.1. Building Information Modelling

The first notions related to BIM surfaced in the early 70s and are credited to Professor Charles M. Eastman [70]. However, the term "Building Information Modelling" would only appear 20 years later, in 1992, in an article by G. A. van Nederveen [71]. Likewise, its acronym, BIM, would only be popularized in 2002, appearing in a white paper by Autodesk entitled "Building Information Modelling" [72].

Thereafter, BIM steadily, yet slowly, increased in popularity within the AEC industry until the early 2010s, when the rise in information and communication technologies enabled its widespread promotion [73-75]. Since then, BIM quickly rose in importance in academic and professional communities, growing from a futuristic scholarly concept towards a central component of the industry [22, 76, 77], completely upending the way we build [76, 78-83].

Throughout the last years, multiple definitions and interpretations were linked to BIM, creating a lack of consensus on what the term signifies. These range from a simple tool to a complex technology, to a methodology or a process-oriented approach. In this thesis, BIM is considered a methodology, supporting the definition proposed by Bilal Succar: “a set of interacting policies, processes and technologies generating a methodology to manage the essential building design and project data in digital format throughout the building’s life cycle” [76]. Thus, BIM entails a set of actions that enable establishing transformative concepts and tools (both revolutionary and evolutionary) into an organisation, contributing to overcome several traditional problems in the AEC industry [75, 78, 84, 85].

BIM has been applied to all stages of the building life cycle, from planning to demolition [78, 86-88], supporting project planning, scheduling, coordination, visualization, decision-making, rapid design generation, documentation, cost estimation, interoperability, among others [25, 26, 62, 78, 86, 87, 89-96]. Its practical benefits have long been documented, with studies linking BIM to increases in project quality [97-100], reduction in costs [101-103], mitigation of errors [104-106], improvement in performance, productivity and efficiency [73-75, 89, 107, 108], as well as ease in communication and information exchange among all project stakeholders [83, 89, 109, 110]. For further information regarding BIM, such as additional advantages, disadvantages, maturity levels and expected future trends, address the following works [75-78, 86, 98, 111-114].

2.2.2. BIM ENERGY ANALYSIS

One of the most identifiable key features of BIM is its digital three-dimensional (3D) representation of a building. This representation, entitled “Building Information Model” or “BIM model”, can be used to store a building’s data, both its geometric descriptions, as well as its non-geometric attributes (i.e. semantically rich information) [25, 110]. One particular and increasingly popular use for these models is to leverage their information to facilitate detailed building performance evaluations, such as structural, acoustic and energy analysis.

Focusing on the latter, previously, the process itself was usually performed separately from BIM. However, this is quickly changing, with BIM allowing for the energy assessment of a building during its early project stages (e.g. initial design and pre-construction) [35, 90, 115], by effortlessly accessing the building information, from materials and weather data to Heating, Ventilation, and Air Conditioning (HVAC) and shading information [116]. This, in turn, allows for the optimization of the proposed solution (or the exploration of different alternatives), leading to improved decision making and better building energy performances [22, 29, 77, 117, 118]. Such an early approach was rarely accomplished when employing Computer Aided Design (CAD)-based solutions, given its impractical application in the early stages of a project, which typically resulted in retroactive modifications of the design, higher costs and lengthier project duration [83, 119].

As such, as seen in [22, 120-122], since 2010, the growing search for higher energy efficiency, reduction of operational costs, building certifications and occupant satisfaction has enhanced the use of BIM energy-related methodologies in the early stages of design, both for new construction and retrofit projects. Consequently, BIM has become an indispensable tool in the decision-making process of building energy optimization [123, 124], enabling a detailed analysis of the building's energy performance through computer-based simulation software [125]. This software allows for the assessment of a building's energy usage, lighting patterns, equivalent CO_2 emissions, solar exposure, orientation, thermal comfort, HVAC systems, renewable energy solutions, among others [22, 77, 126-128].

2.2.3. As-is BIM

As stated in the previous section, BIM energy analysis can be used for multiple purposes. Among these, the impact of different retrofitting solutions on a building's energy performance can be measured to enable the comparison of design alternatives, allowing for improved decision making and retrofitting as a whole [90, 108].

To accomplish this task, given the necessary precision retrofitting requires, typical BIM models, commonly based solely on project documentation, do not fulfil the requirements for an energy retrofit project [39]. This is because solely relying on standard stored information, without questioning the as-is state of the building, may result in inaccurate BIM-based energy simulations, causing ill predictions for the building energy performance and ultimately turning this method unreliable [85, 129]. For example, traditional BIM material databases, typically available within BIM authoring software, cannot be applied since their stored values do not account for the diminished thermal resistances of materials from deterioration [7, 85, 130].

For this reason, there is the need to acquire a BIM model that accurately represents the as-is building conditions to allow for the examination of retrofitting solutions in a realistic scenario [131]. In research, these models are identified as "as-is" models, which come in opposition to "as-designed" and "as-built" models. The differentiation between these models is often unclear; therefore, definitions to distinguish between these terms are presented below [131, 132]. Figure 2.1 illustrates the application of these models in the life cycle of a building.

- as-designed models (also termed as-planned models) refer to BIM models created during the design stage of a project. These models are concluded before construction begins and represent the most commonly found model in the AEC industry, since they are a legal requirement in several countries;
- as-built models arise from the frequent design changes performed during construction. These changes make the as-designed models obsolete, inaccurately reflecting the as-built conditions of a building. Thus, as-built models are created from the constant updates to as-designed models during construction and should portray the state of the building after the construction process ends;
- as-is models represent the building state during operation and maintenance. These models reflect any additions and alterations works carried out during these stages, replacing as-built models that inevitably turn obsolete. At its extreme, as-is models should be virtual copies of their respective buildings, rivalling the increasingly popular Digital Twin concept [133, 134]

and displaying detailed information such as building's energy consumption pattern, occupancy, thermal information, material deterioration, among others.

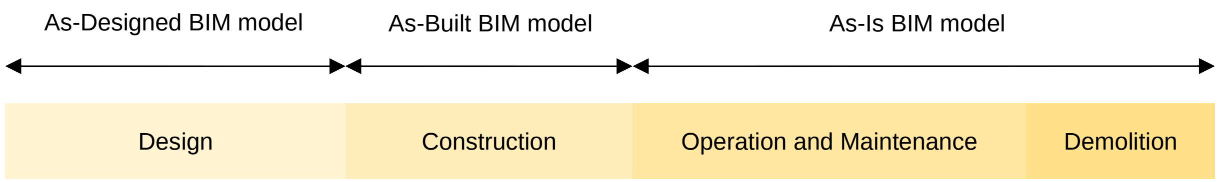

Figure 2.1 – BIM model designation throughout the life cycle of a building

2.2.4. CURRENT LIMITATIONS OF THE AIBEA WORKFLOW

Having covered the related research and base concepts of AIBEA, it is clear that this workflow heavily relies on BIM. The workflow's advantages originate primarily from applying BIM as a database for building as-is information, using its extensive interoperability with building energy analysis tools to directly supply the required data and quickly develop, examine and optimize retrofit solutions.

However, as a recent workflow reliant on considerably new technologies, AIBEA still presents several limitations which restrict its applicability [22-27]. These can be divided into four aspects:

1. the lack of existing standards and auxiliary documentation to support this workflow – as well as any other energy-related BIM project;
2. the still limited, although extensive, interoperability between BIM and energy analysis software;
3. the required exhaustive project documentation review and building surveying that precedes the creation of as-is BIM models;
4. and the time-consuming nature of modelling the as-is building using the surveyed data and existing authoring tools.

Focusing on the first aspect, as in other BIM-related topics (e.g. roles and responsibilities, modelling, clash detection, structural analysis [135-138]), appointing parties [139] should be able to enforce the use of current standards in BIM energy-related projects. Doing so allows for a proper definition of project requirements while also guaranteeing that all active parties (e.g. design team, suppliers, contractors) work under the same guidelines and are evaluated under the same criteria. Furthermore, these standards also typically contribute to a successful communication between stakeholders, guarantee a minimum project quality, and prevent ambiguity [139, 140]. However, despite the availability of BIM standards for other topics and activities throughout a building's life cycle, the author identified a lack of standards for energy-related BIM projects, which jeopardises the successful application of AIBEA. It should be stated that this knowledge gap was also identified by Farzaneh et al. [141].

Regarding the second aspect, it was previously stated that BIM's interoperability with energy analysis software was at the centre of AIBEA, streamlining multiple steps in traditional energy retrofitting projects. As such, it is unusual that it is also presented as a limitation. However, as identified in the multiple research works [26, 77, 106, 118, 142-151], although this interoperability is, in fact, extensive, it still presents some constraints, particularly in what concerns edge cases and the communication between interoperability data schemes and software. These restrictions not only affect the ability to transfer information between both software tools but also severely diminishes AIBEA reliability.

Concerning the third aspect, as stated in Section 2.2.3, as-is BIM models are required for a correct application of the AIBEA workflow. However, although necessary, acquiring an as-is BIM model is usually a challenging task. On the one hand, since most buildings were built before the rise of BIM, they do not have any BIM documentation [23, 131, 132, 152]. On the other hand, the buildings with BIM documentation display obsolete models since their as-designed and as-built models are not adequately updated. Additionally, creating as-is BIM models from two-dimensional (2D) drawings is identified in the literature [10, 153] as requiring highly skilled workers, being time-consuming and not accurate. These and other barriers associated with BIM model updating have been studied in the following works [46, 154-160]. To solve these problems arising from inaccurate, out-of-date, or even missing building information, appropriate techniques must be implemented to capture, manage, and visualize all the required as-is information. This leads to surveying and/or digitalizing substantial amounts of geometrical and energy-related building data, which can be overwhelming [10, 22], disincentivizing AIBEA application.

Finally, in regards to the fourth aspect, after carefully surveying and analysing all the geometric and energy-related building data, the actual BIM modelling of the building can ensue. However, as identified by several works, this modelling process can be characterized as mostly manual, time-consuming, labour-intensive, subjective, and error-prone [22-24, 27-29, 31-34]. Although BIM authoring software has, in recent years, developed tools to assist in modelling existing buildings, this problem still significantly reduces AIBEA efficiency and, as a result, its viability.

Together, these four aspects severely limit the applicability of AIBEA in energy retrofit projects, restraining its ability to accelerate the retrofit of the existing building stock and, ultimately, turning its related energy efficiency and sustainability goals unfeasible. To this end, the present thesis attempts to overcome these limitations by proposing multiple contributions to be incorporated into the AIBEA workflow. These contributions are focused on the following sections.

2.3. ENHANCEMENT OF THE CURRENT AIBEA WORKFLOW

The current section is methodological in nature and allows for a better understanding of the remaining literature review.

As seen in the last section, based on the current literature, AIBEA presents four significant limitations that severely constraint its applicability. To this end, the author proposes tackling these limitations through two distinct perspectives: (1) the development of supporting documentation and tools for an accurate and swift AIBEA, and (2) the integration and automation of the scan-to-BIM process.

While the first perspective targets the first three identified problems in a broader sense, through the development of standards and additional supporting documentation; the second perspective focuses on the fourth identified limitation, attempting to eliminate this drawback through the integration of the scan-to-BIM process, while also trying to overcome this process own limitations through automation.

As such, the following sections focus on these two perspectives, reviewing their related research and presenting the base concepts and nomenclature necessary to better understand the contributions in Chapter 3. The first perspective is explored in Section 2.4, while the second is explored in Section 2.5. For a better understanding, Figure 2.2 illustrates the train of thought presented in the current section.

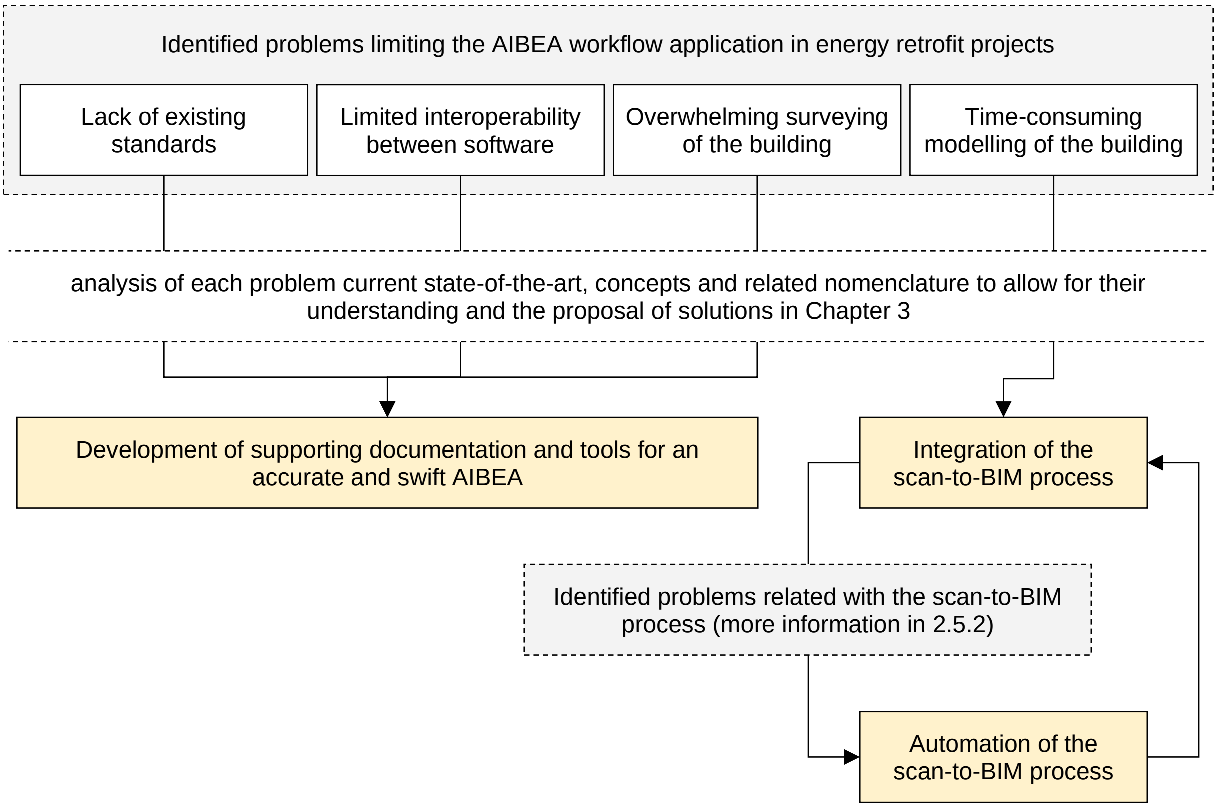

Figure 2.2 – Topics to be tackled for the enhancement of the AIBEA workflow

2.4. Development of supporting documentation and tools for an accurate and swift AIBEA

To properly develop supporting documentation and tools for the first three identified drawbacks, the author proposes analysing the current state of each of these problems, their related literature, concepts and nomenclature. These problems are tackled separately in the following sections, starting with the review of existing standards and documentation to support the AIBEA workflow in Section 2.4.1; followed by the analysis of the current interoperability between BIM and analysis software in Section 2.4.2; and finally, the examination of current as-is building data acquisition methods in Section 2.4.3.

2.4.1. Existing standards and documentation to support the AIBEA workflow

The complexity of BIM workflows, including the digital technologies involved in project delivery, require the use of standards for BIM contract formalisation [139]. These standards help ensure project transparency, quality, communication, among other essential aspects [139, 140]. However, as stated in Section 2.2.4, despite the availability of BIM standards for other topics and activities throughout a buildings life cycle (e.g. the General Services Administration (GSA) Level of Detail (LoD) [161] for model geometric detail), to the author’s knowledge, there is a current lack of standards for energy-related BIM projects, which jeopardises the successful application of AIBEA. To this end, the following sections focus on ISO-19650 as an existing standard that may be expanded upon to create a standard for BIM energy analysis and, by extension, the AIBEA workflow.

2.4.1.1. ISO-19650, Level of Information Need, and the Exchange Information Requirements

One of the most popular standards for BIM projects is ISO-19650 [139]. In this standard, more specifically in clause 11.2, a new term entitled "Level of Information Need" is introduced. The Level of Information Need specifies the level of information to be provided in each project deliverable, helping clients define their minimum information requirements. According to [162], it is essential to avoid the specification of too little information – which increases the risk of subpar deliverables – and the specification of too much information – which decreases project efficiency.

To define the Level of Information Need, the appointing party has at its disposal multiple metrics which are established as part of the project's information standard. The selected metric(s) must define the geometrical and alphanumerical content for each deliverable in terms of quality, quantity, and granularity [139]. If more than one metric is used, these must be complementary and independent. These metrics are then applied by the appointing party when defining the Exchange Information Requirements (EIR).

In ISO-19650, the EIR definition is the starting point in the information delivery cycle [139]. The EIR is a set of documentation used during the project procurement, being identified as an essential element of BIM implementation. It provides the appointing party's intentions and requirements, defining the information, documentation, and models required at each project stage [139, 163-165].

The EIR is organised in three areas: the Managerial, Commercial and Technical aspects [139]. The latter should detail information such as: the Level of Information Need; the applied software; the selected platforms; the formats required for information exchange; the work planning; the coordination and collaboration process; among others [166]. As such, it is in the Technical aspects of the EIR that the appointing party can make the first approach to the energy analysis requirements using the Level of Information Need and its selected metrics.

2.4.1.2. Level of Development as a metric to define the Level of Information Need

Having identified the EIR as a relevant document to stipulate energy analysis-related information, it is now essential to identify a metric that helps define the Level of Information Need.

To this end, BIMForum's Level of Development (LOD) Specification [165] is a detailed interpretation of the LOD schema developed by the American Institute of Architects (AIA). It is a widely used reference tool that allows BIM practitioners to articulate, with a high degree of clarity, BIM-related content and reliability throughout multiple stages of the building's life cycle [165]. The AEC industry has adopted this formal language to describe the reliability of a digital model at any time, while also allowing the stakeholders to understand the evolution of the model elements and their compliance with BIM standards and interoperability requirements [165, 167]. The different LODs covered in this specification are presented in Table 2.2.

Alongside the LOD definition, BIMForum also provides a LOD Specification Table with several Attribute Tables for the different building systems. In these Attribute Tables, among other information, it is possible to identify the baseline (minimum list of attributes) and the additional attributes that can be used to describe a building system. Prior to 2019's version (BIMForum's LOD Specification is updated yearly), the correlation between these attributes and LOD was stated, creating a LOD profile for each attribute [165]. Using this system, a given LOD would only be achieved if all the attributes for that LOD were adequately defined. However, currently, this LOD Profile has been removed from the specification, with the specification guide suggesting the creation of custom correlations between LODs and Attribute requirements, resulting in custom LOD Profiles for each project [165].

Table 2.2 – LOD definition (adapted from [165]).

LOD	DESCRIPTION
100	The model elements are graphically represented with a symbol or other generic representation. The elements are not geometric representations. Examples are information attached to other model elements or symbols showing the existence of a component but not its shape, size, or precise location. Any information derived from LOD 100 elements must be considered approximate.
200	The model elements are graphically represented as a generic system, object, or assembly with approximate quantities, size, shape, location, and orientation. Non-graphic information may also be attached to the model element. Any information derived from LOD 200 elements must be considered approximate.
300	The model elements are graphically represented as a specific system, object or assembly in terms of quantity, size, shape, location, and orientation. The project origin is defined and the element is located accurately with respect to the project origin. Non-graphic information may also be attached to the model element.
350	The model elements are graphically represented as a specific system, object, or assembly in terms of quantity, size, shape, location, orientation, and interfaces with other building systems. This LOD includes the necessary parts for coordination of the element with nearby or attached elements. Non-graphic information may also be attached to the model element.
400	The model elements are graphically represented as a specific system, object or assembly in terms of size, shape, location, quantity, and orientation with detailing, fabrication, assembly, and installation information. Non-graphic information may also be attached to the model element.

The complexity often related to assessing a building's energy performance depends on the amount of modelled information [118]. As such, considering the impact that information has on the available analysis methods, the specification of appropriate LOD requirements is critical [120]. However, there is currently no explicit information in the LOD Specification Tables about the required parameters to create a proper BIM model for energy analysis. In fact, although some of the specified parameters are related to energy studies (e.g. thermal properties, equipment performance), most are not even considered as baseline parameters. Therefore, the energy studies are performed without a clear LOD guideline, compromising, among other aspects, the energy deliverables' reliability and reproducibility.

Previous research works have identified this lack of standard [141]; however, to the authors' knowledge, no study has proposed a set of energy parameters to correct the issue. Although several studies [16, 22, 28, 63, 65, 67, 68, 168-170] include a data acquisition phase or data repository module within their frameworks, the exact parameters, alongside their required accuracy and LOD, are not specified, apart from the ones required in case studies examples. To this end, a clear definition for energy-related parameters must be developed within the LOD Specification, enabling its use as an independent metric for defining the Level of Information Need of a deliverable and ensuring the creation of a standard for BIM energy analysis. This topic will be expanded in Chapter 3.

2.4.2. Interoperability between BIM and energy analysis software

AIBEA relies on two primary types of software solutions:

- BIM authoring software to model the as-is building and manage its non-geometric information;
- and energy analysis software to analyse the building energy performance and examine retrofit solutions to enhance it.

For AIBEA to be applied as intended, BIM authoring software needs to transfer its stored data to the energy analysis software, where this information can be leveraged. Thus, the data exchange process between these two tools is critical for the successful implementation of AIBEA.

Interoperability is commonly referred to as the uninterrupted ability to freely communicate, exchange and use data among different systems or products interfaces [126, 171]. Interoperability recognizes the advantages of transferring data between software without the need for replicating its content, enabling multiple tools to use the same set of files for various purposes [78]. Therefore, AIBEA relies on robust interoperability to enable a digital information flow between its core software tools [77, 172].

To allow for a better understanding of the current interoperability between these two software solutions and shed some light on the current tools in the market, the following sections are dedicated to the analysis of BIM authoring software (Section 2.4.2.1), energy analysis software (Section 2.4.2.2), and finally, existing data exchange schemes and related issues (Section 2.4.2.3).

2.4.2.1. BIM authoring software

Within the AIBEA workflow, BIM authoring software aims to enable the modelling of the as-is building and manage its non-geometric information. BIM authoring software parametric modelling enables a quick modification of the building model, easing the assessment and implementation of multiple retrofit solutions [173]. Additionally, through the application of information exchange data schemes (examined in detail in Section 2.4.2.3), the same model can be transferred to several different expert software, further increasing its value [174]. Further benefits of applying these software tools in the energy analysis evaluation of a building can be seen in [78, 130].

Being a central component of the workflow, the correct selection and adoption of a BIM authoring tool is vital, especially when so many tools were developed and integrated into the market in the last few years. Fortunately, at the same time, several research works focused on these software solutions, analysing their respective features, advantages and disadvantages. For instance, in 2013, Kurul et al. [175] reviewed eleven leading authoring tools, seven of which were among the over one hundred BIM software systems analysed by Abanda et al. [176] in 2015. Additionally, since 2012, the National Building Specification (NBS) has been tracking this software evolution and adoption in the United Kingdom [177-185], with a yearly *National BIM Report*. Throughout these documents, NBS has been reporting an increasing growth in the usage of BIM authoring tools, opposite to the decline of traditional CAD software. This trend is easily verified in Figure 2.3, which presents the yearly authoring tool usage reported by NBS. For instance, by focusing on *Revit*'s and *AutoCAD*'s evolutions from 2012 to 2020, it can be seen that *Revit*, a BIM authoring tool, increased its usage from 17% to 50%, while *AutoCAD*, a CAD authoring tool, decreasing from 50% to 20%.

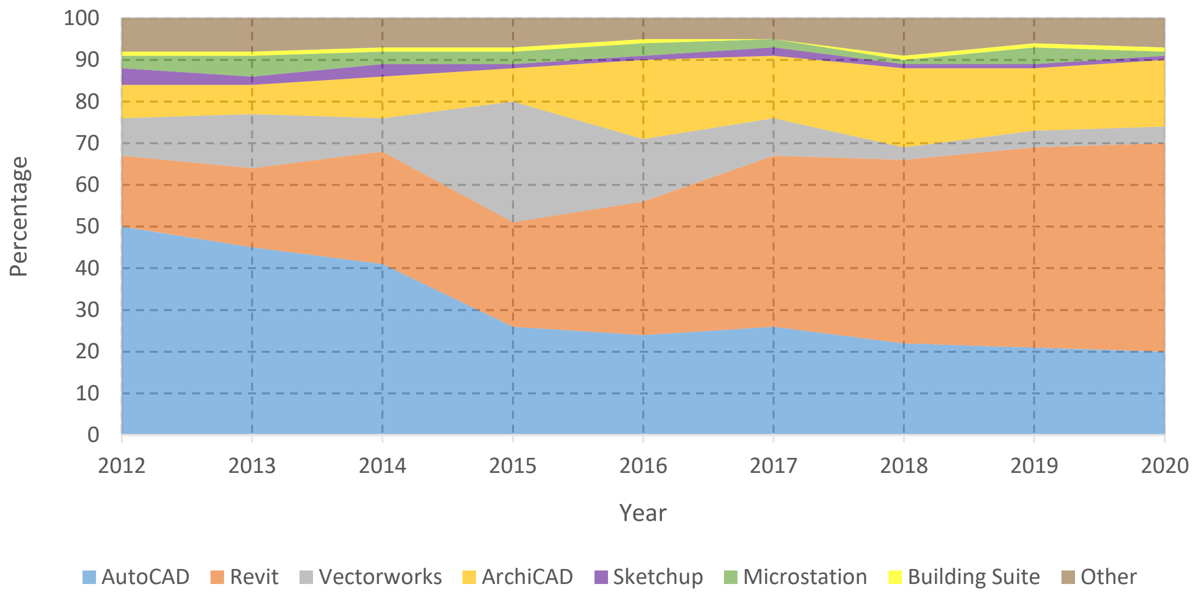

Figure 2.3 – Usage of authoring tools in the United Kingdom according to NBS [177-185]

It should be stated that this evident plethora of available software applications can present a significant challenge for BIM practitioners and BIM adoption, given that modelling techniques, stored information, minimum requirements, and other specifications can vary considerably between software tools. This complicates the training of professional users, decreases efficiency and communication in the AEC industry, and imposes considerable difficulties in software interoperability.

To this end, modelling requirements are often adapted from existing specifications, such as LOD and the Common BIM Requirements (COBIM), to guarantee compliance with BIM standards and improve interoperability [137, 165]. Moreover, model quality verification methods centred on rule-based checking systems, such as *Solibri Model Checker*, *Jotne EDModelChecker* and *FORNAX*, can also be implemented for the same reasons. For more information on these methods, address [186], where Eastman et al. examined and compared five model checking systems, from which the three already mentioned take part.

2.4.2.2. Energy analysis software

Within the AIBEA workflow, energy analysis software receives the developed BIM model as input, automatically creating a building energy model of the building, henceforth entitled “BEM model”, and enabling the simulation and assessment of the building’s energy performance. This automated process streamlines several steps in traditional energy analysis, where BEM models need to be manually created. In fact, through this “BIM to BEM” automated process, engineers cannot only minimize the effort and time required for the development of BEM models but also create a more reliable and consistent analysis across design teams [85, 148]. By enabling the BIM model transfer to multiple energy analysis software, engineers forgo the need to develop several BEM models for different energy analysis applications, completely erasing a significantly time-consuming and error-prone step from the process [143]. As stated by Bazjanac [187, 188], if even a small part of the model data is invalid or inconsistent, the simulation results are no longer credible or acceptable.

In the last few years, similarly to BIM authoring software, many software developers designed energy simulation and analysis tools to virtually evaluate the energy performance of a building [90]. This multiplicity can be best seen in the *Building Energy Software Tools Directory* [189], provided by the United States Department of Energy, where over four hundred energy analysis software tools are currently listed, most of which accept BIM data as an input. Multiple authors extensively reviewed these tools in the past, highlighting their respective usages and functionalities. For instance, in [190], Crawley et al. provided a comparison of the features and capabilities of twenty major building energy simulation programs. In [191], Attia et al. assessed the usage of ten tools (seven of which are among the previous twenty) through a survey with 249 responses. In [192], the authors compared ten energy simulation programs to help design net-zero energy buildings. In another study, Lu et al. [193] reviewed 12 popular BIM software applications developed to improve sustainability performance in buildings, successfully identifying each tool's scope and potential users. Maile et al. [194] described a selection of five energy simulation engines, stating their functionalities and discussing their respective usage over the different life-cycle stages of a building. Finally, Wen and Hiyama [195] reviewed ten programs, focusing on their simplicity and ease of application.

Figure 2.4 presents a summary of the energy analysis tools applied in works cited throughout this literature review, giving, to a certain extent, an overview of the most popular tools related to BIM energy analysis and AIBEA.

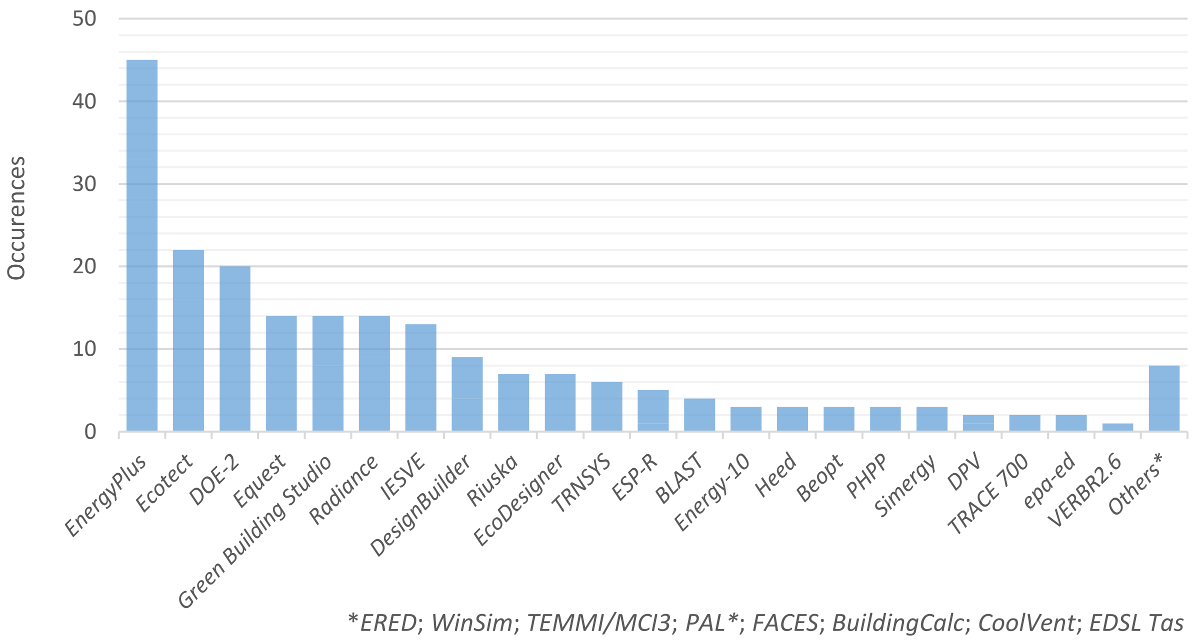

Figure 2.4 – Energy analysis tools applied in works present in this literature review

These tools generally consist of two components: a graphical user interface (GUI) and a simulation engine [85]. The first eases software integration with different types of input data, enables user interaction, and provides a clear output analysis. The second is responsible for the thermal and energy calculations [196]. In multiple cases, GUIs and engines are developed independently. For instance, *DesignBuilder*, *OpenStudio*, *Simergy*, *Hevacomp*, *EFEN*, *Demand Response Quick Assessment Tool*, *CYPE-Building Services*, *Easy EnergyPlus*, *SMART ENERGY*, and *AECOsim* are different applications and GUIs that rely on *EnergyPlus* as a simulation engine [25]. Similarly, *OpenStudio* is an assembly of

GUIs [197]: *OpenStudio SketchUp Plug-in* as the primary geometry editor; *OpenStudio Application* as the main energy editor; *Parametric Analysis Tool* for parametric modulation and analysis; and, finally, *ResultsViewer*.

Regarding software features, both Wen et al. [195] and Stundon et al. [198] identified that "whole building's energy performance prediction throughout a building's life cycle" is the most popular feature among practitioners. However, as highlighted by multiple authors [21, 22, 58, 90, 96, 193, 199-225], these tools offer numerous other capabilities.

For instance, Shahryar Habibi [21] proposed a BIM methodology for assessing office environments, using energy analysis tools to examine a building's solar exposure, natural ventilation, daylight efficiency, acoustic performance, building orientation, and material thermal properties. In [202], Santamouris et al. applied *TRNSYS* to inspect an experimental green roof system and examine its energy-saving potential, while in [222], Kuo et al. investigated the accuracy of energy analysis tools in simulating BIPS for the same purpose.

Regarding building shape and orientation, Toke Nielsen [201] developed a tool for evaluating energy demand and indoor environments in the early stages of building design, using it to generate the optimal building shape for minimum energy consumption; Krstić-Furundžić and Kosić [224] used *PHPP2017* to demonstrate how different concepts of envelope construction affect the energy efficiency of a building; Abanda and Byers [90] assessed how orientation could impact energy consumptions using *Revit* and *Green Building Studio*; and Xu et al. [206] applied *EnergyPlus* to examine the impact of building orientation optimization in the energy savings of chosen cities in China.

Focusing on optimization methodologies, Harmathy et al. [223] used *EnergyPlus*, *Radiance* and *Ecotect* to verify a multi-criterion optimization methodology for overall energy performance improvement of office buildings; Evins [216] presented a multi-level optimization procedure for building design, energy system sizing and operation; and Liu et al. [214] used *Ecotect* for building design optimization and sustainability improvement.

In several other works [200, 203, 207-209, 215, 217], the authors applied multiple energy analysis tools to assess different windows' impact on building thermal and daylight simulations. Studied variables include: window-to-wall ratio; glazing transmittance; window materials; room geometry; type of envelope; and cost.

Both Shoubi et al. [218] and Wang et al. [204] focused on the operational stage of a building, employing *Ecotect* alongside *Revit*, to identify material combinations that diminish operational energy consumption and evaluate the planned operational energy. In another work, Harmati et al. [219] applied the assembled power of *Revit*, *Sketchup*, *OpenStudio* and *EnergyPlus* to analyse, compare and evaluate the performance of four HVAC systems, while Alam and Ham [210] verified the viability of using *EcoDesigner* for energy rating in Australia.

Finally, concerning building energy retrofit, Zmeureanu [199] assessed the energy savings of building retrofit measures using *DOE-2*; Ascione et al. [58] and Chidica et al. [205] utilized *EnergyPlus* to simulate the effectiveness of applying retrofitting practices in historical and office buildings, respectively; Capeluto et al. [211] studied the different European climatic conditions on façade retrofitting; Nagi et al. [212] illustrated the impact of retrofitting measures on temperature supply by analysing a historic building's real retrofit scenario using *EnergyPlus*; and Almeida et al. [220] used

EnergyPlus to quantify and integrate uncertainties in energy consumption during life cycle cost analysis of rehabilitation alternatives.

2.4.2.3. Interoperability data schemes and existing interoperability issues

In the past three decades, the building industry has displayed significant progress in software data exchange through the development and continuous improvement of standard data formats and communication protocols. In the late 80s and early 90s, the first-generation of data exchange models, such as ARMILLA [226], COMBINE [227], IBDE [228], ICADS [229] and STEP [230], displayed a focus on building geometry data. Although required, these models lacked enough information for performance analysis. Consequently, the second-generation of data exchange schemes revealed an expanded model to integrate domain-specific performance information. Both hierarchical models [231] are examples of this second generation. Currently, third-generation schemes have the potential to encompass most, if not all, information related to a building through the entirety of its life cycle. Industry Foundation Classes (IFC) and Green Building Extensible Markup Language (gbXML) are two well-established data schemes of this generation, with most energy analysis applications relying on these schemes for communication [232].

The IFC data scheme was developed by BuildingSMART, formerly known as International Alliance for Interoperability, in 1995 [233]. IFC's main objective is to offer the basis for process improvement and data exchange in the construction and facility management industries [142]. It is an object-oriented data model for buildings, which eases the information exchange process among IFC-compliant software applications [234]. With each IFC release, the model is improved by enhancing its existing structure and creating new classes, enabling further information storage and interoperability among software.

The gbXML scheme was developed in 1999 by Green Building Studio, at the time known as GeoPraxis [142]. Unlike IFC, which presents a broader application area in the AEC industry [235], gbXML focuses on enabling the data exchange between BIM and energy analysis software [232]. In its essence, the gbXML scheme can be perceived as a database to link the building's geometry with its intrinsic descriptive data [236]. gbXML is based on the XML specification, a set of rules for designing text formats, which has been positioning itself as a standard system to define information in BIM [85]. As such, XML provides a non-proprietary, persistent, verifiable, easy to understand file format that organizations may use to create their customized markup language and imbue data schemes with semantic content [232].

Detailed examination and comparison studies of these data schemes can be seen in [232] and [126]. Other works focusing on gbXML can be found in [85, 142], while the IFC data scheme was studied in [144, 237]. It should be noted that interoperability between applications does not depend exclusively on the quality of these data formats but also on how they are adopted and applied by software and practitioners.

Regarding the former, while some tools support only one of these schemes, most tend to support both. For instance, *ArchiCAD*, *DesignBuilder*, *Microstation*, *OpenStudio,* and *Revit* [90, 148, 197, 232, 238] are examples of BIM authoring tools that support both schemes; while energy analysis tools include *Hevacomp*, *Ecotect*, *Green Building Studio*, *eQUEST*, *HAP* and *VE* [25, 90, 142, 232, 239]. A more detailed analysis of these tools' interoperability can be found in the following bullet points:

- *Hevacomp*, a GUI for *EnergyPlus*, can load .xml, .dxf, and .dwg files to acquire the geometry and descriptive data of a building, creating input files for *EnergyPlus* [25];
- *Ecotect* supports multiple file extensions from .xml, to .ifc, through .dxf, .3ds, .obj, among others [173];
- *Green Building Studio*, a web-based software based on *DOE-2.2*'s engine, can be fully integrated with *Revit*, importing all the required data through the gbXML scheme (.xml) [151];
- *eQUEST* may import geometry and descriptive data through .xml and 2D drawing through .dwg. However, some *eQUEST* features are not supported by gbXML [240];
- *RIUASKA*, a GUI for *DOE-2,1E*, can import .ifc files to acquire building geometry information [25, 194];
- *VE* provides an Interoperability Navigator for easier import from various CAD tools while offering *Revit* plugins to extend interoperability. gbXML and IFC are the main data schemes supported [25, 241].

Within AIBEA, energy analysis applications need to receive information regarding the building's location, surrounding environment, geometry, building zones, occupancy, usage, HVAC, materials, among others. As seen in Maile et al. [194], this information can be divided into five stages of data exchange, namely: (1) transfer of the building's location for weather data association; (2) transfer of the building's geometry, construction systems, materials and space types; (3) aggregation of the existing spaces to thermal zones; (4) assignment of space loads (e.g. lighting loads) to the respective spaces; and finally, (5) determination and allocation of HVAC systems and components.

Although most of these steps can be performed seemingly without issues, as indicated in Section 2.2.4, some still reveal interoperability problems [26, 77, 106, 118, 142-146, 148-151, 242, 243]. The following bullet points indicate some of the problems highlighted by the current literature:

- <u>location</u> – the building's surrounding environment is responsible for variables such as local temperature, wind speed and direction, barometric pressure, rainfall intensity, and solar radiation. This data is required for the correct energy analysis of a building and is usually obtained through the nearest weather station, selected using the building's geographic location. Although authoring tools can store this information in data schemes, simulations tools are reported to be incapable of acquiring this information, resetting the building's coordinates to the software default location [148, 243];
- <u>geometry</u> – several inconsistencies have been reported with the transferring of geometrical data between BIM tools. These inconsistencies are mostly related to varying boundaries of rooms and thermal zones, as well as ill interpretation of non-planar geometry [146], which translate into duplicate and/or missing objects, alongside wrongly calculated space volumes [147]. Examples of these problems are the improper determination of walls centrelines [26], the incorrect volume calculations due to false floors and suspended ceilings [148], and the non-determination of space boundaries due to complicated geometries (i.e. freeform shapes and varying wall thickness) [143]. Kim and Yu [149] and Ugliotti et al. [150] reported on the impossibility for current tools to import curved walls using exchange data schemes. Further geometry interoperability issues are described by Maile et al. [147] and Cemesova et al. [106], Panteli et al. [77] and Chen et al. [242];

- material properties – although data schemes may contain very detailed information, often this data is not adequately accessed by authoring or simulations tools. This is especially evident with material properties exchange. Despite data schemes being able to store relevant material properties, the authoring and analysis tools lack the means to import/export these properties [144]. For instance, Jeong et al. [151] reported that the solar and infrared absorptivity parameters, which can be stored in data schemes, are missing in some authoring tools, despite being required by the energy analysis software. Gourlis and Kovacic [26] introduced the material characteristics manually in *EnergyPlus* since both IFC and gbXML schemes could not export the values for thermal conductivity, density, and specific heat capacity of construction layers, despite having the options to provide this data. Kim et al. [118] also reported problems with material properties, designing a manually extendable material database as a solution. Finally, Duygu Utkucu and Hatice Sözer [243] also reported the loss of material data while attempting to use *Revit* with computational fluid dynamics (CFD) simulation tools;
- building systems – most simulation tools display limited interoperability regarding HVAC system components information, which has to be manually introduced by the user. This issue has been increasingly exacerbated by the growing importance of HVAC systems in the energy performance of a building, as well as the lack of solutions in recent versions of the IFC and gbXML schemes [26]. Studies reporting on this problem can be seen in [26, 242, 243];
- building operation – similarly to "location" issues, software tools fail to acquire operation data from data schemes. As such, these programs mostly resort to their default values or user manual inputs. However, Nasyrov et al. [148] stated that *Green Building Studio* successfully exchanges operation data (e.g. building usage, operating schedules, internal loads) with *Revit*, given its integration within the authoring software. Notwithstanding, *Revit* failed to export operation data to other analysis software [242, 243].

To support a proper AIBEA workflow, a solution to these problems must be developed and expanded upon in Chapter 3.

2.4.3. AS-IS BUILDING DATA ACQUISITION

In recent years, driven by technological advances, multiple methods for acquiring geometric and energy-related data have been developed to characterize the as-is conditions of a building [236], enabling the generation of accurate as-is BIM models. The first data type helps create the model shape, enabling the representation of its architecture and the creation of a supporting structure in which to store relevant building data. The second helps depict the building's actual conditions, enabling its analysis [22, 236]. When reviewing these methods, a clear preference for non-destructive approaches is noticeable, as disassembling or damaging the building is often an unfeasible task [129].

To support the creation of documentation and tools that ease the building surveying effort in the AIBEA workflow, the following sections review existing methods for as-is data acquisition. These methods are divided into two groups: (1) geometric and (2) energy-related data acquisition. These are respectively covered in Section 2.4.3.1 and Section 2.4.3.2.

2.4.3.1. Geometric data

Regarding geometric data acquisition, recent technological developments, coupled with the rise in popularity of non-invasive imaging tools and long-range methods, enabled the performance of high accuracy and precision surveys of buildings, allowing for the creation of geometrically detailed as-is BIM models [22, 96, 236, 244, 245].

Various existing survey technologies such as laser scanning, photogrammetry, 3D camera ranging, topographic methods and videogrammetry, were reviewed in [10, 246-251], with the authors concluding that these technologies all require expensive and fragile equipment, trained operators, and may be time-consuming. Other methods such as RGB-D and optical triangulation can be seen in [252, 253], sharing the same conclusions but reporting lesser accuracy and range. Table 2.3 summarizes the information gathered from the works mentioned above. Empty cells refer to unavailable data.

From these methods, two distinguish themselves as the most popular: photogrammetry and laser scanning. Both methods generate point clouds as their output, are considered mass data collection techniques, and are suitable for a wide variety of scales and object complexity levels [96, 254, 255]. These methods are duly reviewed in Section 2.4.3.1.1 and Section 2.4.3.1.2, respectively.

2.4.3.1.1. Photogrammetry

The photogrammetric method, also known as photogrammetry, is defined as the science and technology of extracting qualitative (e.g. shape, textures) and quantitative (e.g. orientation, size) characteristics of an object from photographs [256]. The basic principle behind photogrammetric measurements is triangulation: by photographing an object from at least two different positions, a 3D coordinate can be determined by intersecting the geometrically-mathematically reconstructed rays that travel from the sensor to the object [257, 258].

By repeating this process multiple times for different points, a point cloud is created. A point cloud is essentially a collection of points, typically organized within a 2D matrix, where each row is a captured point, and each column is a variable describing the point [110, 259]. For photogrammetry, there are typically six variables: the X, Y and Z coordinates, used to define the point location in space; and the red, green and blue (RGB) parameters in the RGB colour scheme, used to define the point colour.

Photogrammetry can be divided into two categories depending on their working platform: aerial (e.g. aeroplane, drone) and terrestrial (e.g. handheld, tripod). The terrestrial category can be further specified into close-range photogrammetry, when dealing with ranges below 200 meters [258].

Compared to laser scanning, it is possible to identify advantages regarding the equipment's cost, the operator required knowledge, and the overall operational simplicity during the survey process. However, as seen in [85, 260, 261], finding and matching distinctive features within the scene is required to generate a point cloud using this method, meaning that it works well with highly textured environments but has a poor performance on homogeneous ones [132, 262, 263] – a limitation not affecting laser scanning. Further disadvantages can be linked to its overwhelming manual input requirement and information overlap, which can be time-consuming; its heavy dependence on weather and lighting conditions; as well as reduced resolutions, accuracy, and data processing speed [248, 250, 251, 264-271]. Noticeably, several works have overcome these drawbacks by combining photogrammetry with laser scanning, as shown in [265-268, 270].

Table 2.3 – Methods for as-is building geometric data acquisition

Method	Fieldwork	Automated Spatial Data Retrieval	Spatial Data Accuracy [a]	Spatial Data Resolution [a]	Equipment Cost [b]	Equipment Portability	Range Distance [c]	Data Treatment	Weather and lighting impact
Traditional Method [d]	Simple but time-consuming	No	Low	-	Low	Portable	-	Simple but time-consuming	Low
Topographic Methods	Complex and time-consuming	No	High	-	High	Not portable	High	Complex and time-consuming	Low
Photogrammetry	Complex and time-consuming	Manual or semi-auto.	Medium	Low	Low	Portable	Medium	Simple but time-consuming	High
Videogrammetry	-	Semi-auto.	Medium	High	Low	Portable	Medium	Complex	High
3D Camera Ranging	-	Automated	Medium	Low	Medium	Portable	Low	Complex	Low
Laser Scanning (time-of-flight)	Simple and fast	Automated	High	High	High	Both options	High	Complex	Low
Laser Scanning (phase measurement)	Simple and fast	Automated	High	High	High	Both options	Medium	Complex	Low

[a] High: < 1mm; Medium: 1mm – 1cm; Low: > 1cm
[b] Low: few hundreds; Medium: hundreds; High: thousands
[c] Low: < 10m; Medium: 10m – 1km; High: > 1km
[d] Use of equipment such as flexometers, measuring tape, poles, squares, plumb lines, etc.

This method has been applied in the AEC industry to map a 3D space from 2D photo images, either for acquiring simple measurements [272, 273] or more complex tasks as tracking the construction progress [268, 274].

2.4.3.1.2. Laser scanning

Light Detection and Ranging (LiDAR) technology, also known as 3D laser scanning, measures the distance to a target by illuminating it with a laser and interpreting the results from the reflected light, based on the applied measurement principle [152, 251]. By rotating a mirror in the laser scanner, several targets over a designated area can be measured consecutively, creating a point cloud. In addition to the six variables introduced in the last section, point clouds originated from laser scanning typically present a seventh: the intensity value. This value is determined by the type of material, the atmospheric conditions, and the scanner parameters. This variable will be covered in-depth in Section 3.4.3.2.2. Additionally, in laser scanning, RGB values are acquired by photographing the surveyed scene and corresponding each point in the point cloud to a pixel in the photograph. This mapping is done automatically by laser scanning software.

Regarding the applied distance measurement principle, in the AEC industry, laser scanners usually apply time-of-flight or phase-based principles [110]. In the former, the time taken for an emitted light pulse to return to the scanner is registered and, by knowing the pulse travelling speed, the distance is inferred. In the latter, the phase shift between the emitted and return signal is measured to establish the flight time and, therefore, the distance travelled. Phase-based technology leads to reduced scanning times at the expense of scanning range (under 100m), while time-of-flight leads to higher scanning ranges (above one kilometre) at the expense of scanning time [275].

Similarly to photogrammetry, laser scanners can be divided into three different categories, depending on their working platform:

1. terrestrial – a stationary platform on the ground (e.g. tripod);
2. mobile – a mobile platform on the ground (e.g. car);
3. aerial – an airborne platform (e.g. drone).

Each category has its purpose, intended environment, level of accuracy and precision [254]. Currently, in the AEC industry, terrestrial laser scanning is the most popular approach, given its increased accuracy and lower costs – on average [132].

In comparison to the other survey technologies, laser scanning surpasses the remaining alternatives due to its largely automatic surveying process, fast measuring speed (acquisition of over a million points per second [23, 88, 152]), and improved accuracy – being able to capture complex shape geometries and minute details with a 3D precision of 0.6mm at ten meters range [110, 236, 252, 276, 277]. However, laser scanning is also reported to display some limitations, primarily in its expensive equipment, required knowledgeable operators during data treatment, and stationary field of view, usually requiring the allocation of several station positions to overcome occlusions [88, 249, 278]. Examples of the latter limitation can be seen in [39, 236, 279, 280], where the authors demonstrate case studies in which at least three station positions were required. The use of mobile laser scanners, instead of stationary ones, can also eliminate this drawback, albeit in a trade-off for scanning resolution [46, 131, 281-284]. This limitation may also be partially solved using expert point cloud software. This software is discussed in detail in Section 2.5.1.

In the AEC industry, laser scanning has been applied in construction monitoring and tracking [268, 278, 285-289], project communication [30], quality assurance and control [290-296], energy analysis [28, 39, 62, 85, 297-299], and BIM modelling [27, 29, 300-309]. In particular, the latter topic has attracted the industry's attention in recent years, originating the scan-to-BIM process, thoroughly reviewed in Section 2.5.

2.4.3.2. Energy-related data

Having access to the as-is energy-related information of a building is essential for AIBEA since the actual energy performance of a building can vary significantly from its designed value. This gap has been thoroughly researched in the past, with the author highlighting the following works [7, 310-313]. In its essence, the energy performance of a building is dependent on three aspects [314]: 1) the thermal characteristics of the building and its surroundings; 2) the building energy usage; and 3) the installed services. All three can impact the discrepancy between design and built performances; however, the first two aspects tend to be the most responsible, given their challenge prediction. As such, the following sections review methods by which these two aspects can be determined.

2.4.3.2.1. Thermal characteristics of a building and its surroundings

The thermal characterisation of a building has long been a central research topic in the AEC industry. To this end, multiple methods have been developed for this purpose, from simple device readings to aggregated assessments and complex evaluations. On the latter spectrum, a commonly applied method is the co-heating test.

The co-heating test allows for the post-construction evaluation of a buildings' thermal shell as a complete system [315]. This method is centred around the principle of a balanced energy flow within a steady-state system, meaning that heat input and output are considered equal when averaged across a length of time. This time interval is typically considered 24 hours [316, 317]; however, as seen in [317], smaller periods can also be considered, albeit with a reasonable drop in accuracy. Generally, the method requires significant heating of the building, with the literature indicating a minimum difference of 10 degrees Celsius across the thermal shell [315]. The power required to maintain this temperature is then measured, and regression analysis of the aggregated building data provides the Heat Transfer Coefficient. Sonderegger and Modera [318] originally developed this technique; however, the procedure seen in [316] is generally adopted, given the lack of an international standard supporting the technique.

Regarding research surrounding this method, in [314], Bauwens and Roels made an exhaustive review of the experimental setups, data acquisition practices and data analysis methodologies applied in the assessment of building thermal characteristics using the co-heating test. In another work, Shea et al. [319] compared co-heating tests with computer and laboratory simulations to estimate the hygrothermal performance of an experimental hemp-lime building. In [316, 320], the authors explained the importance of the co-heating test as part of a set of inspections the building should endure when evaluating its hygrothermal performance. Francisco et al. [321] showed the viability of duct retrofits for energy conservation by conducting co-heating tests in 53 residential buildings. Hopper et al. [322] evaluated multiple data collection and analysis techniques (co-heating included) as tools to support thermal performance enhancement of dwellings. In [323], the authors assessed the energy and environmental performance of low energy dwellings on the post-construction stage, comparing them to design expectations. Finally, Eshrar et al. [324] used comparative co-heating tests to assess the fabric and energy performance of five wall systems. For more studies and advances regarding the co-heating test, see [317].

This method is most interesting in what concerns AIBEA not only for its output and evaluation of the building as a whole, but also for the exhaustive survey that accompanies this test. In fact, as seen in the above-referenced studies [314, 316, 319-324], multiple tests can be associated with this method, with Table 2.4 showcasing the ones applied in the previous studies alongside their respective outputs.

Among these tests, in recent years, BIM practitioners have focused on thermography as a method for an automated correspondence between geometric data and energy-related information. This technology goes well in hand with the practice of laser scanning and photogrammetry, with various manufactures designing equipment for their simultaneously use [325]. As such, within AIBEA, infrared thermography stands as a resourceful technique for the acquisition of a building's thermal data.

Through the usage of thermal cameras, this technique can continuously capture wide distributions of surface temperatures, enabling a quick identification of thermal bridges [326], as well as faults related to energy efficiency (e.g. heat losses and air leaks) [327-329]. Yassar El Masri and Tarek Rakha [330] performed an in-depth review of this method, reporting its successful application in identifying materials thickness and physical and dielectric properties [331], measuring the thermal performance of materials, identifying the presence of moisture inside a wall assembly [332], among others uses. In the last few years, multiple methodologies comprising thermography have been developed to measure actual heat transfer conditions, with the authors highlighting the following works [328, 333-336]. Both advantages and disadvantages of this technology have been well documented [7, 85], with its main disadvantages relating to the low field of view and resolution of thermal cameras, translating into an overwhelming amount of thermal images being required to do a proper analysis and representation of the full building. In turn, this makes manually corresponding each image to the geometry of the building a typically time-consuming and poorly accurate process [39].

For this reason, over the past few years, numerous works focused on combining BIM geometric data with thermography [337, 338], allowing for the spatial recognition of a building's thermal properties distribution. These studies can be roughly divided into two groups: visual correspondence; and gbXML based modifications. Visual correspondence relates to the texture modification of BIM elements inside the model, whereas gbXML-based modifications relate to altering the properties values within the gbXML schema.

Recent examples of visual correspondence can be seen in the following works [7, 339], where thermography adds visual information to the 3D building model. In another work, Im et al. [340] proposed a method to visualize 3D thermal models using web-based geospatial systems. In [338], Lagüela et al. presented a methodology to merge point clouds with thermal information acquired through thermography and, more recently, in [39], their work combined laser scanning, photogrammetry and thermography to generate textured 3D BIM elements, both with RGB and thermographic images. Lastly, Borrman et al. [341] created a method for indoor 3D thermal modelling using an automated robot equipped with a thermal camera and a laser scanner.

Table 2.4 – Non-exhaustive survey techniques for the acquisition of energy-related data and respective outputs

Test	Outputs
Air Handler Flow Measurements	▪ Leak identification
Anemometer	▪ Air velocity
Blower Door	▪ Airtightness
Carbon Dioxide Sensor	▪ CO_2 content
Cavity Temperature Measurement	▪ Cavity temperature
Construction Observation	▪ Anomaly identification
Delta-Q Test	▪ Leak identification
Ground Penetrating Radar	▪ Material depth and composition ▪ Moisture detection ▪ Rebar location
Heat Flux Measurement	▪ Envelope thermal resistance (R-values) ▪ Envelope thermal transmittance (U-values)
Hygrometer	▪ Interior relative humidity
Partial Deconstruction	▪ Building element component identification
Pyranometer	▪ Vertical radiation ▪ Window glazing solar transmittance
Smoke Testing	▪ Leak identification
Thermal Anemometry Using Hotwire Anemometers	▪ Fluid velocity ▪ Leak identification
Thermography	▪ Leak identification ▪ Material depth and composition ▪ Thermal bridge detection ▪ Thermal properties
Thermometers	▪ Interior temperature
Tracer Gas Measurement	▪ Air change rates ▪ Leak identification
True Flow Plates Test	▪ Leak identification
Ultrasound	▪ Anomaly identification ▪ Material depth
Weather Station Measurement	▪ Barometric pressure ▪ External air temperatures ▪ External relative humidity ▪ Rainfall ▪ Solar Radiation ▪ Wind direction ▪ Wind speed

Regarding gbXML-base modifications, Lagüela et al. [236] proposed a highly automated methodology to update thermal properties directly in the gbXML files, generating as-is BIM models containing the building thermal characterization. Their work measured as-is thermal properties through thermography, followed by the manual linkage of a single averaged value to the corresponding element in the gbXML schema. In [129] and [85], Younjib Ham and Mani Golpavar-Fard automated this previous method by calculating the thermal properties at the level of 3D points in a meshed BIM, thus allowing for the automatic association of the properties values with the corresponding BIM element in the gbXML schema.

All the above-mentioned studies can identify advantages and limitations for combining BIM, laser scanning and thermography, along with guidelines for better results.

2.4.3.2.2. Building's energy usage

As stated in Section 2.4.3.2, the difficult prediction of a building's energy usage is also responsible for discrepancies between designed and built performances. To answer this problem, recent advances in the field of the Internet of Things (IoT), coupled with the widespread of sensorization technology, enabled the cost-effective and non-intrusive monitoring of a building [342], allowing for the proliferation of post-occupancy databases and the refinement of energy simulation and analysis software engines.

According to Gubbi et al. [343], IoT can be described as an "interconnection of sensing and actuating devices providing the ability to share information across platforms through a unified framework, developing a common operating picture for enabling innovative applications". Although this concept has been popular in research since the late 90s, practical implementations are still in their infancy [344]. However, this is rapidly changing, with the number of worldwide connected devices increasing exponentially in the last few years, currently estimated to be in the tens of billions [345]. As the number of connected devices increases, so does the potential for IoT-based technologies.

Methods reliant on this strategy typically consist of the following four primary layers [342, 346, 347] (also illustrated in Figure 2.5):

- a wireless sensorization network for data collection;
- an online database in which to store and clean the recorded data;
- a data analysis system to examine the stored data, extracting relevant information and key performance indicators;
- and a service system to deliver the extracted information to the user or an autonomous building management system.

Sizes of IoT systems can vary considerably, ranging from a few sensors, in residential buildings, to millions of devices, in complex factory floors and large commercial areas [348]. Data acquired in these sensorization networks travels through the identified layers without requiring human-to-human or human-to-computer interactions. Typically, all data is stored, meaning that the created databases can offer a mixture of live data (e.g. current room occupancy and temperature conditions) and historical data (e.g. room occupancy patterns and energy usage trends) [345]. These databases are frequently referred to as post-occupancy databases.

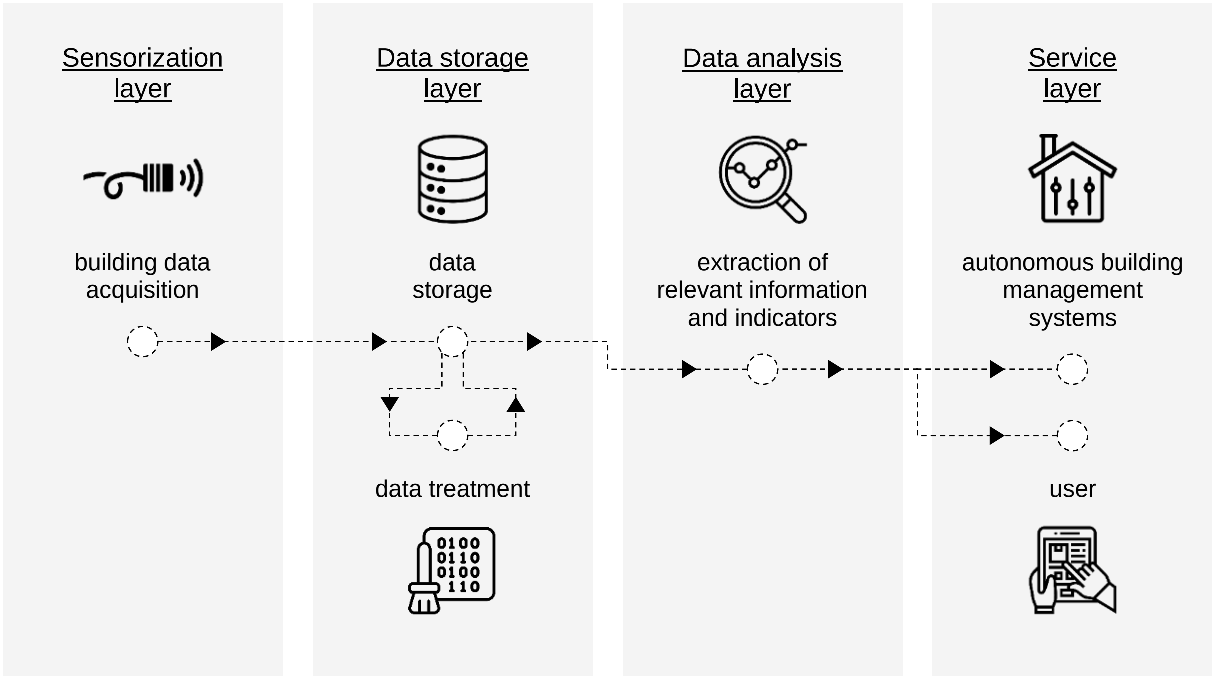

Figure 2.5 – Constituent layers of IoT-based methods for the non-intrusive monitoring of a building

Several works have focused on one or all of these layers in the past few years, with the latter two receiving considerably more focus.

Regarding the first layer, Metallidou et al. [347] and Yaïci et al. [345] presented a comprehensive review of existing sensors used in these methods, identifying their associated smart technologies, typologies, specifications and potential uses.

Regarding the second layer, Sanhudo et al. [349] developed and applied an ML framework for the automated rectification of erroneous or missing data in datasets for building energy analysis.

Finally, regarding the last two layers, multiple authors have leveraged these technologies for numerous purposes such as energy management, construction monitoring, health and safety management [350], building management, and structural stability monitoring [351]. However, as identified in [342], most research focuses on energy-related topics, aiming to maximize a building's energy efficiency and thermal comfort. These topics include:

- building occupancy prediction [352-355], where IoT systems identify the number of occupants in a room and extract occupancy patterns for use in predictive and monitorization systems (e.g. monitor geospatially referenced energy usage);
- real-time energy management at building and city scales [356-358], where IoT systems either automatically intervene in the building systems to achieve a better energy performance (e.g. turn off lights in unoccupied rooms) or deliver generated suggestions to the user;
- effective control and monitoring of HVAC and indoor environment quality systems [359-363], lightening systems [364], hot water systems [365] and BIPS [366];
- energy demand/consumption patterns prediction [346, 367];
- and energy performance benchmarking [368].

In regards to BIM, several of the above-cited works integrate this methodology within their IoT research. In fact, despite BIM's connection with IoT-based data sources being a relatively new development, several studies already identify an exponential increase in research works combining both technologies. For instance, Gerrish et al. [369], Panteli et al. [77] and Tang et al. [370] review several works in this field, identifying the integration of BIM and IoT for energy-related purposes as one of the current major research topics. Similarly, Bottaccioli et al. [371] identify this connection as a vital research objective, stating multiple advantages for integrating both technologies, namely in the effectiveness of potential energy retrofitting actions and the validation of existing BEMs.

As seen by the last few sections, several rising technologies can ease the building surveying effort in the AIBEA workflow, both for geometric and energy-related data. To properly apply these technologies in the AIBEA workflow, a clear framework for their integration needs to be developed. In particular, and considering the second proposed perspective (integration of scan-to-BIM in the AIBEA workflow), the laser scanning technology should be thoroughly analysed, both in terms of its specifications and field application. As such, these topics will be expanded in the proposed contributions in Chapter 3.

2.5. Integration of the scan-to-BIM process in the AIBEA workflow and further enhancement through its automation

As with the first perspective, to properly support the integration and automation of the scan-to-BIM process in the AIBEA workflow, the author proposes analysing this process current state, examining its related literature, concepts, nomenclature, and problems. To this end, the next sections are structured as follows: Section 2.5.1 describes the scan-to-BIM process, further stipulating how to integrate it in the AIBEA workflow; Section 2.5.2 introduces existing problems related to scan-to-BIM, identifying how these can impact AIBEA after its integration; finally, Section 2.5.3 proposes the automation of the scan-to-BIM process as a method to solve the identified problems, examining AI as the primary supporting technology to achieve it.

2.5.1. Scan-to-BIM

The process of transferring point cloud data into a BIM authoring software for modelling is known as scan-to-BIM [152, 288]. This process aims to ease the effort in creating as-is BIM models while also improving their accuracy and detail. Several research initiatives have focused on scan-to-BIM, dividing the process into three main steps [22, 23, 280]: data collection; data processing; and BIM modelling.

Data collection entails the acquisition of the building's point cloud. To do so, traditional surveying methods are replaced with point cloud generation solutions, such as laser scanning or photogrammetry. The former being prevalent. As described in Section 2.4.3.1, these methods are currently advantageous over traditional methods, which increases the scan-to-BIM process appeal.

Data processing comprises the treatment of the acquired point cloud. Expert software, such as *Leica Cyclone*, *Meshlab* and *Autodesk ReCap*, are applied to process the acquired point clouds, allowing for its decimation into lower, homogeneous, and manageable resolutions, the removal of unwanted noise, and the registration of multiple scan stations into a single-shared coordinate system (either manually, semi-automatically, or fully-automatically [372]).

Finally, in BIM modelling the treated point cloud is imported into a BIM authoring software to be manually traced using BIM modelling tools. The interoperability between point cloud and BIM authoring software is supported by multiple file formats, including:

- .pts, .ptx, .txt, and .xyz from ASCII;
- .pcg, .rcp, .rcs, and from Autodesk;
- .e57 from E57;
- .fls, .fpr, and .fws from Faro;
- .las, .ptx, .sc2, .scan, and .xml from Leica;
- .pcd from Point Cloud Library;
- .dbx, .dxf, .msh, .obj, .ply, .ptb, .ptg, and .ptz from several other developers;

as well as multiple point cloud importation and management plugins for BIM authoring tools such as *As-Built* and *CloudWorx*, respectively developed by Faro and Leica.

Regarding research on these three steps, most authors tackle the latter, seldom focusing on the first two. Nevertheless, multiple authors demonstrate scan-to-BIM viability in several AEC industry applications, including: quality assessment and control [292, 296, 373, 374]; construction progress tracking [278, 286-288, 375]; improving project communication [30]; safety management [376]; building performance analysis [22, 35, 377]; sustainability [39, 378, 379]; and facility management [380]. BIM modelling of historic/heritage buildings, typically referred to as HBIM, is also a prevalent topic associated with scan-to-BIM research, given the added detail this process allows and HBIM requires [96, 244, 245, 254, 381-384].

Scan-to-BIM can be integrated into the AIBEA workflow by either including laser scanning or photogrammetry in the first step of AIBEA and using the acquired point cloud data to model the building in the second step (AIBEA main steps can be revisited in Section 2.2).

By accomplishing this integration, the modelling-related difficulties in AIBEA can be drastically improved, solving the last of the four main identified issues in Section 2.2.4. However, as earlier implied, scan-to-BIM also has its own limitations, which prevent it from completely solving this problem. These limitations are focused on in detail in the following section.

2.5.2. Existing problems in conventional scan-to-BIM

In the previous section, scan-to-BIM was proposed to solve the mostly manual, time-consuming, labour-intensive, subjective, and error-prone BIM modelling present in the AIBEA workflow. As demonstrated in the literature, it accomplishes this objective, even allowing for increased model accuracy and detail. Furthermore, by relying on point cloud generation survey methods, scan-to-BIM also indirectly tackles other identified problems, such as the slow and exhaustive building surveying that precedes creating the as-is BIM model (Section 2.2.4).

However, although scan-to-BIM simplifies and increases the speed at which an as-is BIM model can be created, in recent years, the literature has pointed out that this increase may still not be sufficient [22, 96, 385]. Two main reasons are identified for this failure:

- first, although the survey process and subsequent data treatment (i.e. noise removal and point cloud alignment) are faster than in traditional methods (Table 2.3), the latter is still complex and slower than necessary;
- second, although the modelling process is faster and more accurate, the modelling is still slower than required, being completely performed by expert modellers who interpret the point cloud and manually model all the relevant constructive elements in the building [385]. This frequently requires an entirely new modelling workflow, reliant on the creation of auxiliary levels and sections to model the building correctly, which is frequently aggravated by the lack of semantic information in the point cloud, the need to rebuild occluded parts of the building, and the lack of features for point cloud manipulation in BIM authoring environment (e.g. point interaction). Furthermore, although the interoperability between point cloud and BIM authoring software is robust (as identified in the previous section), after importation, BIM authoring tools frequently struggle to work with the point cloud in view, showcasing drastic performance decreases, which result in a sluggish authoring environment. This is a natural consequence of the rapid adoption of laser scanning technology in the AEC industry, which has not been adequately answered by BIM authoring software, resulting in its current inability to work efficiently with the massive amounts of memory interaction associated with point clouds.

To solve these problems and further increase the speed at which AIBEA can be performed, the literature has identified the complete automation of scan-to-BIM as a potential solution [22-24, 27-29, 31-34]. The author agrees with this view, dedicating the following sections to the examination of this approach.

2.5.3. Solving scan-to-BIM limitations through automation

The existing literature identifies the automation of the scan-to-BIM process as a suitable solution to eliminate the previously identified drawbacks. This automation circumvents the manual point cloud treatment and modelling of the building, adjudicating these tasks to algorithms developed for these purposes. In turn, the manual work shifts to evaluating the BIM model outputted by these algorithms, making minor adjustments when necessary. The time required to perform these adjustments is expected to be several times shorter than performing the manual point cloud treatment and modelling, thus drastically increasing the efficiency and implementation speed of the scan-to-BIM process. To achieve this automation, previous works [23, 31, 386] propose using AI and, more specifically, ML.

According to [387], AI can be referred to as a field of computer science dedicated to creating systems that perform tasks generally associated with human intelligence. As such, it can be loosely interpreted as the incorporation of human intelligence into machines, although, in reality, these machines end up performing tasks based on stipulated rules and algorithms. AI is an umbrella term encompassing multiple specific research sub-fields, one of which is ML.

ML is a subset of AI focused on approaches that allow machines to learn from data without being explicitly programmed to do so [388, 389]. The purpose behind ML is to train machines to make decisions based on available data (i.e. training data) and algorithms [390]. The "learning" aspect relates to ML algorithms attempting to minimize their associated error while maximizing their likelihood of success. Thus, ML is merely a method to realize AI [387]. Tom Mitchell [391] provided a more formal definition, defining ML as a computer program able to learn from experience (E) in regards to some task (T) and some performance measure (P) – if its performance on T, as measured by P, improves with experience E, then the program is called a ML program. There are several classifications or types of ML, such as supervised, unsupervised, semi-supervised, and reinforcement learning. These differ according to the nature of the training data and can be examined in greater detail in the following works [388-391], accompanied by popular algorithms for a better understanding.

Using ML, the previously cited works [23, 31, 386] propose dividing the process of automating scan-to-BIM into two main tasks, namely: segmentation of the point cloud into building elements; and modelling of the acquired building elements in a BIM authoring environment. However, in the current thesis, the author proposes expanding this division to six different tasks, since the two previously indicated represent a narrow vision of what scan-to-BIM automation entails. As such, the proposed division consists of:

- point cloud registration;
- point cloud noise removal;
- point cloud segmentation;
- segment classification into building elements;
- geometric modelling of the classified building elements;
- and semantic enrichment of the modelled geometries with non-geometric information.

All tasks must be automated to achieve the complete automation of the scan-to-BIM process. The following six sections (Section 2.5.3.1 to Section 2.5.3.6) expand on each of these tasks by reviewing civil engineering research focused on each of these topics. An additional seventh section (Section 2.5.3.7) presents a brief discussion on the overall state of scan-to-BIM process automation in research.

2.5.3.1. Point cloud registration

Regarding the first task, point cloud registration entails aligning multiple point clouds into a single-shared coordinate system. In the field of civil engineering, no studies were found attempting the automatic registration of point clouds. In 2020, Wang et al. [386] thoroughly reviewed several computational methods of processing point clouds, also failing to identify any civil engineering works tackling point cloud automatic registration. Nevertheless, when expanding the focus to other areas, it is possible to identify that automated registration methods can typically be divided into two classes: (1) coarse and (2) fine registration methods. These can also be referred to as global and local registration methods, respectively. The first typically relies upon detecting key points based on a specific point descriptor and subsequently aligning the point clouds by finding the transformation matrix that minimizes the distance between the detected key points. The second aims to locally optimize the first alignment. Example methods of global registration include 4-Point Congruent Set [392], Greedy Initial Alignment [393] and Sample Consensus Initial Alignment [394]. For local registration, Iterative Closest Point (ICP) [395, 396] is undoubtedly the most popular method, where the goal is to iteratively identify the transformation that correctly moves one point cloud to align with another.

2.5.3.2. Point cloud noise removal

Regarding the second task, point cloud removal entails deleting unwanted noise from the captured point cloud. Contrary to point cloud registration, a few studies were identified tackling this topic in civil engineering research. These include [303, 397], where the authors first identified key building components (e.g. walls, floors and ceilings) and then eliminated the remaining points, which are, by default, classified as noise. The authors agree that this approach is easier to implement and scale while also being computationally efficient.

The inverse approach is used by Ishida et al. [398], which identified the initial noise removal as a vital step in their proposed workflow. The authors justify this approach by demonstrating that point clouds acquired in construction environments can include enough noise levels to diminish the segmentation task performance. To identify the point cloud noise, the authors proposed that any point with a distance d to the nearest point should be considered noise if $d > \alpha D$, where $\alpha \in [1.5; 2]$ and D equals the selected scanning resolution.

2.5.3.3. Point cloud segmentation

Regarding the third task, point cloud segmentation entails dividing the point cloud into multiple continuous segments representing groups or regions of points sharing similar features. Several studies focusing on point cloud segmentation were identified in the focused field. These works typically perform segmentation based on (1) model fitting or (2) region-growth.

The first approach relies on the fact that man-made objects can typically be decomposed into simple geometric primitives such as planes, spheres, and cylinders. Therefore, these primitives can be fitted into point cloud data, with points belonging to the same primitive being labelled as the same segment. Random Sample Consensus (RANSAC) [399] and Hough Transform (HT) [400] are algorithms often applied for this purpose. Reviews on these algorithms can be found in [401-403] and [404-406], respectively for RANSAC and HT, with researchers generally agreeing that RANSAC presents a higher efficiency and accuracy than HT [407]. Research examples for this approach include [408], where the authors fit a column primitive into the point cloud of a bridge, as well as [409-411], where cylindrical shapes are fitted to find pipes. Other examples include [412-414], where RANSAC is used to segment building façades and roofs. However, it should be stated that all these works require a manual pre-processing of the point cloud, in which noise and unnecessary data are manually removed. Figure 2.6 displays two application examples of the RANSAC algorithm.

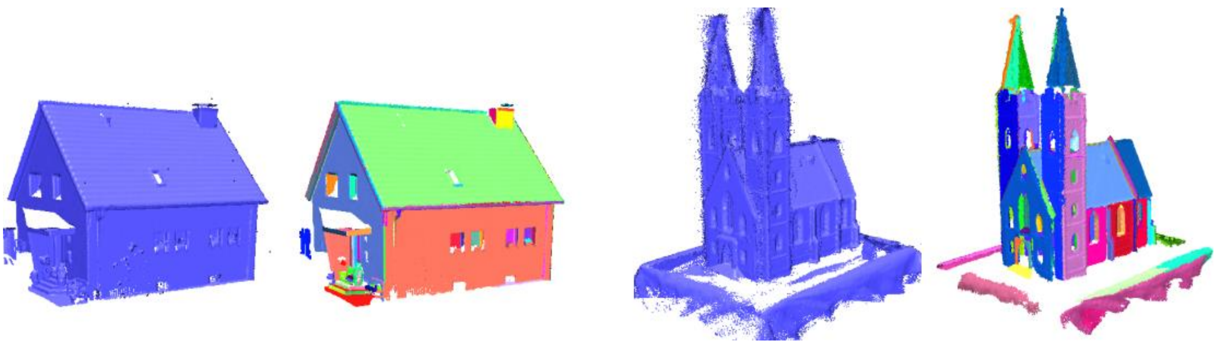

Figure 2.6 – Example applications of the RANSAC algorithm. Adapted from [415]

The second approach relies on the identification of continuous patches of points through unsupervised region-growth clustering algorithms. These algorithms tend to be initialized by identifying one or more seed points, which are then iteratively grown into regions by expanding the seed to neighbouring points using a selected similarity measure. The seed selection and expansion criteria are specified by the user and tend to be based upon common building knowledge. For instance, specifying that walls are strictly orthogonal to floors and ceilings. This is a disadvantage frequently reported on region-growth methods, since the selected criteria can quickly narrow the method's application range [386]. Other disadvantages include frequent over- or under-segmentation [416] (i.e. difficulty determining region boundaries), being computationally intensive [417], and requiring adjustments for application on different datasets [407]. However, these methods are often characterized as robust to noise, which is a significant advantage [418].

To overcome the drawbacks of this approach to a certain extent, after the initial patch segmentation, an optimization procedure can be performed. During this optimization, the final patch dimensions are established, and the building/room boundaries are identified through patch intersection [303]. An example of this optimization approach can be seen in [419], where Valero et al. converted the initial segments into high level surface representations, which are intersected to acquire the final boundaries. Other examples can be seen in [378] and [300], where the authors applied a hard-coded rule-based system to perform this optimization. The hard-coded rules are based upon common building knowledge. A final example can be seen in [416], where Perez-Perez et al. proposed a process to reduce over-segmentation through a learning method based on Markov Random Fields (MRF) [420]. This method enforces coherence between proposed semantic (e.g. wall, ceiling) and geometric labels (e.g. horizontal, vertical), using the neighbourhood context to enhance the semantic labelling accuracy.

The first region-growing algorithm was introduced by Besl and Jain [421] in 1988, with several variations of their proposal being developed since then. Research work examples using such variations include [303] and [422], where the authors applied the k-nearest neighbours (KNN) algorithm alongside the points' normal vector to, respectively, segment building façades and interior rooms (i.e. walls, doors and windows). Similarly, Zhan et al. [423] also used KNN for façade segmentation, this time using the points' colour values.

Another popular region-growing algorithm is DBSCAN (Density-based Spatial Clustering of Applications with Noise) [424], which segments the point cloud based on its density – an in-depth explanation of DBSCAN workflow is presented in Section 3.4.2.4. Recent research works focusing on this algorithm can be seen in [425, 426], where the authors applied DBSCAN to segment building elements' surface planes. In both works, the authors circumvent the common drawbacks of region-growth methods by creating higher dimension embeddings where this algorithm can be applied successfully. However, this process is indicated as resulting in large computational overheads while calculating the embeddings. Another example of this algorithm application can be seen in [427], where DBSCAN is included in an extensive pipeline for rebar diameter classification in point clouds. In particular, the authors apply DBSCAN to remove point cloud noise, which is identified as any point in a low-density region.

2.5.3.4. Segment classification into building elements

Regarding the fourth subtask, segment classification entails labelling point cloud data into building element classes (e.g. wall, ceiling, floor, column, beam). This labelling can be done at the segment-level, where segments of points are classified together into a class (requires pre-segmentation of the point cloud); or at the point-level, where each point is independently classified. If the segmentation is well performed, the first labelling approach is desirable, both in terms of accuracy and computational performance. As in the last task, several works were found tackling this topic in the field of civil engineering.

Wang et al. [386] divided segment classification into three different methods: geometric shape descriptor; hard-coded knowledge; and supervised learning. A fourth method, entitled BIM-vs-Scan, was also proposed, where the building's BIM model is first aligned with the surveyed point cloud and, subsequently, the model semantic information is used for classification. However, since this method requires access to the building's as-is BIM model, which this thesis is trying to create, it falls outside the current review and is not addressed. For more information on this method, see [386].

Regarding the geometric shape descriptor method, it is performed at the segment-level and relies on different building element classes displaying distinct geometric shapes. The method describes the shape of an object based on specific geometric features selected by the user, which are then compared to the geometric features of other building elements previously stored in a digital library [23]. A threshold value is predefined to identify similar geometric features and validate the match between the examined building element and a class stored in the digital library (similarly to the model fitting segmentation approach). As such, this method is heavily dependent on the size of the available digital library, as well as the heterogeneity of the stored building elements. Both Son et al. [428] and Czerniawski et al. [410] presented works based on this method for pipe classification.

Similarly to the previous method, hard-coded knowledge is also performed at the segment-level. It also relies on different building components displaying distinct geometric characteristics; however, instead of comparing extracted geometric features with an existing library, the method relies on previously hard-coded domain knowledge to classify segments (similarly to the region-growth segmentation method). Works using this method include [27, 300, 378, 429-431]. In [378], Want et al. applied this method to classify exterior walls, doors, windows and roofs. Examples of hard-coded knowledge in this work includes: walls being strictly vertical; roofs being above walls and non-vertical; and windows not being doors. In [27], Macher et al. used this method to classify a point into three classes (interior walls, ceilings and floors), using only two rules: parallelism between geometries and minimum distance between wall planes. Finally, in [431], Fatemeh Hamid-Lakzaeian classified façade points into three classes: principal façade; recessed openings; and protrusion. The authors first segment the façade using the RANSAC algorithm, subsequently checking each point according to three hard-coded subroutines that classify the point as one of the three available classes.

As with its segmentation counterpart, hard-coded knowledge works well within a narrow application range of simple geometric building point clouds, failing when faced with irregular variations of building elements (e.g. a tilted wall) or even with elements slightly more intricate (e.g. a relatively simple chair).

Finally, supervised learning methods can be applied at the segment- or point-level. These methods rely on regular ML classifier algorithms to be trained with labelled building point clouds to classify individual points or segments into building element classes. These algorithms frequently require the extraction of handcrafted local and global features from point clouds, enabling an improved classification.

Weinmann et al. [432] identify several popular algorithms related to this method, both at segment- and point-level. The overall process for both levels has been thoroughly detailed in [433] and is shown in Figure 2.7. The process can be divided into three primary stages: feature extraction; feature selection;

and classification. For each stage, Weinmann et al. [433] tested several different methods to compare their performance. The authors conclude that the Random Forest (RF) [434] classifier presents the best performance in several datasets, displaying a good balance between accuracy and efficiency. Further comprehensive and comparative studies on different point-level classifiers can be seen in [386, 435-437].

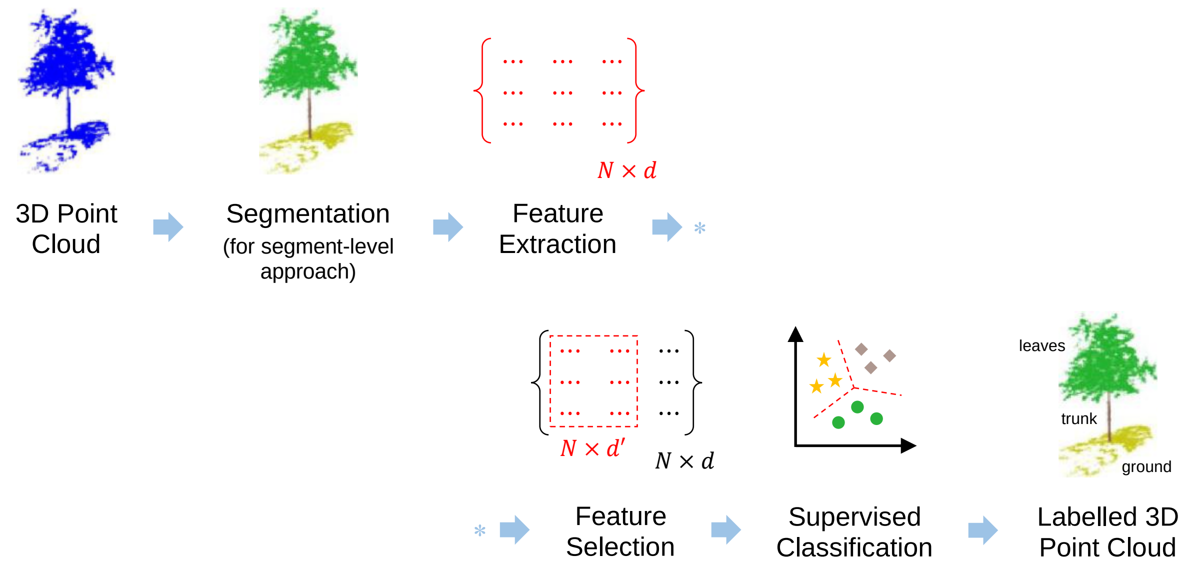

Figure 2.7 – Typical steps in supervised learning classification methods. Adapted from [407]

Research works applying some of the algorithms highlighted in the previous comparative studies (in the topic of point cloud classification) can be seen in the following works: RF [438]; Support Vector Machines (SVM) [439]; AdaBoost (AdB) [440]; MRF [441]; Conditional Random Fields (CRF) [435, 436, 442, 443]; Maximum Likelihood classifier based on Gaussian Mixture Models [444]; and Associative and Non-Associative Markov Networks [445, 446].

Specific examples of point-level applications can be seen in [447, 448]. In [448], Xu et al. applied RF to classify points into different scaffolding elements, allowing for the detection of scaffold units in construction site point clouds. In this study, a new geometric feature entitled "linear straight signature histogram of orientations", or LSSHOT, was proposed to train the classifier. In [447], Wang et al. trained a one-class SVM classifier to identify rebars in point clouds of reinforced precast concrete elements. In this study, no handcrafted features were extracted. Instead, the authors used each point 3D position and colour values to train the model. This simple approach was possible since the targeted class (i.e. rebar), was significantly different from its surrounding environment, both in colour and geometry (i.e. concrete).

Regarding classification at segment-level, a specific example of this application can be seen in [286], where Kim et al. first segmented the point cloud data of a structure into different segments and then classifies the acquired segments into four classes (i.e. column, beam, slab and clutter). The authors applied an SVM classifier, and the selected features for training included the Lalonde feature [449], segment direction, and segment continuity.

Contrary to the hard-coded knowledge method, supervised learning tends to generalize well, displaying a broader application range. However, several disadvantages are still associated with these methods, such as [407]: (1) low accuracies and inefficient computation when faced with large-volume point clouds; (2) required handcrafted feature design and selection – a difficult task in ML; and (3) relative low accuracy even when using complex and computationally intensive ensemble methods.

2.5.3.5. Geometric modelling of the classified building elements

Regarding the fifth task, geometric modelling of the classified building elements, both Hichri et al. [31] and Tang et al. [23] extensively researched this topic, dividing it into a similar range of possible representations. These include: parametric vs non-parametric; global vs local; and explicit vs implicit. Both works present methods to model the building for each of these representations, highlighting Boundary Representation (B-Rep) [450] and Constructive Solid Geometry (CSG) [451] as popular among practitioners. These are, respectively, a traditional method for surface-based representation (i.e. mesh generation) and volumetric representation (i.e. fitting and combining geometric primitives using simple operations like union and intersection). However, despite the detailing of existing methods, both works fail to identify substantial research on this topic in civil engineering, with seldom studies being cited as examples.

Similarly, in the present literature review, few research works were found focusing on the automated geometric modelling of building elements. The identified works included the previously cited research on segmentation through model fitting or CSG [408-411], as well as three extensions of B-Rep [27, 452, 453].

In the first two works focusing on extending B-Rep, De Luca et al. [452] and Macher et al. [27] presented similar approaches to modelling, first identifying the building surface and then extruding it through the application of semi-automated procedures. Both authors were able to geometrically model walls, with De Luca et al. [452] focusing on highly intricate architectural wall geometries (e.g. heritage buildings), while Macher et al. [27] focused on expanding the developed method to floors and ceilings.

In the third extension, Nikoohemat et al. [453] leveraged a mobile laser scanner to capture a building point cloud and perform the volumetric reconstruction of its walls, floors, ceilings and doors. However, strictly speaking, only walls were modelled using the captured geometry, since the remaining elements were modelled using the resulting wall volumes. In fact, following the proposed method, the authors initially detect wall planes in a point cloud, using the detected planes to position strictly vertical volumetric walls, represented by solid boxes. Using the enclosed spaces acquired from the walls' intersection, the floors and ceilings are modelled. Finally, using the registered path of the mobile laser scanner, each time it transverses a wall geometry, a door with predefined dimensions is positioned. As such, the proposed method presents several flaws, namely: it cannot model curved or tilted walls; it cannot model floors or ceilings of open spaces; it cannot model tilted floors or ceilings; it cannot model any openings apart from doors that have been transversed using the mobile laser scanner; and it cannot model the transversed doors with the appropriate dimensions, instead positioning a standard door geometry in the centre of the path-wall intersection.

2.5.3.6. Semantic enrichment of the modelled geometries with non-geometric information

The approaches mentioned in the previous section provide a volumetric representation of the building elements; however, they lack semantic information. To this end, the sixth and final task entails enriching the modelled geometries with sematic data, that is, shifting from simple 3D CAD geometries to BIM elements.

This semantic information can range from simply linking the building elements' designation with the modelled geometries (e.g. wall, floor, ceiling) to specifying its relation with nearby components (e.g. topological, directional), composing materials, and analytical properties.

Seldom works were identified tackling this topic. Among the identified works, both Wang et al. [454] and Kang et al. [455] focused on enriching segmented piping systems with pre-defined BIM element families and material properties. The point cloud segmentation is accomplished using region-growth methods and classified using the geometric shape descriptor method. Each classified geometric shape is checked through a set of mapping rules that identify which semantic information to map onto the geometry. Although having a limited application range, the method works well in reasonably controlled environments, such as pipping systems created from parts of a predetermined supplier.

In [456], Xue et al. focused on modelling repetitive objects, using a multimodal optimization method to identify these objects in a point cloud. The authors present a case study focused on a university lecture hall, where 293 chairs were modelled in *Revit* as BIM elements. These elements contain information regardings the chair's rotation, translation, ground level, and ID. Additionally, since the chairs are identified as a group, each element also presents the previous and next chair's ID. Similarly to the previously cited studies on piping systems, although this method presents a limited application range, it shows a high level of precision in what it can accomplish, in this case: modelling multiple instances of the same element from point clouds.

In another work, Bassier et al. [385] continued their previous work presented in [457], developing a script in *Grasshopper* to successfully reconstruct the geometry and topology of walls from point clouds. The wall elements are modelled in *Revit* and contain information regarding their connections to other walls. The Euclidean distance between element boundaries is used as a criterium for the neighbourhood search and the establishment of connections. However, the proposed method fails to identify openings in walls, modelling walls over existing doors and windows. It also fails to model curved walls, splitting curves into straight segments.

Finally, focusing on energy-related research, most works cited in Section 2.4.3.2.1, concerning both visual correspondence and gbXML-based modifications, can be used as examples of semantic enrichment. As stated in this previous section, works on this topic tend to develop small scripts to introduce non-geometric information in the BIM model, either through the direct modification of the modelled geometries' properties in the BIM authoring software or through the modification of its associated gbXML file.

2.5.3.7. Current state of scan-to-BIM automation

Until this point, it was possible to identify several works stating an urgent need to automate the scan-to-BIM process; however, having examined the research associated with all six proposed tasks for its automation, it is possible to identify a lack of works proposing solutions that: (1) tackle all six tasks simultaneously, automating the entire process of scan-to-BIM; (2) display a wide range of application in civil engineering; and (3) have a high level of performance.

In particular, apart from point cloud segmentation and classification into building elements, the remaining four tasks present little to no research in the field of civil engineering. The few studies that tackle these tasks tend to present restricted solutions and focus solely on modelling the building's geometry (i.e. 3D CAD), not attempting to enrich these geometries with semantic or topological information (i.e. BIM). Existing studies tackling this vital step focus on one single element, with cited examples tackling walls, pipes and chairs. Nevertheless, when focusing on semantic enrichment after the BIM modelling is complete (e.g. insertion of energy-related data), current research presents several works and advanced solutions, which is a positive point.

Focusing on the two remaining tasks, both point cloud segmentation and classification into building elements present substantial research, with most works being published in the last few years. However, these studies focus on traditional ML algorithms and methods as a solution, relying heavily on hard-coded knowledge and extensive object libraries, which severely limit their application range. In addition, most works present either extreme low levels of performance or accuracy, with a balance between both still missing in research.

However, when widening the search to other fields that are not civil engineering, solutions to most of these tasks can be found. This finding is corroborated by the results of a simple string search in the Web of Science Core Collection database , whereby inputting the following string:

ALL=(("scan-to-BIM" AND "artificial intelligence") OR
("scan to BIM" AND "machine learning") OR
("scan to BIM" AND "deep learning") OR
("laser scanning" AND "artificial intelligence") OR
("laser scanning" AND "machine learning") OR
("laser scanning" AND "deep learning") OR
("point cloud" AND "artificial intelligence") OR
("point cloud" AND "machine learning") OR
("point cloud" AND "deep learning"))

the search engine returns 1352 results, only 39 of which are included in the civil engineering or construction building technology categories. This value further decreases to 26 when removing out-of-topic articles, review articles, and the author's own contributions. To this end, solutions proposed in other areas of research need to be adapted and developed to fit the AEC industry and the current problem of scan-to-BIM.

This assessment is valid for all tasks but is especially evident for point cloud segmentation and classification, where research in computer science and electronic engineering has long moved from the traditional ML methods currently proposed in civil engineering works. This indicates that current research in scan-to-BIM automation is detached from the state-of-the-art in point cloud segmentation and classification, which, in 2015, started transitioning to DL approaches for their proven advantages.

As stated in [407], current DL methods for point cloud segmentation and classification far surpass traditional ML methods, showcasing far more efficient handling of large-volume datasets in terms of computational requirements; no need for handcrafted features, hard-coded knowledge or extensive object libraries; and yielding higher levels of accuracy on public benchmark datasets.

Facing these conclusions, the following sections are dedicated to reviewing the current state of DL research in solving point cloud segmentation and classification.

2.5.4. Current DL research for point cloud segmentation and classification

Zhu et al. [458] and Xie et al. [407] identify DL as the most influential and fastest-growing technique in pattern recognition and data analysis. Similarly, in [459], the authors describe DL as the most significant development in the field of computer science in recent times, impacting nearly all scientific fields and disrupting or transforming most businesses and industries.

As a subset of ML, DL builds upon a popular ML algorithm entitled artificial neural networks (ANN), which imitates the behaviour of biological neural networks in the human brain [460]. ANNs accomplish this by comprising three layers: an input layer (which receives the input data); an output layer (which outputs the data processing result); and a hidden layer (which processes the data, identifying and extracting inherent patterns). Each layer contains one or more processing units called neurons, which connect to neurons in adjacent layers. Each connection has an associated weight value determined through training. Data travelling through these connections is multiplied by the connection respective weight and summed at each unit. The resulting value then suffers a transformation based on the chosen activation function, often a sigmoid function, a tan hyperbolic, or a rectified linear unit (ReLU) [461]. For more information on these activations, see [462].

What distinguishes DL from traditional ANNs is its large number of hidden layers in opposition to the sole hidden layer typically used in traditional ANNs (see Figure 2.8). The use of only one layer originates from the late 80s, when George Cybenko [463] showed through the universal approximation theorem that a single hidden layer could solve any continuous problem – also mathematically proven in [464]. These works' findings, in addition to the added computational power incurred by extra hidden layers, deterred DL research until the early 2000s, when the rise of processing power in modern computers allowed for this research to resume. It was quickly found that while a single hidden layer could represent any function, it constituted a far cry from the convenience, efficiency and capability provided by the hierarchical abstraction of multiple hidden layers in DL [459].

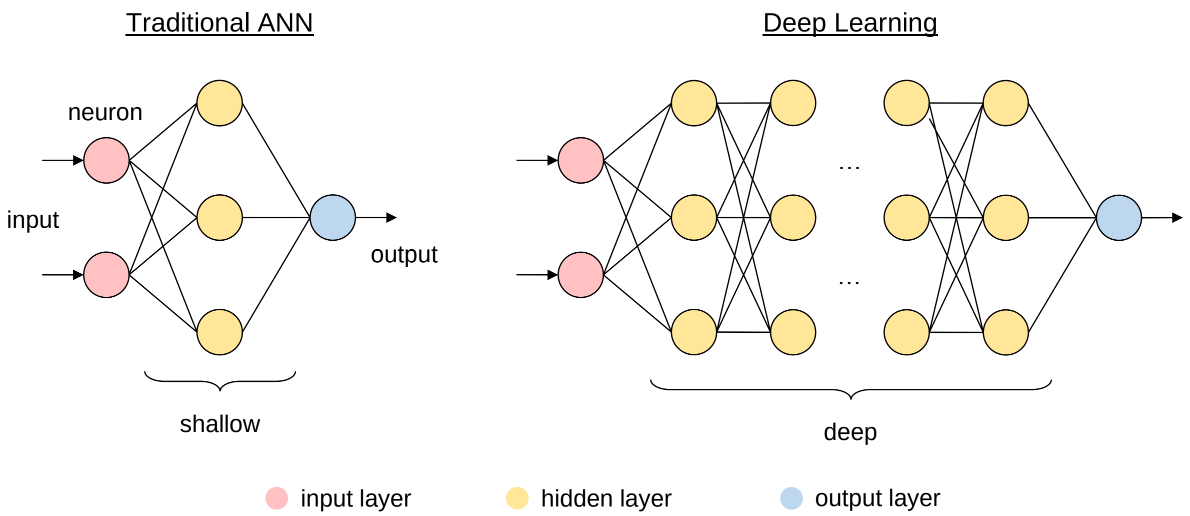

Figure 2.8 – Traditional ANN architecture vs DL architecture

Since DL's resurgence, it has been applied in several research fields, from computer vision to autonomous driving, improving the performance and accuracy of increasingly complex problems [465]. Point cloud research is just one of the latter topics to be tackled by DL, with its application on this topic attracting more and more interest, particularly in the last five years, given its drastic performance increase compared with traditional ML approaches.

DL point cloud-related research was further increased by the advent of point cloud publicly available datasets, such as ApolloCar3D [466], ModelNet [467], NYUv2 [468], Paris-Lille-3D [469], PartNet [470], S3DIS [471], ScanNet [472], ScanObjectNN [473], SceneNN [474], Semantic3D [475], SemanticKITTI [476, 477], ShapeNet [478], and Vaihingen [479]. These datasets allowed for the development of DL methods to tackle several point cloud-related problems, including registration [480], segmentation, shape classification, object detection and tracking [481], pose estimation [482], among others [483, 484]. Reviews on these topics can be found in the following works [407, 485-489]. Guo et al. [465] and Xie et al. [407], in particular, present an excellent overview of current DL methods in point cloud research, examining the chronological evolution of this research, as well as reviewing existing point cloud benchmark datasets and most often used evaluation metrics.

In the present literature review, not all the mentioned problems will be tackled. Instead, the focus will lie on point cloud segmentation and classification. More specifically, these problems are joined into one task, where DL methods simultaneously segment and classify each point in the point cloud. To perform this task, DL methods require the understanding of both the point cloud's local and global geometric structure, as well as each point's fine-grained details [465]. Depending on the segmentation granularity, DL segmentation methods may be classified into one of three categories: semantic; instance; and part segmentation [490]. To date, most research has been focused on semantic and part segmentation, with few studies tackling instance segmentation [490-492].

As a specific example of scan-to-BIM, semantic segmentation requires the division of a point cloud into element classes (i.e. wall, floor, ceiling, column, chair); instance segmentation comprises the division of each of these classes into instances (i.e. chair one, chair two); and part segmentation entails the division of each instance into its constituting parts (i.e. sit, back, legs, and arms of the chair) – see Figure 2.9 for an illustration of this example.

Semantic Segmentation Label: Chairs

Instance Segmentation Label: Chair 1

Part Segmentation Label: Chair's arms, legs, sit, back

Figure 2.9 – Semantic, instance and part segmentation

Within each of these categories, DL research expanded into three different approaches: projection-based; voxel-based; and point-based. These differ in their representation of the input point cloud, meaning they diverge on the required transformations the point cloud must endure before being processed by DL networks.

In fact, in contrast to the point-based approach, which works directly on the point cloud, projection- and voxel-based approaches first transform the raw point cloud into an intermediate regular representation (e.g. multi-view, spherical, volumetric, permutohedral lattice, or other hybrid representation), subsequently segmenting and projecting the acquired results back to the original point cloud.

The transformation into a regular representation is required to go from the inherently unordered, unstructured, and non-uniform [490] nature of point clouds (which are affected by various factors such as perspective effects, radial density variations, and motion [493]) to an organized, structured, and consistent representation that supports 2D and 3D Convolutional Neural Networks (CNN).

CNNs are deep network designs that require a structured medium for application and have been highly successful in a large array of DL tasks, including 2D image classification and segmentation. Given CNNs well-established reputation, projection- and voxel-based approaches attempt to create this medium through several transformations to exploit CNNs' accuracy and efficiency [494]. For a brief explanation of CNNs, see [495, 496], while an in-depth analysis can be addressed in [497, 498]. Interactive and instructive visualizations can be accessed in CNN Explainer (https://poloclub.github.io/cnn-explainer/) or Node Link (https://cs.ryerson.ca/~aharley/vis/conv/), respectively created from the work proposed in [499] and [500].

Each of the three previous approaches and their associated research is tackled in the following sections, starting with projection-based (Section 2.5.4.1), voxel-based (Section 2.5.4.2), and finally, point-based (Section 2.5.4.3). Section 2.5.4.4 further analysing possible hybrid combinations of these three approaches.

2.5.4.1. Segmentation with Projection-based approaches

Considering the historic success of 2D CNNs, initial efforts in point cloud-related DL research focused on projection-based approaches. These approaches attempt to project a 3D point cloud into 2D images, organizing the point cloud information into a 2D structured grid (i.e. pixels). Following this conversion, 2D CNNs can be applied to extract features in the acquired images, using the resulting features to segment the point cloud. This approach can be divided into two categories according to the used representation: multi-view and spherical [465].

Multi-view representation requires the projection of the unstructured point cloud onto 2D planes originated from multiple virtual viewpoints – Figure 2.10. To the author's knowledge, the first work on point cloud related DL was based on this approach, being presented by Su et al. [501] in 2015. In this work, the authors introduced MVCNN, a pioneering work proposing a simple solution of max pooling [502] the acquired features in the virtual multi-views into a global descriptor.

Following MVCNN, several works proposed variations of this approach. For instance, in [503], the authors propose MHBN, a network that acquires local convolutional features through harmonized bilinear pooling to create a compact global descriptor. In another work, Yang et al. [504] first proposed a Relation Network to connect corresponding regions in different viewpoints (i.e. establish interrelationships over a group of views, effectively reinforcing the information of individual images), subsequently integrating these views to obtain a discriminative 3D object representation. Lawin et al. [505] also focused on this representation, applying a multi-stream fully convolutional network (FCN) to predict pixel-wise scores on the acquired synthetic images. Each point on the point cloud was acquired through several different views, with the final semantic label of each point being obtained by fusing the resulting scores for each image.

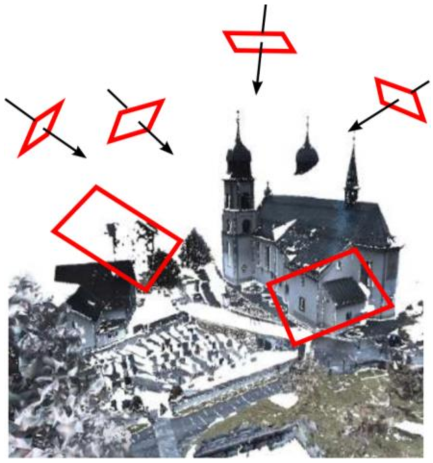

Figure 2.10 – Illustration of a multi-view representation. From [506]

In another approach, Boulch et al. [507] proposed SnapNet, which initially generates multiple RGB-D snapshots of a point cloud through several camera positions, afterwards performing pixel-wise labelling of the resulting images using 2D segmentation networks. Similarly to [505], the predicted scores from the RGB-D images are fused using residual correction [508]. Finally, established on the assumption that point clouds are sampled from locally Euclidean surfaces, Tatarchenko et al. [509] proposed TangentConv, for dense point cloud segmentation. TangentConv first generates per-point surrounding surface geometries, subsequently projecting them into a virtual tangent plane and forming tangent images that can be processed through 2D CNNs. Despite showing advantages in scalability, this method relies heavily on tangent estimation.

Other works on multi-view representation include, GVCNN [510], MV3D [511], RotationNet [512], and other nameless networks [513-518].

Regarding spherical representation, it requires the projection of the 3D point cloud onto a 3D object's surface centred on the laser scanner position – see Figure 2.11. This object is typically a sphere, hence the representation's name; however, other objects have been used, such as cylinders [519].

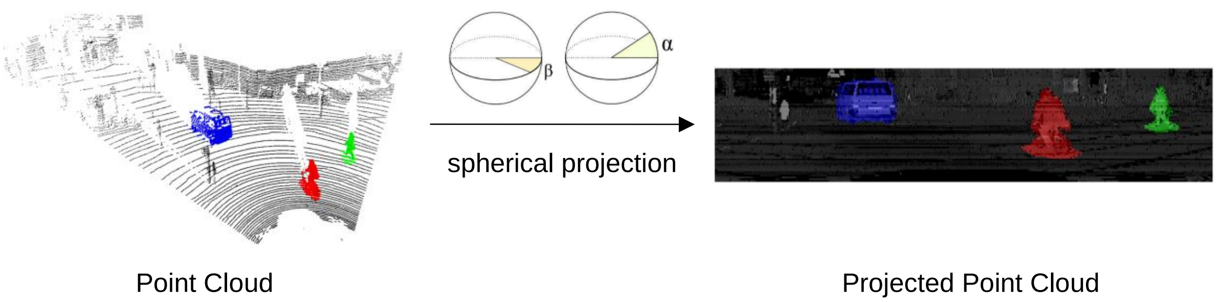

Figure 2.11 – Illustration of a spherical representation. Adapted from [520]

Examples of this representation include SqueezeSeg, proposed by Wu et al. [520], who achieved a fast and accurate segmentation by developing an end-to-end network based on SqueezeNet [521] and CRFs. In a follow-up work, the same authors introduced SqueezeSegV2 [522], improving the previous network segmentation accuracy by applying an unsupervised domain adaptation pipeline to address domain shifts. In another work, Milioto et al. [523] introduced RangeNet++, achieving real-time semantic segmentation of point clouds acquired through LiDAR. The authors further propose an efficient KNN-based post-processing step to alleviate the problem of discretization and blurry CNN outputs, prevalent in projection-based approaches.

Others works on this representation include, PointPillars [519], PointSeg [524], and PointIT [525].

Overall, although multi-view and spherical representations can solve the point cloud structuring problem, the performance of its associated networks are heavily dependent on either viewpoint selection, existing occlusions, point cloud density [465, 526], inconsistencies between multiple 2D predictions [491], or a combination of these factors. Additionally, as noted by Xie et al. [407] and Landrieu et al. [527], these issues are exponentially exacerbated as the point cloud increases in size, making the method unscalable. Finally, this approach does not fully exploit the underlying geometric and structural information of point clouds in 3D space, as the projection step inevitably results in a significant information loss (e.g. underutilizing point cloud sparsity) [465, 526, 528].

2.5.4.2. Segmentation with Voxel-based approaches

The robustness showcased by DL networks in solving segmentation tasks on 2D representations inspired the application of DL networks directly onto structured Euclidean 3D spaces [467, 529-532]. To this end, the point cloud is transformed into voxels, a cube-like structure in 3D space, equivalent to pixels in 2D (see Figure 2.12). Through this voxelization process, points located in the same cell of a 3D grid (which resolution is specified by the user) are aggregated into the same voxel, solving the unordered and unstructured problems associated with the original point cloud and allowing for the application of 3D CNNs. To the author's knowledge, voxel-based approaches were the second explored strategy in point cloud-related DL.

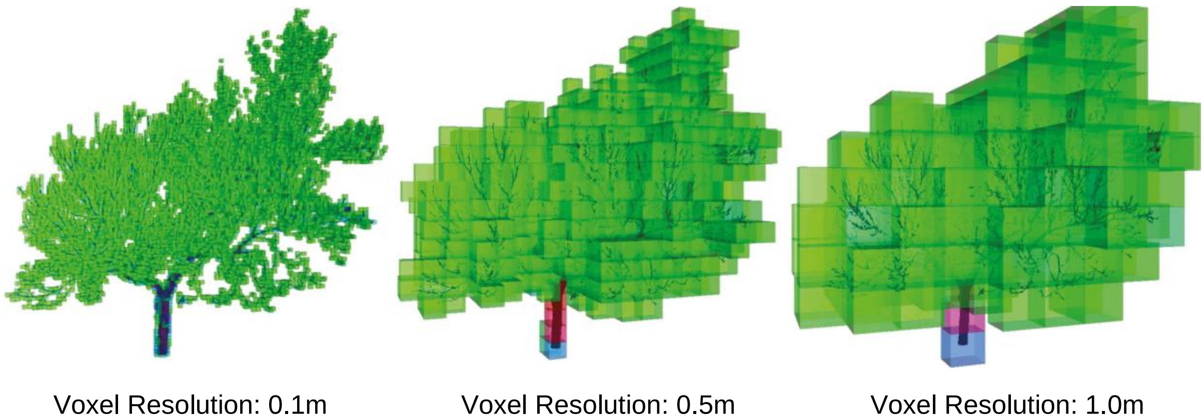

Figure 2.12 – Voxelization of a point cloud for three different voxel resolutions. Adapted from [533]

The first and most popular work on this approach, VoxNet, was proposed in 2015 by Maturana et al. [529] to achieve a robust 3D object recognition. In 2016, Huang et al. [534] proposed a similar work, first voxelizing the point cloud and subsequently feeding the acquired volumetric representation to a 3D FCN for voxel-wise segmentation. Points within the same voxel are assigned the same semantic label as the voxel. In the same year, Qi et al. [535] extended 2D CNNs to 3D, further performing a systemic examination of the relationship between 3D CNNs and multi-view CNNs. In [536], Tchapmi et al. introduced SEGCloud, an end-to-end network that accomplishes fine-grained and global consistent semantic segmentation. The authors developed a deterministic trilinear interpolation to project the coarse voxel predictions produced by a 3D FCN [537] back to the original point cloud, subsequently applying a fully connected CRF to post-process the results and ensure the spatial consistency of the inferred point labels [527].

In another work, Rethage et al. [538] proposed FCPN, the first end-to-end FCN architecture to work on point clouds. The proposed network can process large-scale point clouds, presenting good scalability during inference. It starts by hierarchically abstracting different levels of geometric relations from point clouds using radius search and grouping, subsequently applying 3D convolutions and weighted average pooling operations to extract features and establish long-range dependencies. In the same year of 2018, Dai et al. [539] proposed ScanComplete, a network that receives incomplete point cloud scans (i.e. with partial occlusions) and predicts a complete 3D mesh along with per-voxel semantic labels. The proposed method leverages the scalability of FCNs and can adapt to different data sizes during both training and testing. The author further proposes a coarse-to-fine inference strategy to produce a high-resolution output from the predicted results.

In 2019, Meng et al. [540] proposed VV-Net to first transform unstructured point clouds into regular voxel grids and then apply a kernel-based interpolated variational autoencoder architecture to encode the local geometry within each voxel. Contrary to traditional voxel-based approaches, where voxel occupancy is represented by a Boolean operator, the authors employ Radial Basis Functions (RBF) to compute a local, continuous representation within each voxel. Other studies on voxel-based approaches include [467, 530-532, 541].

Overall, it can be concluded that voxel-based approaches proportionate a stable structure with good memory locality and encouraging performances [407]. However, multiple points are bucketed into the same voxel grid when using low voxel resolutions, making these points undistinguishable and resulting in loss of information. If, in turn, a high resolution is used to preserve the fine point cloud details, the computational cost and memory requirements are significantly increased, making the method unfeasible [490]. Liu et al. [542] showcased this behaviour through a series of experiments, concluding that voxel-based approaches are not scalable since the largest feasible resolution at the time of testing (December 2020) incurred a 42% information loss, while attempts to restrain it to 90% led to over 7× more memory requirements – a value that disallows the network deployment.

In addition, since voxel structures do not solely store occupied cells (i.e. voxels with points in them), naively increasing the voxel resolution decreases this approach's efficiency, since most voxels will be unoccupied [407, 526]. This problem can be alleviated by sparse methods, such as OctNet [543] and O-CNN [544], limiting convolution operations to occupied voxels.

In OctNet, Riegler et al. [543] introduced a hierarchical, flexible and compact structure (i.e. octrees [545]) to partition the 3D space into a set of differently-sized voxels according to the point cloud density, effectively replacing the traditional, dense, static-size 3D grid. More specifically, voxels that contain points are recursively split, stopping at the finest resolution of the tree. As such, voxels differ in size, and the network dynamically focuses its computational and memory resources on relevant regions of the point cloud (see Figure 2.13). The octree structure is efficiently encoded as a bit string representation, and the feature vector of each voxel is indexed by simple arithmetic [465]. This leads to a significant reduction in resource requirements, allowing for a deeper network architecture with higher resolutions. In O-CNN, Wang et al. [544] proposed an octree-based CNN that takes the average normal vectors of a 3D model sampled in the finest leaf octants as input, successively applying 3D CNN operations on the octants occupied by the 3D shape surface. As in OctNet, O-CNN also entails less memory and computational requirements as networks based on traditional voxel grids.

Other works focused on point cloud sparsity include FPNN [546], H-CNN [547], KD-Net [548], LatticeNet [549], MinkowskiNet [550], PointGrid [551], SECOND [552], Sparse3D [553], SPLATNet [554], and SSCN [555]; each proposing an unique approach to the problem. However, as in the traditional voxel-based approaches, these methods may still incur high memory occupancy when faced with deeper networks, as well as losses in geometric detail due to quantization onto voxels.

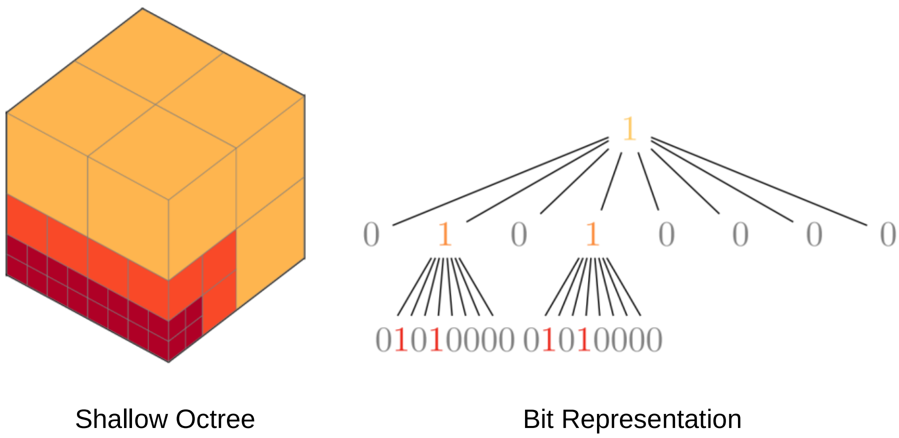

Figure 2.13 – Illustrative voxelization result with OctNet and corresponding bit representation. Adapted from [543]

2.5.4.3. Segmentation with Point-based approaches

In contrast to the two previous approaches, point-based methods directly work on the raw point cloud without any intermediate transformation. As a result, point-based approaches do not experience explicit information loss or added computation; instead, working directly with the points' coordinates, normal and RGB values, creating a compact, efficient, and intuitive network [465, 491]. However, without the point cloud transformation into a structured and organized medium, standard CNNs are unfeasible. As such, different network architectures for feature learning are used in this approach, with the used architecture naming the applied method: pointwise multilayer perceptron (MLP); convolution-based; graph-based; and Recurrent Neural Network (RNN)-based.

- Pointwise MLP methods

In 2017, PointNet [556], the seminal work on point-based approaches, proposed learning per-point features using shared MLPs [557], followed by their aggregation through a global symmetrical pooling function (i.e. max pooling) – a key feature that solves the permutation invariance of point clouds. Given the lack of required intermediate transformations, PointNet can process over one million points per second on modern Graphics Processing Units (GPU) [558], effectively performing tasks in real-time. Zaheer et al. [559] proposed a similar approach with DeepSets, accomplishing permutation invariance by summing all representations and applying nonlinear transformations. Effectively, DeepSets can be considered a generalized model of PointNet [558].

Other works adopted PointNet's simplicity and efficiency, drawing inspiration from this network or even implementing it as their network's backbone [538]. For instance, Joseph-Rivlin et al. [560] proposed Mo-Net, a network with similar architecture to PointNet that takes a finite set of "moments" as its input. Duan et al. [561] proposed SRN to learn structural, relational features between distinct local structures through MLPs. In another work, Lin et al. [562] introduced Justlookup, achieving a 32× speedup of PointNet's inference process by simply developing a lookup table to approximate its variable functions. As rare examples of instance segmentation, both Wang et al. [563] and Pham et al. [491] used PointNet as the backbone of their networks, respectively, SGPN and JSIS3D. Finally, Yan et al. [564] proposed PointASNL, introducing two innovative modules to dynamically adjust the features of points sampled by farthest point sampling (FPS) [565] and further capture their local and long-range dependencies. Other works based on PointNet include PointAugment [566], PointDAN [567], S-NET [568], and SRINet [569], among several others.

However, although computationally efficient, by its design, networks solely reliant on point features cannot capture each point's contextual information (i.e. local structures within neighbouring points), resulting in lower performances when compared with current networks [465].

To solve this problem and exploit local structural information, in a follow-up work, Qi et al. [493] proposed PointNet++, a hierarchical neural network that applies PointNet recursively on overlapping partitions of the point cloud. Each partition results in a set of local features, which are then grouped into larger units to be processed for higher-level features. By doing so, PointNet++ effectively simulates CNN's ability to abstract local patterns through multi-resolution hierarchical data, achieving better generalizability in unseen cases. Figure 2.14 illustrates two methods tested in [493] to acquire the nested partitions. Both methods are thoroughly discussed in the cited work. These partitions are defined as spheres (i.e. ball query) in the underlying Euclidean space, whose parameters include centroid location and scale. To cover the entire point cloud, centroids are selected based on an FPS [565] algorithm.

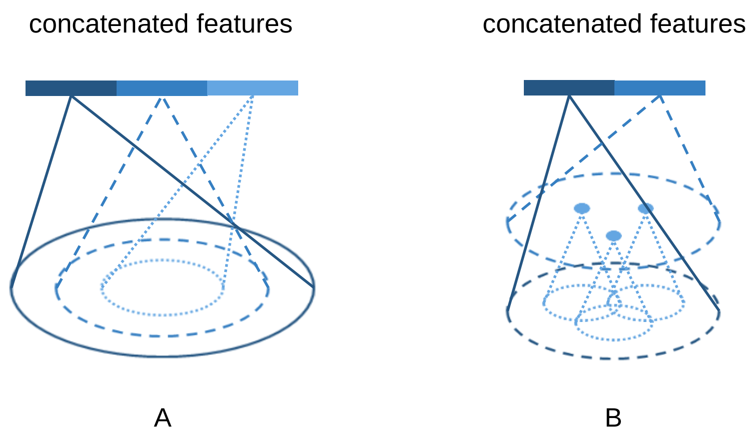

Figure 2.14 – Methods for nested point cloud partitioning: (A) Multi-scale grouping and (B) Multi-resolution grouping. Adapted from [493]

Despite showcasing significant performance improvements compared to its predecessor, PointNet++ incurs higher levels of computation, primarily during the iterative FPS and ball query, which grows linearly with the increase in resolution. Additionally, several works have pointed out that information in local regions may not be well aggregated using only PointNet's max pooling [526].

Nevertheless, following PointNet++ findings, several works proposed networks capable of capturing local and global information, either using hierarchization, neighbouring feature pooling, attention-based aggregation or local-global concatenation. For more information on these methods, see [407, 465].

Examples of such works include PointSIFT [570], in which the authors get inspiration from PointNet and the scale-invariant feature transform algorithm [571] to achieve scale awareness and orientation encoding. PointSIFT can be integrated into PointNet-based architectures to improve their representation capabilities. In another work, Engelmann et al. [572] exchanged PointNet++'s ball query for K-means clustering and KNN, using these algorithms as their grouping mechanism and establishing the assumption that points of the same class are expected to be closer in feature space. In [526], Hengshuang et al. introduced PointWeb, proposing an innovative approach to extract contextual features from local neighbourhoods of point clouds. The authors create a densely connected web of points by linking all existing point pairs in a local neighbourhood, aiming to extract per-point features based on the local region characteristics. To do so, a novel adaptive feature adjustment module is developed to find the interaction between points and adjust the acquired features based on the obtained pairs.

In another study, Hu et al. [573] proposed an efficient and lightweight neural architecture to infer per-point semantics for large-scale point clouds. The key of the developed architecture is to apply random point sampling instead of complex point selection approaches. Although remarkably computation and memory efficient, random sampling can discard key features by chance and, as such, the authors further propose a novel local feature aggregation module to overcome this limitation. Finally, in 3DContextNet [574], the authors use a standard balanced k-dimensional tree [575] to exploit both local and global contextual information and aggregate point features, hierarchically obtaining discriminative 3D signatures. Other works on pointwise methods capable of capturing local and global information include 3D-PointCapsNet [576], ASR [577], LSANet [578], PATs [579], PS^2-Net [580], ShellNet [581], SO-Net [582].

- Convolution-based methods

Convolutional-based methods within the point-based approach attempt to propose effective convolution operators that can be applied directly over point clouds. As such, instead of rearranging the point cloud into a structured representation to better fit the convolution network (as in projection- and voxel-based approaches), these methods attempt to design convolution kernels that can adapt and be flexible enough to deal with the irregularity of point clouds. Depending on the type of convolutional kernel, convolution methods can be divided into continuous and discrete (see Figure 2.15):

- continuous methods define convolutional kernels on a continuous space, meaning weights for neighbouring points are related to the spatial distribution in respect to the centre point;
- discrete methods define convolutional kernels on regular grids, meaning weights for neighbouring points are related to the grid offset in respect to the centre point.

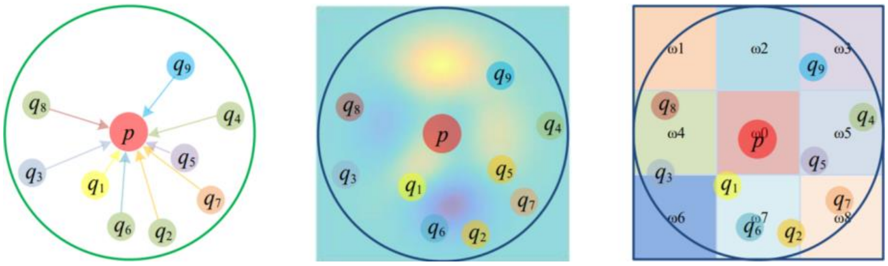

Figure 2.15 – Illustration of a continuous and discrete convolution for a local neighbourhood q_i centred in the point p. Adapted from [465]

As an example of continuous convolution, Thomas et al. [494] proposed KP-FCNN, based on a flexible and deformable convolution operator entitled KPConv. KPConv can work with any number of kernel points, adapting them to the point cloud local geometry. More precisely, the convolution weights in KPConv are calculated using the Euclidean distances to the kernel points. The authors compare the use of a point's coordinates to an image pixel's position, using it as the indexing element. In another work, Wang et al. [583] proposed PCCN, a network based on parametric continuous convolution layers, where the kernel is parameterized by MLPs. Based on this work, Poulenard et al. [584] proposed SPHNet, achieving rotation invariance by employing a spherical harmonics-based kernel at different layers of the network. In [585], Alexandre Boulch proposed ConvPoint, dividing the convolution kernel into two parts: spatial and feature. The locations in the spatial part are randomly sampled from a unit sphere, while the weighting function is learned through an MLP [465]. Finally, Wu et al. [586] and Hermosilla et al. [587] respectively proposed PointConv and MCCNN, defining the convolution as a Monte Carlo estimation and relying on MLP layers to support the weighting and density functions. Other works on the continuous method include 3D Spherical CNN [588], DensePoint [589], Flex-Conv [590], PCNN [591], RS-CNN [592], Spherical CNNs [593], SpiderCNN [594], and Tensor field networks [595].

Regarding discrete convolutions, in 2018, Hua et al. [596] introduced a point-wise convolution operator, in which neighbouring points are binned into a uniform grid of kernel cells and then convolved with kernel weights. The proposed kernel allocates the same weights to all points within the same grid cell, and the layers' output results from weighting and summing the points' mean features. In another work, Lei et al. [597] developed a spherical convolutional kernel by dividing a 3D spherical neighbouring region into several volumetric bins, linking each bin with a learnable weighting matrix. In [598], Li et al. proposed PointCNN, leveraging an innovative X-Conv to initially transform the input points into a latent and potentially canonical order, followed by the application of a typical convolutional operator on the transformed features. X-Conv is implemented through MLPs. Other works focused on this method include A-CNN [599], DPC [600], Geo-CNN [601], InterpCNNs [602], LP-3DCNN [603], RIConv [604], and SFCNN [605]; all proposing innovative kernel designs.

- Graph-based methods

Graph-based methods resort to connecting the point cloud into a graph structure. Each point is considered a vertex for the graph structure, while its connections to neighbouring points are considered the graphs' edges (see Figure 2.16). By performing feature learning over these graph structures, networks can capture the underlying geometric shapes of 3D point clouds [465]. This feature learning can be performed in spatial or spectral domains [606]. For more information on the differences between these approaches, see [607, 608], where the authors present an in-depth review of graph-based networks.

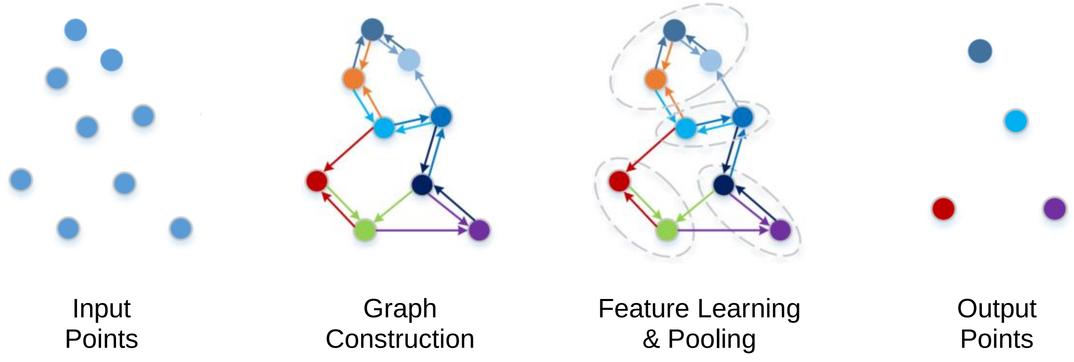

Figure 2.16 – Illustration of graph-based methods. Adapted from [465]

One of the most popular graph-based methods to tackle segmentation was proposed in 2017 by Landrieu and Simonovski [527]. In this work, the authors proposed SPG, a novel point cloud representation with rich edge features encoding the contextual relationship between geometric partitions in point clouds (see Figure 2.17 for an illustration of SPG). The authors first extract simple yet meaningful shapes from the point cloud, called superpoints, subsequently interconnecting them using the graph structure, and finally applying PointNet to finish the segmentation process. In another work, Wang et al. [609] introduced DGCNN, which leverages a novel procedure, entitled EdgeConv, to extract edge features while keeping permutation invariance. Drawing inspiration from DGCNN, Wang et al. [610] developed GAC to capture the structural features of point clouds and prevent feature contamination between different point cloud parts. This feature improves semantic accuracy in point cloud transition areas, such as the limits between a wall and its hosted door. Similarly, Zhang et al. [611] also built upon DGCNN, proposing LDGCNN with improved performances and reduced model size.

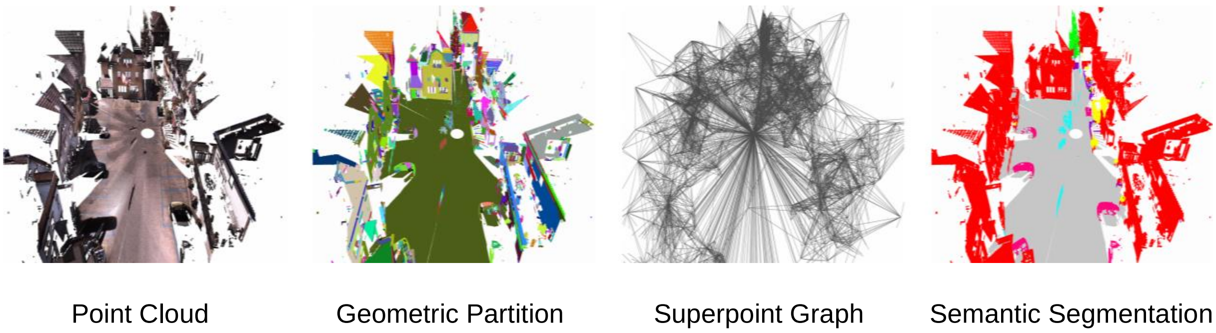

Figure 2.17 – Illustration of the graph-based workflow in SPG [527]

In 2019, Kang et al. [612] introduced two new operators to develop PyramNet, namely, Graph Embedding Module and Pyramid Attention Network. The network relies on these innovative operators to project the point cloud onto a graph structure and explore the relationship between points, improving the local feature expression ability of the model and assigning robust semantic features to each point. Finally, in [613, 614], the authors attempt point segmentation tasks under weak supervision environments (i.e. working with a small portion of labelled points), focusing on graph structures to support their proposed networks. The authors achieve state-of-the-art results with 10× fewer labels. Other works on this approach include 3DTI-Net [615], AGCN [616], ClusterNet [617], DeepGCNs [618], DPAM [619], G3DNet [620], GCNN [621], Grid-GCN [622], HGNN [623], KCNet [624], LocalSpecGCN [625], MoNet [626], PointGCN [104], PointGCR [627], RGCNN [628], SSP+SPG [629].

- RNN-based methods

Contrary to other DL network architectures, where different inputs are analysed separately and considered independent from each other, in RNNs, the network assumes dependencies between the current input and past results. Specifically, RNNs retain information from previous experiences, using feedback loops to keep information in "memory" for an extended period (see Figure 2.18). Despite being especially suited for sequence learning, RNNs are exploited in point cloud DL tasks to infer the inherent contextual information of a point by retaining knowledge about the surrounding points previously analysed by the network. For more information on RNNs, see [630].

Example works focused on this architecture include 3P-RNN [631], where the authors adopt a pointwise pyramid pooling module to capture per-point local features, further employing two-direction RNNs to integrate long-range spatial dependencies. Despite resulting in overall increased accuracy, Zhao et al. [632] identified that this method loses rich geometric features when aggregating the local and global features. To this end, the authors introduce DAR-Net to correctly aggregate these features through a dynamic aggregation operation, while managing permutation invariance in multiple scales. In another work, Huang et al. [633] introduced RSNet, applying RNNs to model local dependencies from ordered point cloud slices acquired from slice pooling layers. In [634], the authors propose Point2Sequences, using RNNs to capture correlations between different areas of the point cloud. It first acquires features at the local region-level using several point cloud scales, later sequencing them and processing them using RNNs. Other works focusing on this architecture include 3DCNN-DQN-RNN [635], RCNet and RCNet-E [636], as well as Engelmann et al. [637] research on extending PointNet to incorporate larger-scale spatial context.

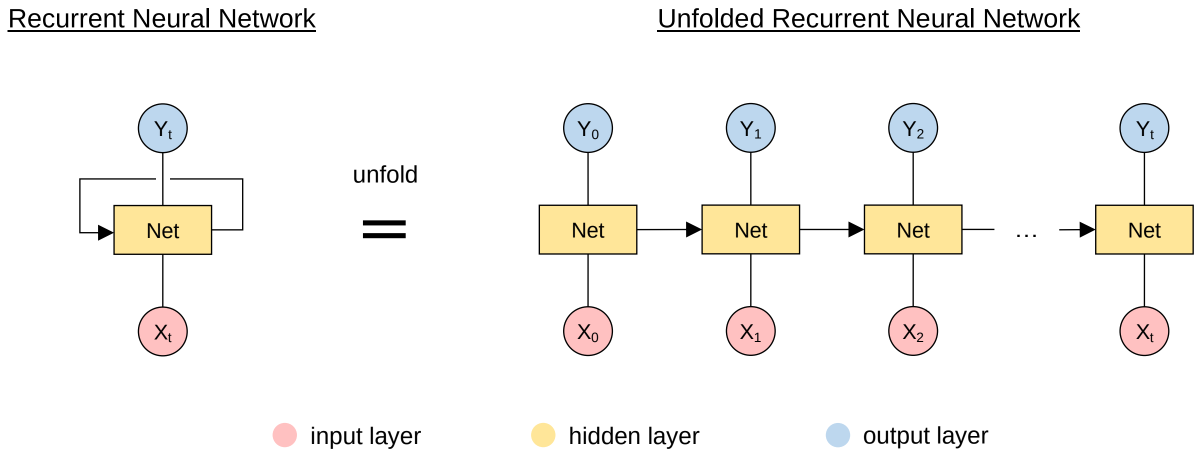

Figure 2.18 – Illustration of an RNN in both folded and unfolded forms

- Drawbacks of Point-based approach

Overall, although PointNet initially introduced a memory and computation efficient network, it lacked the context modelling capability to achieve the high performance displayed by other approaches. To this end, later research tackled this limitation by aggregating neighbourhood information in the point domain using several methods, from hierarchically partitioning the point cloud to retaining previous results in the network's memory. However, these methods introduced several drawbacks, from irregular memory access patterns to dynamic kernel computation overheads, which become the efficiency bottleneck of point-based approaches. Once again, Liu et al. [542] showcased this behaviour through a series of experiments, concluding that the collective overhead between irregular memory access and dynamic kernel computation ranges from 55% (in DGCNN) to 88% (in PointCNN), meaning that most computation is wasted on solving the irregularity of the point-based representation.

2.5.4.4. Segmentation with Hybrid approaches

Hybrid approaches combine two of the three previous strategies to reduce their associated disadvantages while maximising their respective advantages. To do so, methods related to this approach typically leverage multiple data representations to learn multi-modal features.

As examples of fusing point- and projection-based approaches, in 2018, Dai and Nießner [638], Qi et al. [639], and Ku et al. [640], respectively proposed 3DMV, Frustum PointNet, and AVOD, to combine multi-view RGB features and point cloud spatial-geometric features, acquired through 2D and 3D CNNs. Other works focusing on the combination of these approaches include PVNet [641], PVRNet [642], as well as Jaritz et al. [643] and Chieng et al. [644] works.

As the sole identified example of combining projection- and voxel-based approaches, in 2019, Hou et al. [645] tackled instance segmentation with 3D-SIS. The network first relies on 2D convolutions to extract 2D RGB features from images, subsequently back-projecting them onto a voxel grid to jointly learn from both the voxel geometric structure and the RGB data using 3D convolutions.

Finally, as examples of fusing point- and voxel-based approaches, in 2019, Yin Zhou and Oncel Tuzel [646] proposed VoxelNet, while Liu et al. [542] proposed PVCNN.

VoxelNet [646] is an end-to-end trainable DL network that divides a point cloud into equally spaced voxels and transforms the points within each voxel into a unified feature representation. To do so, the authors introduce a novel voxel feature encoding (VFE) layer, which essentially combines point-wise features with a locally aggregated feature. By stacking multiple VFE layers, the network is able to learn complex features that characterize the local information in each voxel.

PVCNN [542] is a network aimed at real-time application, with a heavy focus on efficiently combining both point- and voxel-based approaches. The authors mitigate both approaches' limitations by representing the point cloud data in the sparse and irregular point representation, while performing the required convolutions for increased performance in a dense, regular voxel representation. This strategy effectively allows the network to extract individual point information and model local and global information. During testing, PVCNN shows a reduction in the memory footprint and irregular memory access, achieving two times speedup over PointNet, as well as improved performances – being the current leader of several point cloud-related benchmarks. PVCNN will be further examined in Chapter 3.

2.6. SUMMARY OF THE LITERATURE REVIEW AND IDENTIFIED KNOWLEDGE GAPS

As indicated throughout the present chapter, multiple knowledge gaps were identified during the literature review. The following points summarize the most important findings and stress the knowledge gaps, which, in the author's opinion, are most relevant to the current thesis.

- Throughout the initial sections of Chapter 2, it was possible to identify a clear deficit in the pace at which buildings are being retrofitted, threatening the success of existing international energy and sustainability goals imposed in the AEC industry. Currently, the literature identifies AIBEA as a suitable solution to accelerate this retrofit; however, as described in Section 2.2.4, the process displays four primary limitations which restrict its swift application;
- The first of these limitations is the current lack of standards to support the AIBEA workflow, as well as any other energy analysis-related BIM project. By reviewing existing standards for BIM in Section 2.4.1, it was possible to identify ISO-19650 as an existing standard that may be expanded upon to correct this issue. It was further identified that this expansion could be accomplished by establishing and integrating key energy parameters in BIMForum's LOD Specification, enabling its use as an independent metric for defining the Level of Information Need of a deliverable, supporting the creation of a standard for BIM energy analysis. This expansion will be a focus of Chapter 3;
- The second limitation is the current state of interoperability between BIM authoring and energy analysis software, which, although existent, is still too limited to enable the full potential of the AIBEA workflow. Section 2.4.2 identified several of these software solutions and summarized an extensive list of issues related to their interoperability, which will have to be revisited and solved in Chapter 3;
- The third identified limitation is the labour-intensive and time-consuming survey process needed to develop an as-is BIM model for the correct application of AIBEA. Although this process cannot be circumvented, as seen in Section 2.4.3, several rising technologies can ease the building surveying effort, both for its geometric and energy-related data. However, despite the increasing popularity of these technologies, no research has been found to provide a complete framework for acquiring both data types, with most studies focusing on the process after the data is acquired and exported to BIM. This gap will be revisited in Chapter 3, with laser scanning, in particular, being focused on as the chosen technology for geometric data acquisition, given its high potential and numerous open challenges;
- Finally, the fourth identified limitation relates to the creation of the building's as-is BIM model using the surveyed data and existing authoring tools. Although vital to the proper performance of AIBEA (as identified in Section 2.2.3), this model is challenging to develop, given the lack of adequate support in authoring tools. Section 2.5 presented the scan-to-BIM process as the literature's identified solution for this limitation; however, as with AIBEA itself, several issues still constrain the scan-to-BIM process' application, as identified in Section 2.5.2;
- To solve these issues, the literature proposes the complete automation of the scan-to-BIM process, despite, to date, few works attempting such a solution. In the existing works related to the automation of scan-to-BIM, the process is divided into only two tasks: segmentation of the point cloud into building elements; and modelling of the acquired elements in a BIM environment. In the author's opinion, this is an oversimplification of the process and does not lead to its full automation. As such, the current thesis divides the automation of scan-to-BIM

into six distinct tasks, which, as identified in Section 2.5.3.7, are severely lacking in the current literature, either by presenting scarce related research (i.e. point cloud registration and noise removal), by focusing on outdated methods (i.e. point cloud segmentation and classification), or by failing to accomplish the proposed objective (i.e. performing CAD modelling instead of BIM, given the lack of semantic content). To solve these issues, Section 2.5.4 presented point cloud-related research in the field of DL, which currently outperforms by several degrees the current methods applied in civil engineering research for the same purpose. These methods will be revisited in Chapter 3 to enable the scan-to-BIM process automation and integration in AIBEA.

3

METHODOLOGY FOR AN ENHANCED AS-IS BIM ENERGY ANALYSIS

The current chapter presents and examines the proposed methodology for an enhanced AIBEA. It starts by briefly outlining the methodology, dividing it into five unique modules, justifying and contextualizing their application within the AIBEA workflow. This allows for an overview of the developed work, laying the foundation for a better understanding of each module's contributions in the following sections.

3.1. OVERVIEW OF THE PROPOSED METHODOLOGY

The proposed methodology for an enhanced AIBEA is comprised of five unique modules. These modules aim to answer all the research gaps identified throughout the literature review, tackling the problem from the two already developed perspectives: (1) creation of supporting documentation and tools for an accurate and swift AIBEA, and (2) integration and automation of the scan-to-BIM process. Modules 1, 2 and 5 lean more on the first perspective, while Modules 4 and 5 lean more on the second. However, in practice, all five modules support each other, blurring the division between the two viewpoints. The key technologies identified during the literature review (i.e. laser scanning, AI and BIM) were applied throughout the different modules to support their development.

A summarized graphic overview of the methodology is presented in Figure 3.1, identifying each module's name, primary contributions, tasks, and interaction with the remaining modules. In addition, a comprehensive overview of each module is present in Figure 3.2, Figure 3.3, Figure 3.4, Figure 3.5, and Figure 3.6, which respectively illustrate, in detail, the workflows of Modules 1 to 5. The following paragraphs further detail each module.

The methodology starts in Module 1, "identification of AIBEA requirements". This module focuses on creating standard information for AIBEA contract formalisation, helping the appointing party identify the project's requirements through the specification of the desired BIM model geometric detail and the identification of the energy simulations to perform. This information is then used to stipulate the building survey requirements, specifically, the minimum point cloud resolution and the building energy-related information to acquire. Two well-known independent and complementary metrics are used to specify this information, allowing for a straightforward definition of the Level of Information Need and, ultimately, the EIR of a project.

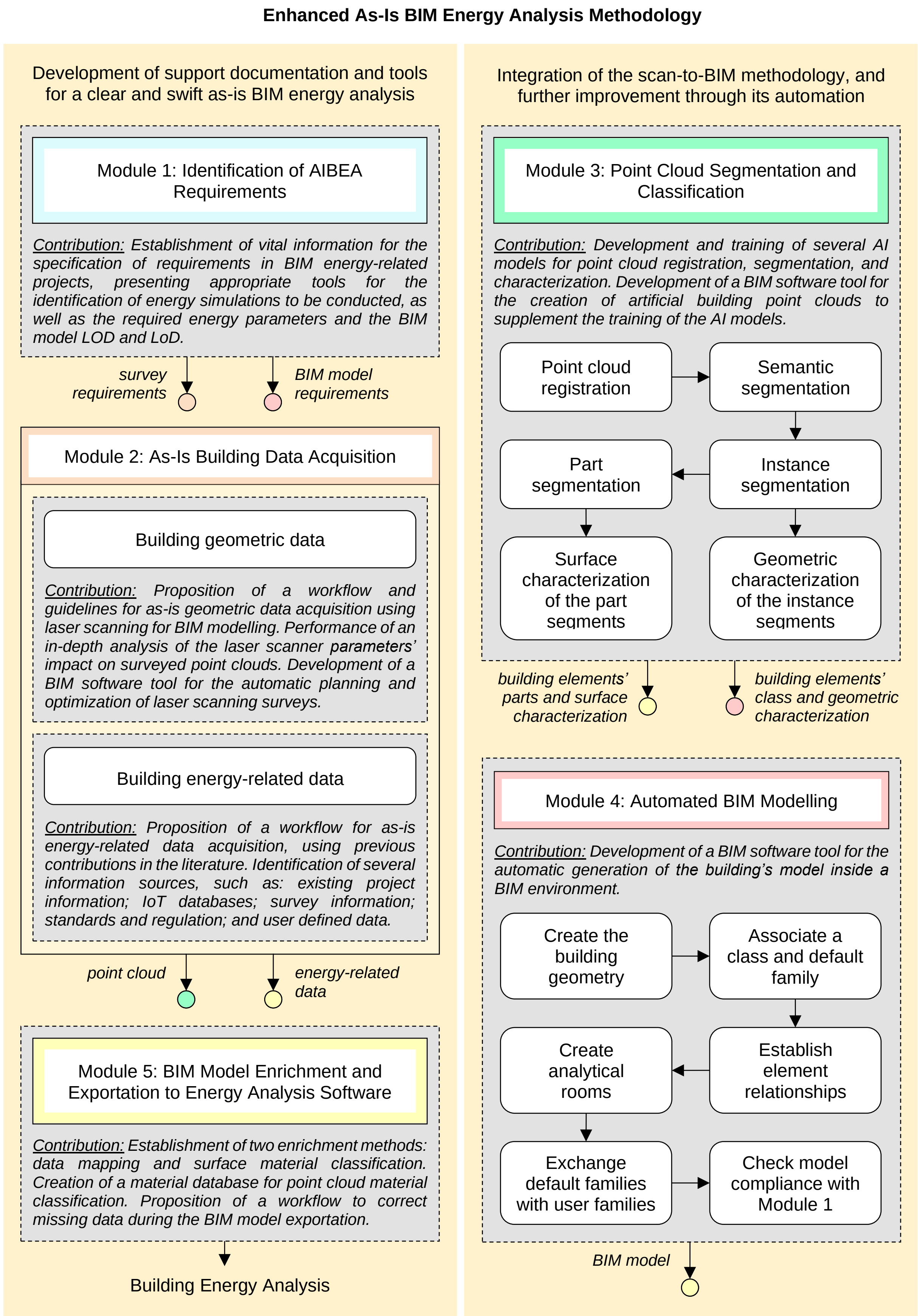

Figure 3.1 – Overview of the proposed methodology

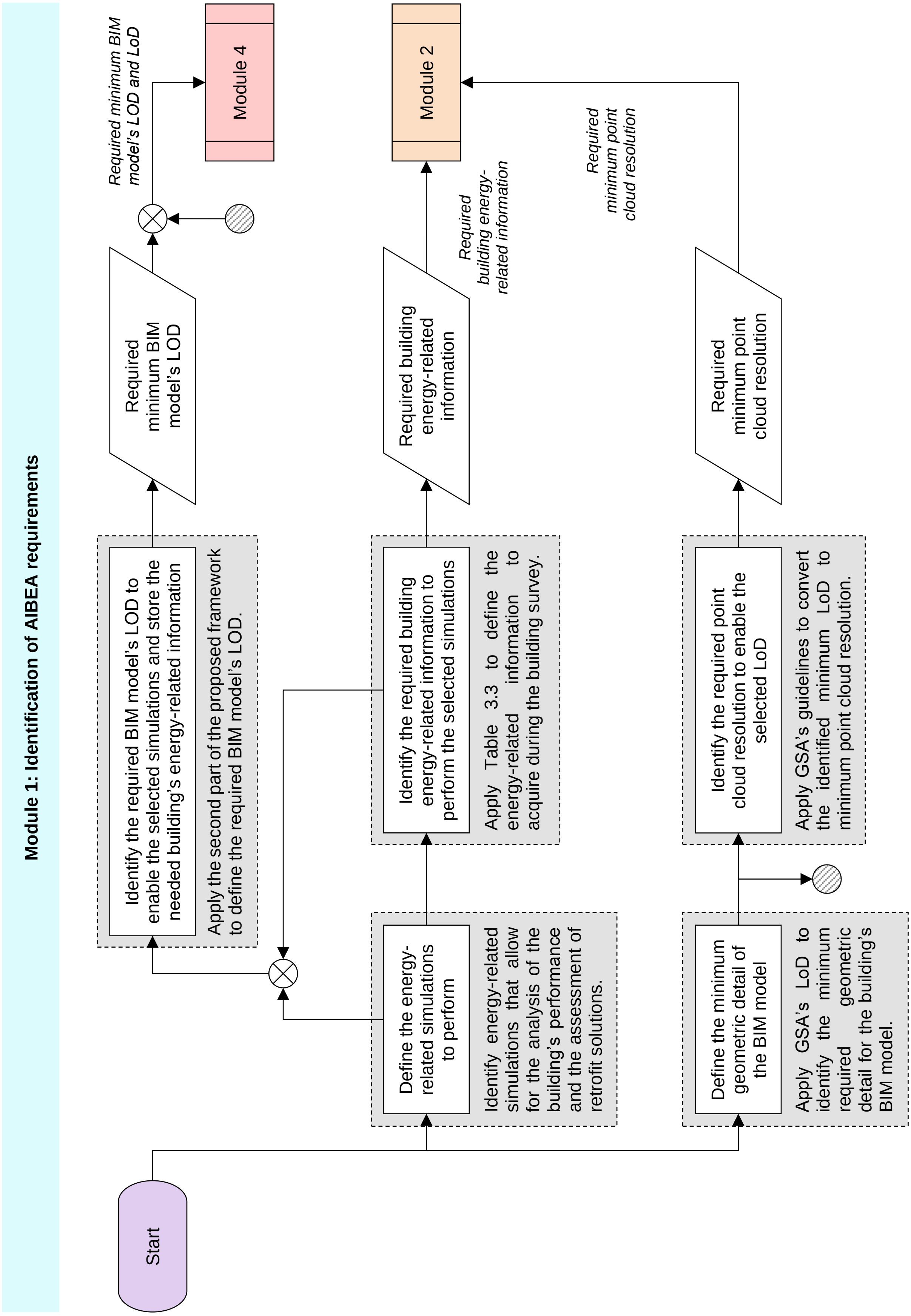

Figure 3.2 – Module 1

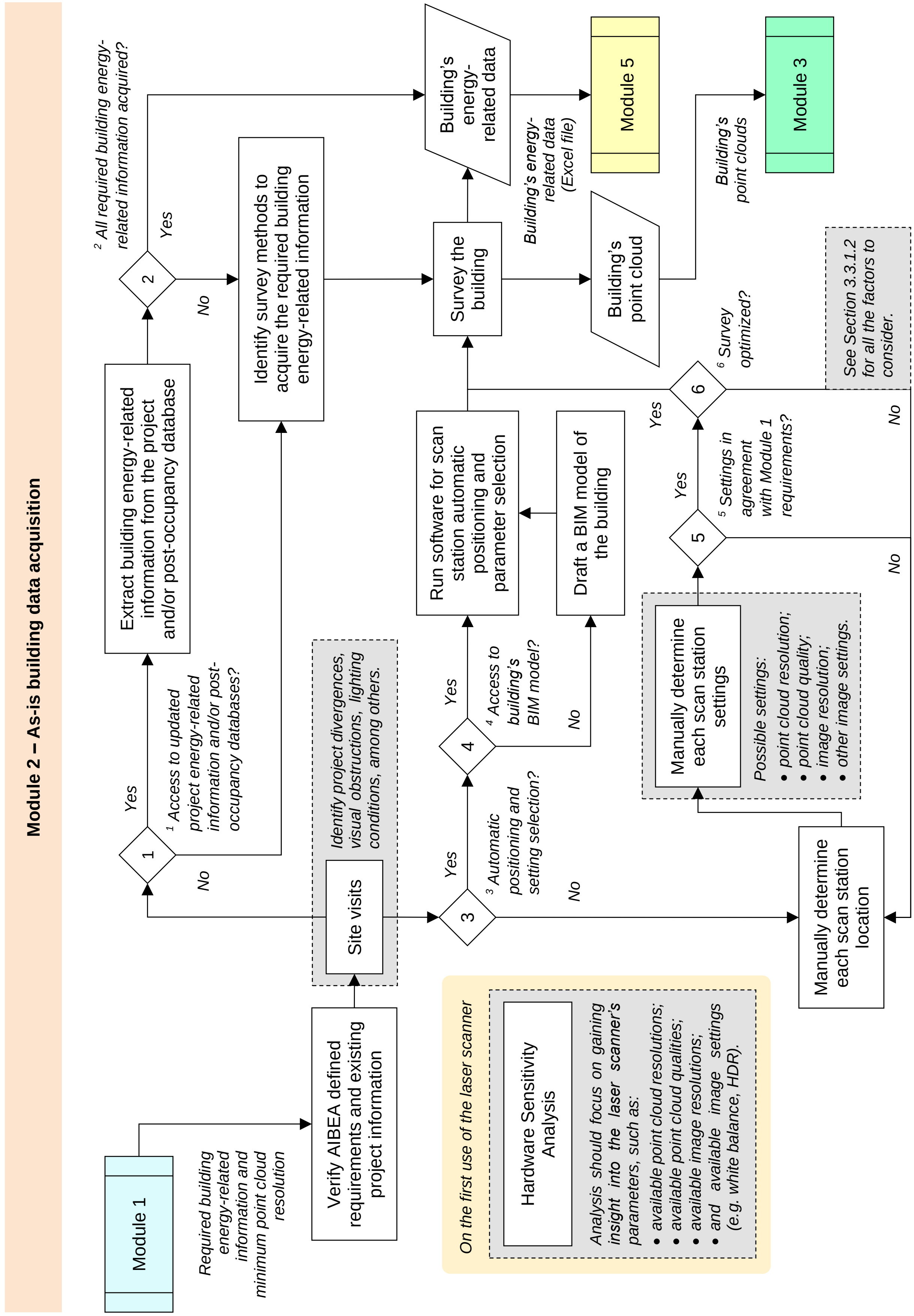

Figure 3.3 – Module 2

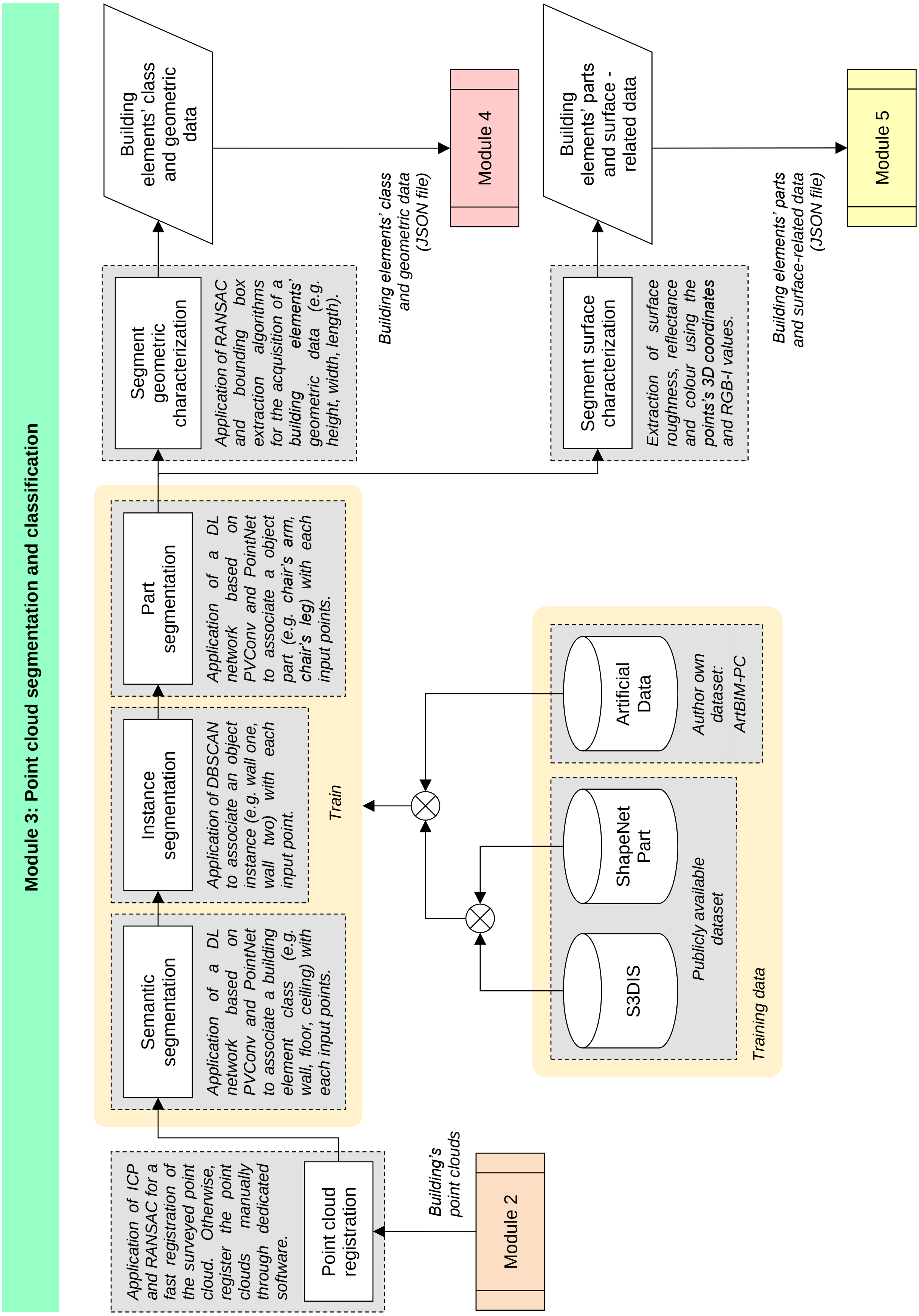

Figure 3.4 – Module 3

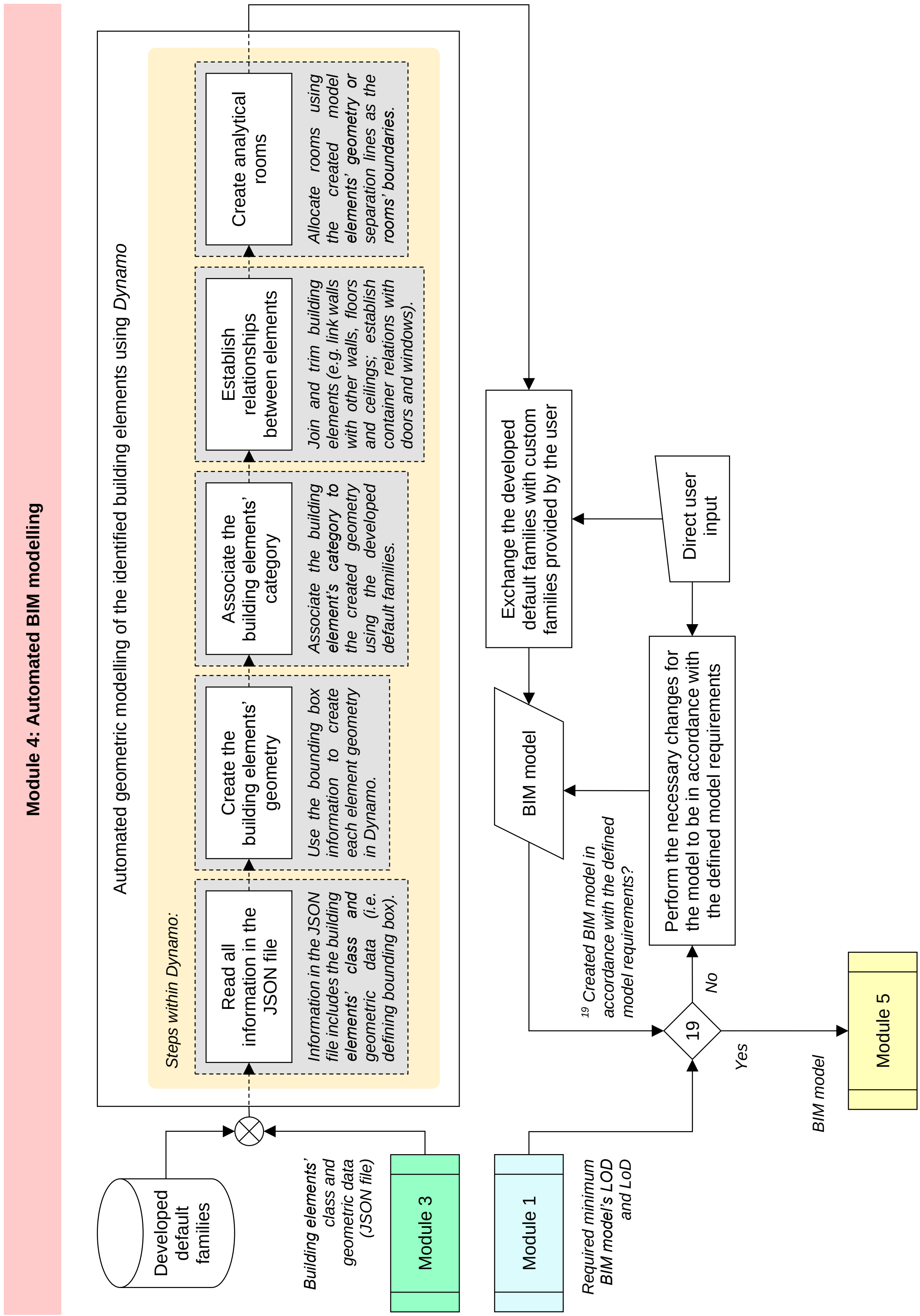

Figure 3.5 – Module 4

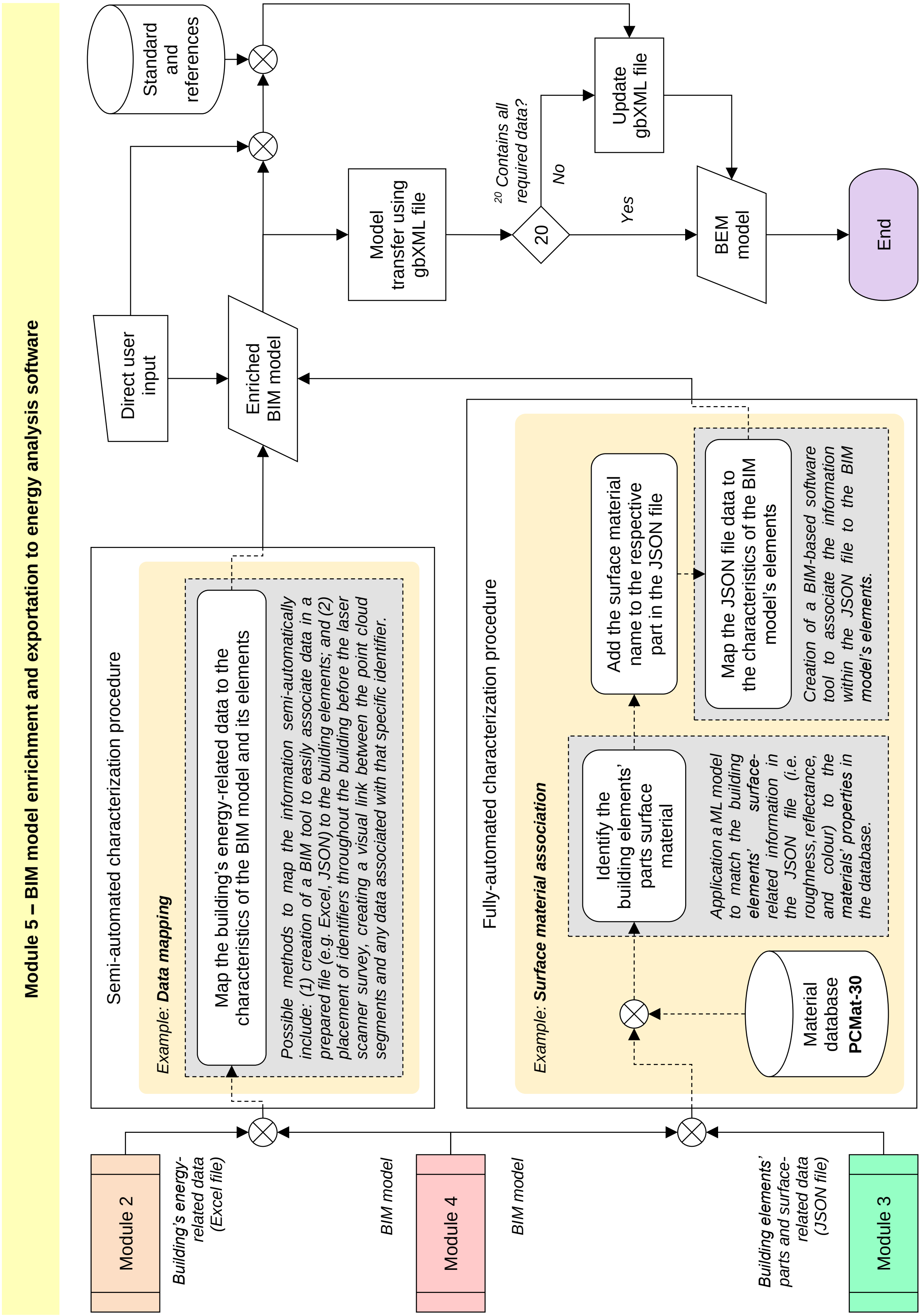

Figure 3.6 – Module 5

The second module, “as-is building data acquisition”, receives the survey requirements from Module 1, using them to identify the building’s energy-related data to be acquired, as well as the resolution of the building’s point cloud to be obtained using laser scanning – the selected method for as-is geometric data acquisition. It focuses on creating guidelines for a complete survey of the as-is building, both in terms of its geometric and energy-related information. Since laser scanning is a relatively unexplored technology in current research, when compared to energy-related data acquisition methods, a higher focus was put on developing the geometric portion of the guidelines, with most of the energy-related portion being based on existing literature solutions. Additionally, the module further introduces two other significant contributions: an in-depth analysis of the laser scanner parameters; and a BIM software tool for optimising laser scanning surveys that automatically positions and selects the parameters of the required scan stations.

The third module, “point cloud segmentation and classification”, receives the surveyed point clouds from Module 2, subsequently treating and registering them either automatically (through a combination of developed algorithms) or manually (through the use of typical point cloud software). The module then focuses on the semantic, instance and part segmentation of the treated point cloud through the application of three distinct AI models. Afterwards, the acquired instance segments (i.e. building elements) are characterized using their geometric information (i.e. acquisition of the segments height, width, length, volume, plane and bounding box), while the acquired part segments are characterized using their surface information (i.e. roughness, reflectance and colour). As another significant contribution, the module further introduces a BIM software tool to create artificial point clouds, with which to train the developed models.

The fourth module, “automated BIM modelling”, receives the building elements geometric information from Module 3 and feeds it into a developed BIM software tool. This software exploits *Dynamo*’s access to *Revit*’s Application Programming Interface (API) to generate the building’s model inside a BIM environment. Within *Dynamo*, the BIM model is generated by applying the retrieved information to (1) model the geometry of the building elements, (2) associate a class and default family with each of the modelled geometries, and (3) establish relationships between these geometries, which, by this point, are considered BIM elements. With this process finished and the BIM model acquired, analytical rooms are automatically created, and the user is prompted to exchange the default families with custom families containing further detail and analytical properties. If, after this process, the BIM model complies with Module 1 requirements, then the model is finished. Otherwise, the user must perform additional modifications until it conforms to the requirements.

The fifth and final module, “BIM model enrichment and exportation to energy analysis software”, receives the building energy-related data from Module 1, as well as the parts and surface-related data from Module 3, using this information to enrich the BIM model acquired from Module 4. It can perform this enrichment through several different methods, which are grouped in two distinct categories, namely, semi-automated and fully-automated enrichment processes. After the BIM model enrichment is complete, it is exported to a BIM energy-analysis software for performance assessment. The exportation can be completed either through dedicated transfer plugins or through a gbXML file. For either option, the model can be exported using the created analytical rooms or the building elements’ analytical properties. In case any information is lost during the exportation process, semi-automatic processes reliant on standard information and user input are proposed to correct the missing data. Two additional and noteworthy contributions in this module include developing an AI model for surface material classification (using the acquired surface-related information) and creating a material database to train the developed model. The developed AI model is proposed as an example of a fully-automated enrichment process.

3.2. Module 1 – Identification of AIBEA requirements

The first module of the proposed methodology establishes vital information to help the appointing party identify project objectives and requirements during the AIBEA project formalisation. It aims to establish a clear, levelled, common ground for project development, increasing project communication and transparency, while also providing all parties with an instrument to control the quality of intermediate and final deliverables. The module's workflow can be seen in detail in Figure 3.2.

Initially, the appointing party defines the minimum desired BIM model's geometric detail and the energy-related simulations to conduct during the assessment of the building's energy performance. In the author's opinion, these are the two most important aspects of the project from the appointing party's point of view, since they effectively control the core outputs of an AIBEA project: the building's as-is BIM model and the energy-performance assessment report.

To specify the minimum desired BIM model's geometric detail, as stated in Section 2.4.1, the appointing party can resort to GSA's LoD [161]. This standard has the added benefit of proposing a conversion method from LoD to point cloud resolution, which can be leveraged to define the building's geometric survey requirements. Table 3.1 displays GSA's proposed conversion between LoD and point cloud resolution.

It should be stressed that, as recognized by the GSA's BIM guide for 3D imaging [647], the uncertainty of individual point positions cannot be theoretically quantified. Thus, the specification relies on performing discrete comparisons between the point cloud and the actual physical measurements. To avoid this process and guarantee full compliance with the resolution and tolerance goals described in the GSA's LoD specification, real-world applications should account for this uncertainty by increasing the laser scan resolution and/or positioning the scanning station accordingly [35].

Table 3.1 – GSA's proposed LoD conversion to point cloud resolution

LoD	Resolution (mm)	Tolerance (mm)
1	152x152	±51
2	25x25	±13
3	13x13	±6
4	13x13	±3

To specify the energy-related simulations for assessing the building's energy performance, the appointing party can resort to Table 3.2 and Table 3.3, developed to provide an initial base for discussion.

Table 3.2 proposes suitable energy simulations for each project's design stage, as well as its respective simulation objectives. Table 3.3 indicates the necessary energy-related information to include in the

BIM model for the performance of said simulations. The latter can be leveraged to define the building's energy-related survey requirements.

Table 3.2 – AIBEA project formalisation: proposed simulations and respective objectives per design stage

	Conceptual Design	Schematic Design	Design Development / Retrofit
Simulations	• Shadow analysis; • Solar radiation studies; • Wind studies.	• Shadow analysis; • Solar radiation studies; • Natural ventilation assessment; • Construction solutions' assessment; • Heating and cooling loads analysis; • HVAC systems testing.	• Heating and cooling loads analysis; • HVAC systems testing; • Building systems assessment; • Construction solutions assessment; • Interior daylighting analysis; • Greenhouse gas emissions analysis.
Objectives	• Optimise the building's form and orientation; • Increase sunlight and solar gains; • Optimise passive strategies.	• Define the final building geometry and orientation; • Narrow appropriate construction solutions; • Roughly define the HVAC systems.	• Define the final construction solutions; • Define the HVAC systems; • Define the illumination solutions; • Define the control strategies (illumination, HVAC, shading).

Table 3.3 – AIBEA project formalisation: proposed parameters and respective LODs per design stage

Parameters	Conceptual Design	Schematic Design	Design Development	Retrofit
GENERAL INFORMATION				
Location (*weather file*)	LOD 300	LOD 300	LOD 300	LOD 300
Building orientation	LOD 100	LOD 200	LOD 300	LOD 300
Building geometry	LOD 100	LOD 200	LOD 300	LOD 300
Building type/function	-	LOD 300	LOD 300	LOD 300
Nearby constructions	LOD 100	LOD 100	LOD 100	LOD 100
	Whole building		*By room/space*	
Area	LOD 100	LOD 200	LOD 300	LOD 300
Volume	LOD 100	LOD 200	LOD 300	LOD 300
Occupancy *	-	LOD 200	LOD 300	LOD 300
Metabolic Information (*activity*) *	-	LOD 200	LOD 300	LOD 300
Domestic Hot Water (*consumption: l/m^2.day*) *	-	LOD 200	LOD 300	LOD 300
Heating temperature set point *	-	LOD 200	LOD 300	LOD 300
Cooling temperature set point *	-	LOD 200	LOD 300	LOD 300
RH humidification set point (*%*) *	-	LOD 200	LOD 300	LOD 300

RH Dehumidification set point (*%*) *	-	LOD 200	LOD 300	LOD 300
Fresh air (*l/s.person*) *	-	LOD 200	LOD 300	LOD 300
Mechanical ventilation per area (*l/s.m²*) *	-	LOD 200	LOD 300	LOD 300
CONSTRUCTION SOLUTIONS				
External Walls	LOD 100	LOD 200	LOD 300	LOD 200
Internal Walls	-	LOD 200	LOD 300	LOD 200
Roofs	LOD 100	LOD 200	LOD 300	LOD 200
Ceilings	-	LOD 200	LOD 300	LOD 200
Floors	LOD 100	LOD 200	LOD 300	LOD 200
Doors	-	LOD 200	LOD 300	LOD 200
Airtightness – Infiltration Constant rate (*ac/h*)	-	LOD 200	LOD 300	LOD 200
OPENINGS				
Windows and Skylights (*glazing type*)	LOD 100	LOD200	LOD300	LOD 200
Shading windows and local shading	LOD 100	LOD200	LOD300	LOD 200
Type				
Position				
Control type *	-	-		
SYSTEMS				
Equipment	-	LOD 200	LOD 300	LOD 200
Room/Space name (*location*)	-	-		
Power density (*W/m²*)	-			
Schedule	-			
Fuel	-			
Lighting	-	LOD 200	LOD 300	LOD 200
Room/Space name (*location*)	-	-		
Power density (*W/m²*)	-			
Schedule *	-			
Luminaire type	-			
Control type *	-	-		
Natural Ventilation	-	LOD 200	LOD 300	LOD 300
Room/Space (*location*)	-	-		

Outside air (*ac/h*) *	-	Approximate	Accurate	Accurate
Mechanical Ventilation	-	LOD 200	LOD 300	LOD 200
Room/Space (*location*)	-	-	Accurate	Accurate
System type	-	Approximate	Accurate	Accurate
Outside air (*ac/h*) *	-	Approximate	Accurate	Accurate
Schedule *	-	Approximate	Accurate	Accurate
Fans type	-	Approximate	Accurate	Accurate
Fans pressure rise (*Pa*)	-	Approximate	Accurate	Approximate
Fans total efficiency (*%*)	-	Approximate	Accurate	Approximate
Heat recovery type	-	-	Accurate	Accurate
Heating and Cooling	-	LOD 200	LOD 300	LOD 200
Room/Space (*location*)	-	-	Accurate	Accurate
System type	-	Approximate	Accurate	Accurate
Fuel	-	Accurate	Accurate	Accurate
System seasonal COP	-	Approximate	Accurate	Approximate
Max. or Min. supply air temperature (*ºC*)	-	Approximate	Accurate	Accurate
Max. or Min. supply air humidity ratio (*g/g*)	-	Approximate	Accurate	Accurate
Operation schedule *	-	Approximate	Accurate	Accurate
Domestic Hot Water	-	LOD 200	LOD 300	LOD 200
Room/Space (*location*)	-	-	Accurate	Accurate
Type	-	Approximate	Accurate	Accurate
DHW COP	-	Approximate	Accurate	Approximate
Fuel	-	Accurate	Accurate	Accurate
Delivery temperature (*ºC*)	-	Accurate	Accurate	Accurate
Operation schedule*	-	Approximate	Accurate	Accurate

Symbolic Approximate Accurate

* parameters which can use real data gathered in operational databases

The information in Table 3.3 is specified through the establishment of key energy parameters, which are associated with predefined LODs. When adequate, an indication of the key parameter's accuracy is also presented under three categories: symbolic; approximate; and accurate. The definition of these parameters and respective LOD was based upon ASHRAE Standard 209-2018 [648] and BIMForum's LOD Specification [649], making it applicable at all stages of the building lifecycle, from early concept development to post-occupancy, either to new buildings or major renovations and additions. The proposed accuracy levels should be discussed and agreed upon with all participating parties.

For the specific case of AIBEA, the "retrofit" stage column is undoubtedly the most important. However, it was decided to expand the proposed tables to the remaining design stages since no current standard presents this information – as identified in the literature review. Also, depending on the magnitude of the retrofitting works, the information on the remaining stages may apply to AIBEA projects.

Throughout the design phases, the quantity of information increases and becomes gradually more accurate. The framework translates this into the proposed LOD, with its overall value following a similar behaviour. However, this does not imply that every model element displays the same LOD for a given stage, as this seldom occurs in practice. For instance, as seen in previous BIMForum's LOD Specifications [650], during the schematic design stage, the model can include elements with LODs ranging from 100 to 400. Table 3.3 mimics this behaviour, as different LODs are indicated for each stage, depending on the required parameters.

It should be stated that through the application of these two tables, the appointing party effectively has at its disposal a set of predefined LOD Profiles, one for each of the proposed key parameters. This can be considered a step back in BIM standards, since after 2017's version of BIMForum's LOD Specification [165] this feature/information was removed. However, it is the author's opinion that during the initial stages of energy-related BIM standardisation, the use of predefined LOD Profiles is essential, since a merely descriptive approach may be insufficient to guarantee an unambiguous definition of the project requirements, at least while all the intervening parties gain experience in this field. After an appropriate period, similarly to the current LOD Specification progression, the predefined LOD Profiles can be removed in favour of custom profiles determined between all the intervening parties, thus fulfilling the approach favoured by the Level of Information Need standards.

Finally, by grounding the specification of both the BIM model's geometric detail and the energy-related simulations in two independent and complementary metrics (i.e. LoD and LOD), the Level of Information Need of a deliverable can be easily specified using these metrics, which, in turn, allows for the straightforward incorporation of energy-related requirements in a project's EIR. This is a desirable scenario, given the widespread adoption of ISO-19650 in BIM-related projects.

The contributions present in this module were published in peer-reviewed journals [29, 35] as central tools to support the specification of information requirements in energy-related BIM projects. Additionally, performed case studies dedicated to testing the framework and detailing the model creation process can be seen in [651].

3.3. MODULE 2 – AS-IS BUILDING DATA ACQUISITION

The second module of the proposed methodology entails the as-is building survey, both in terms of its geometric and energy-related information. To accomplish this objective, the workflow seen in Figure 3.3 was implemented in Module 2.

Initially, the requirements regarding the building energy-related information and minimum point cloud resolution are acquired from Module 1. Then, existing project information is gathered, and site visits are scheduled to (1) identify divergences between the as-is building and the existing project information and (2) start planning the required surveys. While gathering existing project information, special attention should be given to existing CAD plans, construction materials, glazing, HVAC and illumination specifications, among other energy-related information. As for the site visits, special attention should be given to unexpected visual obstructions, existing lighting conditions, and the presence of reflective surfaces, since these can significantly impact the geometric survey through laser scanning.

After the site visits are concluded, the module workflow diverges into two separate paths: one for geometric information and another for energy-related information. These are respectively reviewed in Section 3.3.1 and Section 3.3.2.

3.3.1. GEOMETRIC DATA ACQUISITION

As stated in Section 3.1, the chosen method to survey the building's geometric data was laser scanning. This technology was chosen for its clear advantages over the remaining survey methods, as previously identified in Section 2.4.3.1.2. Furthermore, this technology is a point cloud generation solution, which is a requirement to enable the scan-to-BIM process.

Despite the relatively recent dissemination of this technology, several authors have already researched its practical applications in the AEC industry with high levels of success, as identified in the literature review. However, as stated in [29], no research has provided a complete workflow for the acquisition of points clouds to be applied in BIM, with most studies focusing on the process after the point cloud data has been exported.

As such, to properly develop a workflow for geometric data acquisition using this technology, an in-depth analysis of each of the laser scanner parameters was first performed to understand their impact on the resulting point cloud. The results of these tests were critical in the development of the geometric data acquisition workflow, which is why the analysis process itself was also included in Figure 3.3. The performed analysis process can be seen in the following section or in [29], as published in an international peer-reviewed journal.

3.3.1.1. In-depth analysis of the laser scanner parameters

An in-depth analysis of *Leica's ScanStation P20* parameters was performed to understand their impact on the acquired point clouds and support the development of Module 2. Although *Leica's ScanStation P20* was the utilized laser scanner, as seen in [652, 653], the examined parameters are shared by several other laser scanners, unrestricting the conclusions of this study to the equipment at hand.

The analysis comprised the performance of ablation studies for each laser scanner parameter. The ablation studies involved acquiring 32 point clouds of the same controlled environment, each with different scanning parameters, subsequently analysing their impact on the average scanning time, the point cloud file size, and the point cloud geometric information. The selected controlled environment was the Construction Department's rain chamber in *Faculdade de Engenharia da Universidade do Porto* (FEUP), visible in Figure 3.7. The rain chamber was selected for its isolated conditions and the detailed geometrical features provided by the ground frame and the sample containers on the wall. The examined parameters are described below:

- Resolution – sets the distance (in millimetres) between captured points, both vertically and horizontally, for a radius of 10 meters measured from the laser scanner position. The larger the distance, the lower the accuracy and the density of points captured. The examined laser scanner has seven pre-sets: 50; 25; 12.5; 6.3; 3.1; 1.6; and 0.8mm@10m;
- Quality – relates to the precision with which a given point is acquired. Greater quality translates into a lengthier scan rotation duration so that each point can be acquired with higher precision. The examined laser scanner has four pre-sets ranging from 1 to 4;
- White Balance – allows the acquisition of white tones and the overall photograph colour correction. The examined laser scanner displays four pre-sets: Sunny; Cloudy; Cold Light; and Warm Light. These pre-sets should be set according to the predominant type of environment lighting. The first two are used when predominantly subject to natural light (with a high or small sun exposure, respectively), while the last two are used for artificial light (with fluorescent lamps or tungsten bulbs, respectively);
- Image Resolution – defines the number of pixels, both vertically and horizontally, for the acquired photographs. Higher resolution translates into a sharper image with higher overall image quality and less blur; however, it also increases the scan duration and file size. The examined laser scanner has three pre-sets: 640×640; 960×960; 1920×1920;
- High Dynamic Range (HDR) –extends the dynamic range of an image, meaning the ratio between the lightest and darkest value. Several photographs with different levels of exposure are taken, with the final photograph resulting from a balance between these images. This parameter should be turned on when faced with extreme lighting conditions environments.

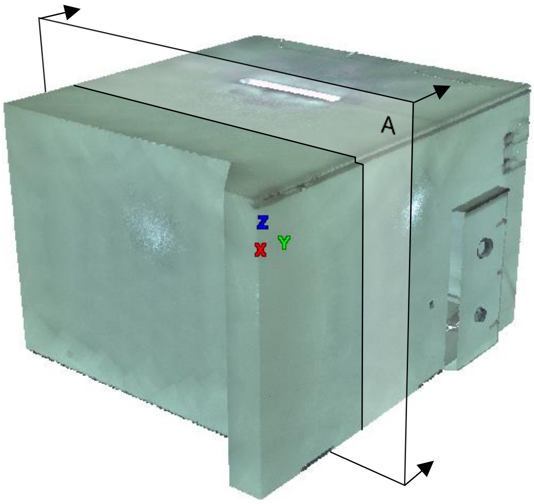

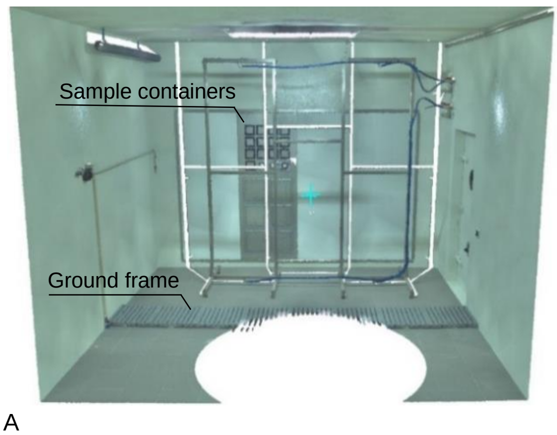

Figure 3.7 – 3D interior view (left) and section A (right) of the rain chamber

During the capture of the 32 point clouds, according to the rain chamber's lighting conditions, the HDR and White Balance parameters were, respectively, turned off and specified as "Cold Light" for all the tests. Table 3.4 presents the parameter combinations for each of the 32 performed tests, as well as the resulting point cloud file size and average scanning time.

Through Table 3.4 analysis, it can be concluded that the impact of scan and image resolutions on file size is roughly proportional to the number of points in the cloud or pixels in the acquired images. It also shows that the scanning time depends mostly on the scan resolution and quality, as the number of photographs is constant for each scan, regardless of the selected image resolution.

However, the scan resolution's influence over the total file size and average scanning time is far more significant than the remaining two parameters. Indeed, Table 3.4 indicates that changes in scan resolution can originate increments of over 20 GB in file size and 105 minutes in estimated time. Meanwhile, changes in image resolution only prompt changes of around 400 MB for the file size and 1 minute for the estimated time. As for the scan quality, these values are even lower.

The graphics seen in Figure 3.8 demonstrate the exponential impact the scan resolution has over these two variables, clearly emphasizing the importance of planning each scan station position and parameters. An overestimation of these parameters can undoubtedly negatively impact the survey duration and the required hardware specifications. The displayed values were averaged from Table 3.4 values.

Regarding the point cloud geometric information, Table 3.5 presents 12 scans acquired using two different scan qualities and six scan resolutions at a range of five meters. By observing the displayed scans, it can be concluded that a modification in scan quality does not provide any noticeable difference in geometric information, at least in the conditions present within the rain chamber.

Conversely, changes in scan resolution display an extreme impact on this subject, since using a scan resolution of 25.0mm@10m delivers far less geometrical information than a resolution of 1.6mm@10m, as seen in Table 3.5. Still, it can also be concluded that resolutions above 3.1mm@10m result in minor information gains, at least at the tested range – thus, the 0.8mm@10m resolution scan not being shown.

As for the image resolution's impact on the geometric information of the point cloud, given that the taken photographs are only used as a source of RGB values to map onto the point cloud, a natural method to study this impact comprises comparing the RGB values of point clouds with different image resolutions. The point clouds from tests 16, 17 and 18 were used for this purpose, respectively displaying an image resolution of 640×640, 960×960, and 1920×1920.

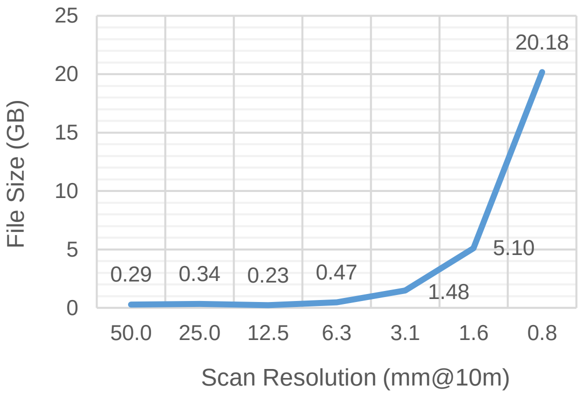

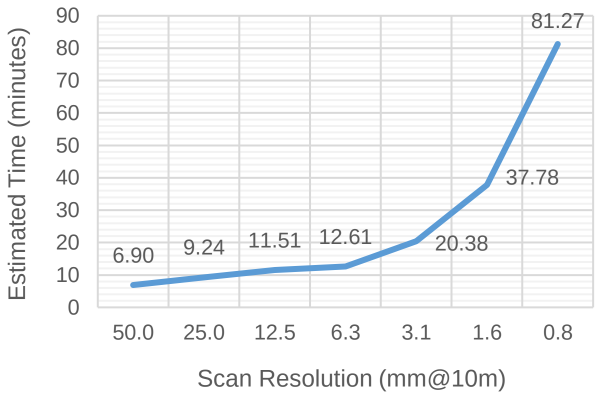

Figure 3.8 – Average file size and estimated time for the respective scan resolution at ten meters

Table 3.4 – Parameter combinations tested

Test	Scan Resolution (mm@10m)	Scan Quality	Image Resolution	Point Cloud File Size (MB)	Images File Size (MB)	Total File Size (MB)	Average Scanning Time (min.)
1	50.0	1	960x960	6	144	150	6.43
2		2	960x960	6	148	154	6.43
3		3	1920x1920	6	566	572	7.83
4	25.0	1	960x960	21	148	168	6.65
5		2	960x960	21	151	171	6.65
6		3	960x960	21	148	168	7.67
7		4	1920x1920	20	571	591	9.83
8	12.5	1	960x960	80	171	251	7.67
9		2	960x960	80	148	228	7.92
10		3	960x960	80	151	231	9.60
11		4	960x960	80	151	231	12.97
12	6.3	1	960x960	319	145	464	8.17
13		2	960x960	318	147	465	9.60
14		3	960x960	318	147	465	12.97
15		4	960x960	318	148	466	19.72
16	3.1	1	640x640	1269	67	1335	9.42
17		1	960x960	1269	147	1415	9.60
18		1	1920x1920	1269	568	1837	10.77
19		2	960x960	1271	148	1419	12.97
20		3	960x960	1270	148	1418	19.70
21		4	640x640	1270	68	1337	33.00
22		4	960x960	1270	149	1418	33.18
23		4	1920x1920	1270	575	1845	34.37
24	1.6	1	960x960	5087	149	5236	19.75
25		2	960x960	5091	149	5240	33.27
26		3	960x960	5089	148	5237	60.32
27	0.8	1	640x640	20328	68	20396	60.13
28		1	960x960	20328	149	20478	60.30
29		1	1920x1920	20329	575	20903	61.48
30		2	640x640	20339	68	20407	114.20
31		2	960x960	20339	149	20488	114.38
32		2	1920x1920	20339	575	20914	115.55

Table 3.5 – Visual representation of Table 3.4's scans for their respective scan quality and resolution

Scan Resol.	Scan Quality	
	1	4
50.0mm@10m	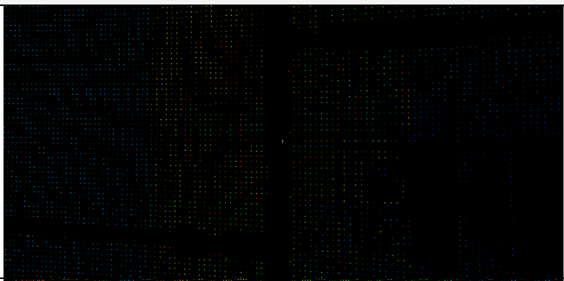	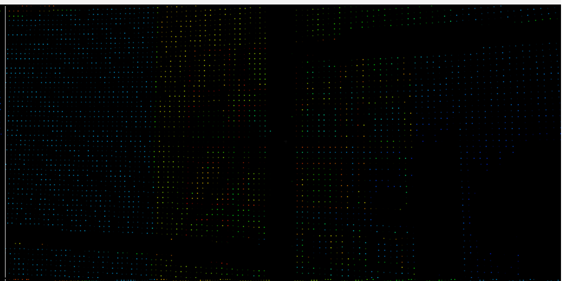
25.0mm@10m	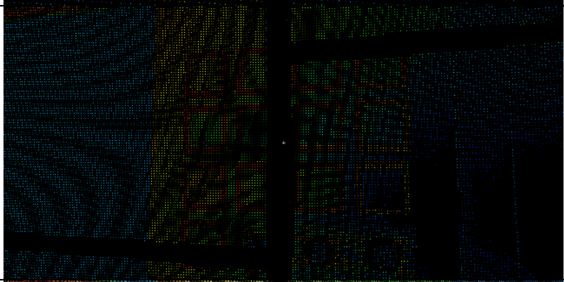	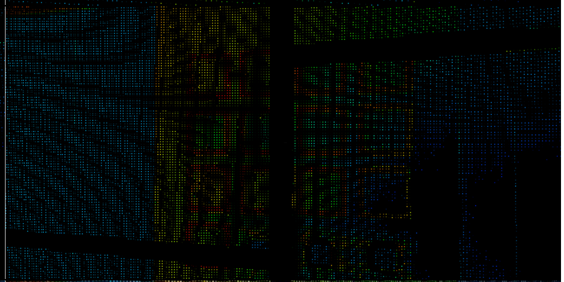
12.5mm@10m	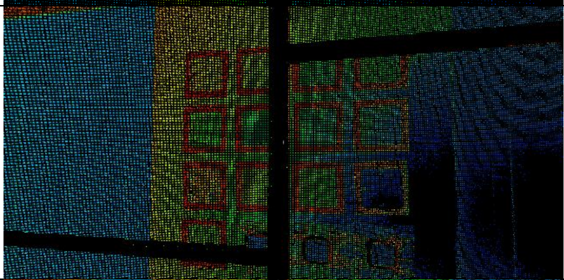	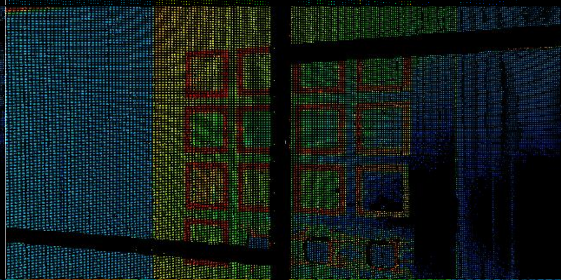
6.3mm@10m	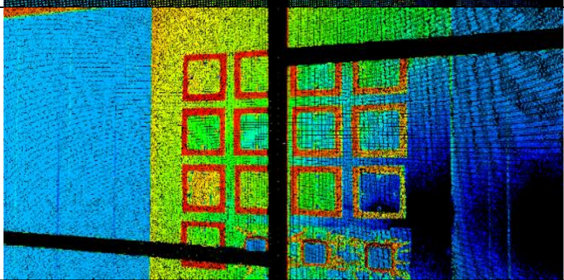	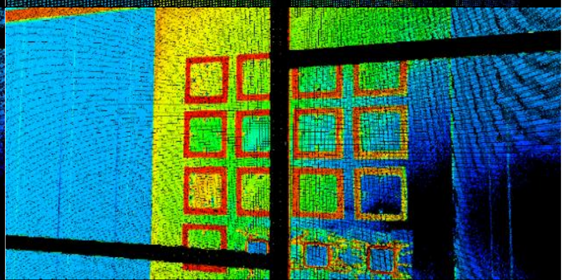
3.1mm@10m	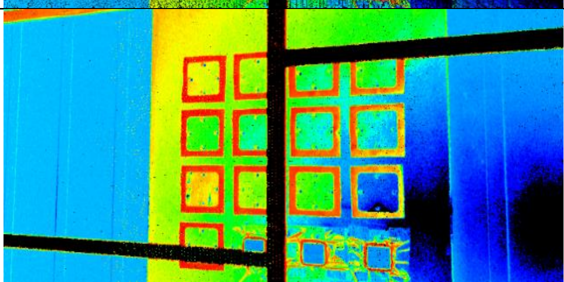	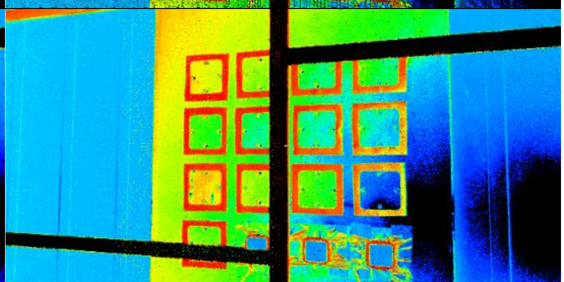
1.6mm@10m	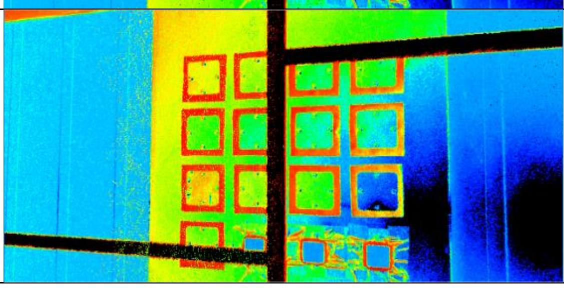	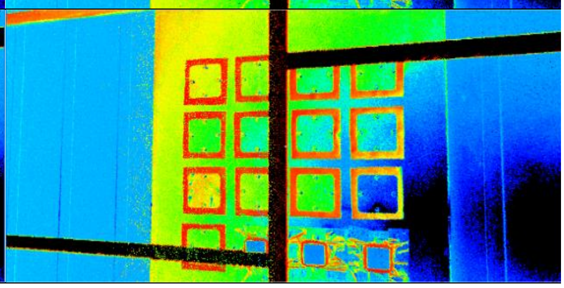

Two different methods were applied to compare the RGB value [654]. The first method entailed computing the Euclidean distance d between the RGB values of two point clouds ($PC1$ and $PC2$) as shown in Equation 3.1:

$$d(RGB_{PC1}, RGB_{PC2}) = \sum_{i=1}^{n} \sqrt{(R1_i - R2_i)^2 + (G1_i - G2_i)^2 + (B1_i - B2_i)^2} \tag{3.1}$$

, where $R1_i$, $R2_i$, $G1_i$, $G2_i$, $B1_i$, and $B2_i$ correspond to the RGB values of the i^{th} point in point clouds one and two, respectively. This method returned an average distance of 16.17 (between the 640×640 and 960×960 resolutions) and 17.16 (between 960×960, and 1920×1920 resolutions) for the pairs of points from each point cloud, effectively translating into a vector module variation of only 3.7% and 3.9%, respectively.

The second method entailed computing the colour histograms of each point cloud [655] and compare their values. For this second method, only the points referring to the wall holding the sample containers were used (40,986,009 points), since it was identified as showing the highest colour range, and thus, being considered the worst-case scenario. This method resulted in Figure 3.9, which displays a clear overlap between the colour values of the three studied point clouds.

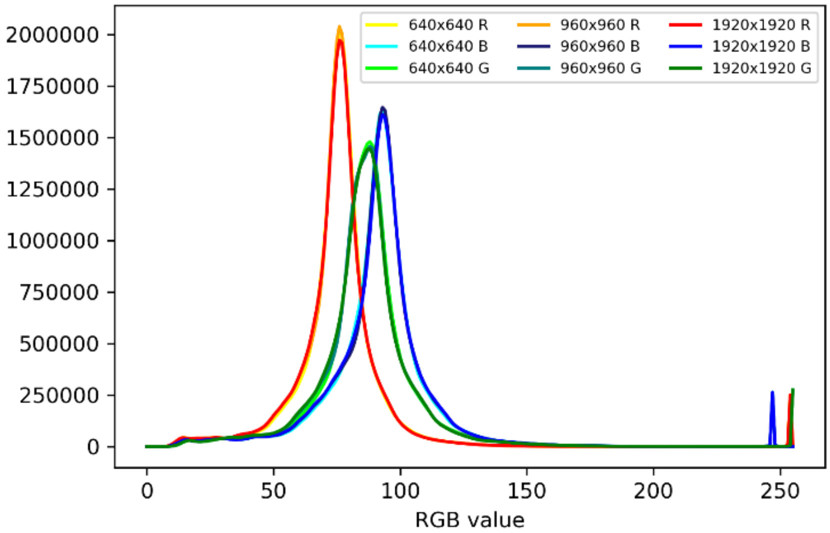

Figure 3.9 – Colour histograms for the examined point clouds

As such, from the performed laboratory tests, it is possible to conclude that:

- The scan resolution is the most critical parameter, greatly influencing all three studied aspects (average scan time, point cloud file size, and point cloud geometric information). Thus, the selection of this parameter should be carefully examined to optimize the survey;
- The scan quality contributes significantly to the average scan time and point cloud file size, yet its impact on the point cloud geometric information is negligible. Thus, limiting this parameter to its lowest values should translate into higher efficiency surveys. However, its use could be considered when faced with highly unfavourable environment conditions (e.g. multiple glass surfaces, distant targets, humid environments);

- Similarly to scan quality, the image resolution contributes considerably to the average scan time and point cloud file size, yet its impact on the point cloud geometric information is not significant. As such, restricting this parameter to its lowest value should increase the survey efficiency.

3.3.1.2. Software for scan station automatic positioning and parameters selection

From the analysis of laser scanner parameters, it is clear that a proper selection of each scan station parameters is required for the optimization of the building's geometric survey, especially regarding scan resolution. However, performing this optimization manually can be complex and time-consuming, given the multiple factors influencing it. Additionally, most factors are inherently correlated, making it impossible to isolate and optimize them separately. These factors include:

- each parameter's dissimilar influence over the average scan time and final point cloud file size – the latter further influencing the time required to export the acquired point clouds from the laser scanner into the point cloud software;
- the building geometry;
- the number of scan stations;
- the scan stations positions;
- the field of view of each scan position;
- the required link between scan stations for registration of the acquired point clouds;
- the required time to transport and set up the laser scanner;
- the survey team size;
- and the compliance with Module 1 point cloud resolution requirements;

Considering this process complexity and importance, the author developed a BIM software tool that optimizes the positions and parameters of the scan stations to perform the geometrical survey of a building. The software was developed using *Dynamo* and *Python*.

Depending on the decision to use this software, the steps taken during Module 2 can change considerably, namely:

- If the developed software is applied, then a draft of the building must be designed in a BIM authoring software to support its use. This can seem contradictory since the software aims to optimize a geometric survey, which resulting information will be used to create the building's as-is BIM model. However, it should be considered that the precision required for this auxiliary model is minimal and should not require the same duration to be complete as an as-is BIM model. In fact, a single site visit or having access to the building's CAD plans should allow for its swift creation. As an example, while performing a laser scanning survey of bus terminal "24 de Agosto", in Porto, Portugal, the author's manual planning of the survey took approximately two full workdays to be complete, while the required BIM sketch of the station took less than three hours using the available CAD plans.
- If, on the other hand, the scan stations positioning and parameter selection is performed manually, then a dedicated examination of the required scan stations ensues, where the previously identified factors must be taken into account for an efficient geometric survey. Performing this process manually is not advised since it can quickly turn into a time-consuming,

labour-intensive, subjective, and error-prone process depending on the scale and complexity of the building. In fact, performing this process manually will most likely never result in an optimal survey, with the survey efficiency being significantly reliant on the workers' experience. A safe approach would be to either use a high number of scan stations with low resolutions or a low number of scan stations with high resolutions – the former, typically being favourable since it requires less planning and the precision required for the development of 3D models for energy simulations is usually modest.

For any of these approaches, as stated in Module 1, the acquired point cloud minimum resolution should be slightly superior to the one specified in the requirements to guarantee full compliance with GSA's tolerance goals.

Regarding the software tool itself, it performs the survey planning and optimization by iterating over multiple scan stations positions and parameter combinations. These scan stations are represented in the BIM model as spheres of radius r, acquired through Equation 3.2:

$$r = \frac{Module1Resol \times 10}{TestedResol} \tag{3.2}$$

, where $Module1Resol$ corresponds to the minimum point cloud resolution determined in Module 1 and $TestedResol$ corresponds to the tested resolution during the iterative process. These spheres also represent the scan station's field of view, meaning they intersect and deform around the BIM model geometry.

To identify the most efficient combination of scan stations and respective parameters, the iterative process searches the combination that complies with the following four conditions:

1. the minimum resolution of the acquired point cloud must fulfil Module 1 requirements;
2. all the building geometry must be surveyed;
3. a scan station must share at least 2% of its field of view with one or more scan stations;
4. and Equation 3.3 must be minimized.

From these conditions, the first two are quite straightforward and self-explanatory. The first is guaranteed by Equation 3.2. The second is tracked through the intersections between the scan stations spheres and the BIM model.

The third condition ensures the registration of the acquired point clouds – the 2% value was decided through testing and guarantees a minimum overlap between scan stations' fields of view, which, when unrestricted, might not be sufficient.

The fourth condition entails minimising a cost function that considers the previously listed factors influencing the geometric survey through laser scanning. These factors are grouped into three different processes, represented by each line on Equation 3.3. These processes consist of (1) setting up the laser scanner, (2) performing the laser scan, and (3) exporting the acquired point cloud from the laser scanner to the point cloud software. Each of Equation 3.3 lines essentially translates the time (in minutes) associated with each of these processes, using the analysis present in Section 3.3.1.1, as well as the data from multiple performed surveys to support its formulation. Some of these surveys can be seen in [28-30, 33, 36, 656].

$$
\begin{aligned}
Cost(ScanStation_i) = &-0.735 \times ln(TeamSize_i) + 3.1391 \\
&+ScanDuration(ScanQuality_i; ScanResol_i) \\
&+0.0338 \times \left(\frac{12478}{ScaResol^2} + 0.0001 \times ImgResol_i^2 + 0.0201 \times ImgResol_i - 4.5\right)
\end{aligned}
\tag{3.3}
$$

, where $TeamSize_i$, $ScanQuality_i$, $ScanResol_i$, and $ImgResol_i$ respectively represent the team size, scan quality, scan resolution, and image resolution for the i^{th} scan station in the survey.

To formulate the first line of Equation 3.3 (related to the first process), the set-up of over 140 scan stations was timed. The set-up included disassembling, repositioning, assembling and choosing the parameters of a scan station. From these timed scan stations, 48 were performed by a team size of one, 75 by a team size of two, and 21 by a team size of three. The resulting times were averaged and plotted in Figure 3.10, from which a trendline was extracted to represent the first process in Equation 3.3.

To acquire the time taken in the second process, Table 3.6 is directly applied. This table contains the scan durations reported in the field manual of the utilized laser scanner (*Leica's ScanStation P20* [657]), according to the selected scan quality and resolution. In Equation 3.3, this table is represented by the second line term $ScanDuration(ScanQuality_i; ScanResol_i)$.

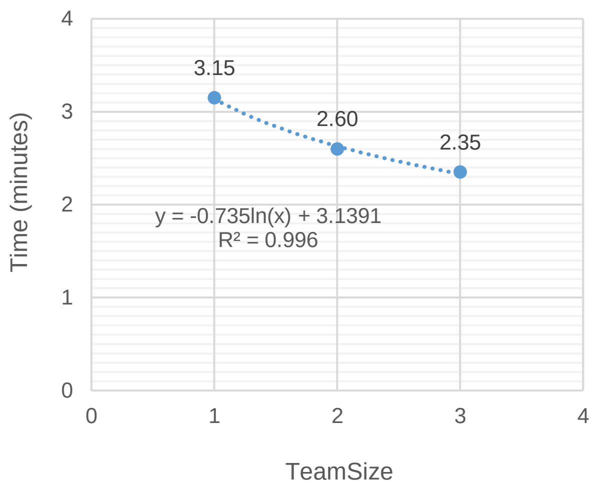

Figure 3.10 – Trendline used on the first process of Equation 3.3: setting up the laser scanner

Table 3.6 – Scan duration (minutes) as reported in the field manual of *Leica's ScanStation P20*

Scan Quality	Scan Resolution (mm@10m)						
	50.0	25.0	12.5	6.3	3.1	1.6	0.8
1	0.3333	0.5500	0.9667	1.8167	3.5000	13.5500	54.1167
2	0.3333	0.5500	1.7333	3.4167	6.7833	27.0667	108.2167
3	0.4667	0.8833	3.4000	6.7667	13.5000	54.1167	-
4	-	1.7167	6.7667	13.5000	26.9833	-	-

Finally, to formulate the third line of Equation 3.3 (related to the third process), the point cloud exportation process for the 32 tests in Section 3.3.1.1 was timed, resulting in an average exportation speed of 29.5858 MB per minute. This speed value is used to convert the total survey file size to minutes. The total survey file size is acquired from the sum of the trendline equations seen in Figure 3.11, which were acquired using the average of file sizes seen in Table 3.4.

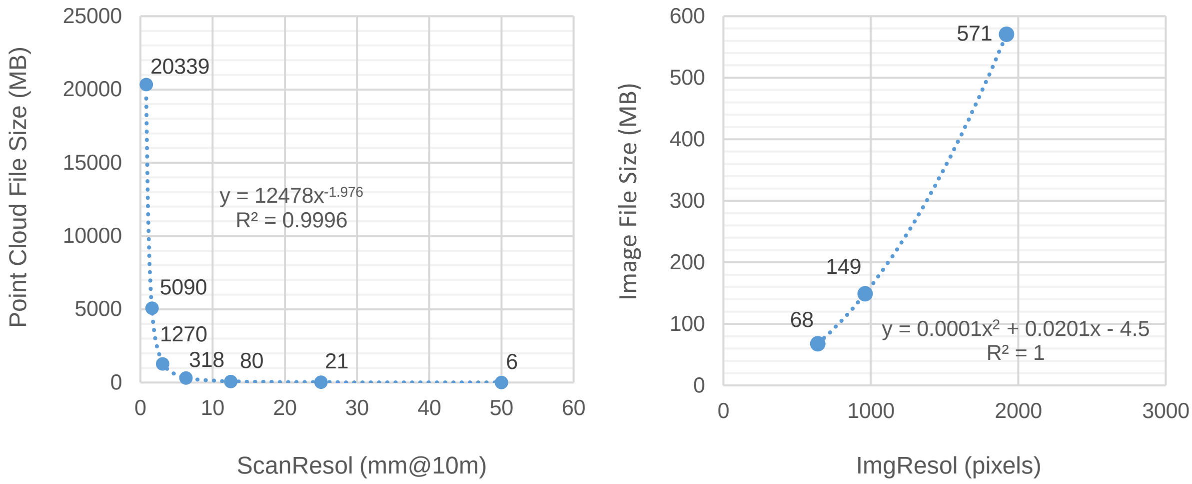

Figure 3.11 – Trendlines for the total file size. Point cloud file size on the left and images file size on the right

Taking into account how Equation 3.3 was formulated, it is clear the equation is heavily dependent on the used hardware and software; as such, for any other combination of hardware and software, this equation should be re-formulated, allowing for an higher precision of its output. For clarity, the following hardware and software were used:

- laser scanner: *Leica's ScanStation* P20;
- point cloud software: *Leica Cyclone 2020.1.0*;
- computer station specifications: *Intel I7-6700K* (4.00GHz); *MSI GeForce GTX 1050 Ti Gaming X 4G*; 32GB (2x16GB) DDR4-2400MHz CL15; SSD 2.5'' 500GB SATA 3.

Having understood all four conditions, as previously stated, the software performs the optimization through an iteration process. This process consists of seven steps:

1. create a set of possible scan station locations throughout the BIM model using a spaced grid, which spacing is indicated by the user;
2. create all possible parameter combinations for each scan location;
3. identify the combinations of scan locations and parameters that comply with conditions 1 to 3;
4. calculate the cost function for each of these combinations;
5. select the combination that minimises the cost function;
6. establish new possible locations in the vicinity of the selected combination using a reduced grid (half the previous spacing);
7. repeat this process until a new combination is less efficient than the previous one.

Figure 3.12 showcases this optimization process for an illustrative BIM model, with some of the performed combinations being illustrated at ground level in 2D.

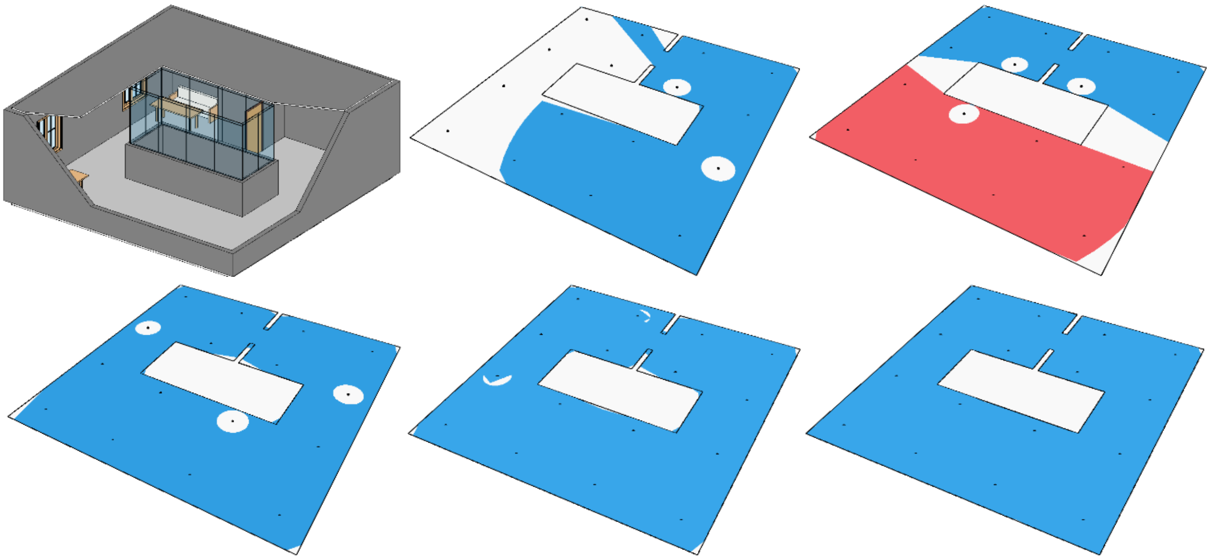

Figure 3.12 – Assessment and iterative optimization of multiple scan station positions and parameters using the developed software

With the scan stations planned and optimized, the building's geometric survey can be performed, resulting in the acquisition of the building's point clouds to be used in Module 3. During the survey, any modification to the plan should be duly noted.

3.3.2. Energy-related data acquisition

Regarding energy-related information, after the site visits are performed, the gathered project information is reviewed for all of the specified key parameters in Module 1. This review should extend to existing post-occupancy databases in case these are available. Table 3.3 specifies which of the key parameters are more frequently encountered in post-occupancy databases, hopefully simplifying this process.

After reviewing all the available information in the project and post-occupancy databases, if any required information remains undetermined, survey methods are identified to acquire the remaining information from the as-is building. Any of the methods indicated in Table 2.4 can be selected, depending on the required data. Non-destructive methods are preferred; however, depending on the retrofit scale and building state, destructive methods may be viable and even advantageous.

With the methods chosen, the building's energy-related survey can be performed, with the resulting data being stored in a predefined file structure to be sent to Module 5. The predefined structure enables the use of data mapping algorithms for BIM model enrichment (further information in Module 5), which, in the case of the present thesis, constitutes an *Excel* file with a similar structure as Table 3.3. This file structure can be edited to correspond to any worker/company preferences; however, it requires the corresponding modifications to be performed in the mapping algorithms.

The workflows and guidelines proposed in Module 2 were applied during several case studies published in international peer-reviewed journals [22, 28-30] and conference papers [36, 656, 658].

3.4. Module 3 – Point cloud segmentation and classification

The third module of the proposed methodology entails the registration of the surveyed building points clouds, its subsequent segmentation and classification into building elements, and the characterization of the acquired elements in terms of their geometric (e.g. height, width, length) and surface (i.e. roughness, reflectance and colour) information. For an overview of the third module, please address Figure 3.4.

The registration process can be performed manually, through the use of dedicated point cloud software (e.g. *Leica Cyclone*, *Meshlab* and *Autodesk ReCap*), or automatically, through a developed AI model reliant on the RANSAC [399] and ICP algorithms [395, 396]. This process is examined in great detail in Section 3.4.1.

Regarding segmentation and classification, these tasks are tackled simultaneously, essentially morphing both into a semantic segmentation task. This task was taken a step further, also performing instance and part segmentation, resulting in a better BIM modelling and building element characterization, respectively covered in Module 4 and Module 5, respectively.

As alluded to in Section 2.5.3.7, DL networks were the selected method to accomplish these segmentations. The developed networks were based on previous works, namely PointNet [556], as the backbone network, and PVConv [542], as the primary primitive. However, the instance segmentation task was performed using the DBSCAN algorithm instead of the developed DL network, after initial tests with the latter yielded unsatisfactory results. An in-depth discussion for choosing these components and algorithms is presented in Section 3.4.2, where the semantic, instance and part segmentation tasks are thoroughly examined.

As for the geometric and surface characterization processes, these were done separately on distinct data sets. The geometric description was performed on the instance segments, while the surface information was acquired from the part segments. The first relied primarily on RANSAC [399] and a general bounding box generation algorithm. The second was based on the work by Yuan et al. [659]. These characterization processes are examined in Section 3.4.3.

The data used for training the developed networks and models was acquired from publicly available datasets, as well as datasets artificially created using a software tool developed by the author. This tool is covered in Section 3.4.4.

3.4.1. Point cloud registration

As identified in the literature review, point cloud registration entails aligning multiple point clouds into a single-shared coordinate system. However, in the proposed methodology, four different tasks were included in this process, namely:

- Simplification/decimation – this task involves homogenising the surveyed point clouds' resolution by eliminating points in denser areas. The target resolution is the minimum required in Module 1 while taking into account the added resolution for compliance with GSA's tolerance requirements;
- Cleaning – this task requires eliminating the noise in the surveyed point clouds, such as moving objects or incorrectly captured points;

- Registration – this task entails aligning all the surveyed point clouds into a single-shared coordinate system;
- Unification – this task requires converting the aligned point clouds into a single point cloud. Duplicate points acquired from different scan stations are eliminated during this process.

These tasks can be performed automatically or manually. Until recently, the latter was considered preferential, given its increased precision, despite the added work effort. However, with AI advances in recent years, the author believes that this no longer is the case. Nevertheless, both methods were researched, with Section 3.4.1.1 and Section 3.4.1.2 proposing solutions for manual and automatic approaches, respectively.

3.4.1.1. Manual registration

To perform a manual point cloud registration, the surveyed point clouds must first be imported into a dedicated point cloud software. In this thesis, the applied software was *Leica Cyclone*. During the importation step, most software tools include a decimation feature, which may be used to perform the first task and homogenize the point cloud to the target resolution. If no such feature is available during importation, the simplification is done after all point clouds are imported. Different software tools use different algorithms for simplification; however, popular simplification algorithms include voxel downsampling [660] and Poisson Disc Sampling [661].

With the point clouds decimated, the cleaning process ensues. Point cloud management software applications are equipped with various tools to eliminate noise, such as fence, select, and delete. Figure 3.13 illustrates the cleaning process using the identified tools, while Figure 3.14 displays the same point cloud before and after cleaning. As seen in these figures, deleting all the unwanted points can be a laborious task.

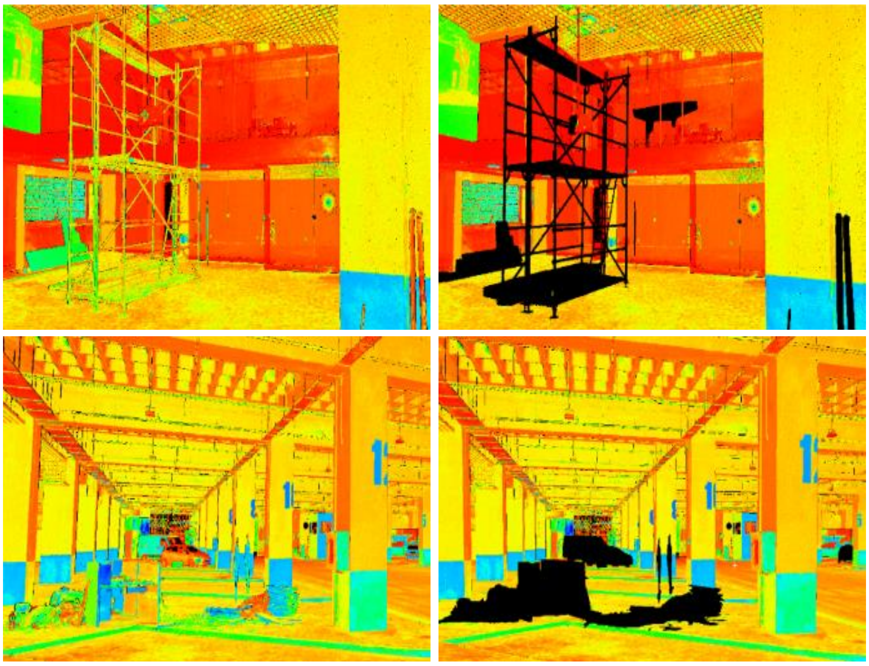

Figure 3.13 – Two point cloud examples undergoing the elimination of unwanted points

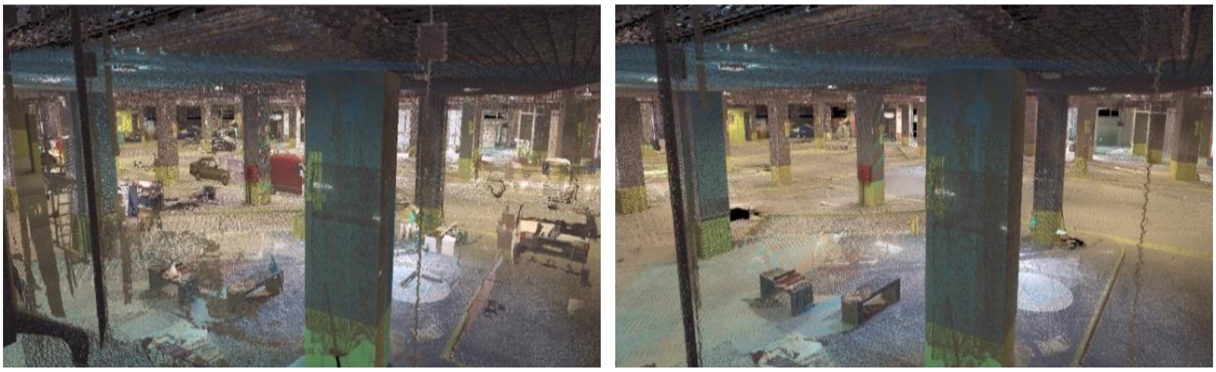

Figure 3.14 – Example of a point cloud before (left) and after (right) completing the cleaning task

After eliminating all the identified noise, the registration process first requires establishing links between the performed scan stations. These links indicate to the software which scan stations share portions of their point clouds. All scan stations must be linked into a single scan station network to allow for a complete registration. With all links created, point cloud software tools typically require establishing constraints between linked scan stations. These constraints merge the different point clouds using at least three pairs of non-collinear points, which are manually indicated. Figure 3.15 showcases this process, with the user searching both points clouds at the bottom of the figure for non-collinear points. With the points established, the software searches their vicinity, trying to determine a proper match. After multiple manual constraints, the software automatically suggests and generates new constraints using the relative positions of the previously constrained point clouds.

Finally, with registration complete, the unification is performed by simply selecting this feature in the software. During this task, some software tools present an option for keeping or deleting overlapping points. The latter option is preferable since there is no advantage in keeping duplicates.

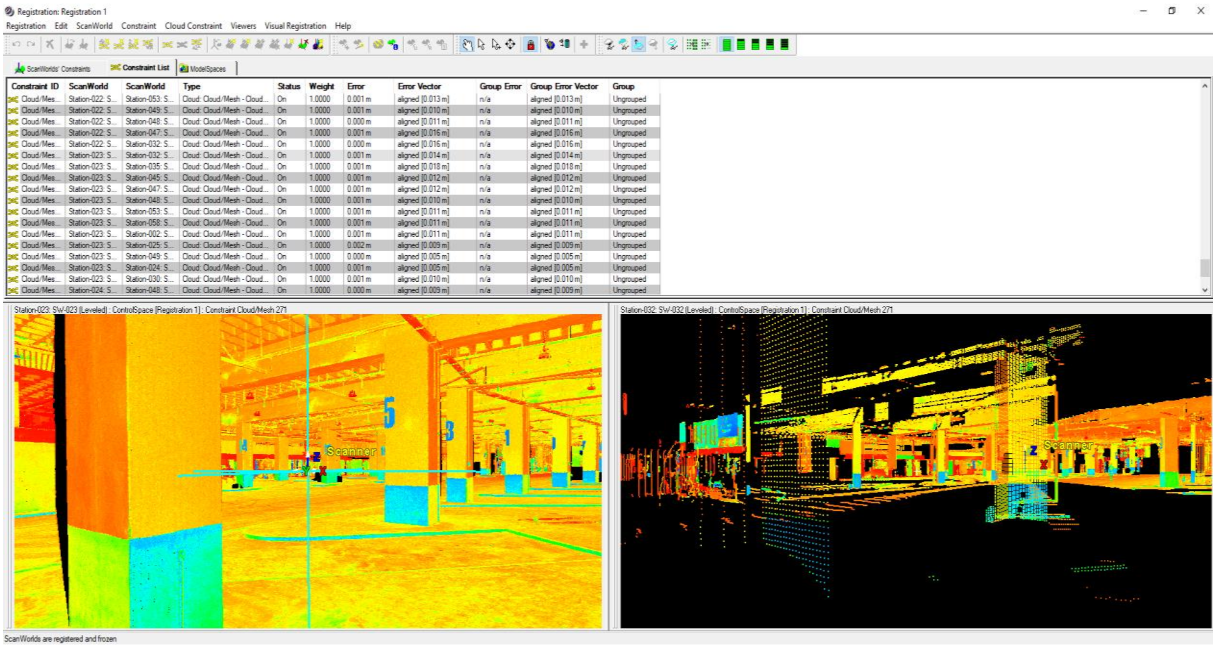

Figure 3.15 – Registration process in *Leica Cyclone*

3.4.1.2. Automatic registration

To perform the automatic point cloud registration, an ML model was developed to perform each of the four tasks consecutively. The model starts by simplifying all acquired point clouds by using the voxel downsampling algorithm [660]. This algorithm was selected over Poisson Disc Sampling [661] purely for preference reasons, since no impactful difference was noted when testing both algorithms. The developed algorithm was adapted from pseudo-code seen in [660].

With the point clouds decimated, the cleaning process is performed by applying a statistical outlier removal algorithm [660], meaning that relatively isolated points are considered noise. This assumption introduces some degree of bias, yet, in the tested scenarios, the algorithm performed the noise removal correctly, thus being selected. It should be stated that a second algorithm for cleaning was tested, namely, the radius outlier removal proposed in [662]. However, this second algorithm removed useful information in the tested scenarios, thus not being selected. The pseudo-code from which the algorithm was adapted can be seen in [660]. Figure 3.16 showcases the application of this algorithm.

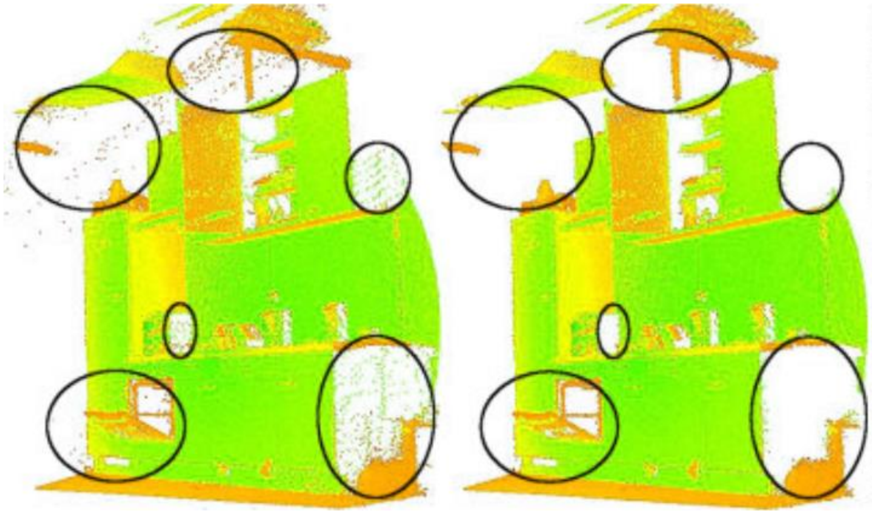

Figure 3.16 – Illustrative application of the statistical outlier removal algorithm. Adapted from [663]

After eliminating all the identified noise, the registration process ensues. As stated in the literature review, AI registration methods are typically divided into global and local registration methods. While the second generally results in more precision, it is also more computationally intensive. To solve this issue, the author proposes using a mixed approach, where a global registration is initially applied to produce a loose alignment of the point clouds and, afterwards, a local registration is employed to refine and tighten the alignment.

For the global registration, an algorithm based on Rusu et al. [394] Fast Point Feature Histograms (FPFH) was developed. The algorithm first computes the FPFH for each point p_i^j in the surveyed point cloud v_j, where p_i^j correspond to the i^{th} point in the j^{th} surveyed point cloud. This results in the acquisition of a 33-dimensional feature vector that describes the local geometry around each examined point. Then, RANSAC is applied to register the point cloud. The selected RANSAC parameters are based on Choi et al. [664]. In each RANSAC iteration, four points are randomly picked from the base point cloud v_j, and their corresponding points in the target point cloud v_{j+1} are acquired by querying the respective nearest neighbours in the FPFH feature space. Pruning algorithms are applied to accelerate this process and quickly disregard false matches, as suggested in [665]. To identify v_j and v_{j+1} the algorithm uses the stipulated links during the planning of the survey – thus the importance of duly noting any modifications to the survey plan in Module 2.

With the point clouds loosely aligned, the Point-to-Plane variation of ICP, proposed in [396], is applied to refine the global alignment. This algorithm consists of two iterative steps: one for data correspondence between the base and target point clouds; and a second step to compute the transformation between both clouds, based on the performed data association.

The objective is to find the correspondence set $C = \{(p_i^j, p_i^{j+1})\}$ transformed with the current transformation matrix T, and update T so that the objective function $E(T)$, defined over the correspondence set C, is minimized:

$$E(T) = \sum_{(p_i^j, p_i^{j+1}) \in C} \left(\left(p_i^j - T p_i^{j+1}\right) \cdot n_{p_i^j} \right)^2 \tag{3.4}$$

, where $n_{p_i^j}$ is the normal of point p_i^j.

With v_j, and v_{j+1} tightly aligned, the point clouds are unified by simply applying the voxel downsampling algorithm used during the simplification task to eliminate duplicate points and save the point clouds as one aligned point cloud V. This process continues with the alignment between V and v_{j+2}. The registration process ends when V is aligned with the last point cloud in the scan station network.

3.4.2. Point cloud segmentation

As stated at the beginning of the present module, the developed DL networks rely on an existing backbone network and primitive. As such, for a better understanding of the developed models, these are respectively covered in Section 3.4.2.1 and Section 3.4.2.2, before tackling the semantic, instance, and part segmentation in Section 3.4.2.3, Section 3.4.2.4, and Section 3.4.2.5, respectively.

3.4.2.1. Backbone network: PointNet

The term backbone is typically used to refer to the feature extractor network, which researchers frequently adopt from previous works for two main reasons: (1) historic success; and (2) the time-consuming and challenging nature of performing ablation studies for network architecture optimization.

In this thesis, PointNet [556] was the selected backbone to extract the local and global features, given its pioneering status and importance as a milestone in point cloud deep learning [494, 573].

As displayed in Figure 3.17, PointNet's architecture can be divided into two portions: the classification network and the segmentation network. Both share a large section of their structures, with the second effectively extending the first.

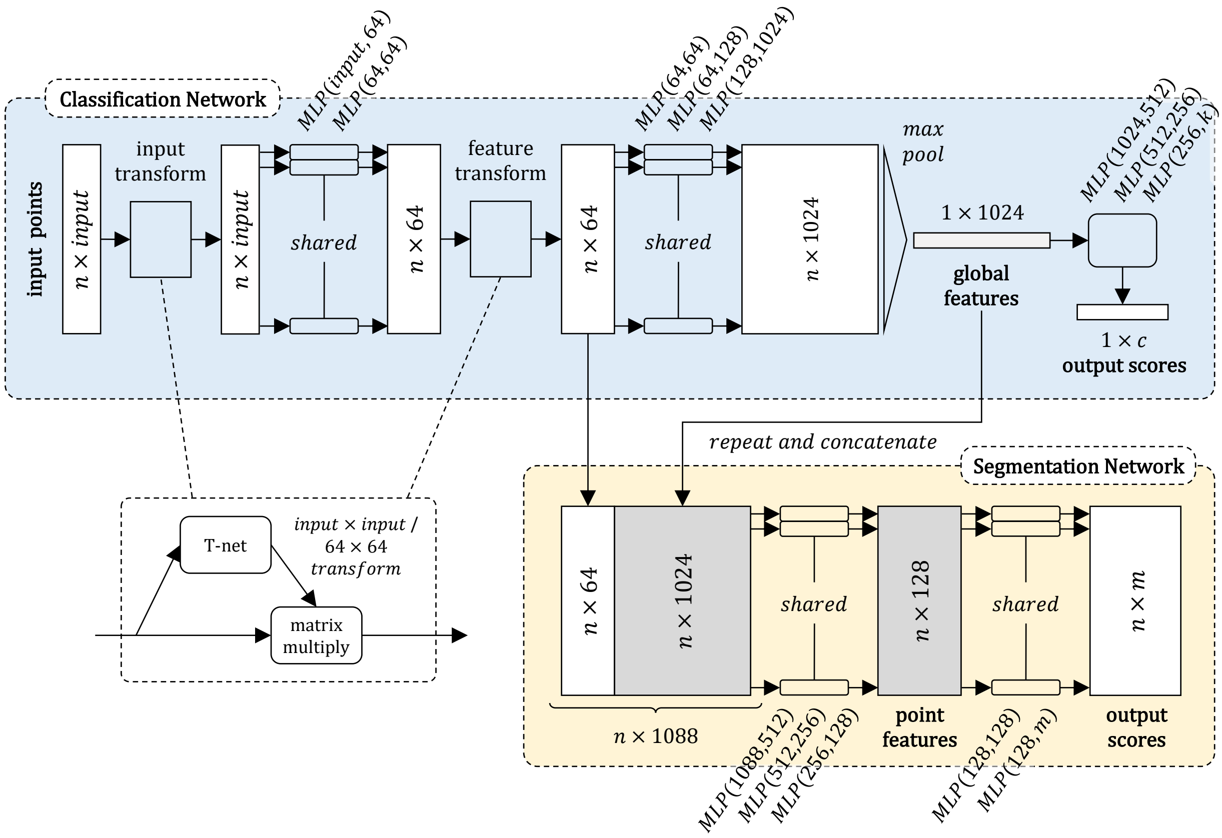

Figure 3.17 – PointNet architecture. Adapted from [556]

PointNet starts by receiving n points with $input$ dimensions (the latter being dependent on the number of existing point features), subsequently applying input and feature transformations, as well as shared MLPs, to acquire per-point features. The input and feature transformations are achieved through a mini-network, T-net, which resembles PointNet itself and has its own basic modules of point independent feature extraction, max pooling and fully connected layers. For more information on T-net and shared MLPs, see [556, 557].

The acquired per-point features are then aggregated into a global feature vector through the symmetric function max pooling. Max pooling takes n vectors as input and outputs a new vector invariant to the input order, thus making the model invariant to input permutation. Essentially the network learns a set of optimization functions that identify noteworthy points of the point cloud and encode the reason behind their selection. This is an essential step in PointNet, whose core idea is to approximate a general function defined on a point set by applying a symmetric function on transformed elements in the set:

$$f(\{p_1, \dots, p_n\}) \approx g\big(h(p_1), \dots, h(p_n)\big) \tag{3.5}$$

, where $f : 2^{\mathbb{R}^N} \to \mathbb{R}$, $h : \mathbb{R}^N \to \mathbb{R}^K$ and $g : \underbrace{\mathbb{R}^K \times \dots \times \mathbb{R}^K}_{n}$ is a symmetric function used to solve the unordered nature of point clouds.

The introduced MLPs approximate h, representing the per-point local features, while g, representing the global features, is approximated by a single variable function and max pooling composition.

After acquiring the global features, the classification and segmentation networks diverge. In classification, output scores for c classes are produced by aggregating the learnt global descriptor using shared MLPs. In segmentation, the global features are concatenated with per-point local features that have been previously stored, subsequently extracting new per-point features from the combined knowledge of both local and global descriptors. This last process is also done through MLPs, with the resulting output being a collection of $n \times m$ scores for each of the n points and the m semantic labels.

3.4.2.2. Primitive: Point-Voxel Convolution

PVConv was the chosen primitive to be used in the developed DL networks. This primitive was introduced by Liu et al. [542] to tackle the large memory and computation overheads in the current state-of-the-art networks. It successfully achieved this objective, outperforming several existing networks with 10× lower memory consumption and 7× speedup, while achieving better evaluation metric scores in segmentation tasks. To do so, as the name implies, PVConv combines the advantages of point-based and voxel-based methods to, respectively, reduce the memory footprint through point cloud sparsity and obtain a contiguous memory access pattern through voxel-based convolution.

As illustrated in Figure 3.18, PVConv is composed of two separate branches. The lower branch tackles the voxel-based portion of PVConv, while the upper branch tackles the point-based portion. The lower branch focuses on acquiring low-resolution information (per voxel), while the upper branch focuses on high-resolution information (per-point). Both branches are merged at the end of PVConv, resulting in per-point features which contain both the acquired aggregated neighbourhood information (lower branch) and the extracted individual point features (upper branch). These two portions of information complement each other. Both branches are thoroughly examined in the following sections. Their architectures are detailed in Figure 3.19.

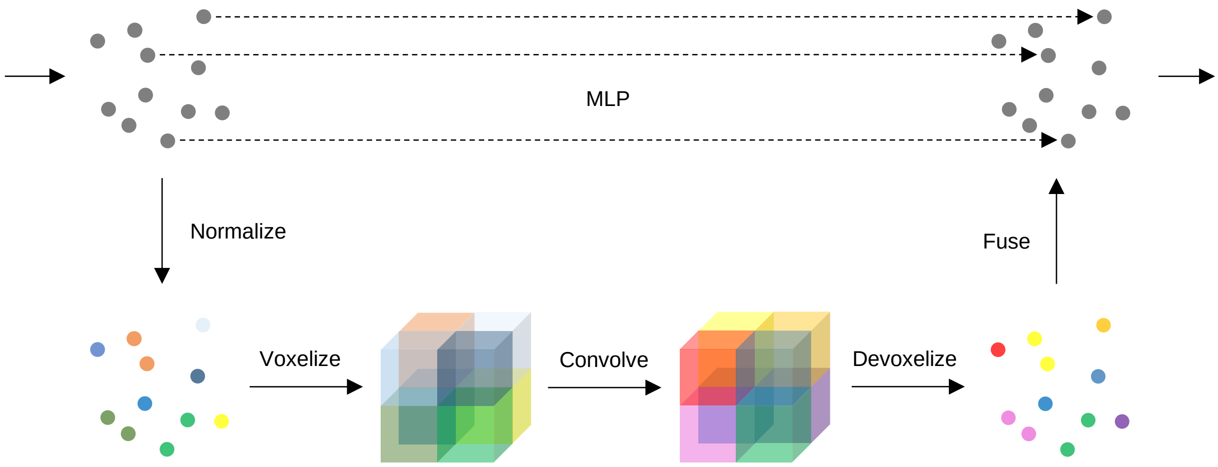

Figure 3.18 – PVConv. Adapted from [542]

3.4.2.2.1. Lower branch: Aggregated neighbourhood information

The lower branch of PVConv aggregates the neighbourhood information to extract the points' local features, meaning information regarding the points' surroundings. This task is performed in the volumetric domain instead of the point domain, given its inherent regularity.

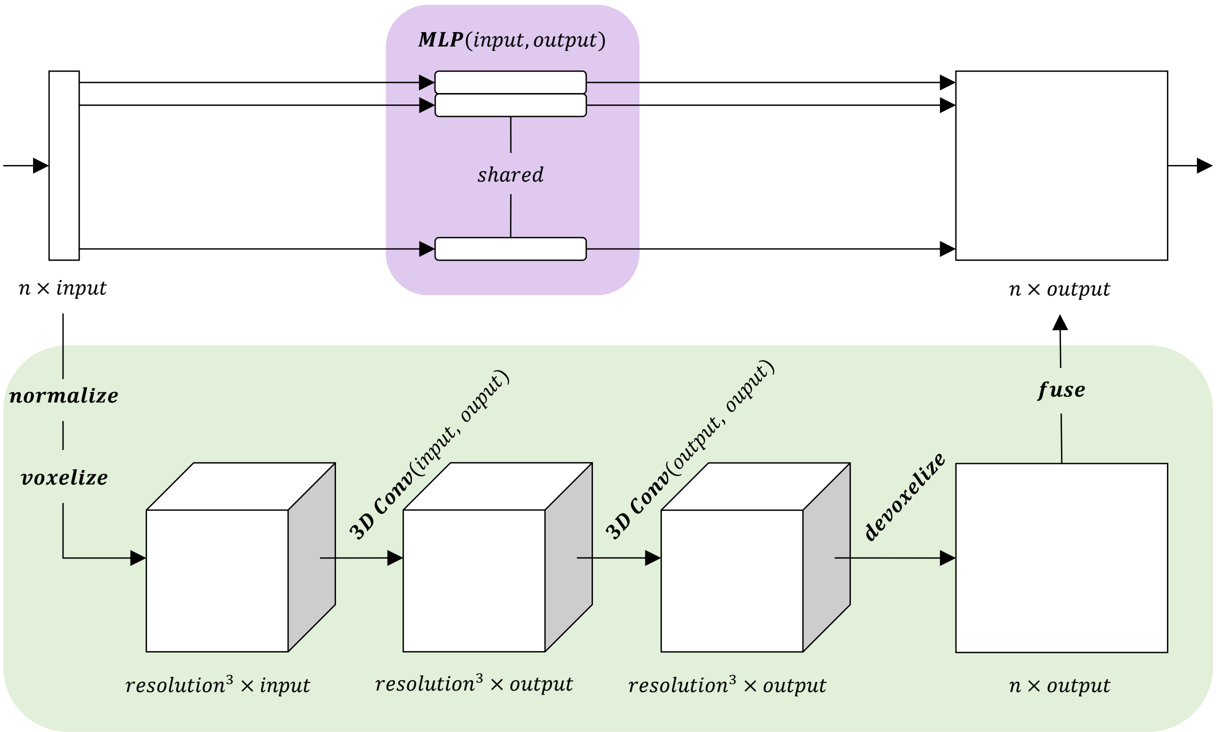

Figure 3.19 – PVConv architecture. Operations are denoted in italic bold, while layer sizes are solely italic

To adequately explain this branch, let us denote a 3D point as $p = \{p_i\} = \{(c_i, f_i)\}$, where c_i signifies the 3D coordinate of the i^{th} input point and f_i its corresponding features. Initially, the n input points are normalized to account for different point cloud scales. This procedure only affects the points' 3D coordinates $\{c_i\}$, with the respective features $\{f_i\}$ remaining unchanged. The normalized coordinates are denoted as $\{\hat{c}_i\} = \{(\hat{x}_i, \hat{y}_i, \hat{z}_i)\}$.

After the normalization process, voxelization ensues. As explained in Section 2.5.4.2, voxelization is the process by which points are aggregated into low-resolution voxels, here denoted as $\{V_{u,v,w}\}$. These voxels are created by averaging the features $\{f_i\}$ of points whose normalized coordinates $\{\hat{c}_i\}$ fall into the voxel grid (u, v, w), as per Equation 3.6:

$$V_{u,v,w} = \frac{1}{N_{u,v,w}} \times \sum_{i=1}^{n} f_k \times \mathbb{I}[floor(\hat{x}_i \times r) = u, floor(\hat{y}_i \times r) = v, floor(\hat{z}_i \times r) = w] \tag{3.6}$$

, where $N_{u,v,w}$ denotes the normalization factor (i.e. number of points within the voxel grid), $\mathbb{I}[\cdot]$ the binary indicator (i.e. whether $\{\hat{c}_i\}$ falls into the voxel grid), and r the voxel resolution.

With the points converted into voxels, a stack of two 3D volumetric convolutions is applied to aggregate the voxel-based features. These convolutions are identified in Figure 3.19 as $3D\ Conv$, each containing two parameters within brackets. These parameters indicate the input and output dimensions of each layer, respectively. Each convolution is followed by a batch normalization [666] and a nonlinear activation function [462]. The chosen function is Leaky Rectified Linear Function (LReLU) [462] to prevent possible dead neurons. For more information on this problem, see [667].

Finally, to allow merging the acquired voxel-based features with the individual point features from the upper branch, a devoxelization process is performed to return the acquired voxel-based features to the point cloud domain. In the original article [542], the authors discuss two different devoxelization processes, deciding on a trilinear interpolation [668]. This approach guarantees that each point is mapped with distinct features. The resulting features are denoted as $\{f_i^{voxel}\}$.

3.4.2.2.2. Upper branch: Individual point features

With the points' local features $\{f_i^{voxel}\}$ acquired, the upper branch focuses on extracting the individual points' features, denoted as $\{f_i^{point}\}$. To do so, the upper branch directly operates on each n input point to extract its distinctive information using a shared MLP model. As indicated in [556, 557], this shared MLP is implemented using a series of 1D convolutions, batch normalization and ReLU operations. As seen in Figure 3.19, the shared MLP also presents two parameters within brackets, once again indicative of the input and output dimensions. It should be stated that the convolutions are configured so that the weights are shared across the input point cloud.

3.4.2.2.3. Branch merger: Point-Voxel features

Since both branches provide complementary information, at the end of PVConv, the aggregated neighbourhood information and individual point features can be merged through a simple concatenation. The resulting output features are denoted as $F_i = \{f_i^{voxel}, f_i^{point}\}$, with the n output points of PVConv being represented as $p = \{p_i\} = \{(c_i, F_i)\}$.

3.4.2.3. Semantic segmentation

Using the selected backbone and primitive, the network seen in Figure 3.20 was developed for semantic segmentation. The network has clear parallels to its backbone, PointNet, maintaining (1) the increasing level of abstraction throughout its layers; (2) the use of a max pooling layer to aggregate information from all points into the global descriptor; and (3) the concatenation of the acquired global feature vector with previously extracted point features – which is then used to extract new point features while aware of both local and global information. The input and output are also the same, with the former being a point cloud of n points with $input$ dimensions (e.g. 3D coordinates, RGB colour values, normal vector, intensity) and the latter a collection of $n \times m$ scores for each of the n input points and the m semantic labels (e.g. wall, ceiling, floor, beam, column).

The remaining portions of the network are, however, significantly different. In particular, in the feature extraction portion of the network (shaded blue in Figure 3.20), the original transforms and shared MLPs in PointNet are replaced with PVConv. Additionally, instead of storing only one layer of the acquired per-point local features, all layers are stored to acquire information regarding different voxel resolution levels. The utilized resolutions can be seen in Figure 3.20, where PVConv modules show, between brackets, from left to right, the volumetric convolution input channels, output channels, and resolution. Similarly, shared MLPs and normal MLPs also display, between brackets, from left to right, their input and output channels.

As in PVConv, the used shared MLPs are constituted by a 1D convolution, followed by batch normalization and a ReLU activation function. Normal MLPs are identical apart from the use of a fully connected layer instead of the convolution.

The kernel size is 3 for 3D convolutions and 1 for 1D convolutions. In 3D convolutions, the padding and stride are also set to 1.

It should be stated that a dropout ratio of 0.3 is used between the last three shared MLPs to prevent overfitting [669]. Additionally, no batch normalization or activation functions are used in the last layer.

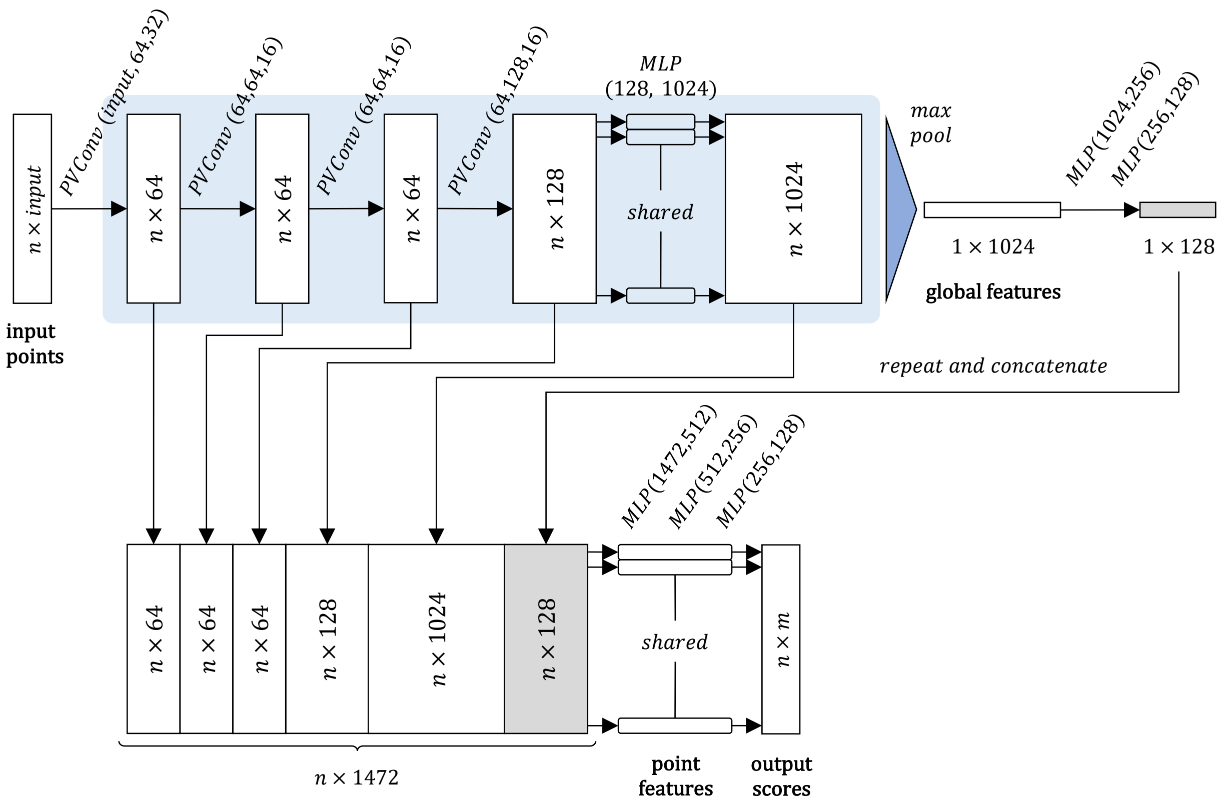

Figure 3.20 – Semantic segmentation network's architecture

3.4.2.4. Instance segmentation

Through the semantic segmentation network presented in the previous section, each of the n input points p is associated with one of m semantic labels S (e.g. wall, ceiling, floor, beam, column). The chosen semantic label for each point is the one producing the highest score in the output score matrix. As such, $p = \{p_i\} = \{(c_i, f_i, S_i)\}$, where S_i signifies the semantic label of the i^{th} input point. All points with the same semantic label S belong to the same building element class.

Using this information, the n points can be partitioned into m individual point clouds v_k, representative of the existing instances, so that $n = (v_1, v_{k,} \dots, v_m)$ and $v_k = \{p_i\} : S_i = S_k$.

These point clouds can then be separately analysed for instance segmentation. Two different approaches were tested to accomplish instance segmentation.

The first approach was heavily influenced by the research presented by Pham et al. [491]. In this approach, the previously proposed network was slightly modified to further output an instance label I, representing a instance object (e.g. wall one, wall two). As such, $p = \{p_i\} = \{(p_i, f_i, S_i, I_i)\}$, where I_i signifies the object instance of the i^th input point. All points with the same instance label I belong to the same building element object.

To accomplish this, the loss function proposed in the original PointNet [556] and applied in the semantic segmentation network was modified to the one presented in Equation 3.7:

$$\mathcal{L} = \mathcal{L}_{prediction} + \mathcal{L}_{embedding} \tag{3.7}$$

, where the prediction loss $\mathcal{L}_{prediction}$ is defined by the cross-entropy as usual, and $\mathcal{L}_{embedding}$ is a discriminative loss function inspired by [670]. This embedding loss is calculated using three different losses, as shown in Equation 3.8:

$$\mathcal{L}_{embedding} = \alpha \cdot \mathcal{L}_{pull} + \beta \cdot \mathcal{L}_{push} + \gamma \cdot \mathcal{L}_{reg} \tag{3.8}$$

The embedding loss can be intuitively perceived as a mechanism where $\mathcal{L}_{pull}$ attracts the point embeddings towards the instance centroids and the $\mathcal{L}_{push}$ keeps these centroids apart from each other. The regularisation loss $\mathcal{L}_{reg}$ acts as a small force that draws all centroids towards the origin. For more information on this function, see [670] and [491].

Initially, after preliminary tests, this approach seemed a viable solution. However, after extracting the instance segments' geometric data (Section 3.4.3) and automatically modelling the segments in BIM (Module 4), it was concluded that this approach would not output the desired results, since it led to several cases of stacked elements in the final BIM model.

This stacking problem derives from mislabelled points, typically near an object's boundary, as illustrated in Figure 3.21. The illustration attempts to represent the mislabelling of a chair's point as the origin of the problem, leading to the stacking of the resulting chair and table BIM elements.

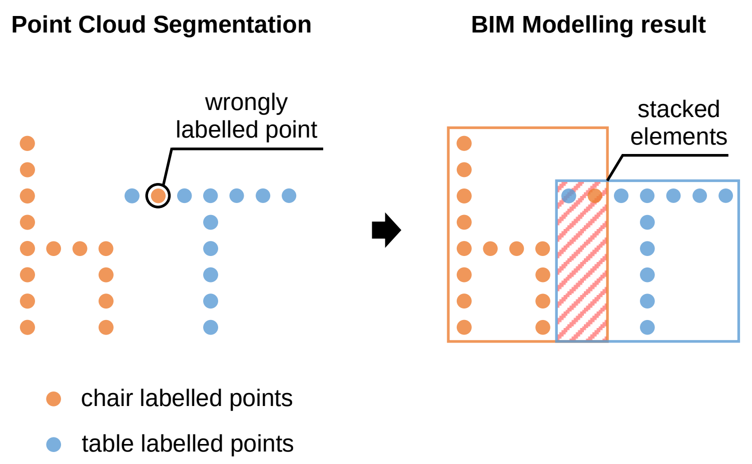

Figure 3.21 – Illustration of the stacking problem originated from the first segmentation approach

Such cases could be avoided by post-processing the instance segmentation results with clustering techniques; however, it seems easier and more efficient to apply these clustering techniques from the beginning as the instance segmentation approach. This was the basis for the second tested method.

As such, following this first approach, the second approach continued previous research works by the thesis' author [33, 671], where an unsupervised clustering model based on the DBSCAN [424] was developed and applied to fully segment a single room of reduced dimensions and simple architecture (i.e. orthogonal walls, floor and ceiling). Work on this approach had been halted, given DBSCAN propensity to over-segmentation in high-density, complex rooms, without resorting to higher dimensions embeddings where this algorithm could be applied successfully – a process that would result in large computational overheads as already discussed in Section 2.5.3.3.

However, by applying DBSCAN after the initial semantic labelling, this problem is effectively circumvented, since most instances of the same class are already well defined in space. As such, DBSCAN was the chosen algorithm to perform the point cloud instance segmentation. The complete pseudo-code from which the DBSCAN implementation was based can be seen in [672], with a few modifications based on [673] being applied for optimization. A quick summary is presented in the following paragraphs.

Facing a point cloud v_k, DBSCAN starts by selecting a point p_i as an initial seed, denoted as $\bar{p}_i$. Then, all $\bar{n}$ neighbouring points within distance d, provided by the user, are identified. If the number of neighbouring points is larger than a user-predefined threshold $\bar{T}$, so that $\bar{T} \geq |\bar{n}|$, then $\bar{p}_i$ is regarded as a core point, and a cluster is former. This cluster includes the core point itself and all its neighbouring points. If the threshold is not surpassed, the point is regarded as noise, eliminated, and the algorithm will advance to a new randomly selected seed, which was not yet visited. In the first scenario, the neighbouring points will be defined as new seeds $\bar{p}_i$ from which a new search for $\bar{n}$ neighbouring points within distance d is performed. If one of these new seeds has sufficient neighbouring points to surpass the user-predefined threshold, these neighbouring points are also added to the cluster. This process is repeated until no more neighbouring points can be added to the cluster. At which point the algorithm will search for a new randomly selected seed $\bar{p}_i$ that was not yet visited, repeating the same process to create a new cluster. DBSCAN stops when all points have either been attributed to an instance cluster $p = \{p_i\} = \{(p_i, f_i, S_i, I_i)\}$ or eliminated by being classified as noise.

Figure 3.22 attempts to illustrate DBSCAN workflow, where d represents the user specified search distance, C represents the red cluster's core point, points A and B are being analysed to be included in the red cluster, and point N is already identified as noise.

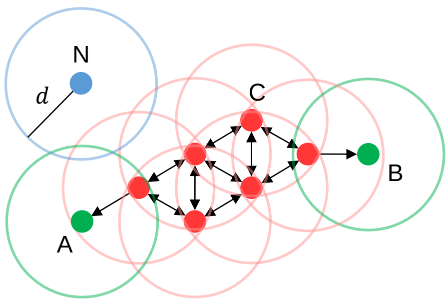

Figure 3.22 – Illustration of the DBSCAN algorithm. Adapted from [672]

3.4.2.5. Part segmentation

Regarding part segmentation, the DL network approach was once again followed. As such, by applying the selected backbone and primitive, the network seen in Figure 3.23 was developed. This network's architecture is similar to the previous network in Section 3.4.2.3; however, this time, the network displays an increased number of neurons in its layers, which are concatenated with the global features and a new one-hot vector. This one-hot vector indicates the points' semantic labels S previously acquired.

PVConv, shared MLP and regular MLP modules all retain their specifications. However, the dropout ratio is decreased to 0.2, instead of the previous 0.3. Additionally, although the input is the same, a point cloud of n points with $input$ dimensions, the output is different, this time corresponding to a collection of $n \times l$ scores for each of the n input points and the l part labels P.

The chosen part label for each point is the one producing the highest score in the output score matrix. As such, $p = \{p_i\} = \{(c_i, f_i, S_i, I_i, P_i)\}$, where P_i signifies the part label of the i^{th} input point. All points with the same part label P belong to the same building element part.

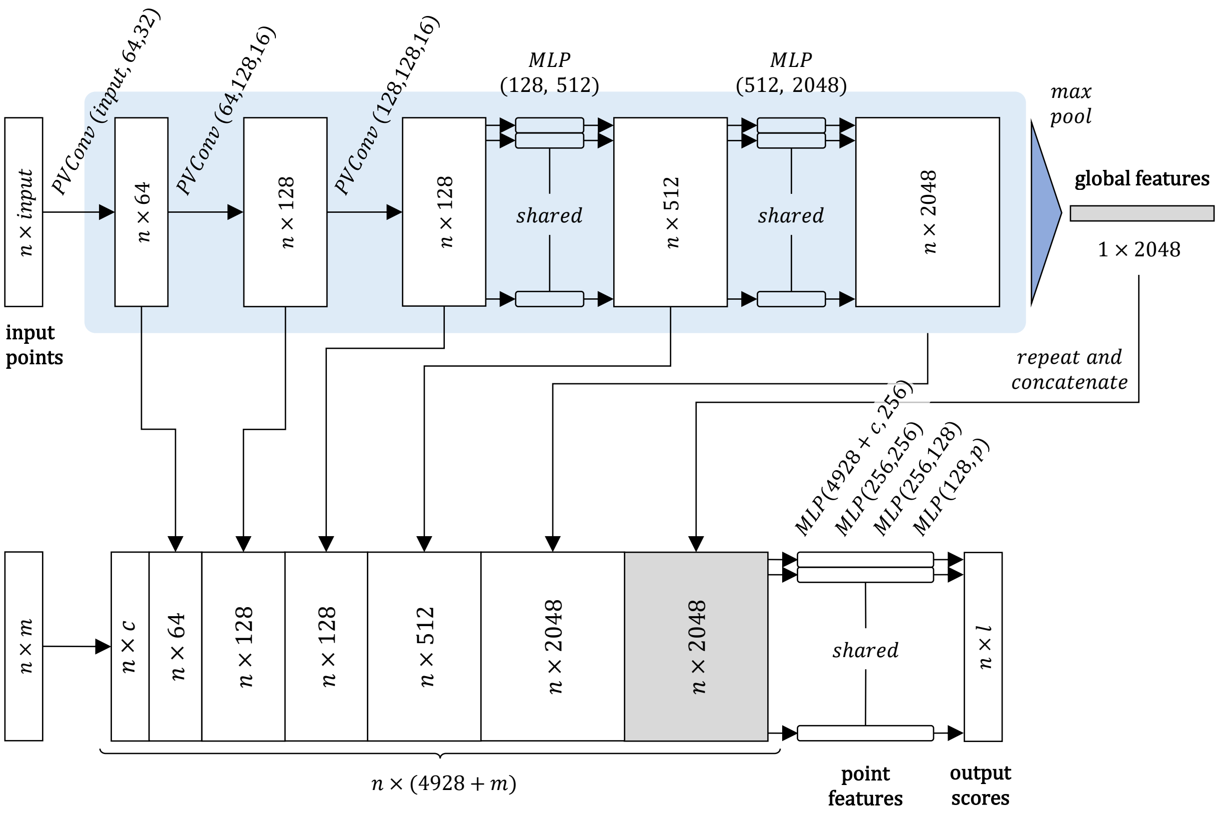

Figure 3.23 – Part segmentation network's architecture

3.4.3. Segment characterization

With the point cloud segmentation complete, all points in a point cloud are now associated with a semantic (i.e. building element), instance (i.e. object), and part label. The point cloud has also been successfully divided into m point clouds v_k, representative of the existing instances. A similar process is performed for each instance point cloud v_k, where these are subdivided into l point clouds v_u, representative of their constituting parts, so that $v_k = (v_1, v_{u,} \dots, v_l)$ and $v_u = \{p_i\} : P_i = P_u$.

With all these point clouds acquired, two different characterization processes ensue. The first aims to characterize the instance point clouds v_k according to their geometric information. The second aims to characterize the part point clouds v_u according to their surface-related information. These processes are respectively explored in Section 3.4.3.1 and Section 3.4.3.2.

3.4.3.1. Segment geometric characterization

The geometric characterization of the instance point clouds aims to acquire the required geometric information to model the identified building elements inside a BIM environment. To do this, two main algorithms were applied: RANSAC [399] and a generic bounding box algorithm. The bounding box algorithm was used in all tested building element classes while RANSAC was only applied in a selected few, namely: walls; floors; ceilings; beams; doors; tables; boards; and stairs. These were building element classes where the prior definition of planes could increase the bounding box generation's accuracy by creating well-defined surface limits.

For instance, Figure 3.24 exemplifies the application of RANSAC for the definition of a table top's plane, which is then used to create a bounding box. This bounding box serves as an auxiliary tool to generate the table's geometry inside the BIM environment, where the floor elevation defines the table's bottom limit, and the top and lateral limits are defined by the corresponding limits in the auxiliary bounding box.

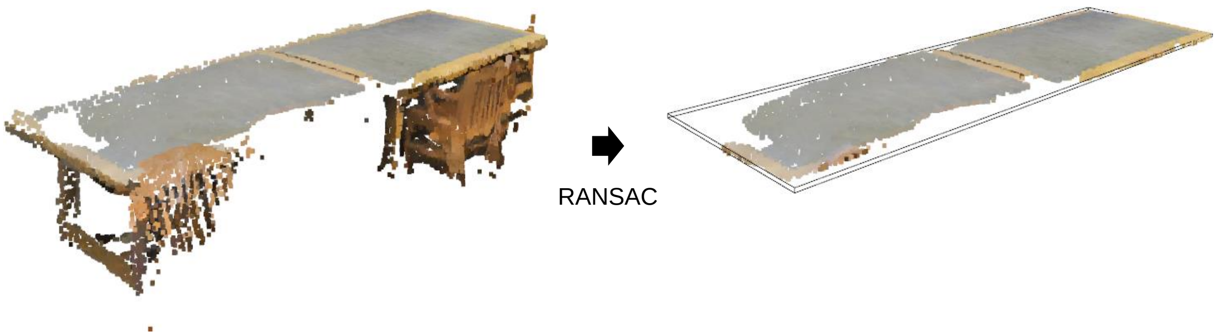

Figure 3.24 – Example of RANSAC application for geometric characterization

The RANSAC algorithm's application was similar for the remaining identified elements classes except for the "stairs" class, where its use focused on the identification of risers and treads, essentially acquiring the needed information to count the stairs' steps.

As for the bounding box algorithm, two different bounding box types were thoroughly tested. These were:

- axis-aligned minimum bounding box (AABB);
- and object-oriented minimum bounding box (OOBB);

Both bounding boxes attempt to identify the minimum volume to enclose all points within a cuboid shape, differing in their limits' alignment: AABB has its limits aligned with the coordinate system's axes, while OOBB has its limits aligned to the object primary orientations.

A third bounding box type based on the element's convex hull was also assessed. However, this approach was quickly deemed overly complex for the tackled problem, since the resulting surfaces (see Figure 3.25) would decrease the developed BIM modelling tool efficiency and over-complicate the BIM model generation and design.

Figure 3.25 showcases the different results in the application of these algorithms. Open3D library [674] was used to implement all three approaches during testing, albeit with slight modifications to improve their performance. Through testing, OOBB was selected as the used bonding box type, since it resulted in a better fit for the building elements.

With the instance segments' bounding boxes acquired, their height, length, width, volume, and centre can be easily extracted. A JavaScript Object Notation (JSON) file (structure illustrated in Figure 3.26) is used to store this information alongside the instance (*instance_class* + *instance_id*) and semantic labels (*instance_class*). This file is sent to Module 4.

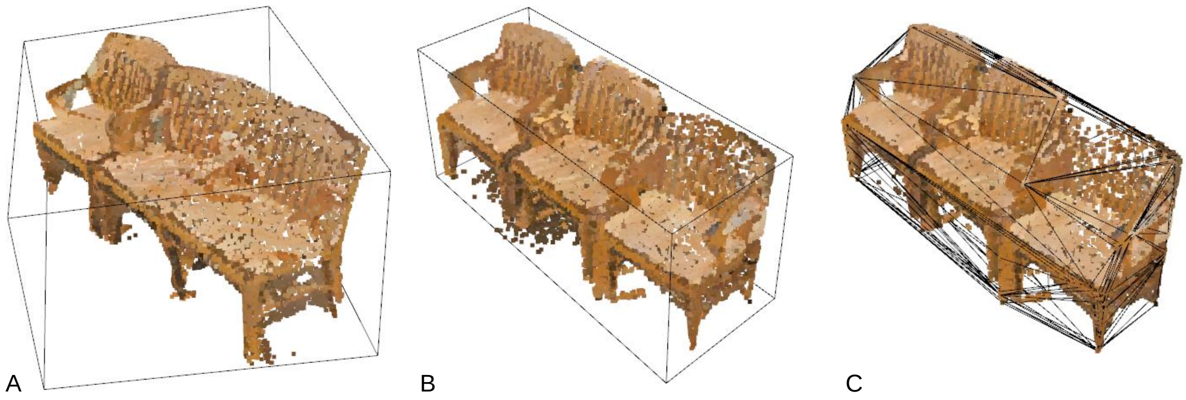

Figure 3.25 – Tested bounding boxes algorithms: AABB (A); OOBB (B); and convex hull (C)

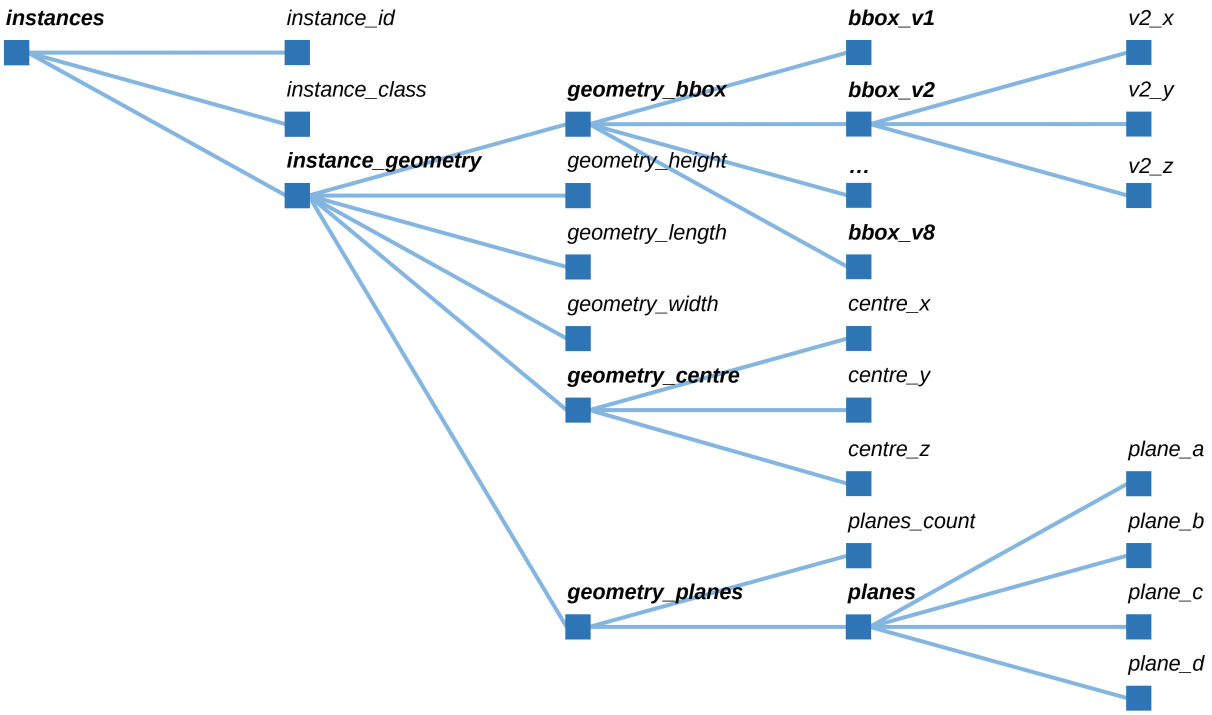

Figure 3.26 –JSON file structure containing the segment geometric information

3.4.3.2. Segment surface characterization

The surface characterization of the part point clouds aims to acquire the required information to identify the surface material in Module 5.

Three surface characteristics were acquired from the part point clouds to accomplish this characterisation: surface roughness, reflectance, and colour. Their determination was based on Yuan et al. [659] work and requires that each point contains information regarding its 3D coordinates, RGB values, and intensity value – all standard information in point clouds acquired through laser scanning.

It should be stated that although these characteristics are used to describe the point cloud surface, their determination is done per-point. Each characteristic is tackled separately in the following sections

3.4.3.2.1. Surface roughness

As stated in Valero et al. [675], the surface roughness R measures the irregularity of an area. This roughness can be calculated for a given point p_i using Equation 3.9:

$$R_i = \sqrt{\frac{1}{N}\sum_{j=1}^{N}\left(d_j - \mu\right)^2}\,, with\ \mu = \frac{1}{N}\sum_{j=1}^{N} d_j \tag{3.9}$$

Essentially, R_i is calculated as the standard deviation of the orthogonal distances d_j between the j^{th} neighbouring point and a plane F fitting all N neighbouring points. The neighbouring points are identified by establishing a bounding box centred on p_i, with dimensions $s_1 \times s_1 \times s_1$. The fitted plane F is determined through RANSAC and can be expressed as $Ax + By + Cz + D = 0$. The distances d_j are calculated using a simple point to plane distance, as seen in Equation 3.10:

$$d_j = \frac{\left|Ax_j + By_j + Cz_j + D\right|}{\sqrt{A^2 + B^2 + C^2}} \tag{3.10}$$

Figure 3.27 illustrates the process of calculating the surface roughness.

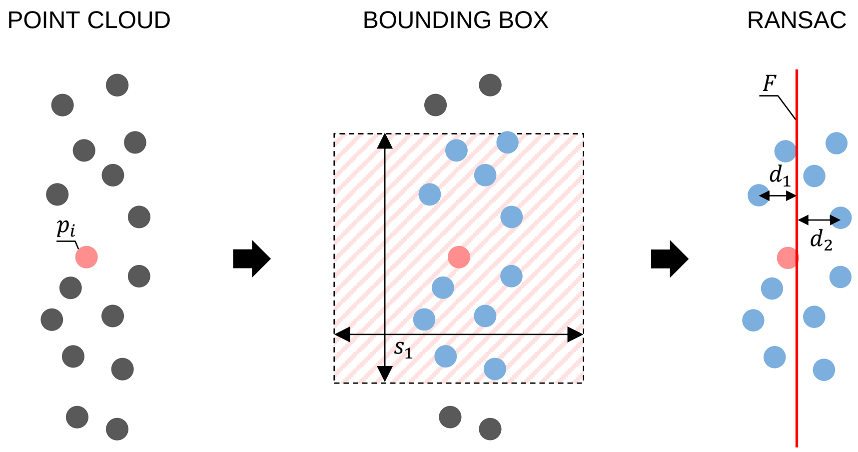

Figure 3.27 – Surface roughness R based on the distances of the N neighbouring points to the fitted plane F

3.4.3.2.2. Surface reflectance

As stated in [659, 676, 677], the surface reflectance ρ for a a given point p_i can be determined, or at least approximated, through the examination of its intensity value I_i.

Following the workflow presented in [659] and according to [678], a point's received intensity value I_r can be obtained as the laser power per unit area:

$$I_r = \frac{P_r}{\Delta S} \tag{3.11}$$

, where P_r is the received laser signal power and ΔS is the unit area. P_r can be determined using Equation 3.12 [679]:

$$P_r = \frac{P_t D_r^2}{4\pi R^4 \beta_t} \eta_{sys} \eta_{atm} \sigma \tag{3.12}$$

, where P_t designates the transmitted power, D_r corresponds to the receiver aperture diameter, R equals the range from the laser scanner to the target, β_t is the laser beam width, η_{sys} is the system transmission factor, η_{atm} is the atmospheric transmission factor, and σ is the effective target cross-section.

According to Höfle et al. [679], Equation 3.12 can be simplified into Equation 3.13:

$$P_r = \frac{P_t D_r^2 \rho}{4R^2} \eta_{sys} \eta_{atm} \cos\theta \tag{3.13}$$

, where θ corresponds to the incident angle between the laser beam and the scanned point. An in-depth explanation on this simplification can be seen in [659, 679]. By combining Equation 3.11 and Equation 3.13, Equation 3.14 is acquired:

$$I_r = \frac{P_t D_r^2 \rho}{4R^2 \Delta S} \eta_{sys} \eta_{atm} \cos\theta \tag{3.14}$$

Since P_t, D_r, ΔS, and η_{sys} can be fixed for the same laser scanner, and η_{atm} can be regarded as a constant for the same scanned region, these variables can be exchanged by the coefficient K:

$$I_r = \rho K \frac{\cos\theta}{R^2} \tag{3.15}$$

However, as noted by Yuan et al. [659], previous studies [680, 681] identify that I_r and $\cos\theta / R^2$ present linear relationships and are not proportional. As such, according to these studies, Equation 3.15 should be expressed as:

$$I_r = \rho K \frac{\cos\theta}{R^2} + b \tag{3.16}$$

, where b is a constant term. Finally, by following the illustration seen in Figure 3.28, I_r can be obtained as:

$$I_r = \rho K \frac{\sqrt{\frac{x^2 + y^2}{x^2 + {}^2 + z^2}}}{x^2 + y^2 + z^2} + b \tag{3.17}$$

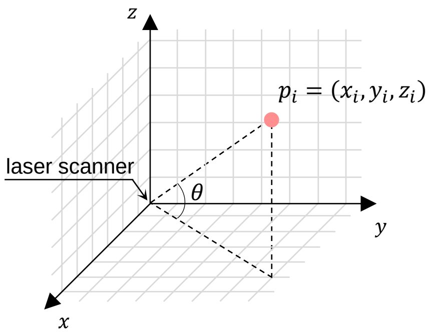

Figure 3.28 – Illustration of point p_i in relation to the laser scanner. Adapted from [659]

Since K is fixed for the same laser scanner, ρK is used to represent the material reflectance. This allows computing ρK using a simple linear regression $y = ax + b$, where $y = I_i$, a $= \rho K$, and x $= \cos\theta / R^2$. To perform this linear regression, similarly to the surface roughness calculation, all N neighbouring points are first identified by establishing a bounding box centred on p_i, with dimensions $s_2 \times s_2 \times s_2$. Then $\cos\theta_j / R_j^2$ is calculated and I_j is retrieved for each j^{th} neighbouring point. Finally, the linear regression is performed, acquiring $\rho_i K$. Figure 3.29 illustrates the process of calculating the surface reflectance.

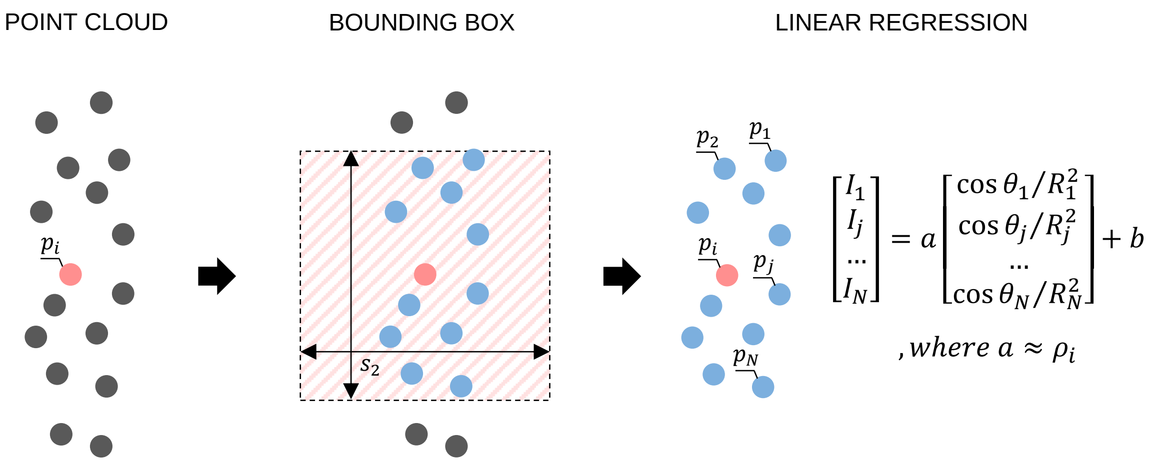

Figure 3.29 – Surface reflectance ρ based on a simple linear regression using the N neighbouring points

3.4.3.2.3. Surface colour

Determining the surface colour is relatively straightforward since each point is already associated with a set of RGB values. In fact, the only computing required is the transformation of the RGB values to the Hue-Saturation-Value (HSV) colour scheme, since the literature identifies this colour scheme as more robust to changes in illumination conditions [682], a desirable characteristic when tackling the identification of both indoor and outdoor surface materials. The transformation was computed using the formulas described in [683]:

$$r = \frac{R}{255}, g = \frac{G}{255}, b = \frac{B}{255}$$

$$Ma = max(r, g, b), Mi = min(r, g, b), \Delta = Ma - Mi$$

$$H = \begin{cases} 0º, if\ Ma = Mi \\ 60º \times \frac{g - b}{\Delta} + 0º, if\ Ma = r\ and\ g \gg b \\ 60º \times \frac{g - b}{\Delta} + 360º, if\ Ma = r\ and\ g < b \\ 60º \times \frac{b - r}{\Delta} + 120º, if\ Ma = g \\ 60º \times \frac{r - g}{\Delta} + 240º, if\ Ma = b \end{cases} \tag{3.18}$$

$$S = \begin{cases} 0, if\ Ma = 0 \\ \frac{\Delta}{Ma}, otherwise \end{cases}$$

$$V = Ma$$

With all three surface characteristics determined, a JSON file (structure illustrated in Figure 3.30) is used to store this information alongside the part (*part_class* + *part_id*) and instance (*instance_class* + *instance_id*) labels. Once again, although these characteristics describe the point cloud surface, they are calculated per-point (*points*). This file is sent to Module 5.

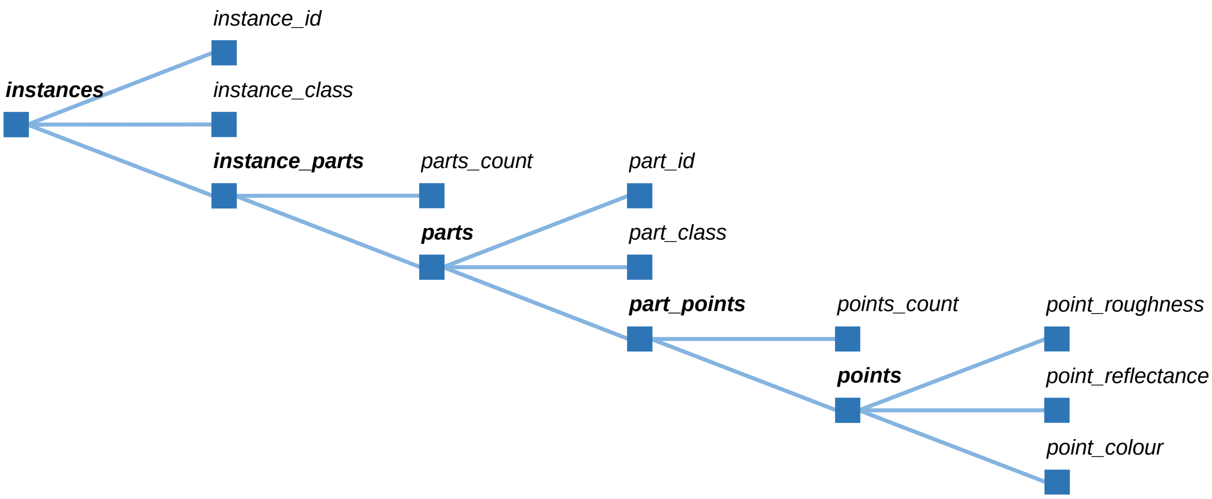

Figure 3.30 –JSON file structure containing the segment surface information

3.4.4. Training Data and Data Augmentation

As stated in the present module's overview and indicated in Figure 3.4, the data with which to train the developed models was acquired from publicly available datasets, such as Stanford 3D Indoor Scene (S3DIS) [471] and ShapeNet-Part [684], as well as artificially created using a BIM software tool developed for this purpose. The data available in the public datasets is thoroughly examined in Chapter

4, while the developed software to generate the artificial data and the generated data itself are analysed in Section 3.4.4.1 and Section 3.4.4.2, respectively.

3.4.4.1. Software for artificial point cloud generation

A BIM software tool was developed using *Dynamo* and *Python* to create artificial point clouds based on a building's BIM model geometry, allowing for the augmentation of the models' training data acquired from publicly available datasets (i.e. S3DIS, ShapeNet-Part).

This software essentially mimics a laser scanner's behaviour within a BIM environment, performing a laser scanning survey of a building's BIM model. To select the scan stations for this survey, the software introduced in Section 3.3.1.2 is applied, allowing for the complete automation of the artificial point clouds generation: the first software positions the scan stations, while the second mimics each scan station execution.

Regarding the second software workflow, it starts by retrieving each scan station's selected position and parameters from the first software. Then, for each position, a point is created at a height h, indicated by the user, or left as default at $h = 1.6$ meters. This point symbolizes the laser scanner and is the origin of the laser scanner's beams. After the points are created, the first laser beam is fired parallel to the XY plane. This beam's length is given by Equation 3.2 and is dependent on the optimized parameters selected by the first software. With the first beam established, several copies are created through a horizontal rotation centred in the beam's origin. The rotation's angle α is calculated (in degrees) through Equation 3.19:

$$\alpha = \tan^{-1}\left(\frac{TestedResol}{10}\right) \tag{3.19}$$

, where $TestedResol$ equals the same resolution tested and selected in Equation 3.2. The rotation process is repeated until it performs a full 360º rotation.

With the horizontal laser beams created, a similar rotation process is applied for all beams, where these are vertically rotated until covering the [-45º, 225º] range. The vertical rotation's angle is the same rotation angle α given by Equation 3.19. Figure 3.31 illustrates a laser scanner performing these two rotation processes.

With all the laser scanner beams created within the BIM environment, each time a beam intercepts the building's BIM model, the first interception is registered as a point in the artificially created point cloud. The point contains information regarding its 3D coordinates, RGB values (acquired from the BIM model surface), normal vector, as well as semantic and instance labels. It should be stated that each registered point has a slight chance to move between [0,1] millimetres in any direction, replicating existing noise. The chance is dependent on the selected quality parameter, decreasing with higher qualities.

Figure 3.32 and Figure 3.33 showcase an illustrative artificial point cloud generated using the developed BIM software tool for the BIM model presented in Figure 3.12. The different colours stand for different object instances.

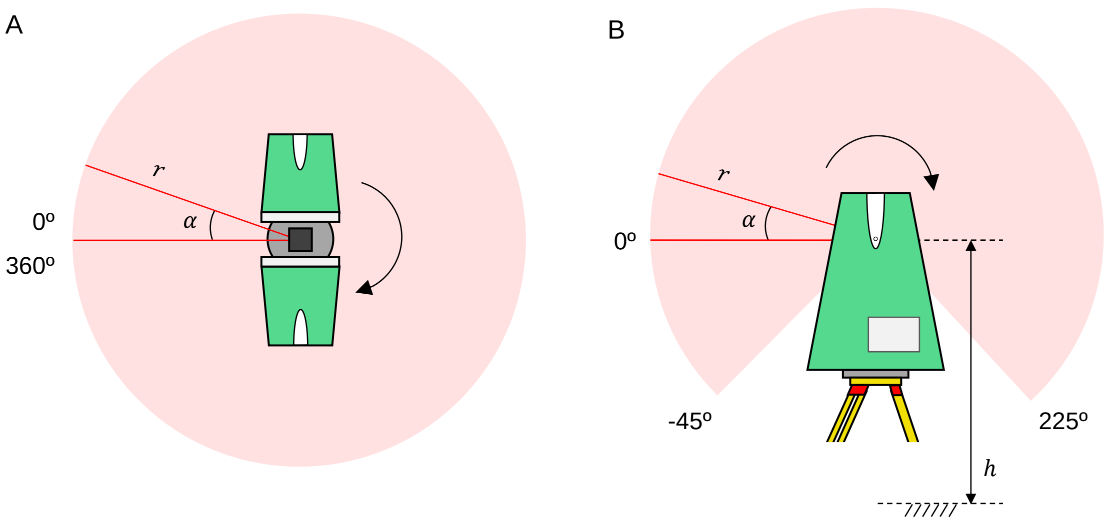

Figure 3.31 – Laser beam rotation. Plan (A) and elevation (B) view

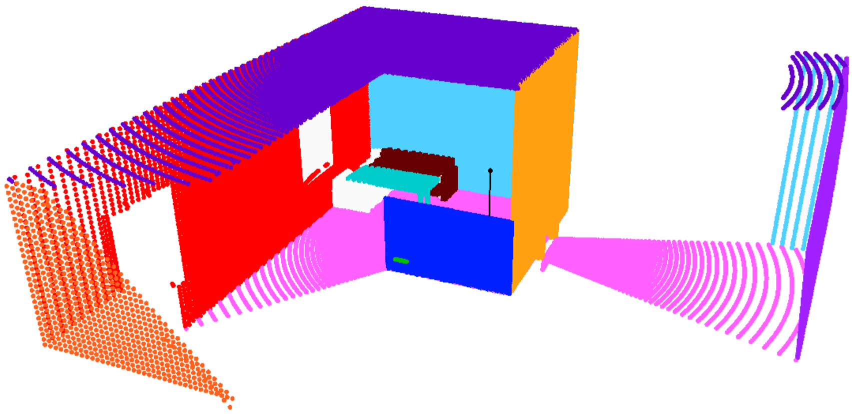

Figure 3.32 – Illustrative artificial point cloud generated using the developed software

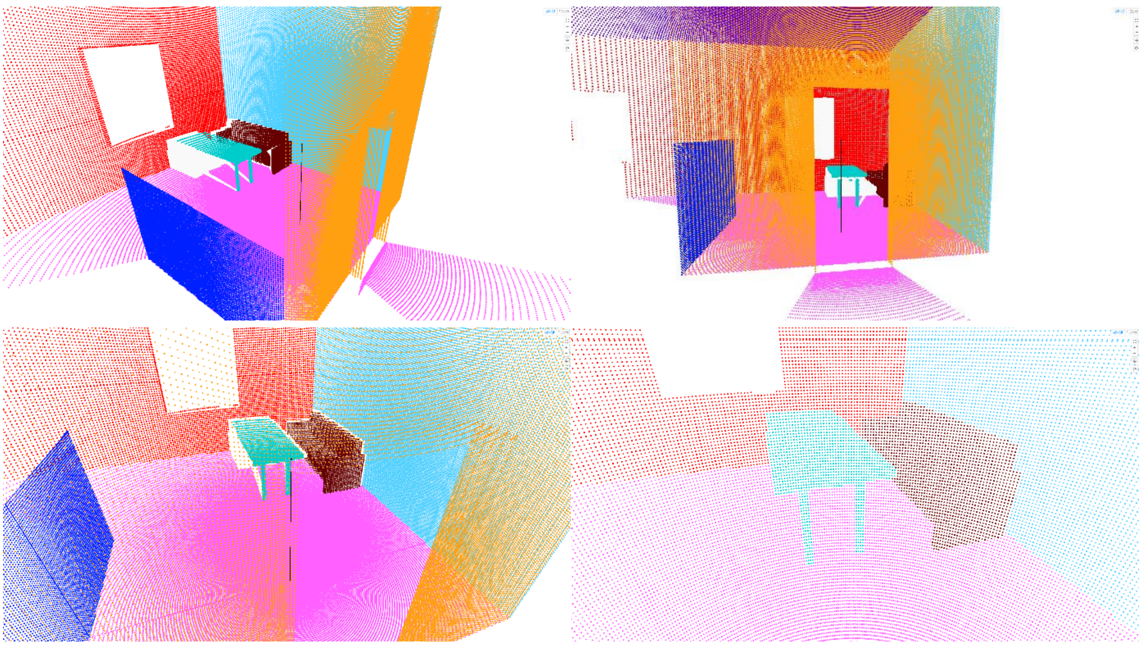

Figure 3.33 – Closer views of the illustrative artificial point cloud in Figure 3.32

3.4.4.2. Training data and data augmentation

As stated in Section 3.4.4, the software presented in the previous section was used to generate artificial point clouds of BIM models. This artificial data was then used to augment the publicly available datasets. Data augmentation with artificial/synthetic data is common practice in AI, where training data is frequently scarce or difficult to acquire. This is especially apparent for DL, where models frequently require massive amounts of training data. For more information on artificially generated data, please address [685, 686].

In this thesis, the data augmentation was targeted at stairs' point clouds, with this element comprising a large portion of the generated points. The focus on stairs originated from the need to classify this element during a case study in Chapter 4, despite the publicly available datasets not containing this specific label.

To this end, 20 BIM models heavily focused on modelled stairs were used to create the artificial point clouds. The models were divided into two groups according to their size. The first group comprised five larger models averaging 418,000 points after the artificial point cloud generation, while the second group comprised 15 smaller models with an average of 157,000 points. In total, 4,449,930 points were artificially generated using these 20 models, which were stored in a small, yet easily expandable, artificial BIM point cloud dataset, entitled, "Artificial BIM Point Clouds" or "ArtBIM-PC".

Table 3.7 presents the number of generated points divided according to their respective building element. Figure 3.34 shows four of the created BIM models (two from each group), and their respective artificially generated point clouds. As seen in this figure, the larger models focused more on the continuation of the stair throughout multiple building levels, while the smaller models focused more on different stair models with distinct designs and geometries. As seen in the displayed images, particularly in model D, the software can only capture the stairs' risers and treads, since it was the only geometry that could be accessed through *Revit*'s API – the chosen BIM authoring software.

Table 3.7 – ArtBIM-PC points per building element

Building element	Stair	Floor	Wall
#points	730,842	1,521,067	2,198,021

3.5. MODULE 4 – AUTOMATED BIM MODELLING

The fourth module of the proposed methodology entails the automated modelling of the surveyed building in a BIM environment. To accomplish this objective, the workflow seen in Figure 3.5 was implemented in Module 4. To better understand the automated BIM modelling process, this section is divided into three parts, namely: automated modelling workflow (Section 3.5.1); user input (Section 3.5.2); and degree of generalization (Section 3.5.3).

3.5.1. AUTOMATED MODELLING WORFKLOW

Initially, the JSON file containing the building elements' classes and geometric information (e.g. height, length, width, centre) is acquired from Module 3. Then, this data is sent to *Dynamo*, where the information is extracted. *Dynamo* was selected to perform the automated BIM modelling, given its access to *Revit*'s API and easy use of *Python*.

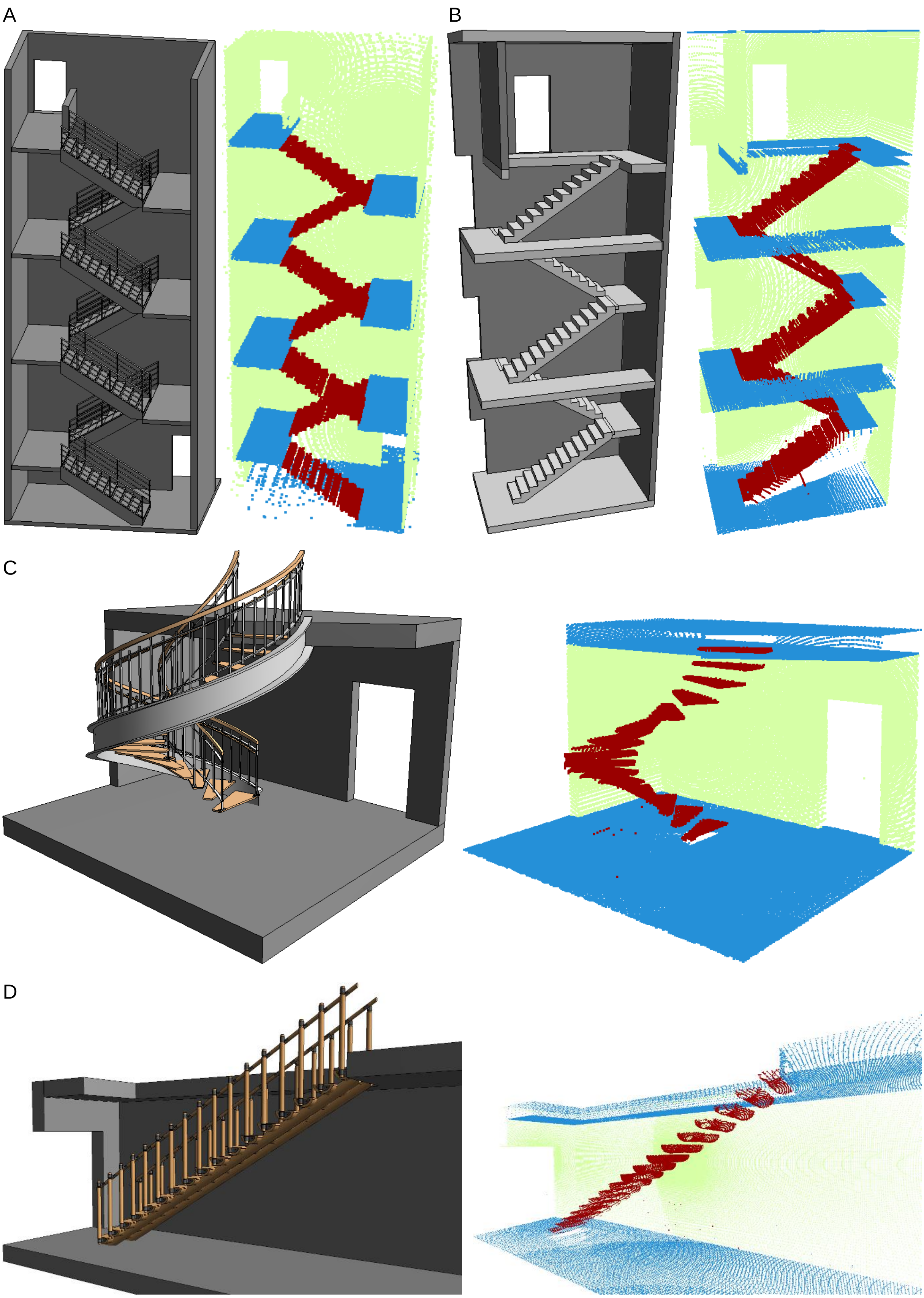

Figure 3.34 – Examples of BIM models and respective artificially generated point clouds. Models A and B are representative of the larger BIM models, while C and D are representative of the smaller models

With all the JSON file information extracted, the geometric data is used to start creating the building elements' geometry. The generation of this geometry is largely dependent on the building element being modelled since each building element is (1) modelled according to dissimilar parameters within *Revit* and *Dynamo,* and (2) acquired differently using a laser scanner.

To this end, five different classes of objects were created, each having its own distinct modelling methodology: *structure elements*; *hosted elements*; *furniture elements*; *stairs*; and *clutter*. Each of these classes houses different elements, namely:

- Structure elements – ceiling, floor, wall, beam, column;
- Hosted elements – door, window (regular, skylight or curtain wall), board, painting;
- Furniture elements – table, chair, sofa, bookcase;
- Stairs – stairs;
- Clutter – any elements still not recognized by the developed algorithms (i.e. not trained) or not adjudicated to one of the four previous classes.

By developing a general modelling methodology for each class, the modelling process was greatly simplified, since each element inside the same class roughly follows the same methodology. In fact, these differ only on small details related to *Revit*'s API. As such, as seen in Figure 3.5, the modelling process is as follows.

Initially, the information from the JSON file (Figure 3.26) is extracted for each of the identified building elements (i.e. *instances*). This information includes its geometric data (i.e. *instance_geometry*), as well as the element's category (i.e. its semantic label stored in *instance_class*).

Afterwards, the extracted information, namely the bounding box vertices (*geometry_bbox*) and the planes equations (*geometry_planes*), is used to develop a general view of the building. This step includes the distinction between straight and tilted elements; the extraction of *floor* and *ceiling* levels; as well as the generation of structure elements' boundaries (i.e. creation of enclosed surface volumes representative of this class' elements, including the extraction of curved surfaces for walls).

Using the created surfaces and the generated levels, semantic BIM objects are created for the structural elements. These elements are placed inside the BIM authoring environment using default families created by the author (see Figure 3.35).

These families, as per Table 2.2, are created at LOD 300 in most graphical parameters, the sole distinction being their shape, which is classified at LOD 200. As such, elements are graphically represented as specific objects within the BIM environment, with precise width, length, height, and orientation, but with a generic cuboid shape, as displayed in Figure 3.35.

With the structural elements class created, its elements are finished by establishing relationships and connections between elements, namely: wall-to-floor constraints; wall-to-ceiling constraints; wall-to-wall constraints; column-to-floor constraints; column-to-ceiling constraints; and beam-to-ceiling constraints. Beam-to-wall constraints were also attempted; however, this step cannot be currently automated given the lack of support for such an option in *Revit*'s API. This is a well-known issue in *Revit*'s community, which will hopefully be solved in future versions of the software, thus enabling its automation.

With all the structural elements completed, the next step is the placement of the hosted elements class. To do so, the centre (*geometry_centre*) of the element volume is used to identify the host element (e.g. wall, ceiling), and the JSON information is used to establish the element geometry. If the element is a door or a window, its thickness equals the host element. If the element is a board, the geometric information in the JSON file is used to specify its thickness (*geometry_height*, *geometry_length*, and *geometry_width*). As an example, Figure 3.36 shows modelling results for the hosted elements class.

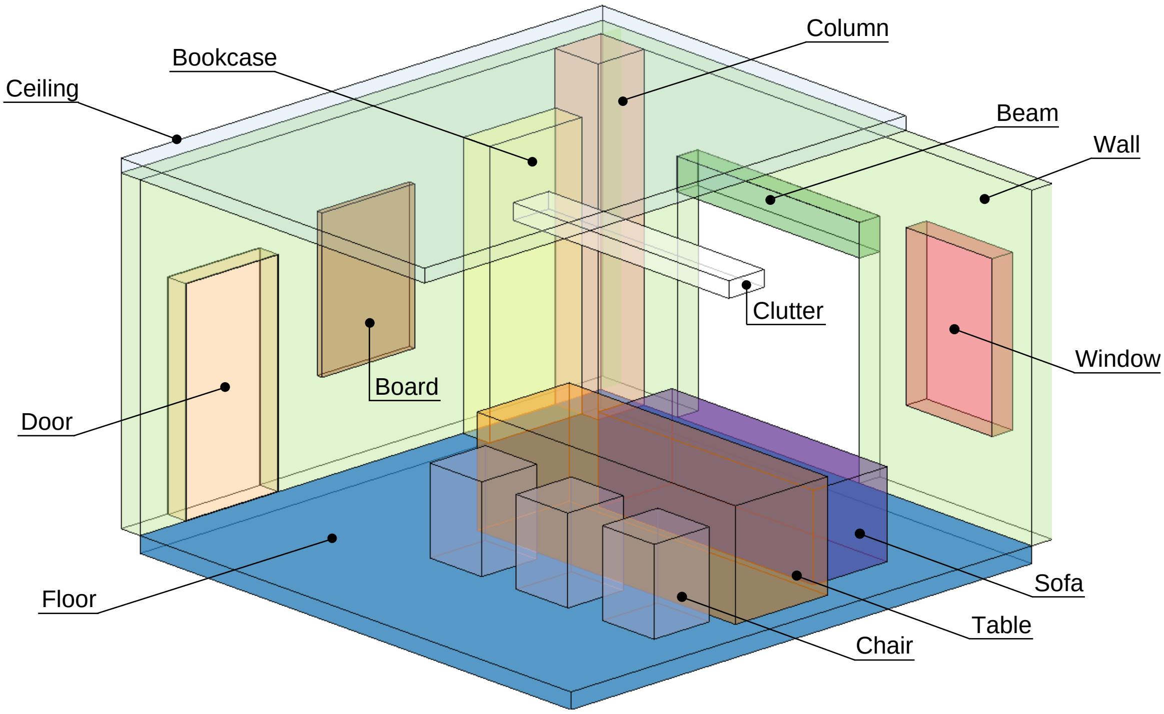

Figure 3.35 – Default families developed for the modelling software

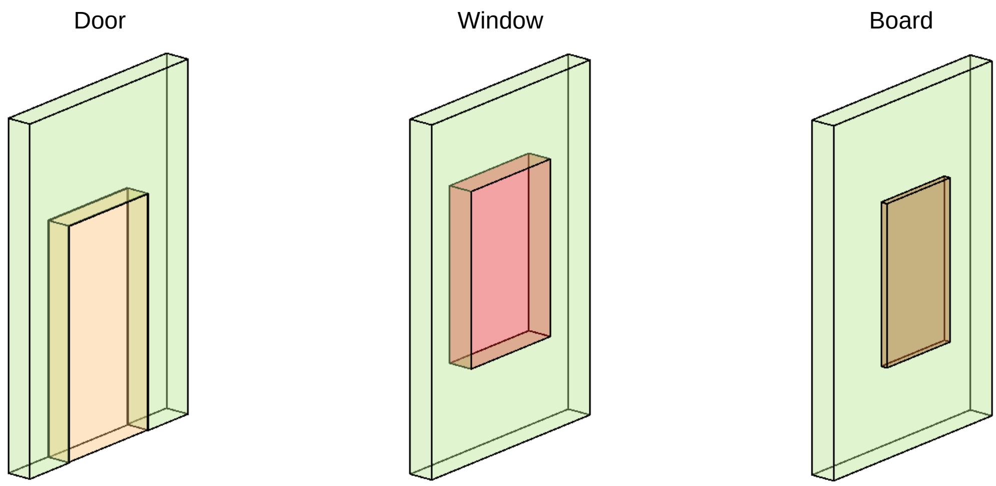

Figure 3.36 – Modelling results for the hosted elements class

With the hosted elements generated, the furniture elements follow suit. These are generated using the elements bounding box information retrieved from the JSON file to place their default families in the BIM environment. Apart from the elements being constrained to the floor, no further relationships are created.

With the furniture elements created, the clutter class is modelled using the same workflow as the furniture elements class, minus the floor constraint.

As the last class/element to be modelled, stairs were the most challenging to automate. To do so, initially, the stair's bounding box, retrieved from the JSON file (Figure 3.26), is used to carve an opening in the *floor* and *ceiling* elements, in case these are obstructing the stairway. Using the top- and bottom-most points of the stair, the orientation of the stair is extracted and the default family is generated. Finally, as the last step in the stair creation, the number of risers in the default stair is updated to equal the number of vertical RANSAC surfaces identified in the stair's point cloud (half the *planes_count* in the JSON file). As a default option, no handrail is included; however, this can also be easily enabled in *Dynamo*, as showcased in Figure 3.37. In terms of constraints, only the stair's landings are constrained to floors, with its sides being unable to be constrained to adjacent elements, such as walls, given the lack of options to do so in *Revit*'s API.

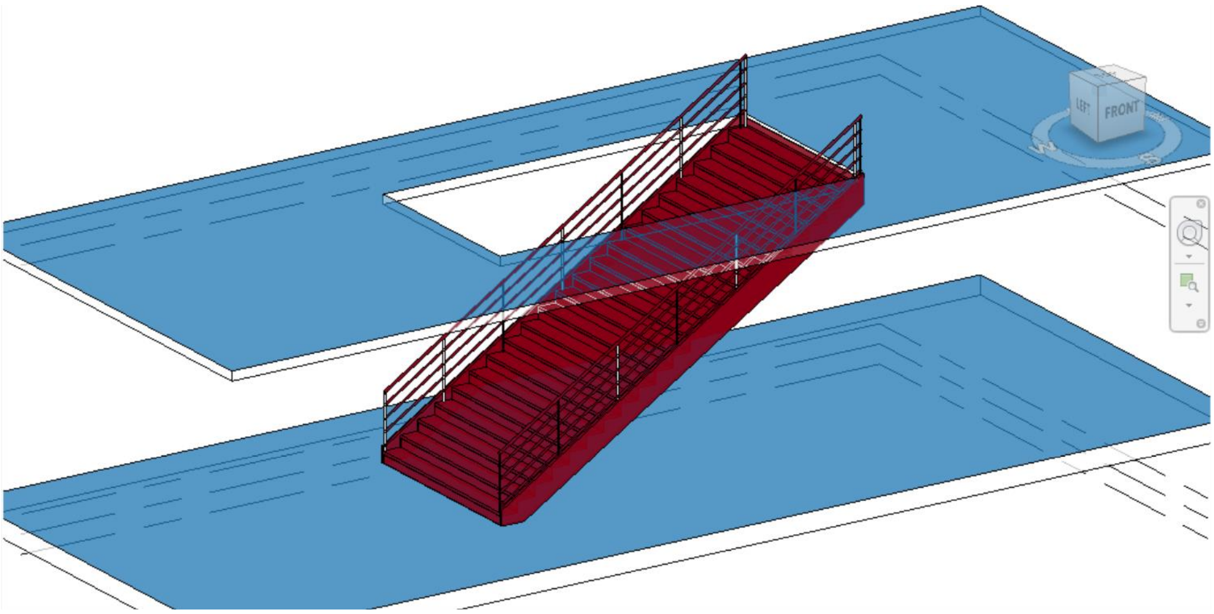

Figure 3.37 – Modelling result for the stair class

As the last step in the automated modelling process, analytical rooms are placed in Revit. These rooms are key components in exporting the BIM model information to energy analysis software, and are created according to the existing floor and ceiling elements. Essentially, the floor and ceiling provide the room's bottom and top boundaries, while the floor's perimeter is used to identify the room's lateral boundary conditions. In fact, the perimeter is first used to check for existing walls surrounding the room. If these walls are in place, they are used as lateral boundaries. If not, a room separation line is generated within *Revit* to create a virtual "air" boundary. The difference between these boundaries is important for the energy analysis software since wall boundaries and "air" boundaries have distinct thermal conductivity values.

3.5.2. User input

With all the element classes in place, the user is prompted to exchange the current elements in the BIM authoring software with custom families. This is easily performed, since the elements have been modelled with their correct categories. As an example, Figure 3.38 displays this step's simplicity by exchanging all skylights' default families in the model with a different family provided by the user.

With all the families exchanged, Module 1 requirements regarding the minimum BIM model's LOD and LoD are verified. If any of the requirements are not met, the user must perform the necessary changes to the model so as to fulfil the requirements. When the model meets all requirements, it is sent to Module 5.

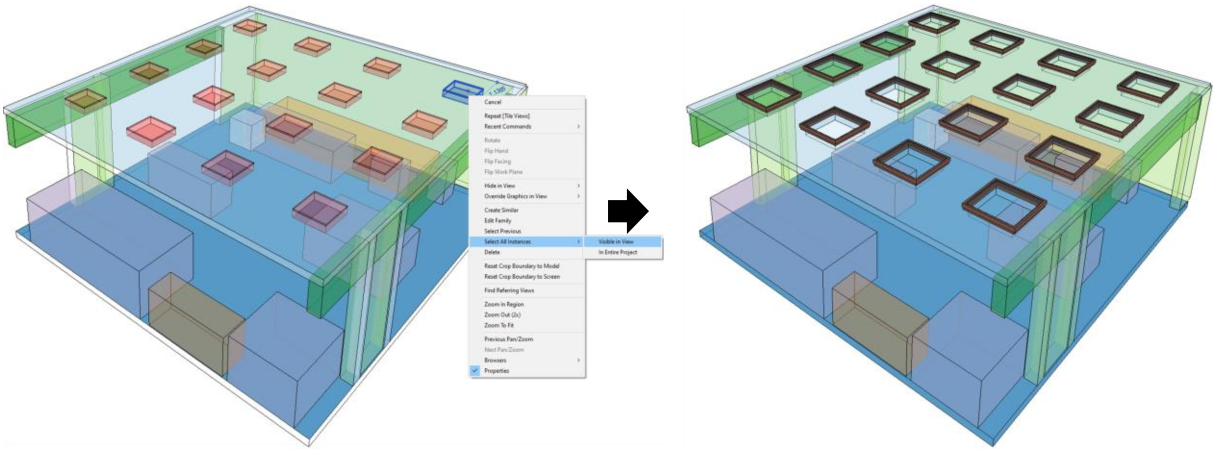

Figure 3.38 – Example of exchanging all elements of a default family in a model (skylights) with a custom family provided by the user

3.5.3. Degree of generalization

One crucial point central to the modelling workflow, which was not yet adequately covered, was the degree of generalization introduced in the *Dynamo* algorithm. This topic is especially important when tackling the modelling of geometric information, which was not captured during the laser scanning survey, either because of existing obstructions, hidden elements, or simply bad practices.

As seen during the state-of-the-art review, most previous works on scan-to-BIM automation tend to significantly generalize the modelling process, from neglecting the correct wall openings' dimensions to modelling tilted or curved walls as straight. In the author's opinion, this is due to the lack of precise geometric information (i.e. less accurate point cloud segmentation), which in turn creates an unreliable modelling when only using the extracted geometric data.

However, since the proposed segmentation and geometry extraction algorithms have a high precision and accuracy, the opposite approach was adopted in the proposed modelling workflow. As such, the level of generalization is negligible, essentially limiting itself to filling *floor* occlusion, which may result from in-place furniture (e.g. tables, chairs, sofas).

In the author's opinion, this is an advantage of the proposed workflow, since it is easier to identify the lack of modelling in a building (i.e. a gap in a wall) than to identify cases in which wrong information was modelled from the resulting generalization.

For instance, in the final version of the workflow, walls, ceilings and floors are created with a default thickness of 2cm so as not to interfere with opposite rooms (e.g. the same wall in two adjacent rooms). Initially, as proposed in the author's Research Thesis Project [671] and included in the first iteration of the software [33], a simple neighbourhood check was implemented to unite these elements by default. However, doing so could lead to joining elements that should not be united (e.g. cavity walls – see Figure 3.39). As such, this feature is, by default, disabled, with the option to enable it being set in *Dynamo*.

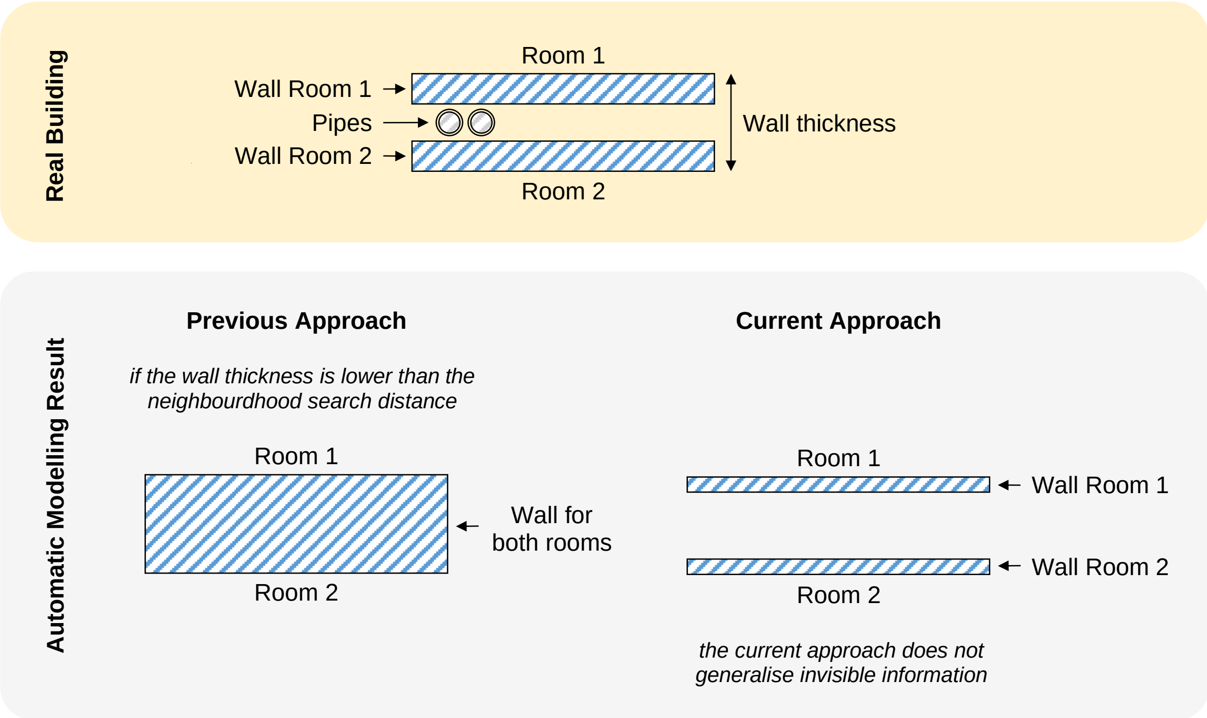

Figure 3.39 – Previous vs current approach regarding the generalisation of invisible information

3.6. Module 5 – BIM model enrichment and exportation to energy analysis software

The fifth module of the proposed methodology entails enriching the BIM model with non-geometric data and subsequently exporting the model to a building energy analysis software.

Regarding the enrichment process, the non-geometric data used for this purpose consist primarily of the acquired building energy-related data in Module 2 (i.e. the *Excel* file) and the part and surface-related information acquired in Module 3 (i.e. JSON file). Additionally, direct user input may be provided.

To this end, the enrichment process is divided into two approaches: fully-automated and semi-automated enrichment processes. These differ in the amount of required user intervention. Section 3.6.1 and Section 3.6.2 focus on these characterization processes, using, as respective examples, surface material association and data mapping.

Regarding the exportation process, two approaches were examined to transfer the BIM model from authoring to energy analysis software. These were: a direct approach using exportation plugins; and an indirect approach reliant on the gbXML data scheme to bridge both tools. Both approaches present challenges to which solutions are proposed. This process is focused on Section 3.6.3.

As in the previous modules, Figure 3.6 presents the fifth module workflow in detail.

3.6.1. Fully-automated enrichment processes – Surface material association

As the name implies, fully-automated enrichment processes do not require any user intervention to be performed. These processes are envisioned as heavily reliant on AI models, using the survey or model information to extract relevant characteristics regarding the building.

Only one work was identified in the literature attempting an automated BIM model enrichment process [687]. In this work, the authors focused on automatically classifying a room type in *Revit* by acquiring its area, floor level offset, number of doors, windows and boundary lines, as well as the connections to adjacent rooms. This information was used as features in a traditional ML classifier, achieving a maximum accuracy of 82% for 15 different room labels (i.e. room types). Only ANN was tested as the classifier.

In this thesis, a different yet similar process is proposed as an example. This process automatically identifies the building elements' surface material using, as in [687], a traditional ML classifier. The selected features for this classifier were the roughness, reflectance, and colour computed in Module 3. As stated in that same module, these features were acquired per-point, meaning that the material predictions are also per-point. To acquire the overall material of each identified part, the mode of the points' predictions for each part is used. This information is kept at a part level instead of a building element level since the latter can be composed of several surface materials, while this is rarely the former's case.

Ten different ML classifiers were trained to perform this task, with the best performing classifier being selected. These included five base models and five ensemble methods, namely:

- <u>Base models</u>: Decision Tree (DT) [688]; KNN [689]; Logistic Regression (LR) [690]; MLP [691]; and Multiclass SVM [692];
- <u>Ensemble methods</u>: AdB [693]; Extremely Randomized Forest (ExT) [694]; Gradient Boosting (GrB) [695, 696]; RF [434]; and Majority/Hard Voting [697].

A point cloud material dataset containing 30 different materials was developed to train the algorithms. This dataset was entitled "30 Point Clouds Materials" or "PCMat-30", and its development process is described in Chapter 4. The models training and tunning processes are also detailed in this chapter, with the best performing classifier being identified in Section 4.5.2.

With all the parts' surface material identified, the JSON file containing the parts and surface-related information (Figure 3.30) is updated to contain the identified material, as well as its average roughness, reflectance, and colour values. The resulting JSON file structure can be seen in Figure 3.40. This file's information is then automatically inserted into the BIM model elements using a simple *Dynamo* algorithm developed for this purpose. The algorithm essentially uses the *instance_id* and *instance_class* in the JSON file to identify the corresponding building element and update its information using the *part_class*, *part_material*, *part_avg_roughness*, *part_ avg_reflectance* and *part_avg_colour* data. This information is purely descriptive, with the element's geometry and design remaining unchanged.

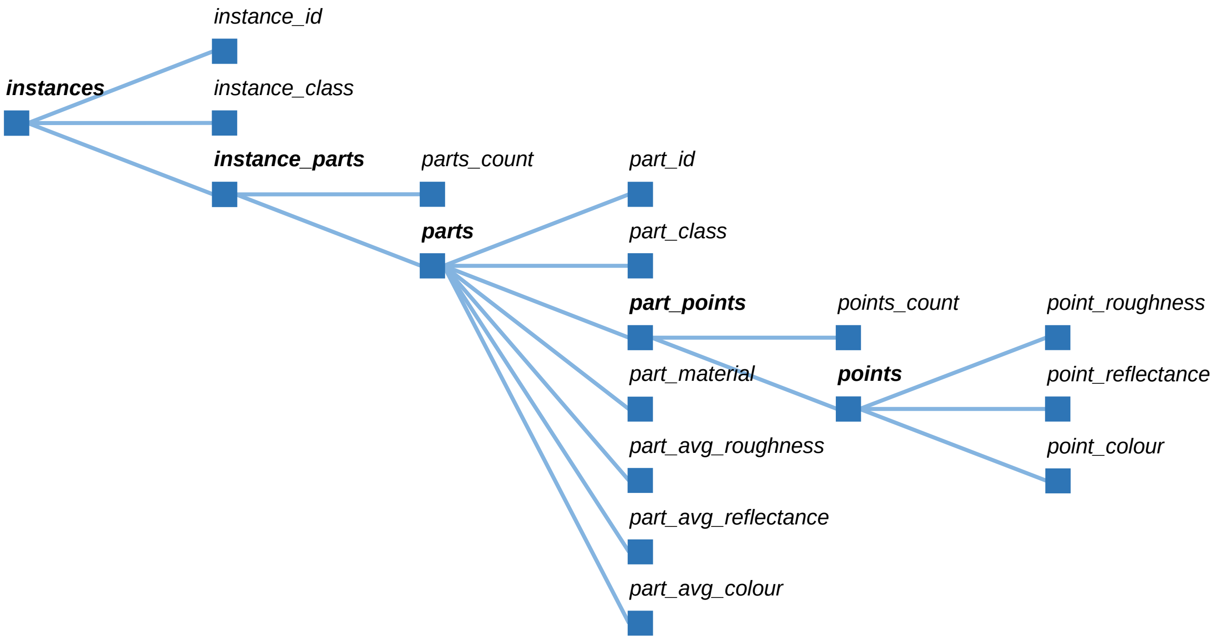

Figure 3.40 – Updated JSON file structure containing the building elements' parts information

3.6.2. Semi-automated enrichment processes – Data mapping

Contrary to the previous methods, semi-automated enrichment processes require some user intervention to be performed. These processes are envisioned as simple software tools or plugins that can be used to ease the BIM model enrichment.

There are undoubtedly several research works with such tools, as they are relatively common even within the practical community. In fact, *Dynamo*'s primary purpose is to develop simple software tools that simplify BIM model design and data manipulation, with its enrichment being one of the most popular tasks – either in terms of energy-related information or any other subject as structural or geotechnical data. Nevertheless, the works present in [236] and [698] are appropriate examples. In both these works, the authors apply thermography to extract a building element's thermal resistance and subsequently map these values into a gbXML-based BIM file to link the BIM elements with the identified thermal resistance.

In this thesis, a similar process is proposed. This process also maps building energy-related data into BIM; however, it does so by directly modifying the model's properties instead of its gbXML file. To do so, a simple *Dynamo* script was created to extract the building energy-related information from the *Excel* file created in Module 2 and subsequently update the BIM model's general, systems, and constructive elements information. If a specific parameter is available in the *Excel* file but not in the user's custom families, a warning message is created alerting to that fact. In prior versions of the developed script, *Dynamo* would simply create the parameter in the user's custom family and insert the available information. However, this was changed to a warning message, given that the BIM model has already passed the LOD requirements in Module 4. As such, all BIM elements already have the required parameters to store the established key parameters in Module 1, meaning that the extra parameters in *Excel* can be seen as non-required, and the decision to include this extra information should be left to the user.

3.6.3. Exportation to building energy analysis software

With the BIM model fully characterized, the model can now be exported from the BIM authoring tool to an energy analysis software. However, as stated in the literature review (Section 2.4.2.3), there are multiple issues related to the interoperability of these software tools, which need to be addressed in the proposed AIBEA workflow.

To this end, a study focused on this topic was performed to acquire further insight into the literature findings and better understand how to integrate existing solutions proposed in the literature. The chosen software tools to test the interoperability were *Autodesk Revit* and *DesignBuilder*, respectively as the BIM authoring tool and the energy analysis software. These tools were selected for their availability, as well as their popularity in current research and practice, as identified in Section 2.4.2.

This study focused on the assessment of two different workflows for transferring the BIM model's information into the energy analysis software, namely:

- leveraging *DesignBuilder*'s plugin for *Revit* to automatically transfer the BIM model between both tools;
- and exporting the BIM model from *Revit* to *DesignBuilder* using the gbXML data scheme.

A third option focusing on the direct usage of *Revit*'s web-based energy analysis tool (*Insight* – spiritual successor of *Green Building Studio*) was also assessed, which directly runs within the authoring software, meaning, no data transfer is required. However, although interoperability results were promising, this software's features were too scarce, limiting its scope and applicability within the AIBEA workflow. As such, its analysis is not focused on this section.

To further the study of *Revit-DesignBuilder* interoperability, four different models were tested (Model A to D). These models showcased different levels of complexity and objectives, following Table 3.3 proposed modelling information:

- Model A was modelled following the proposed information for Conceptual Design;
- Model B was modelled following the proposed information for Schematic Design;
- and Model C and D were modelled following the proposed information for Design Development and Retrofit. These two models differ only on the added MEP system detail that Model D has in comparison with Model C.

Table 3.8 displays the 3D view of these four models, as well as the ground and first floor plants.

Additionally, when possible, two different approaches were used to retrieve the energy information from *Revit*, namely, using its Energy Settings or its Room Volumes. These two options differ on the first requiring the indication of the building's energy information using the software's options dialog, while the second exports the building volumes and acquires the energy information from the room's analytical surfaces. The first has the added advantage of enabling the detailing of certain energy systems in greater detail, while the second is fully automated.

Through the combination of all these options, the tests seen in Table 3.9 were performed. Model A only endured two tests, since its low LOD negated the option of exporting the model using Room Volumes.

The acquired results and conclusions from these tests were published in the same report as the AIBEA requirements [651], alongside an extensive analysis of the developed models characteristics and assessed exportation methods. The report's findings were applied in [28, 29, 35] to support the proper exportation of the BIM model information.

The acquired results from the performed tests can be seen in Table 3.10 to Table 3.12, where each of the modelled energy parameters is specified as being successfully exchanged between software tools. Table 3.10 displays the results from Model A; Table 3.11 for Model B; and Table 3.12 for both Model C and D since these returned the same results.

Table 3.8 – Developed BIM models for the interoperability assessment: 3D view (left); ground floor plant (centre); and first floor plant (right)

Model A
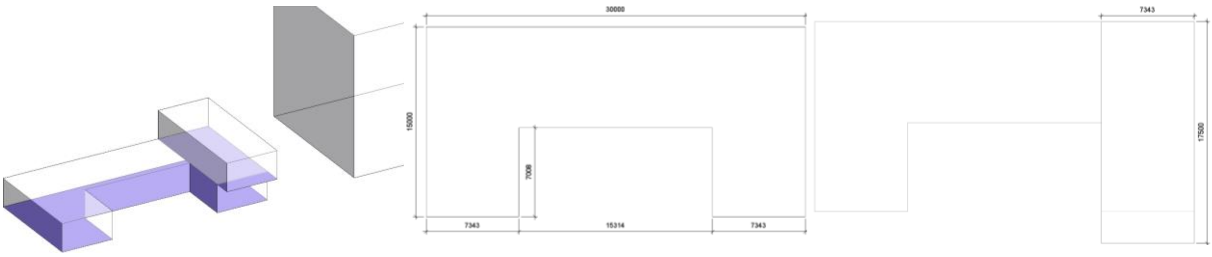
Model B
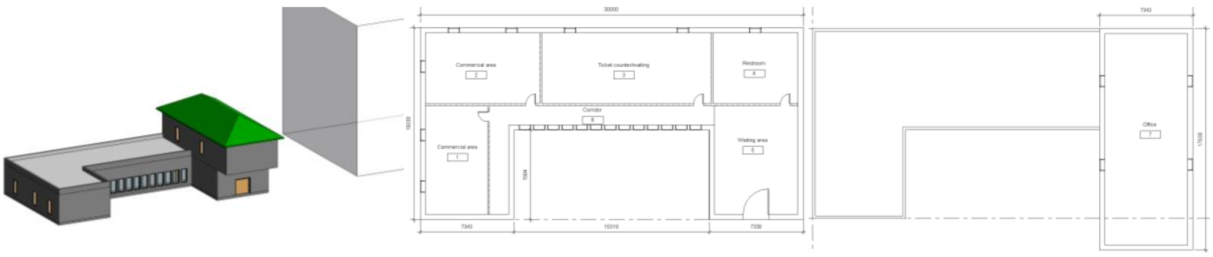
Model C
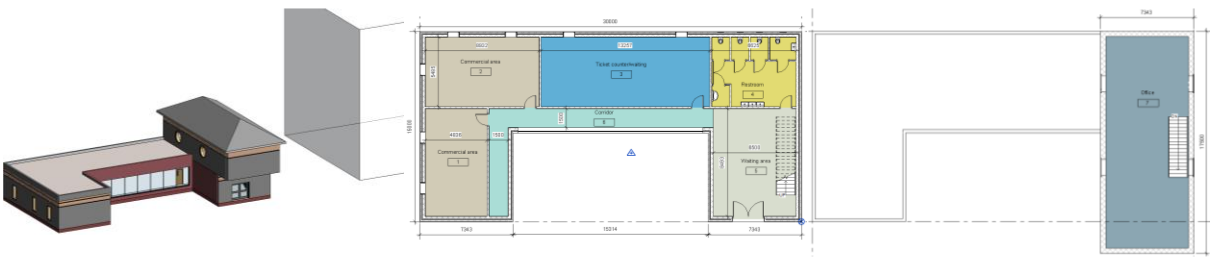
Model D
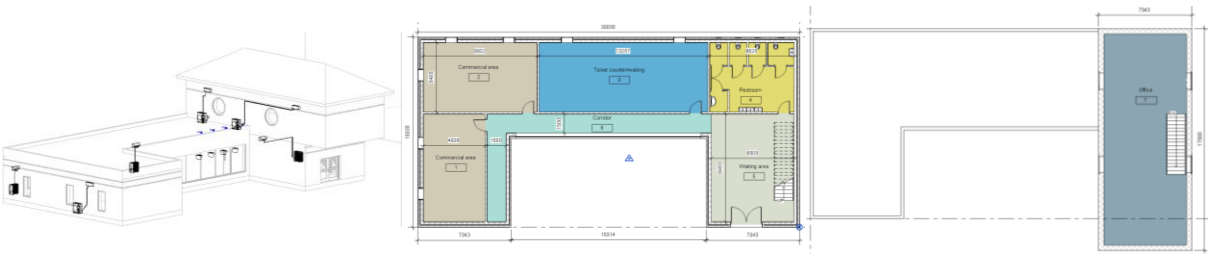

Table 3.9 – Performed tests during the interoperability assessment

Test	Model	Exportation method
A1	Model A	gbXML with Energy Settings
A2		DesignBuilder’s plugin for Revit with Energy Settings
B1	Model B	gbXML with Energy Settings
B2		gbXML with Room Volumes
B3		DesignBuilder’s plugin for Revit with Energy Settings
B4		DesignBuilder’s plugin for Revit with Room Volumes
C1	Model C	gbXML with Energy Settings
C2		gbXML with Room Volumes
C3		DesignBuilder’s plugin for Revit with Energy Settings
C4		DesignBuilder’s plugin for Revit with Room Volumes
D1	Model D	gbXML with Energy Settings
D2		gbXML with Room Volumes
D3		DesignBuilder’s plugin for Revit with Energy Settings
D4		DesignBuilder’s plugin for Revit with Room Volumes

Table 3.10 – Interoperability analysis results for Model A

Parameters		Exportation Method	
		Energy Settings	
		gbXML file (A1)	DesignBuilder’s plugin (A2)
Location (*weather file*)		×	✓
Building orientation		✓	✓
Building geometry		Loss of ~10% in volume	Loss of ~7% in volume
Building type/function		×	×
Area per person		×	×
Lighting load density		×	×
Power load density		×	×
Building operating schedule		×	×
HVAC type		×	×
Constructive solution	Walls	×	×
	Roofs	×	×
	Floors	×	×
	Exterior windows	×	×
Nearby construction (external mass)		✓	✓

Table 3.11 – Interoperability analysis results for Model B

Parameters		**Exportation Method**			
		Energy Settings		**Room Volumes**	
		gbXML file (B1)	**DB's plugin (B2)**	**gbXML file (B3)**	**DB's plugin (B4)**
Location (*weather file*)		×	✓	×	✓
Building orientation		✓	✓	✓	✓
Building geometry		Gain of ~1% in volume	Gain of ~3% in volume	✓	Loss of ~1% in volume
Building type/function		×	×	×	×
Area per person		×	×	×	×
Sensible heat gain per person		×	×	×	×
Latent heat gain per person		×	×	×	×
Lighting load density		×	×	×	×
Power load density		×	×	×	×
Occupancy schedule		×	×	×	×
Lighting schedule		×	×	×	×
Power schedule		×	×	×	×
Building Operating Schedule		×	×	×	×
HVAC type		×	×	×	×
Rooms		×	×	✓	✓
Constructive solution	Exterior walls	✓	✓	✓	✓
	Interior walls	✓	✓	✓	✓
	Roofs	✓	✓	✓	✓
	Floors	✓	✓	✓	✓
	Doors	✓	✓	✓	✓
	Exterior windows	✓	✓	✓	✓
	Operable windows	×	×	×	×
	Operable windows schedule	×	×	×	×
Nearby construction (external mass)		✓	✓	×	×

Table 3.12 – Interoperability analysis results for Model C and D

Parameters		**Exportation Method**			
		Energy Settings		**Room Volumes**	
		gbXML file (C1/D1)	**DB's plugin (C2/D2)**	**gbXML file (C3/D3)**	**DB's plugin (C4/D4)**
Location (*weather file*)		×	✓	×	✓
Building orientation		✓	✓	✓	✓
Building geometry		Gain of ~1% in volume	Gain of ~2% in volume	✓	Loss of ~1% in volume
Building type/function		×	×	×	×
Area per person		×	×	×	×
Sensible heat gain per person		×	×	×	×
Latent heat gain per person		×	×	×	×
Lighting load density		×	×	×	×
Power load density		×	×	×	×
Occupancy schedule		×	×	×	×
Lighting schedule		×	×	×	×
Power schedule		×	×	×	×
Building Operating Schedule		×	×	×	×
HVAC type		×	×	×	×
Rooms		×	×	✓	✓
Constructive solution	Exterior walls	✓	✓	✓	✓
	Interior walls	✓	✓	✓	✓
	Roofs	✓	✓	✓	✓
	Floors	✓	✓	✓	✓
	Doors	✓	✓	✓	✓
	Curtain walls	✓	✓	✓	✓
	Exterior windows	✓	✓	✓	✓
	Operable windows	×	×	×	×
	Operable windows schedule	×	×	×	×
Nearby construction (external mass)		✓	✓	×	×

It should be stated that the results presented in the previous tables differ slightly from the result in the identified report [651], since new runs with new versions of both authoring and energy analysis software were performed to identify any new developments. However, despite the three year gap in software versions (2018 in the report and 2021 in the present thesis), by comparing both tables findings, it can be concluded that apart from the building geometry (which interoperability improved substantially), the remaining parameters remain virtually in the same state, keeping the report findings relevant to date.

Additionally, it can also be concluded that all methods still display limitations in the information that can be transferred between both applications, namely:

- When comparing the use of Energy Settings to Room Volumes, it can be concluded that Energy Settings has the advantage of transferring nearby construction, which presents a key role in analysis such as shadow and daylight simulations. However, it is less accurate in transferring geometric information and does not transfer room data, which can be helpful in not only visualizing the model in *DesignBuilding*, but also in correcting the missing information. Additionally, as previously stated, Room Volumes exportation is fully automated, while Energy Settings requires the specification of extra information in *Revit* – information which is not transferred using any of the assessed methods. As such, Room Volumes is currently the favored option.
- As for the comparison between *DesignBuilder*'s plugin and the gbXML data scheme, it can be concluded that the gbXML file is more reliable, resulting in the only workflow that transfers the exact same geometry as in the BIM model (B3 and C3/D3). In addition, the use of gbXML exportation is prevalent in current methods to solve interoperability issues between BIM authoring and energy analysis software [22, 85, 699], since the exported gbXML file can be modified to correct any existing issues, while modifying third party software is often an unrealistic approach. As such, the use of the gbXML data scheme is currently the prefered option.

Focusing the current literature solutions to solve these interoperability issues, authors generally focus on post-processing the exported gbXML file before sending it to the energy analysis software. This solution relies on developing a software tool for file checking, which essentially runs through a list of pre-established variables and verifies their existence in the gbXML file. If a variable is missing/empty, the software tool creates/fills that variable with information acquired from either the BIM model, current standards and references, or direct user input. This is a simple yet elegant solution to the current problem, especially since most of the lost information can be considered analytical data, such as the building location, type/function, occupancy schedule, among others. This type of data comes in opposition to geometric data, which would be harder to modify within the gbXML file.

To this end, the author's proposes to adopt Chong et al. [699] solution, establishing an intermediate step in the exportation of the BIM model to the energy analysis software. The steps proposed in this work were already integrated into Module 5's workflow, as seen in Figure 3.6.

4

VALIDATION

The present chapter aims to validate the proposed contributions through their application in five different experiments. These experiments are tackled separately from Section 4.2 to Section 4.6, being preceded by a general overview of the experiments in Section 4.1, and succeeded by a summary of the obtained results in Section 4.7.

4.1. OVERVIEW OF THE EXPERIMENTS

Five unique experiments were carried out to validate the proposed contributions. Each of these experiments is tackled in their respective sections, which start by introducing and detailing the experimental setting, the performed tasks, the used evaluation metrics, and the applied dataset. Regarding the latter, throughout the experiments, four datasets are applied. These are: S3DIS [471]; ShapeNet-Part [684]; PCMat-30; and ArtBIM-PC.

As summarized in Table 4.1, these experiments focus on distinct parts of the methodology, evaluating different portions of the proposed modules. Namely:

- the first experiment focuses on evaluating the contributions of Module 3 and Module 4, targeting the semantic and instance segmentation of point clouds, followed by the automated BIM modelling of the identified elements. This experiment focuses on the usage of diverse point clouds with multiple semantic labels, enabling the overall assessment of the developed DL networks and BIM tools;
- similarly, the second experiment also targets the contributions of Module 3 and Module 4, focusing, however, on predicting a semantic label primarily trained with artificial data (i.e. stairs), instead of targeting a wider variety of labels. In addition, the data acquisition guidelines proposed in Module 2 were applied for the surveying of FEUP and the acquisition of the testing dataset;
- regarding the third experiment, it focuses solely on Module 3, particularly in the part segmentation of point clouds;
- the fourth experiment focuses on Modules 3 and 5, assessing the developed material classification algorithm proposed as a fully-automated enrichment process;
- and, finally, the fifth experiment focuses on Module 5, evaluating the exportation of an automatically generated BIM model to the selected energy analysis software.

As identified throughout the thesis, it should be noted that further experiments focusing on these Modules were published in both international peer-reviewed journals [28-30, 35], conference papers [33, 36, 37, 656], and project reports [651].

Table 4.1 – Overview of the performed experiments

	First Experiment	Second Experiment	Third Experiment	Fourth Experiment	Fifth Experiment
Training Data	S3DIS ArtBIM-PC	S3DIS	ShapeNet	PCMat-30	S3DIS
Testing Data	S3DIS	FEUP	ShapeNet	PCMat-30	S3DIS
Performed Tasks	Sematic and instance segmentation of point clouds, followed by the automated modelling of the identified elements. Focus on the usage of diverse point clouds with multiple semantic labels	Sematic and instance segmentation of a surveyed point cloud, followed by the automated modelling of the identified elements. Focus on the prediction of a semantic label that was primarily trained with artificial data	Part segmentation of point clouds	Point cloud material classification with distinct point clouds	Transference of an automatically generated BIM model to an energy analysis software

4.2. First Experiment

4.2.1. Experimental setting – S3DIS

The first experiment focuses on semantic and instance segmentation, as well as automated BIM modelling. As such, Section 3.4 and Section 3.5 contributions are assessed, excluding the part segmentation network, since no part information is available. The applied dataset was S3DIS.

S3DIS [471] is a large-scale semantic indoor scene parsing dataset consisting of 3D RGB point clouds acquired using a Matterport Scanner [700]. It consists of six floors from three different buildings split into 272 individual disjoint spaces. These spaces show diverse properties in architectural style, appearance and usage, including, among others, office rooms, conference rooms, restrooms, educational and exhibition spaces, storage areas, open spaces, lobbies, pantries, lounges, and hallways.

Each point p_i in the scene is associated with an instance label I_i and one of 13 semantic labels S_i. These include seven structural elements (ceiling, floor, wall, beam, column, window and door), five commonly found items and furniture (table, chair, sofa, bookcase and board), and a clutter/noise class for the remaining data. Each point p_i further contains information regarding its 3D coordinates $c_i = \{x_i, y_i, z_i\}$ and six features $f_i = \left\{R_i, G_i, B_i, n\ _i, n_{y_i}, n_{z_i}\right\}$, its RGB values and normal vector.

All point information is used as input: $p_i = (c_i, f_i)$. For evaluation metrics, overall accuracy ($oAcc$), mean accuracy over classes ($mAcc$), and per-class accuracy (Acc) are calculated according to Equation 4.1, Equation 4.2, and Equation 4.3, respectively:

$$oAcc = \frac{Corrected\ Predictions}{Total\ Predictions} \times 100 \tag{4.1}$$

$$mAcc = \frac{\sum_S^m (Acc_S)}{m} \tag{4.2}$$

$$Acc_S = \frac{Corrected\ Predictions_S}{Total\ Predictions_S} \times 100 \tag{4.3}$$

, where m represents the total number of semantic classes, and S represents the evaluated semantic label. While $oAcc$ and Acc are commonly evaluated metrics, $mAcc$ is less used. This metric was calculated to better represent the model performance facing the class imbalance in S3DIS. Images of the segmented point cloud and the final BIM models are provided for a qualitative evaluation.

Regarding the test/train split, the dataset is originally divided into six building areas, as seen in Figure 4.1. Table 4.2 and Table 4.3 present information concerning these areas. As per the dataset authors [471], and following the most common validation protocol for S3DIS, Areas 1, 2, 3, 4, and 6 were used for training, while Area 5 was left for testing. This split is used since portions of the training areas share similarities in appearance and architectural features, which could influence the testing results.

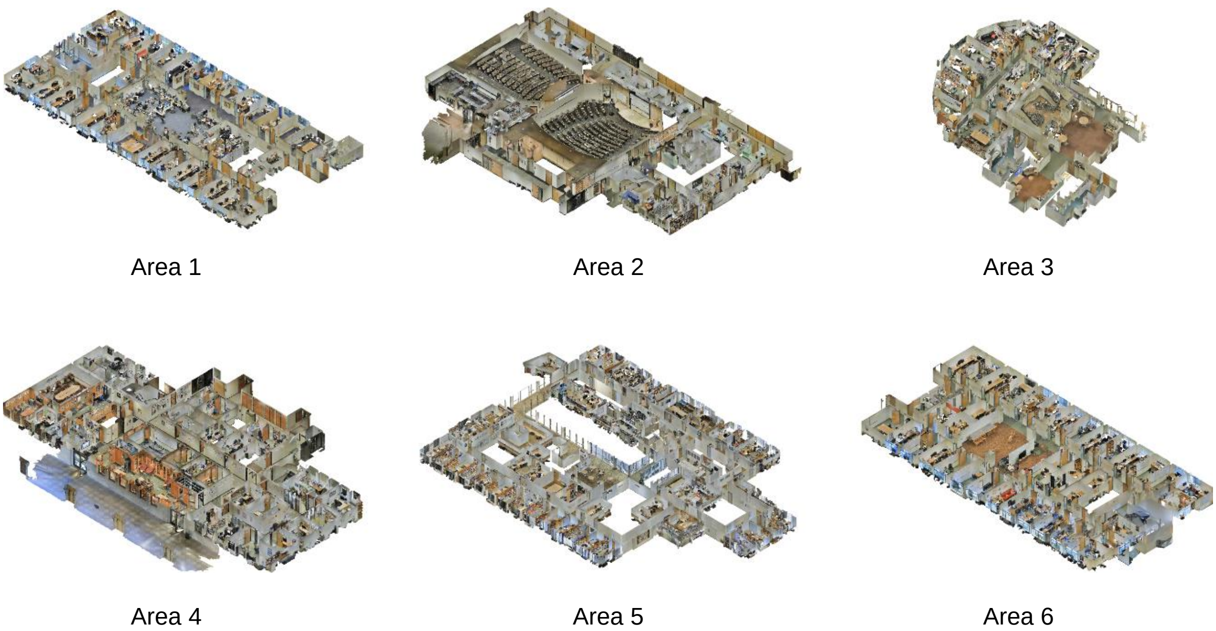

Figure 4.1 – Building areas in the S3DIS dataset

However, as seen in Table 4.4, Area 5 has a meagre number of points for the beam class, which is not enough for a representative evaluation. Thus, despite sharing similarities with other areas, a second test/train split was performed with Area 6 as the testing data. The analysis of the acquired results from this second split took into consideration this existing bias.

It should be stated that since the original dataset is no longer publicly available, the dataset used in this thesis is a pre-processed version of the original provided by [491]. Nevertheless, this version of the dataset is currently used in the literature for validation, and its results should be accepted for comparison with the existing state-of-the-art.

4.2.2. Results and discussion

S3DIS is a challenging dataset with classes such as wall-hidden columns and white boards on white walls. To support the analysis and discussion of the carried experiment, quantitative results are presented in Table 4.5 and Table 4.6, while qualitative results are displayed from Figure 4.2 to Figure 4.13.

Starting with the quantitative results, Table 4.5 presents the overall accuracy ($oAcc$) and mean accuracy over classes ($mAcc$) for several existing models, as well as the proposed approach. Table 4.6 presents the per-class accuracy (Acc) for the proposed approach in Areas 5 and 6.

Table 4.2 – Disjoint spaces information per building area

Building Area	**Area (m^2)**	**Volume (m^3)**	**Office**	**Confer. Room**	**Auditor.**	**Lobby**	**Lounge**	**Hallway**	**Copy Room**	**Pantry**	**Open Space**	**Storage**	**WC**	**Total**
Area 1	965	2,850	31	2	-	-	-	8	1	1	-	-	1	44
Area 2	1,100	3,065	14	1	2	-	-	12	-	-	-	9	2	40
Area 3	450	1,215	10	1	-	-	2	6	-	-	-	2	2	23
Area 4	870	2,780	22	3	-	2	-	14	-	-	-	4	4	49
Area 5	1,700	5,370	42	3	-	1	-	15	-	1	-	4	2	68
Area 6	935	2,670	37	1	-	-	1	6	1	1	1	-	-	48
Total	6,020	17,950	156	11	2	3	3	61	2	3	1	19	11	272

Table 4.3 – Object class information per building area

Building Area	**Ceiling**	**Floor**	**Wall**	**Beam**	**Column**	**Door**	**Window**	**Table**	**Chair**	**Sofa**	**Bookcase**	**Board**
Area 1	56	45	235	62	58	87	30	70	156	7	91	28
Area 2	82	51	284	62	58	94	9	47	546	7	49	18
Area 3	38	24	160	14	13	38	9	31	68	10	42	13
Area 4	74	51	281	4	39	108	41	80	160	15	99	11
Area 5	77	69	344	4	75	128	53	155	259	12	218	43
Area 6	64	50	248	69	55	94	32	78	180	10	91	30
Total	391	290	1,552	165	260	549	174	461	1,369	61	590	143

Table 4.4 – S3DIS dataset information regarding Areas 5 and 6

Class	**Area 5**		**Area 6**	
	#points	**%points**	**#points**	**%points**
Ceiling	7,286,031	25.96	3,310,010	24.53
Floor	6,685,246	23.82	2,927,011	21.69
Wall	5,603,217	19.96	2,016,502	14.95
Beam	6,158	0.02	668,815	4.96
Column	317,406	1.13	336,230	2.49
Window	508,649	1.81	175,400	1.30
Door	701,934	2.50	623,804	4.62
Table	1,267,817	4.52	777,433	5.76
Chair	742,458	2.65	649,088	4.81
Sofa	95,654	0.34	62,163	0.46
Bookcase	1,985,434	7.07	303,998	2.25
Board	195,873	0.70	128,440	0.95
Clutter	2,669,915	9.51	1,513,330	11.22
Total	28,065,792	100	13,492,224	100

Table 4.5 – S3DIS segmentation results. Overall accuracy ($oAcc$) and mean accuracy over classes ($mAcc$) for the proposed approach and existing models in the state-of-the-art

Method	**Area 5**		**Area 6**	
	oAcc (%)	**mAcc (%)**	**oAcc (%)**	**mAcc (%)**
SEGCloud [536]	-	57.35	-	-
KPConv [494]	72.80	-	-	-
PointNet [556]	78.60	48.98	-	-
PointCNN [598]	85.91	63.86	-	-
SPG [527]	86.38	66.50	-	-
ASIS [701]	86.90	60.90	-	-
Pointweb [526]	86.97	66.64	-	-
MV-CRF [491]	87.40	-	-	-
PVNet [542]	87.48	-	-	-
SASO [702]	87.50	63.50	-	-
Proposed Approach	87.64	62.80	90.52	83.19
JSNet [703]	87.70	61.40	-	-
PointTransformer [528]	**90.80**	**76.50**	-	-

Table 4.6 – S3DIS segmentation results. Per-class accuracy (Acc) for the proposed approach

Area	ceiling	floor	wall	beam	column	window	door	table	chair	sofa	bookcase	board	clutter
5	95.32	98.13	95.01	0.15	23.42	68.11	36.96	80.29	89.92	28.26	70.31	60.86	69.64
6	98.65	99.17	91.3	86.36	74.99	94.17	93.95	84.53	88.72	71.23	69.97	58.44	69.88

As seen in Table 4.5, compared to current methods, the developed segmentation network is well-positioned in both metrics for Area 5, surpassing PointNet [556] and PVNet [542], which served as significant components for the proposed network. Additionally, these metrics are achieved using PVConv, one of the most computationally efficient primitives in the literature. This comes in opposition to PointTransformer [528], released in December 2020 and current leader in S3DIS, which is considered computationally expensive, particularly in memory requirements.

Regarding Area 6, although no existing comparisons were found in research, it can be concluded that this area achieved significantly better metrics, particularly regarding $mAcc$. Although the previously stated bias can undoubtedly influence these results, it alone should not produce such improvements.

After further inspection, it can be concluded that this area is far more forgiving in terms of false predictions, which significantly improves the metric scores. In particular, Area 6's points are significantly better distributed through the existing classes (see Table 4.4), with the beam and column classes (which produced the worst predictions in Area 5 – see Table 4.6) having an additional 680,000 points and more than six times their Area 5's class percentages. By expanding this search to the ten minor classes in Area 5, it can also be concluded that their relative sizes increased by over 8.5%.

Through further inspection of both areas' results, it can also be concluded that the proposed approach works exceedingly well with ceilings, floors and walls while failing to achieve the same level of performances in the remaining classes. This behaviour can be attributed to the dataset imbalance (the first three classes constitute over 60% of all data), which either prevents the model from generalizing the minor classes as well, or simply does not have enough data for their proper training. Nevertheless, these classes accuracy could easily be improved by acquiring more training data.

Moving to the qualitative evaluation, Figure 4.2 to Figure 4.13 display the surveyed point clouds of several rooms in S3DIS, as well as the entire process of semantic and instance segmentation, geometric characterization and BIM modelling. These rooms were selected for showcasing examples of existing errors resulting from the proposed algorithms. To this end, to simplify this evaluation, the following analysis focuses on the identified errors, implying the overall success of the remaining segmentation and modelling processes.

For the semantic segmentation process, three errors were identified. These were labelled, by the author, as: feature contamination; island clusters; and outright mislabelling of entire elements.

Feature contamination was already briefly mentioned in Section 2.5.3.3 and Section 2.5.4.3, appearing when surrounding segmentation classes appear within another class's boundary. This issue can be seen in Figure 4.7, where the limits of tables and chairs point clouds are classified as the opposite adjacent class. However, apart from tables and chairs, no more classes were found suffering from this issue, which may point to two simple solutions:

- the first is to increase these classes respective training data. This problem can be associated with the lack of training data for two reasons: first, chairs and tables only cumulatively present around 8% of the total training data; second, other classes with higher training data should also present the same problem while interacting with other classes such as: wall-bookcase; wall-board; wall-door; floor-chair; among others;
- the second is to perform a hierarchical segmentation for these two classes, in which the algorithm first determines that the point can belong to the chair or table classes, and then further analysis which of these two labels should be selected. This approach typically solves cases as the previous one, albeit, in a trade-off for the added computation and training of a second algorithm to just focus on differentiating between these two classes.

Island clusters are the author's description of small wrongly labelled clusters appearing within other well-labelled elements. An example of this issue can be seen in Figure 4.5, where small clusters of wall labels appear amidst the curtain wall element, largely correctly labelled as a window. Cases such as this one are fairly rare but also difficult to identify, since these are typically not as sizable and thus not as visible as in Figure 4.5. To correct this issue, a CRF-based solution could be implemented after the initial segmentation to optimize the results. However, once again, this would incur further computation. Additionally, although incorrect, these small clusters do not influence the final modelling, since small clusters such as these ones are not validated by the DBSCAN minimum point threshold for clustering. As such, it is the author's opinion that this issue can, for now, be simply ignored, since it does not jeoperdize the final result. It is also possible that by increasing the training data, the network solves this issue on its own. This is especially true for Figure 4.5, since there is only around 1.5% window points, a fraction of which belong to curtain walls.

Finally, regarding the outright mislabelling of elements, this can be clearly signalled as a very uncommon issue. It was only identified in Figure 4.4, where a table in the middle of the hallway is wrongly classified as a chair, and in Figure 4.7, where a garbage can is also wrongly labelled as a chair (both cases identified by an arrow in their respective figures). Since this problem is so rare and, once again, only associated with minor classes (training data wise), for now the issue should simply be monitored until further training data is used. Nevertheless, as stated in the Section 2.5.3 and identified in Figure 3.5, the automated modelling process is followed up by a user's input, where mislabellings must be identified, since a fully-automated DL process will always have a an accuracy and performance associated that is not 100%.

For the instance segmentation model, Figure 4.2 and Figure 4.3 showcase how well it performs when instances of the same class are well defined in space since it is based on the DBSCAN algorithm. However, when the opposite occurs, as in Figure 4.7, where all the chairs are clumped together, the model has difficulties isolating each instance. This behaviour is evidence by Figure 4.8, which showcases different chairs being grouped in the same instance because of their proximity. A solution to this problem would be to fine-tune the DBSCAN parameters to each class and not only to the point cloud resolution. This would mean that intricate and more problematic classes in instance segmentation, such as chairs and tables, would present a smaller search radius when attempting to find neighbouring points. However, this tunning would have to be carefully performed, since decreasing the search radius too much may end up dividing the own element into multiple clusters. Nevertheless, it should be stated that cases such as this one were only identified in chairs, with the remaining classes, and most importantly, the structural classes, having their instances adequately segmented.

Regarding BIM modelling, as seen throughout Figure 4.2 to Figure 4.11, the developed software performs perfectly in most scenarios. These figures present all available classes is S3DIS properly modelled, even when facing dissimilar types of wall enclosers: closed room in Figure 4.2; u-shaped hallway in Figure 4.4; straight hallway in Figure 4.5; and isolated walls in Figure 4.7.

Additionally, exchanging the default classes is easily performed without issues, as exemplified in Figure 4.9, where the walls, ceiling, floor and even the existing tables are all quickly exchanged using a simple "select all" and "change family" command.

The bottom line is that the Dynamo algorithm will always generate a model geometrically identical to the geometry acquired in the point cloud, which means that any existing errors in the model do not originate on the side of the Dynamo algorithm but on the original point cloud or the segmentation and instance portions of the code.

Errors such as these can be seen in Figure 4.10 and Figure 4.11, where a portion of the room was not properly surveyed, resulting in a lack of information to model the entire room. In most rooms, where the surveyed point cloud did not acquire the entire room, this issue was solved by implementing a simple search mechanic, in which certain elements, such as walls, floors, and ceilings, are virtually extended to search for nearby connections. If a connection is found, the model predicts how the room's geometry should be and models it. However, since this search was limited to an extension of just 10cm, cases as the one in Figure 4.10 are not solved. The search could be further extended to 20, 30, or 50cm, but these could result in elements being wrongly extended and connected, which, in the author's opinion, is a worse scenario than having to manually extend unsurveyed portions of the model as in Figure 4.11 (i.e. simply applying the "extend" tool).

Finally, as the last figures related to this first experiment, Figure 4.12 and Figure 4.13 showcase the importance of a good laser scanning survey of the building, exemplifying that the proposed algorithms and workflows do not perform correctly when the building is not adequately surveyed. In fact, these two figures present the point cloud of a storage room, where several portions of the point cloud are not visible, because of an outright lack of station positions. To add to what was already a fairly complicated room to model (given the several clutter elements in the room), most of the ceiling and floor of the room are not acquired and obstructions were left unchecked. These conditions result in the algorithms only being able to correctly identify a few classes in the point cloud, namely, the bookcase and the shelves, lacking the identification of a door, and failing to properly extract the remaining classes' geometry.

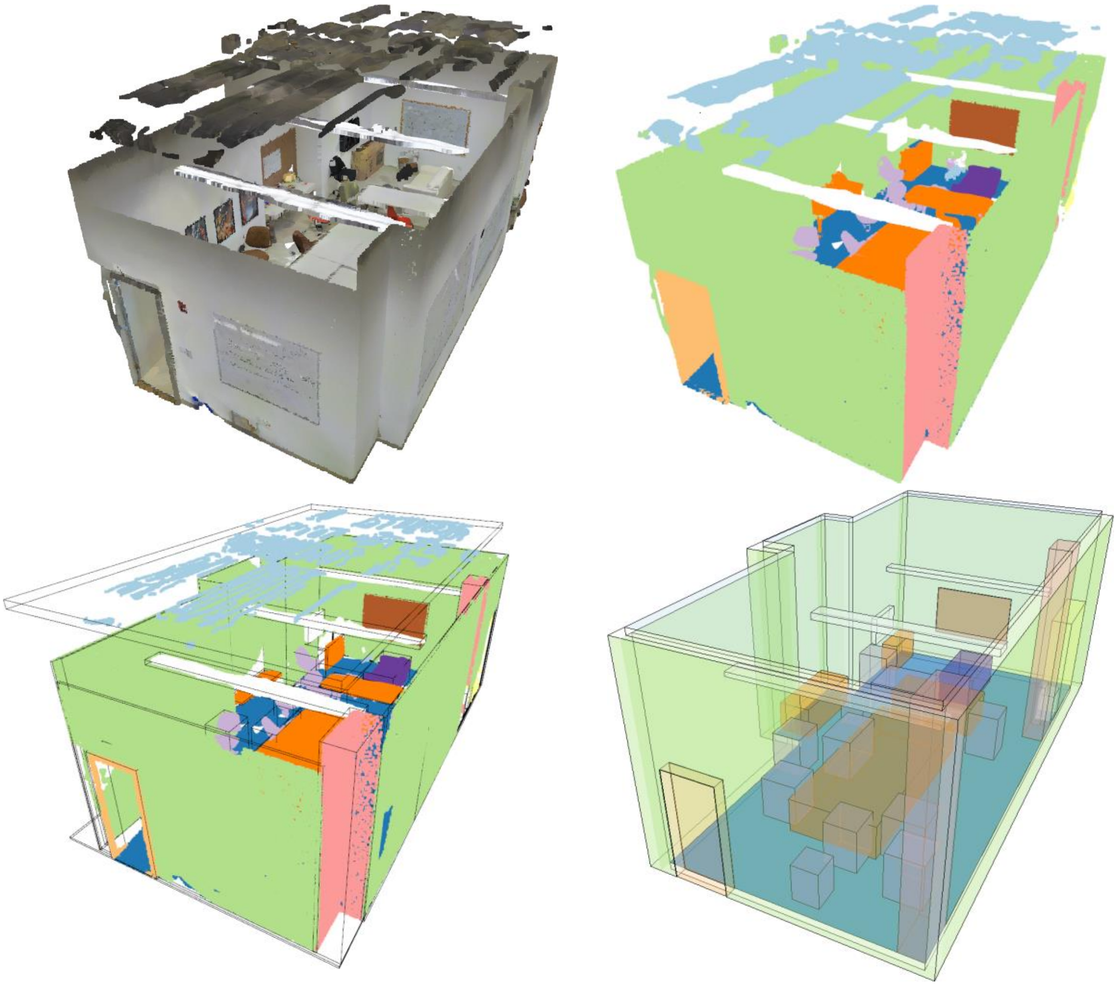

Figure 4.2 – Segmentation, geometric characterization and BIM modelling of a conference room

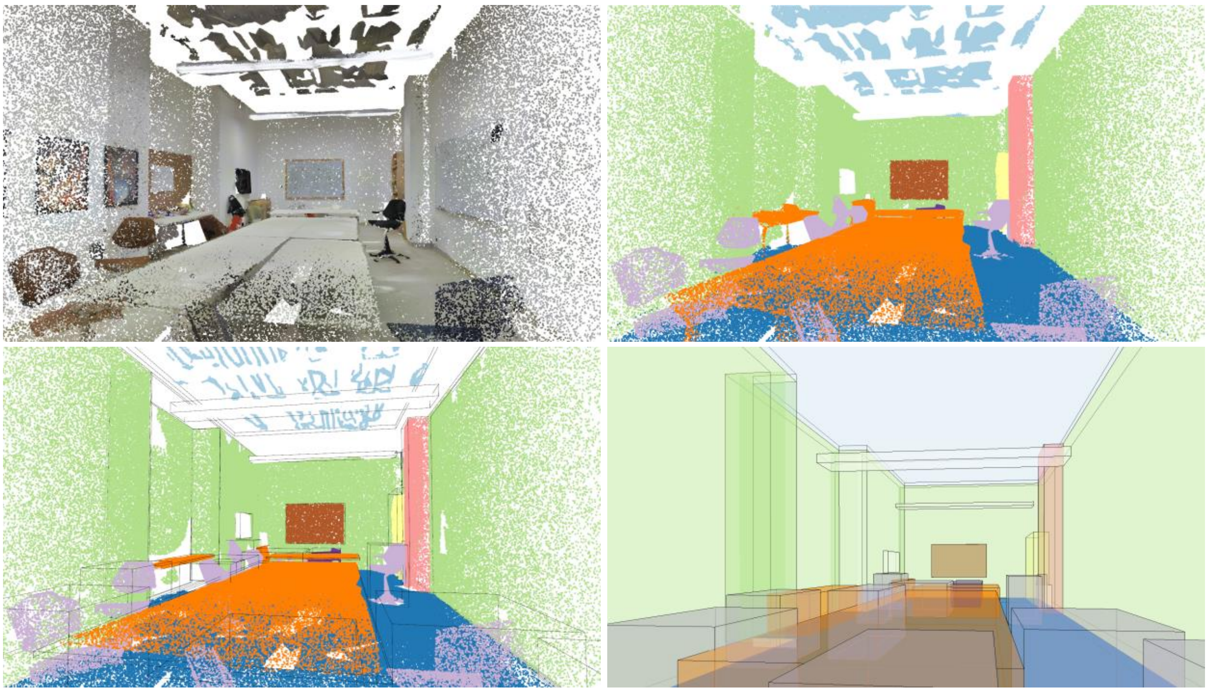

Figure 4.3 – Segmentation, geometric characterization and BIM modelling of a conference room: interior view

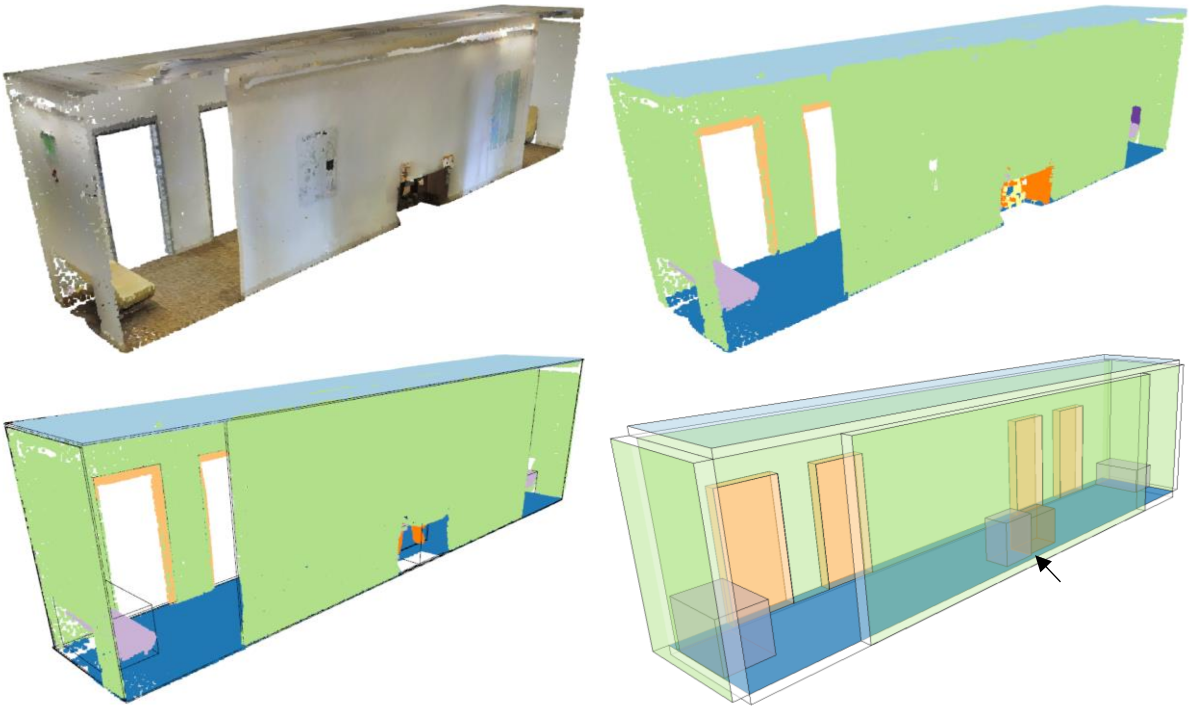

Figure 4.4 – Segmentation, geometric characterization and BIM modelling of a hallway

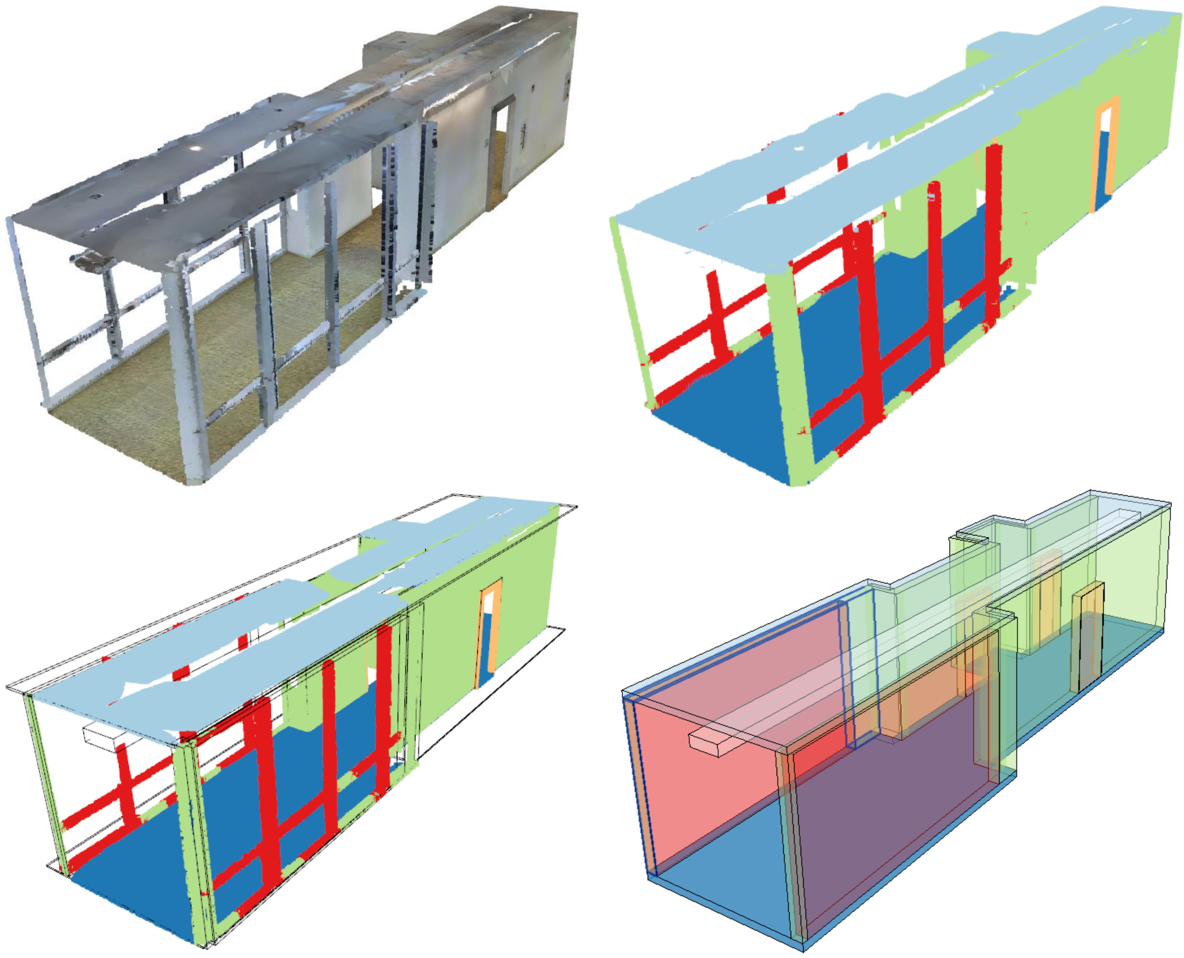

Figure 4.5 – Segmentation, geometric characterization and BIM modelling of a hallway with glazing

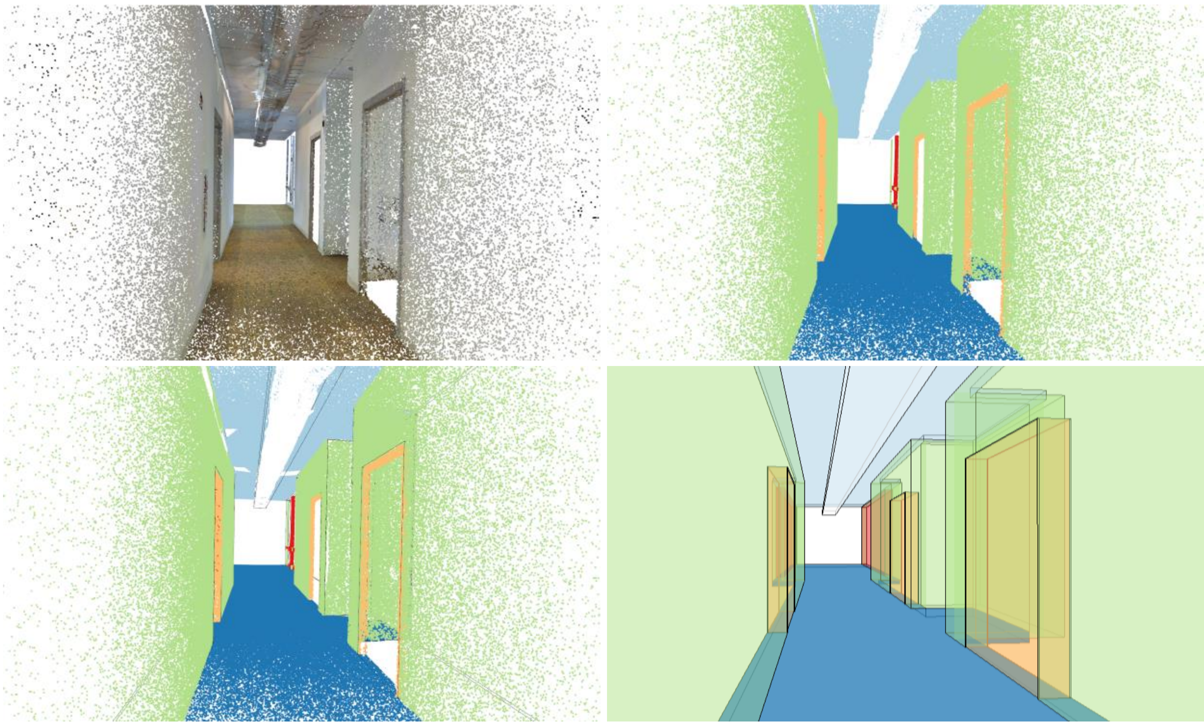

Figure 4.6 – Segmentation, geometric characterization and BIM modelling of a hallway with glazing: interior view

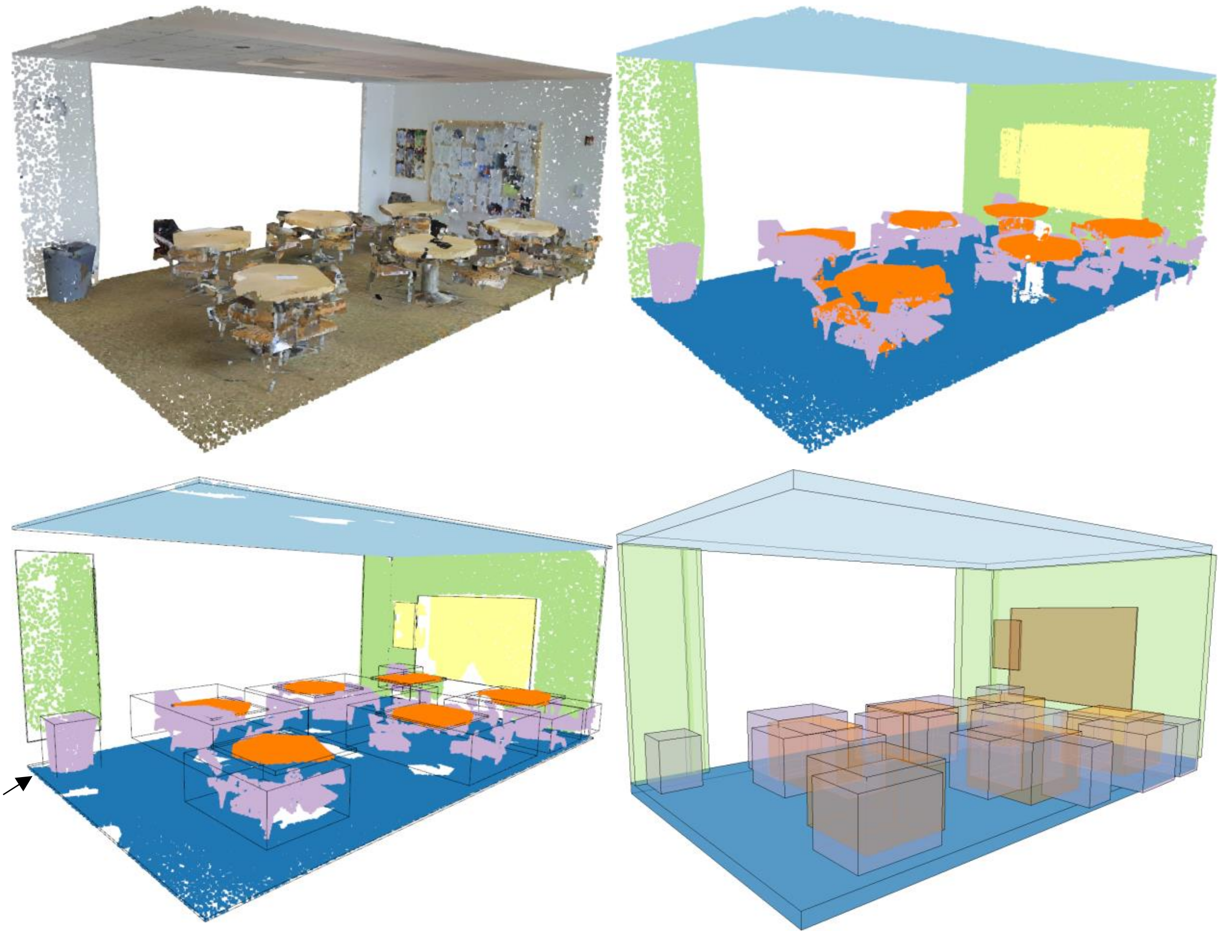

Figure 4.7 – Segmentation, geometric characterization and BIM modelling of a lobby room

Figure 4.8 – Instance segmentation of the chairs seen in Figure 4.7

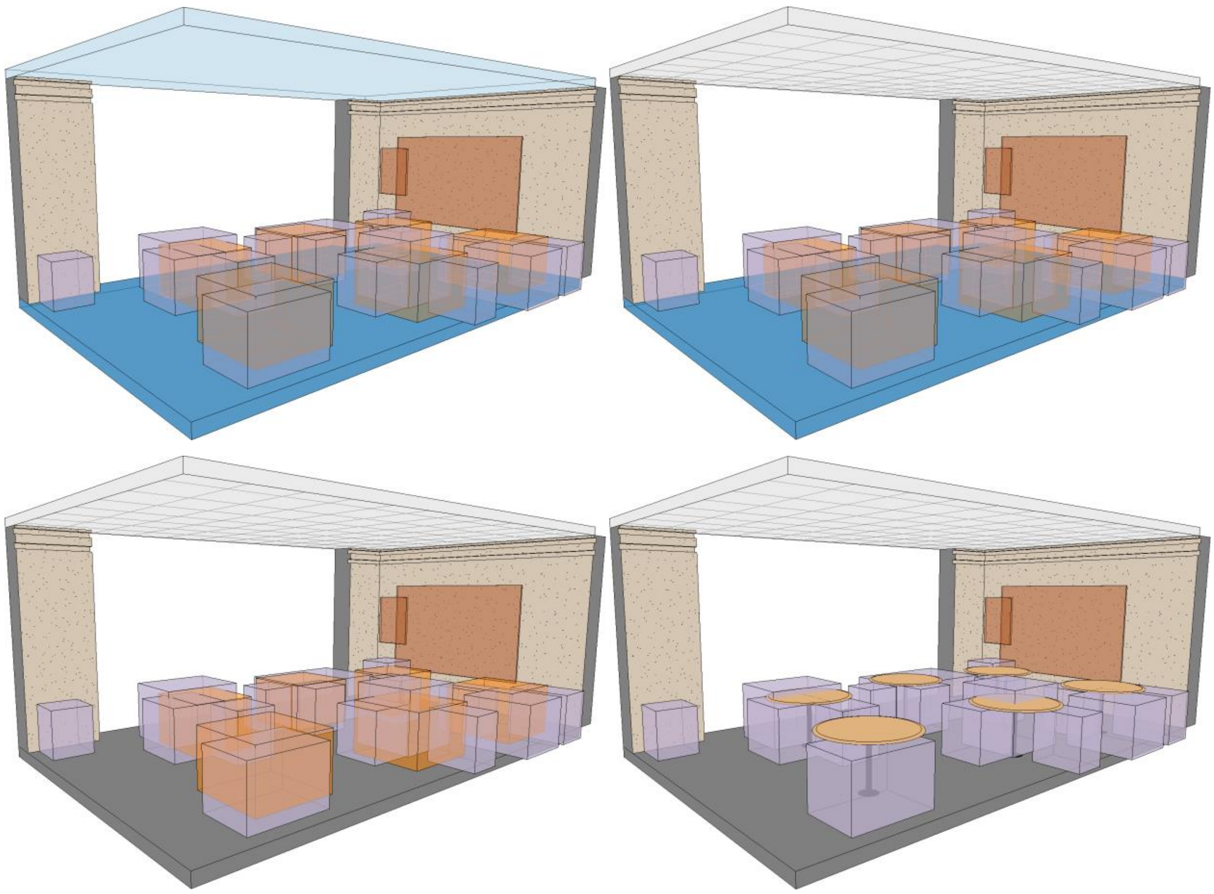

Figure 4.9 – User manual exchange of the modelled default families with custom families provided by the user

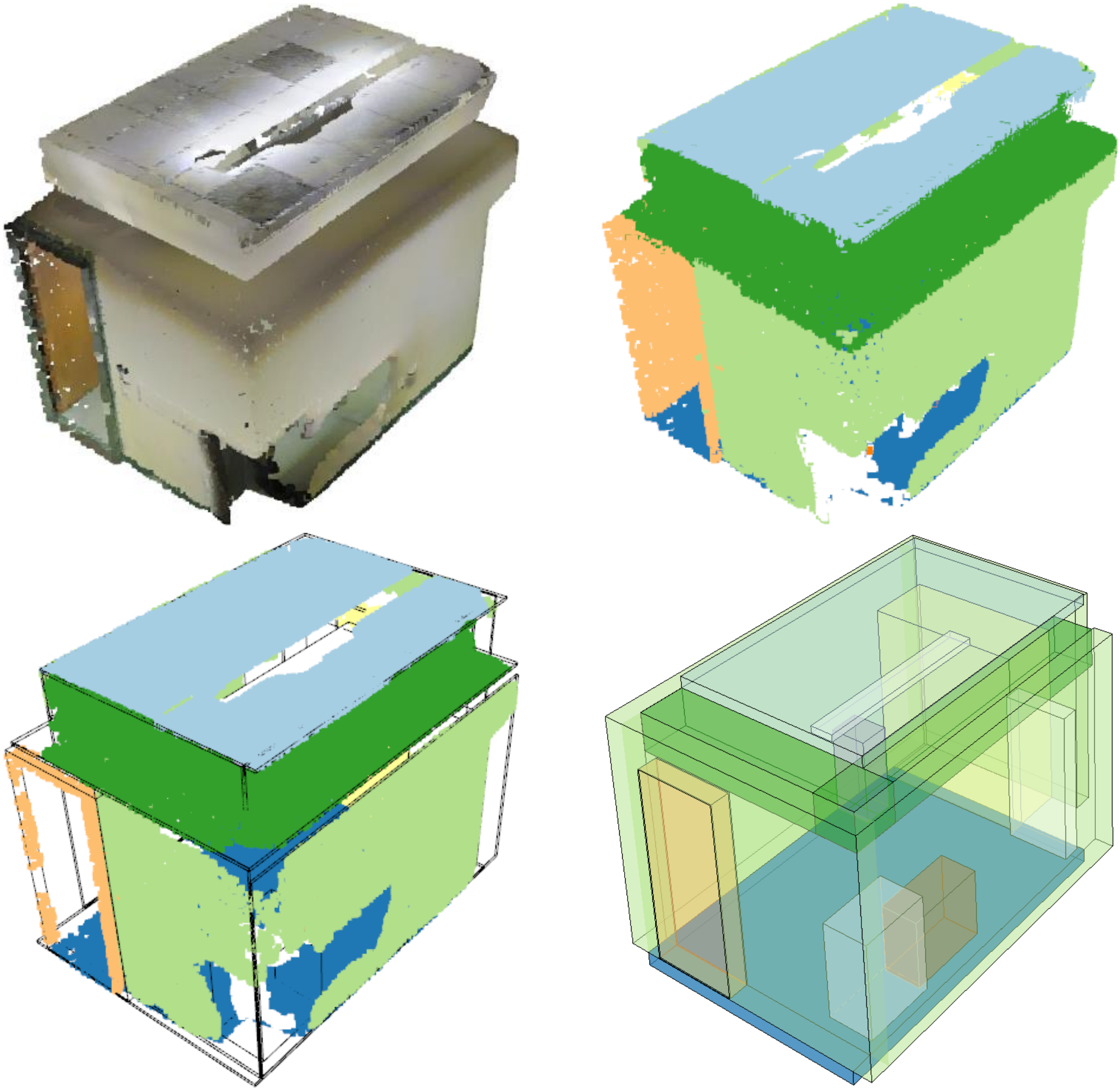

Figure 4.10 – Segmentation, geometric characterization and BIM modelling of a pantry room

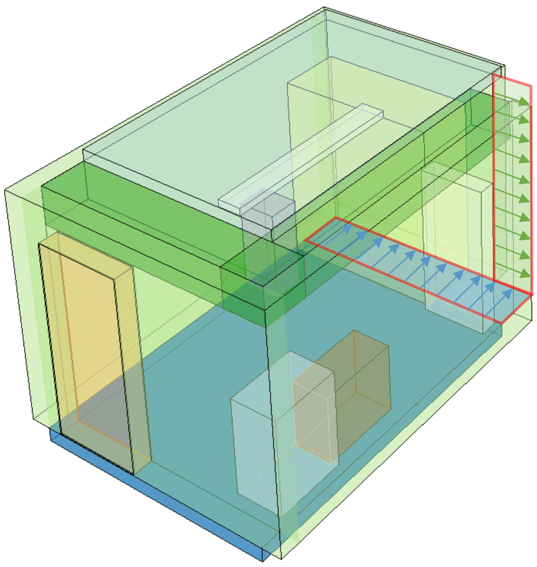

Figure 4.11 – Extension of the floor and wall elements to correct the lack of modelling shown in Figure 4.10

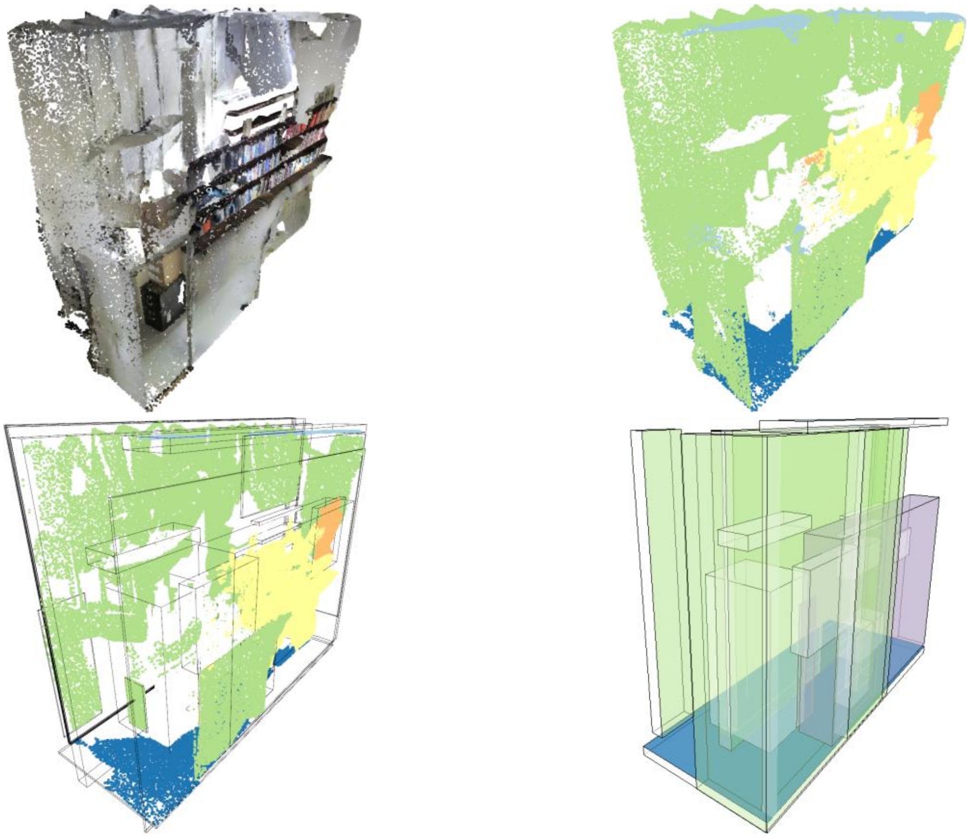

Figure 4.12 – Segmentation, geometric characterization and BIM modelling of a wrongly surveyed storage room

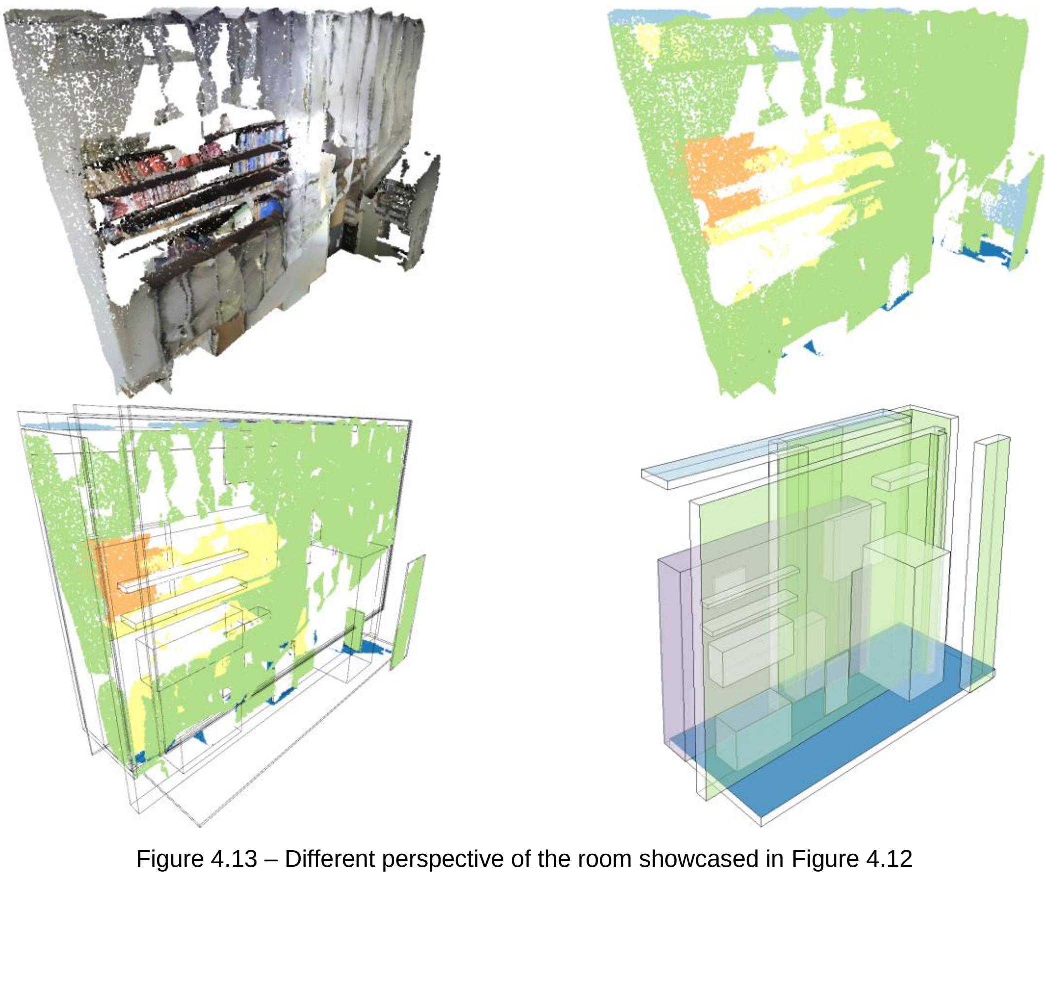

Figure 4.13 – Different perspective of the room showcased in Figure 4.12

4.3. SECOND EXPERIMENT

4.3.1. EXPERIMENTAL SETTING – FEUP

As in the first experiment, the second experiment focused on the segmentation and BIM modelling of a building's point cloud. However, in this experiment, S3DIS was not the sole source for training data, with ArtBIM-PC being applied as an augmentation dataset. This augmentation was done to allow the classification of stairs in a small building point cloud of FEUP, the selected test data. FEUP's point cloud was acquired using *Leica ScanStation P20* and the proposed data acquisition guidelines. As such, in addition to Section 3.4 and Section 3.5 contributions, this experiment also validates Section 3.3 contributions.

Regarding the point cloud information, as stated earlier, each point p_i in both S3DIS and ArtBIM-PC contains information regarding its 3D coordinates $c_i = \{x_i, y_i, z_i\}$ and six features $f_i = \left\{R_i, G_i, B_i, n_{x_i}, n_{y_i}, n_{z_i}\right\}$, its RGB values and normal vector. Both datasets also associate each point with an instance label I_i and one of 14 semantic labels S_i. These include eight structural elements (*ceiling*, *floor*, *wall*, *beam*, *column*, *window*, *door* and *stairs*), five furniture items (*table*, *chair*, *sofa*, *bookcase* and *board*), and a *clutter* class for the remaining data.

All point information is used as input for training the developed models, meaning: $p_i = (c_i, f_i)$. For evaluation metrics, only the *stairs* class accuracy is presented. This metric is calculated according to Equation 4.3.

The main reason for only presenting the evaluation metric for the *stairs* class is that each point in the point cloud had to be manually labelled since the surveyed point cloud did not contain any semantic or instance information. This led to several doubts regarding point labelling, which could significantly influence the resulting accuracies. As such, to not present misleading results, and since the remaining categories had already been evaluated in the first experiment, it was decided to solely include the *stairs* class in the quantitative evaluation, leaving the remaining categories for a qualitative assessment.

Regarding the test/train split, both ArtBIM-PC and S3DIS were used to train the models, while FEUP's point cloud was used for testing. However, S3DIS had to undergo a few modifications to be used, given that eight of its 277 rooms contained stairs. As such, these had to be manually relabeled from *clutter* (as per the original labelling) to *stairs*. These eight stairs range from a few steps to full flights, although most are incomplete (Figure 4.14). It should be noted that only the steps were relabelled to *stairs*, with the handrails remaining as *clutter*.

4.3.2. RESULTS AND DISCUSSION – FEUP

To support the analysis and discussion of the carried experiment, quantitative results are presented in Table 4.7, while qualitative results are displayed from Figure 4.16 to Figure 4.20.

From analysing Table 4.7, it can be concluded that the *stairs* class showcases an good performance, with a class accuracy of 92.95%. This value rivals the best performing classes in S3DIS (i.e. the *ceiling*, *floor* and *wall* classes), at least in the conducted tests – Areas 5 and 6 in the first experiment. As such, it can be determined that the data augmentation with the generated artificial point clouds was successful, validating the developed software tool and generated dataset. Figure 4.15 enables a visual comparison between one of the artificial *stairs* point clouds and the surveyed point cloud, reinforcing these conclusions, given their similarities. The surveyed point cloud has still to suffer its decimation, so it has a higher resolution. Nevertheless, the similarities are apparent.

Figure 4.14 – All existing stairs point clouds in S3DIS, originally labelled as *clutter* and changed to *stairs*

Table 4.7 – *Stairs* class classification accuracy for FEUP's point cloud

True Label	Predicted Label	#points	%points
Stairs	Stairs	461544	92.95
	Wall	15159	3.05
	Floor	12953	2.61
	Ceiling	5451	1.10
	Clutter	1443	0.29

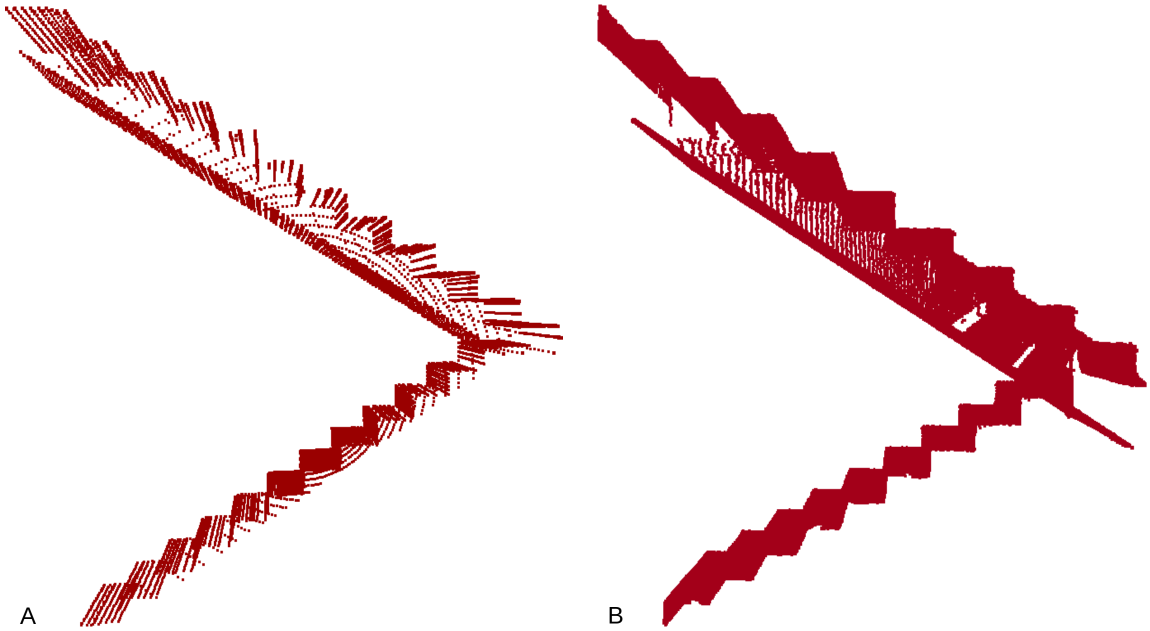

Figure 4.15 – Comparison between the artificially generated point cloud (A) and the surveyed point cloud (B)

Regarding the qualitative evaluation, Figure 4.16 to Figure 4.20 showcase the surveyed point clouds, their segmentation, automated modelling and manual modelling. The manual models are presented to allow for a comparison with the automatically generated models. As in the previous experiments, the analysis focuses on the identified errors, implying the overall success of the remaining point cloud segmentation and modelling.

Starting with the survey itself, Figure 4.16 showcases two errors in data acquisition. These errors influence the automated BIM modelling by not providing enough data to model certain elements, namely, (1) the sidewall of the elevator entrance and (2) the suspended ceiling's "wall" under the flight of stairs. These errors are highlighted in Figure 4.16, Figure 4.17 and Figure 4.20 using a red circle. Additionally, small portions of the areas below the scan stations' location were left unsurveyed. However, given how the automated floor modelling is performed, this was not an issue.

Regarding semantic segmentation, only one error was identified. This error consists of classifying the point cloud segment below the second floor and near the second flight of stairs as a *wall* instead of a *beam*, the most likely element. It is stated as "likely" since the beams' locations cannot be pinpointed without additional survey methods or access to FEUP's structural plans, both of which were unavailable. This possible error is highlighted in Figure 4.19 using a blue circle. It should be stated that this error allowed for the identification of the same error in the ArtBIM-PC dataset, where the stairs are never resting upon beams. Thus, ArtBIM-PC point clouds will be regenerated to include beams when applicable, and this element will be kept in mind when expanding the dataset.

Regarding the automated BIM modelling, two errors were identified:

- the first is related to the continuing difficulty in modelling beams, given how these are configurated in *Revit*'s API. This error is highlighted in Figure 4.18 and Figure 4.20 using a purple circle, where a portion of the modelled beams collide with the modelled walls;

- the second error is similar to the first in that it relates to *Revit*'s API, this time in the context the *stairs* element. More precisely, as stated in Section 3.5.1, the sides of the stairs cannot be united to adjacent elements (when modelled through *Dynamo*), meaning that the stairways' walls do not find an intersection and continue their height until reaching the base level, instead of stopping at the *stairs*, as intended. This error is highlighted in Figure 4.16, Figure 4.17 and Figure 4.18 using an orange circle;

It should be noted that the white clutter boxes near the flights of stairs' beginning and end indicate portions of the handrails where there was a sufficient point cloud density to create a cluster in DBSCAN. These could either be deleted or used to identify the rail height. If the user required the continuing rail, instead of just its extremities, the required DBSCAN density could be lowered. In opposition, increasing the density requirement would lead to no handrail elements.

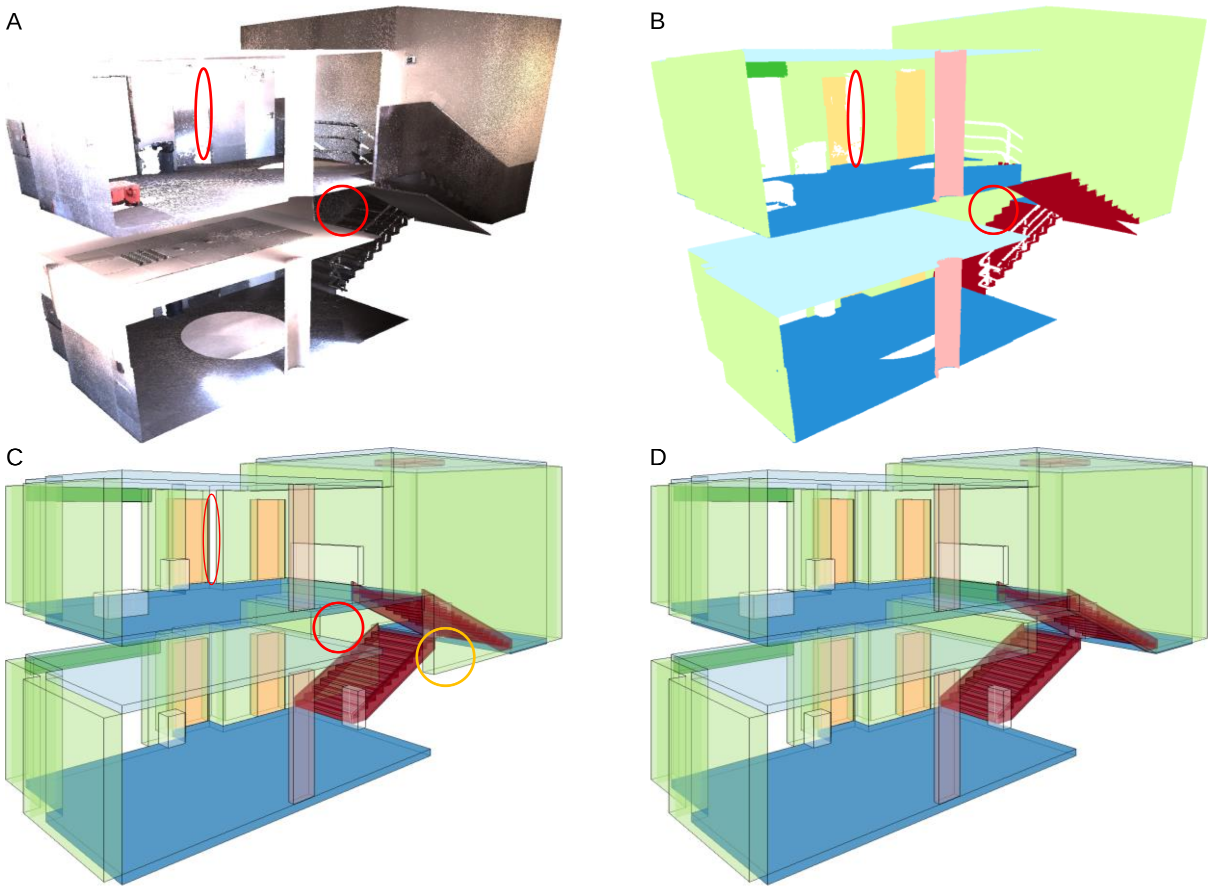

Figure 4.16 – FEUP's point cloud front view: survey (A), segmentation (B), automated modelling (C), and manual modelling (D)

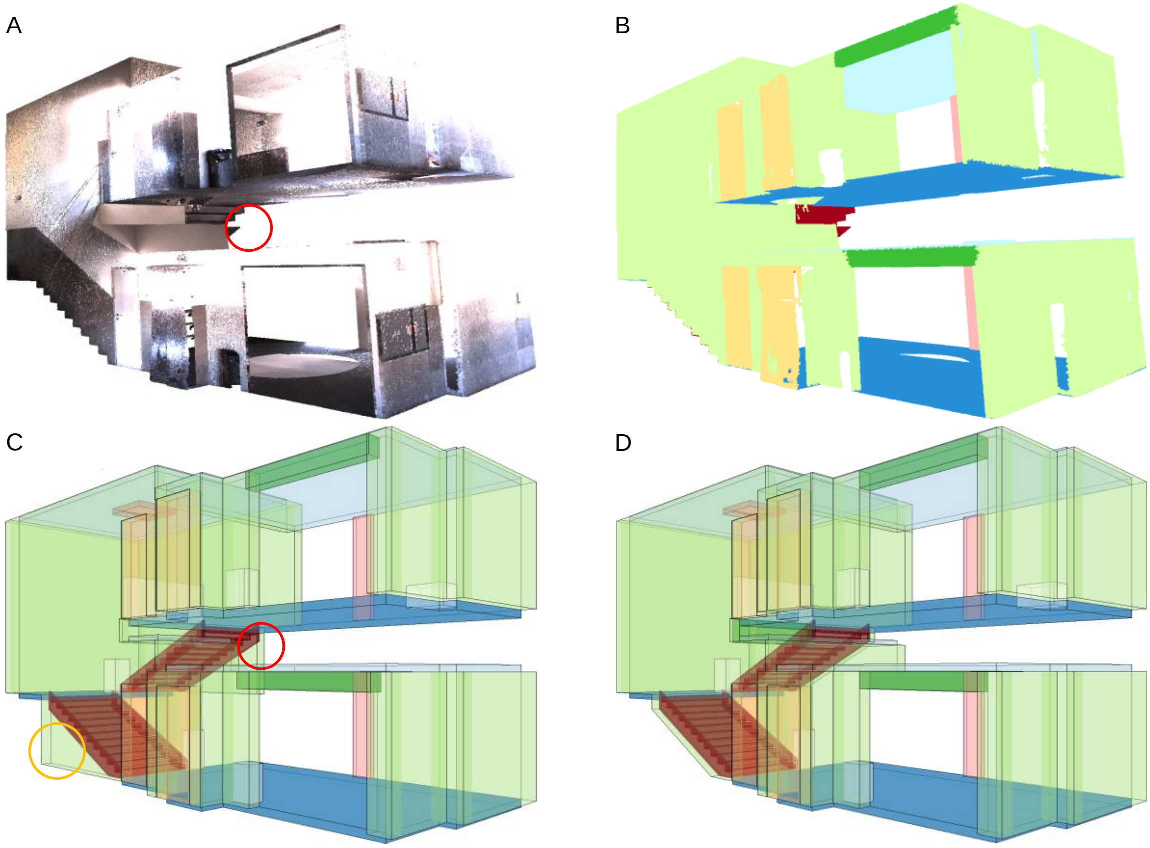

Figure 4.17 – FEUP's point cloud back view: survey (A), segmentation (B), automated modelling (C), and manual modelling (D)

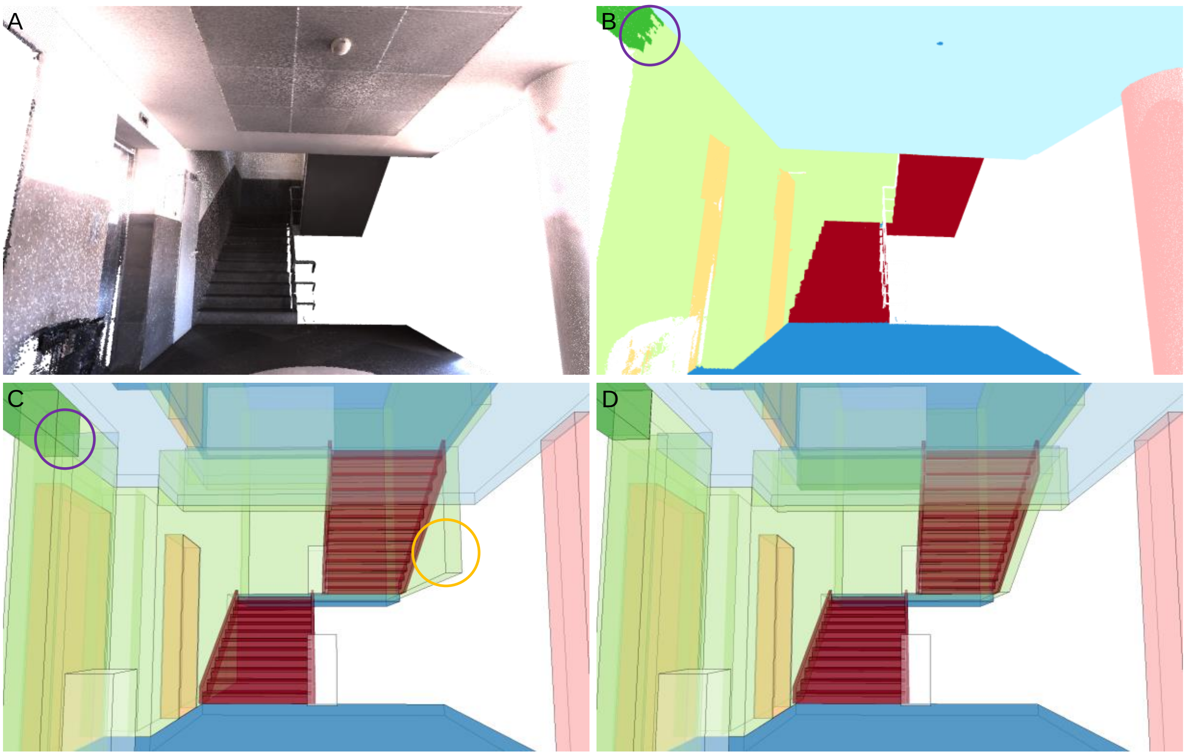

Figure 4.18 – FEUP's point cloud first-floor interior view: survey (A), segmentation (B), automated modelling (C), and manual modelling (D)

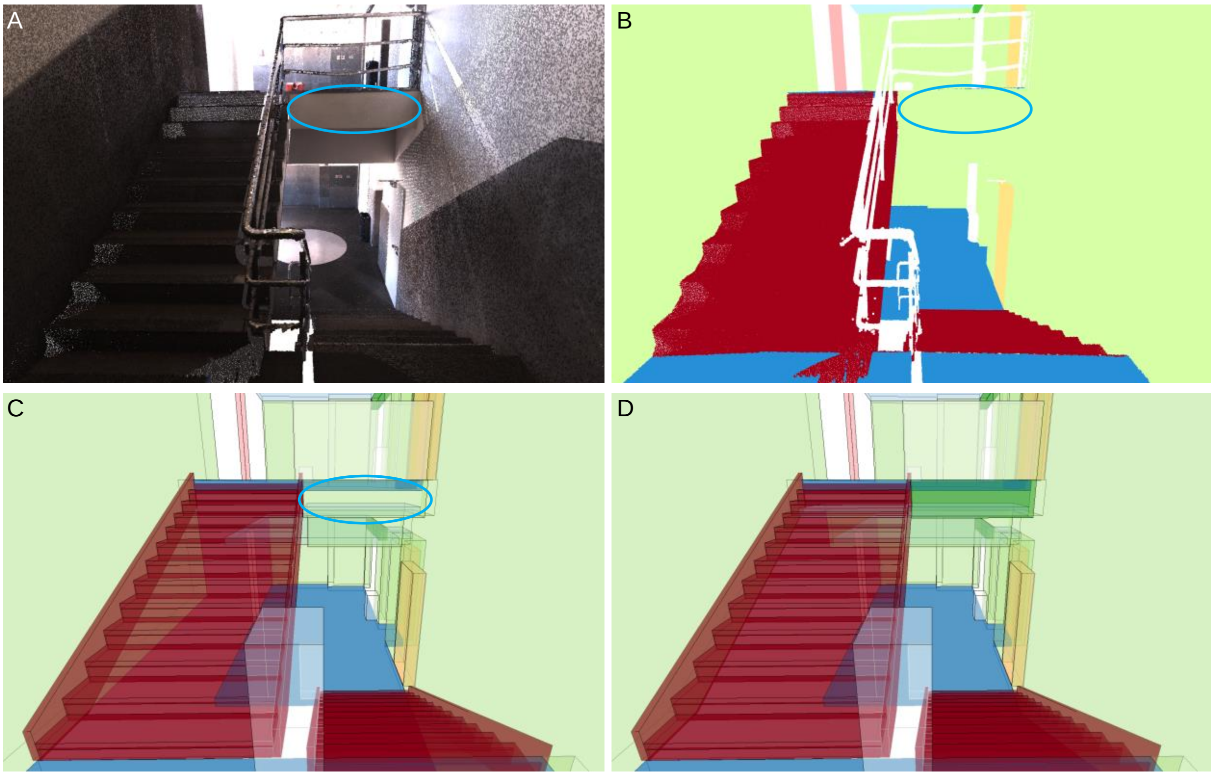

Figure 4.19 – FEUP's point cloud stairs interior view: survey (A) segmentation (B), automated modelling (C) and manual modelling (D)

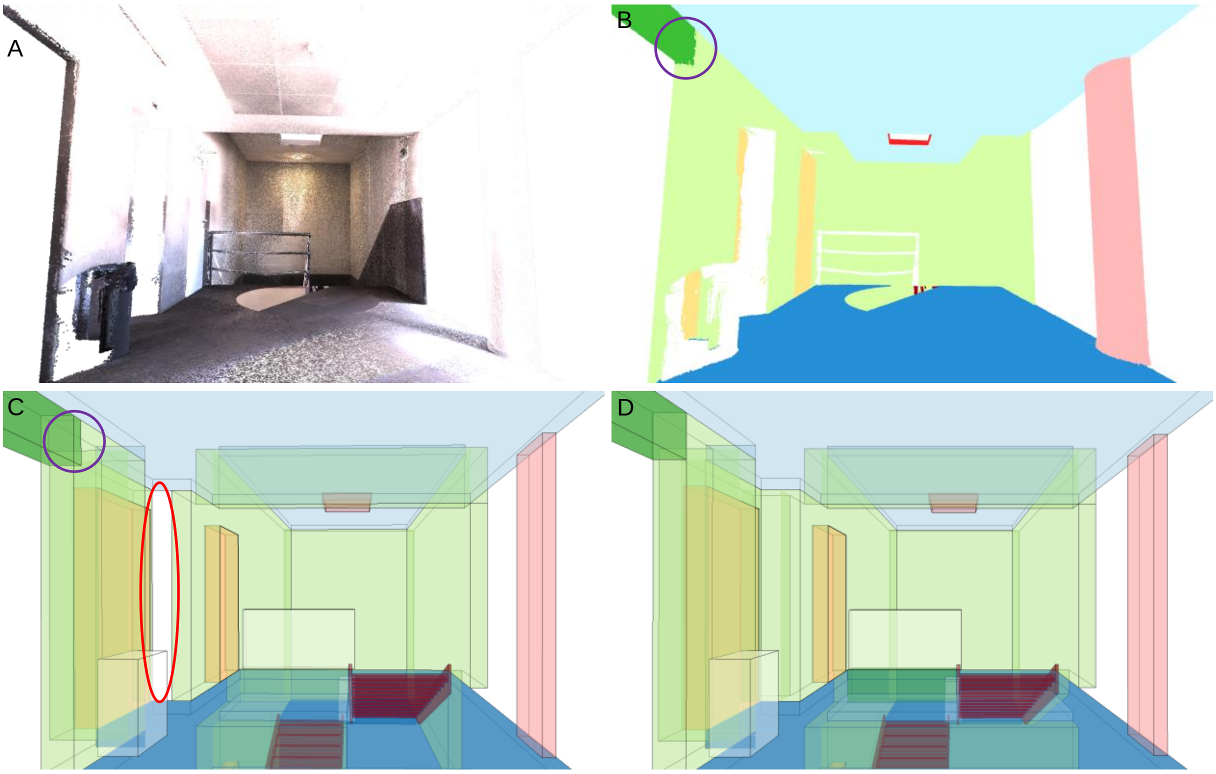

Figure 4.20 – FEUP's point cloud second-floor interior view: survey (A), segmentation (B), automated modelling (C), and manual modelling (D)

4.4. THIRD EXPERIMENT

4.4.1. EXPERIMENTAL SETTING – SHAPENET-PART

The third experiment focused purely on part segmentation, thus assessing the developed part segmentation network presented in Section 3.5. The applied dataset was ShapeNet-Part [684].

ShapeNet-Part is a large-scale 3D object part segmentation dataset consisting of 3D RGB point clouds of 16,881 geometric models from 16 different semantic classes. These are: *airplane*; *bag*; *cap*; *car*; *chair*; *earphone*; *guitar*; *knife*; *lamp*; *laptop*; *motorbike*; *mug*; *pistol*; *rocket*; *skateboard*; and *table*. Each class is divided into two to six parts, and there are 50 different parts in total. Table 4.8 presents further information regarding these classes, while Figure 4.21 showcases some examples of model point clouds in the dataset.

Table 4.8 – ShapeNet-Part dataset information

Class	#models	#points	%points	#parts	Parts
Airplane	2,690	6,934,600	15.74	4	Fuselage / Engine / Tail / Wing
Bag	76	208,959	0.47	2	Case / Handle
Cap	55	144,734	0.33	2	Brim / Crown
Car	898	2,481,901	5.63	4	Frame / Hood / Roof / Wheel
Chair	3,758	10,133,843	23.00	4	Arm / Back / Leg / Seat
Earphone	69	172,272	0.39	3	Cable / Earphone / Headband
Guitar	787	1,852,525	4.20	3	Body / Head / Neck
Knife	392	845,376	1.92	2	Blade / Handle
Lamp	1,547	3,398,202	7.71	4	Base / Canopy / Shade / Tube
Laptop	451	1,227,288	2.79	2	Base / Lid
Motorbike	202	552,602	1.25	6	Tank / Handle / Light / Seat / Wheel / Frame
Mug	184	518,322	1.18	2	Cup / Handle
Pistol	283	730,116	1.66	3	Barrel / Grip / Trigger
Rocket	66	155,667	0.35	3	Body / Fin / Nose
Skateboard	152	384,491	0.87	3	Deck / Truck / Wheel
Table	5,271	14,326,407	32.51	3	Leg / Skirt / Top
Total	16,881	44,067,305	100	50	

Each point p_i in ShapeNet-Part is associated with a part label P_i and contains information regarding its 3D coordinates $c_i = \{x_i, y_i, z_i\}$ and its normal vector $f_i = \left\{n_{x_i}, n_{y_i}, n_{z_i}\right\}$.

Once again, all point information is used as input for the network: $p_i = (c_i, f_i)$. Mean intersection-over-union over parts ($mIoU$) is calculated as the evaluation metrics using Equation 4.4 and Equation 4.5:

$$mIoU = \frac{\sum_{P}^{l}(IoU_P)}{l} \tag{4.4}$$

$$IoU_P = \frac{Predicted\ Area_P \cap Groundtruth\ Area_P}{Predicted\ Area_P \cup Groundtruth\ Area_P} \times 100 \tag{4.5}$$

, where l represents the total number of parts and P represents the evaluated part. For a better understanding of this metric, see Figure 4.22.

As in [528, 542, 555, 558, 598], 14,006 models are used for training, while 2,874 are left for testing.

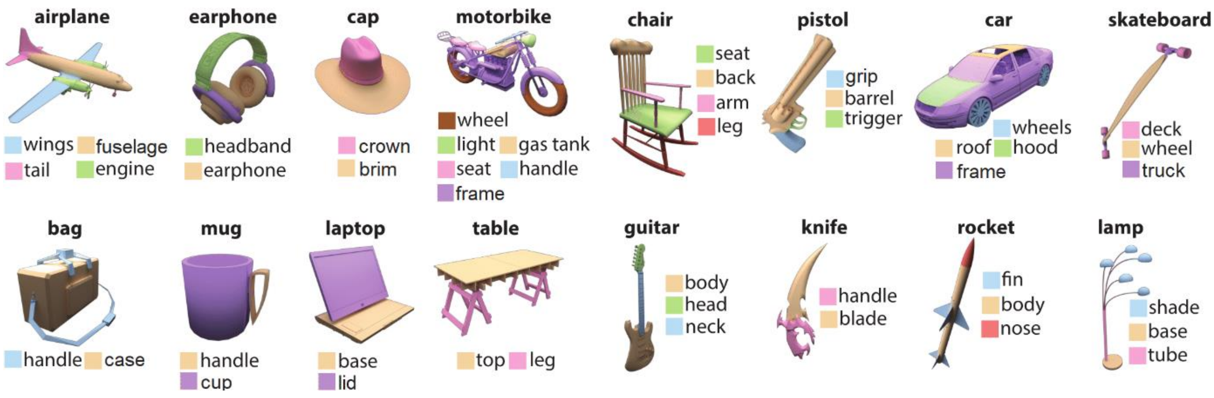

Figure 4.21 – Exemples of models and parts for each class in ShapeNet-Part. Adapted from [684]

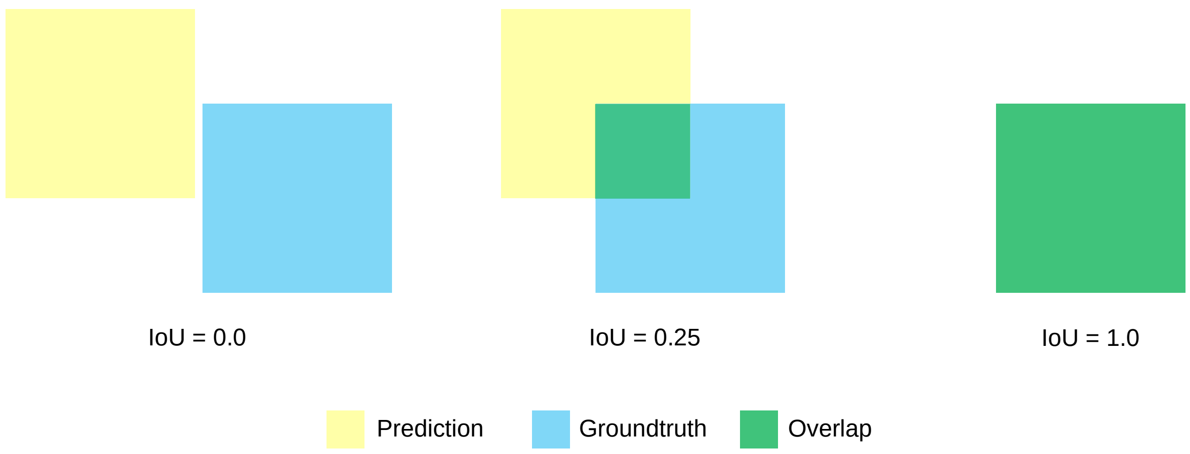

Figure 4.22 – Visualization of IoU. The prediction and groundthruth areas are given by the respective point cloud masks

4.4.2. Results and Discussion

The carried experience's quantitative results are presented in Table 4.9, while qualitative results are displayed in Figure 4.23.

Focusing on Table 4.9, it can be seen that the existing literature on this dataset is quite extensive, with the author identifying at least 24 models. The proposed approach is well placed when compared with these models, once again surpassing PointNet [556] despite staying below PVNet [542], with less 0.3% $mIoU$. As in S3DIS, PointTransformer [528] leads the ranking in ShapeNet-Part.

Regarding Figure 4.23, it can be seen that the network correctly part segments the chosen representative classes, namely, *chair*, *lamp*, and *table*. Seven dissimilar examples are displayed for each class, demonstrating the generalization capabilities of the proposed network. The chosen classes were selected for their relative prevalence in the context of scan-to-BIM, as well as their presence in S3DIS's semantic labels (lamps can be found classified as *clutter* in S3DIS).

Table 4.9 – ShapeNet-Part segmentation results. Mean intersection-over-union over parts ($mIoU$) for the proposed approach and existing models in the state-of-the-art

Method	mIoU
SAFRA [684]	81.4
KD-Net [548]	82.3
PointNet [556]	83.7
SPLATNet [554]	84.6
SSCNN [704]	84.7
RSNet [633]	84.9
SO-Net [582]	84.9
PointNet++ [493]	84.9
ASIS [701]	85.0
DGCNN [609]	85.2
P2Sequence [634]	85.2
SpiderCNN [594]	85.3
PointConv [586]	85.7
JSNet [703]	85.8
SGPN [563]	85.8
ConvPoint [585]	85.8
Proposed Approach	85.9
SSCN [555]	86.0
PointASNL [564]	86.1
PointCNN [598]	86.1
PVNet [542]	86.2
RS-CNN [592]	86.2
KPConv [494]	86.4
SASO [702]	86.4
PointTransformer [528]	**86.6**

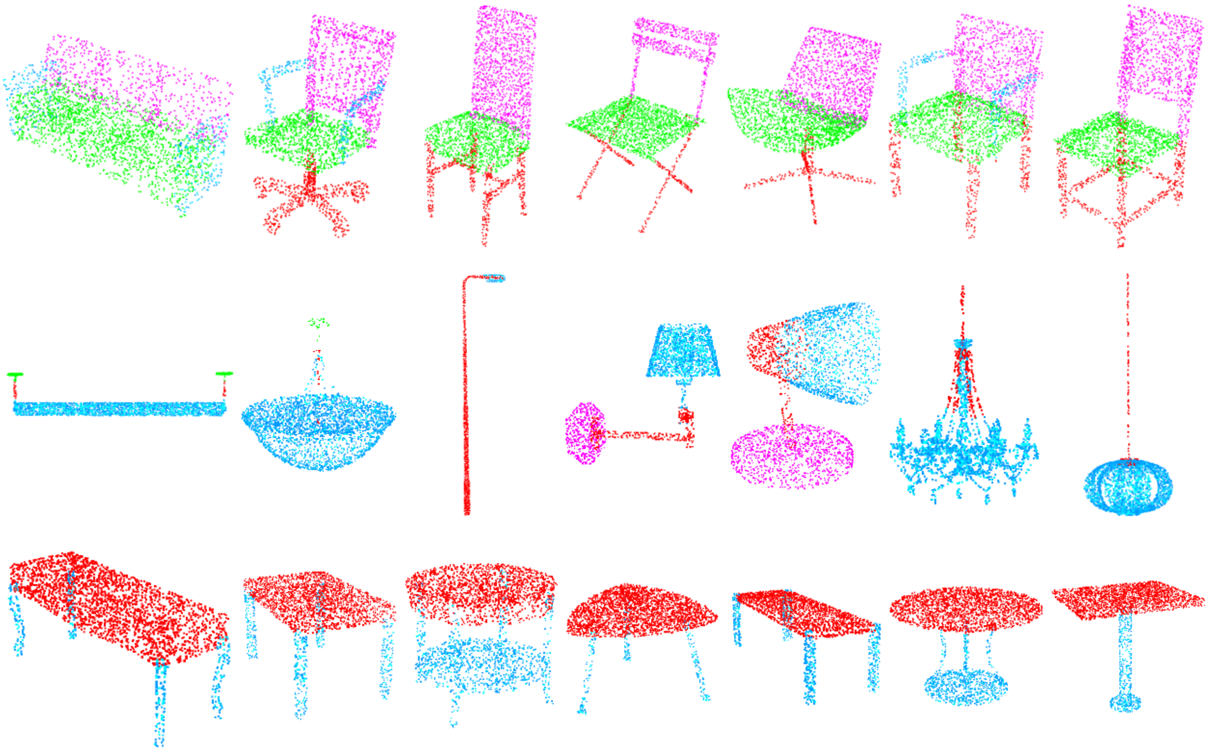

Figure 4.23 – Segmentation examples for the classes “chair”, “lamp”, and “table”, using the proposed approach

It should be stated that although ShapeNet-Part is an extensive dataset suitable to assess the proposed network, it does not include many classes relevant to the scan-to-BIM process. In fact, from the 14 trained labels during semantic segmentation (i.e. the 13 classes from S3DIS and the *stair* class from ArtBIM-PC), only three are included in ShapeNet-Part. These are: *chair*; *sofa*; and *table*; with the *sofa* class being included in ShapeNet-Part through its *chair* class – see Figure 4.23. Even when accounting for identified objects within the *clutter* class of S3DIS, such as lamps, the dataset is still outside the focused topic.

Nevertheless, ShapeNet-Part was selected to train and test the developed network given the lack of a better-suited dataset and its prevalence in the literature.

For clarification, in a real-world scenario, if no part data were available to train a determined semantic label (e.g. wall), that label would be constituted by a single part representing its entire geometry. Thus, when performing the BIM model enrichment with part data, only one part would be described for these building elements.

4.5. Fourth Experiment

4.5.1. Experimental setting – PCMat-30

The fourth experiment focused solely on material classification, thus assessing the proposed fully-automated enrichment process proposed in Module 5. The applied dataset was PCMat-30.

As indicated in 3.6.1, PCMat-30 is the author's own material classification dataset consisting of 27.000 3D RGB point clouds from 30 unique material classes. Sample point clouds for each available material can be seen in Table 4.10, while Figure 4.24 presents the number of points per material.

The dataset's creation process was as follows: initially, each material class was captured in three distinct conditions, resulting in 90 different point clouds. The conditions were made distinct through variations in lighting (e.g. indoor or outdoor), incidence angle (i.e. the angle between the laser and material surface), size (e.g. a large wooden table top or a slender wooden table leg), primary plane (e.g. stone wall or stone floor), colour (e.g. blue and red carpet), and pattern (e.g. different brick designs). Some of these distinctions can be visualized in Table 4.11.

Leica ScanStationP20 [657] was used as the laser scanner for all captures. The settings for the scan resolution and quality were, respectively, 0.8mm@10m and four. All materials were acquired within ten meters of the laser scanner, meaning the point clouds' final resolution is sub 0.8mm. The laser scanner's internal camera was used to photograph the scanned scene and map the resulting photographs' colours onto the acquired point cloud. All photographs were captured with a resolution of 640×640 and the appropriate lighting settings.

After their acquisition, the 90 initial point clouds were modified to augment the dataset. These modifications include:

- the decimation of the resolution from sub 0.8mm to 3.1mm, 6.3mm, and 12.5mm (see Table 4.12), resulting in 270 point clouds;
- the subdivision of each of the resulting point clouds into five differently sized point clouds (see Figure 4.25), resulting in 1,350 point clouds;
- the artificial modification of the point clouds' brightness (see Table 4.13), resulting in five different brightness levels $\{-10, -5, 0, 5, 10\}$% and 6,750 point clouds;
- and the implementation of random dropout (see Table 4.12), resulting in four different dropout levels $\{0, 5, 10, 15\}$% and the final 27,000 point clouds.

It should be stated that reducing the point resolution and performing random dropout is inherently different: the former systematically removes points based on the minimum distance between two points; the latter randomly removes points based on chance until achieving the target dropout percentage. Additionally, it should be emphasized that by augmenting the dataset with multiple resolutions and differently sized point clouds, the resulting models will be able to have a better generalization.

Each point p_i in PCMat-30 is associated with a material label and contains information regarding its 3D coordinates $c_i = \{x_i, y_i, z_i\}$ and seven features $f_i = \left\{R_i, G_i, B_i, n_{x_i}, n_{y_i}, n_{z_i}, I_i\right\}$, its RGB values, normal vector and intensity value.

All point information is used as input: $p_i = (c_i, f_i)$. For evaluation metrics, overall accuracy ($oAcc$), mean accuracy over classes ($mAcc$), and per-class accuracy (Acc) are calculated according to Equation 4.1, Equation 4.2, and Equation 4.3, respectively.

Table 4.10 – PCMat-30 dataset material classes

Brick 0	Brick 1	Cardboard 0	Carpet 0	Carpet 1
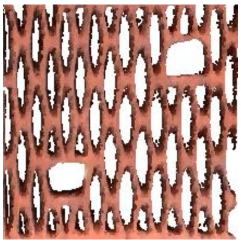				
Cloth 0	Cloth 1	Cobblestone 0	Concrete 0	Concrete 1
	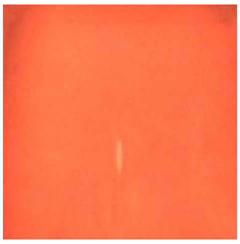		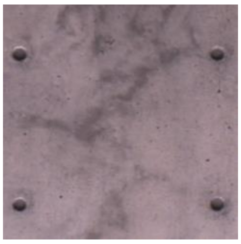	
EPS 0	Fiber 0	Grass 0	Grass 1	Gravel 0
	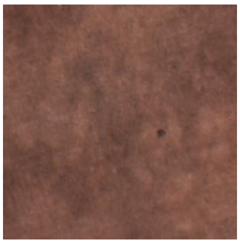		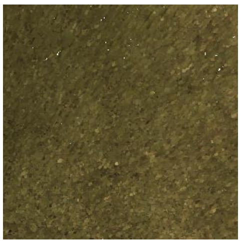	
Grid 0	Leather 0	Metal 0	Metal 1	Mortar 0
	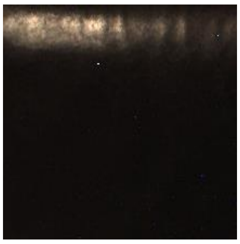			
Plaster 0	Plastic 0	Stone 0	Stone 1	Stone 2
			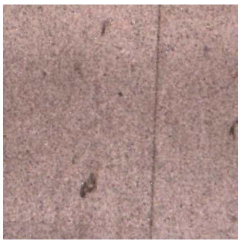	
Rubber 0	Tar	Tile 0	Wood 0	Wood 1
			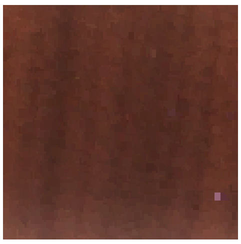	

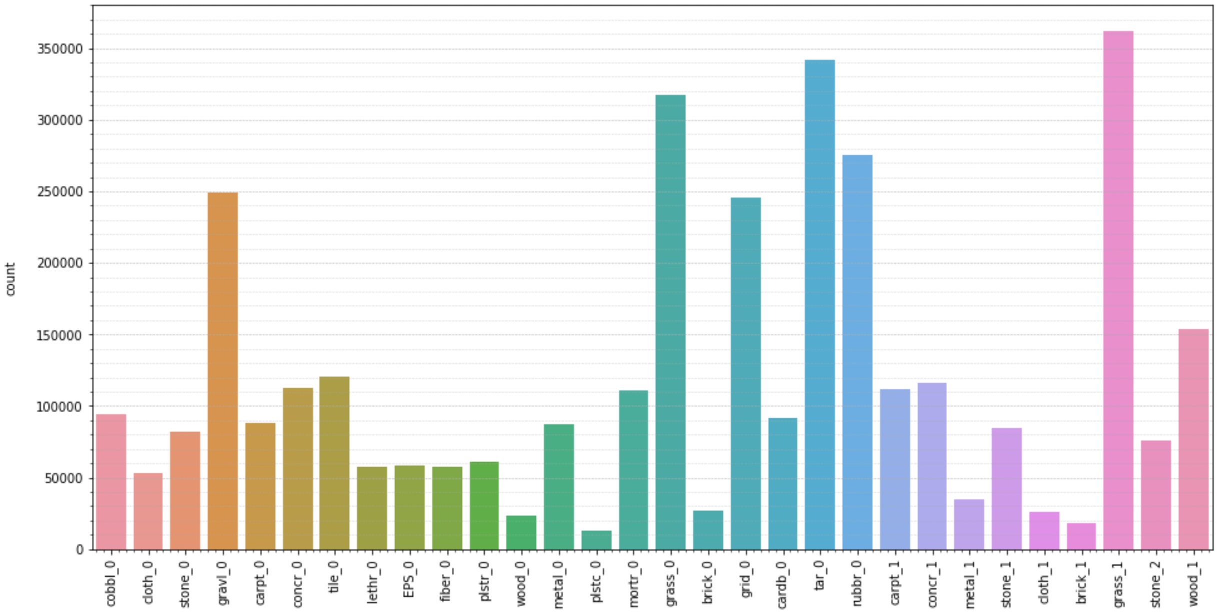

Figure 4.24 – Point distribution per material class in PCMat-30

Table 4.11 – Visual comparison between distinct point clouds of the same material

Cobblestone 0	Concrete 0
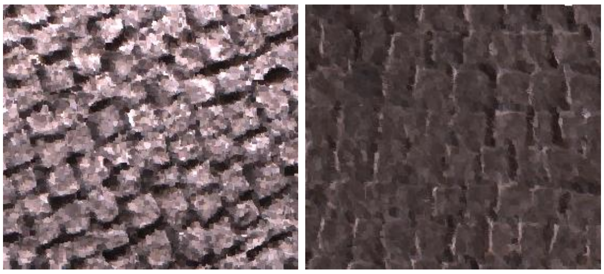	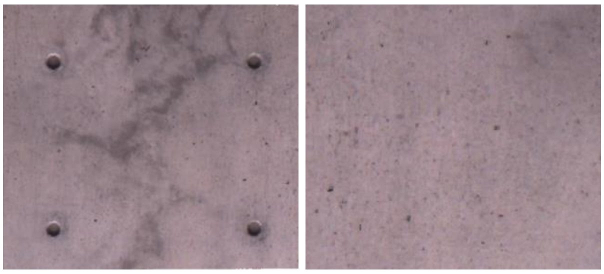
Concrete 1	**Metal 0**
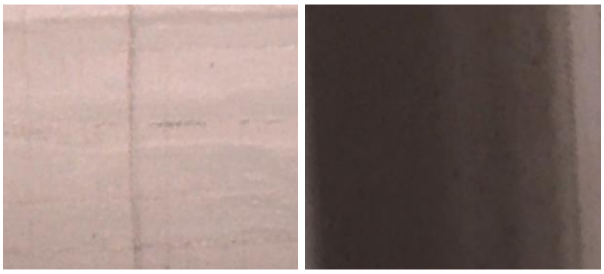	
Mortar 0	**Stone 1**
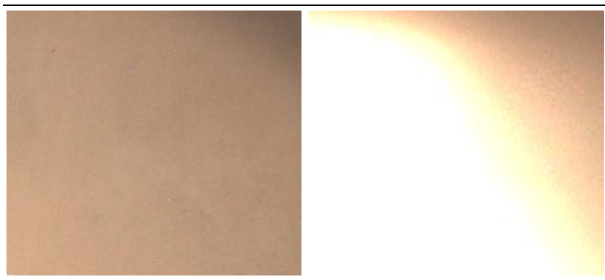	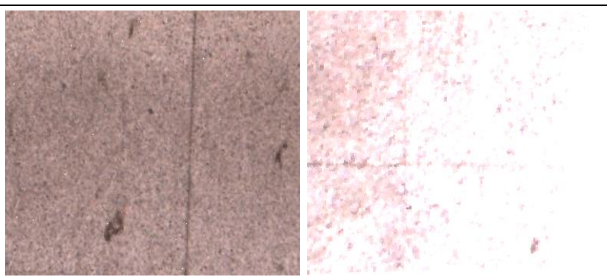

Table 4.12 – Visual comparison between all three resolutions available in the material dataset, as well as between Random Dropout (RDp) of 0% and 15%

Res.	3.1mm		6.3mm	12.5mm
RDp	0%	15%	0%	0%
Plastic Grid Point Cloud	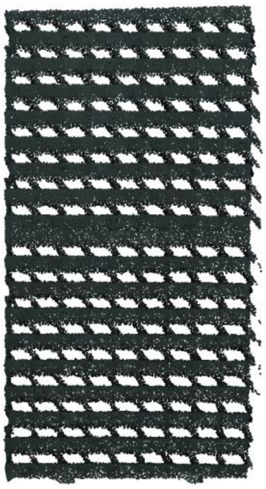	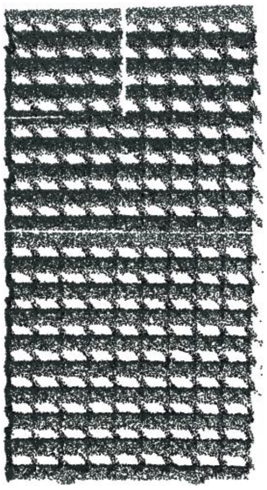	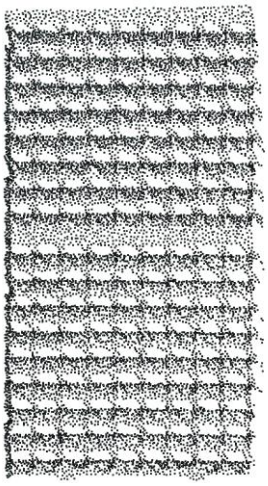	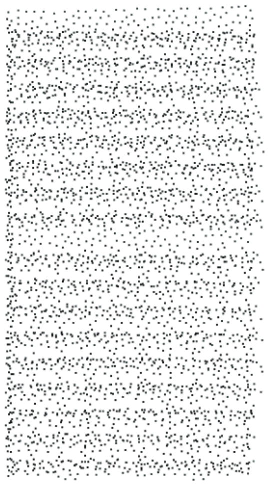

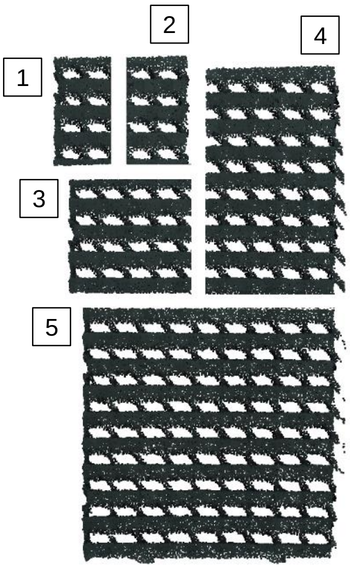

Figure 4.25 – Typical subdivision of the point cloud into five differently sized point clouds

Table 4.13 – Visual comparison between all five levels of artificial brightness in the material dataset

Brightness Level				
-10%	-5%	0%	+5%	+10%

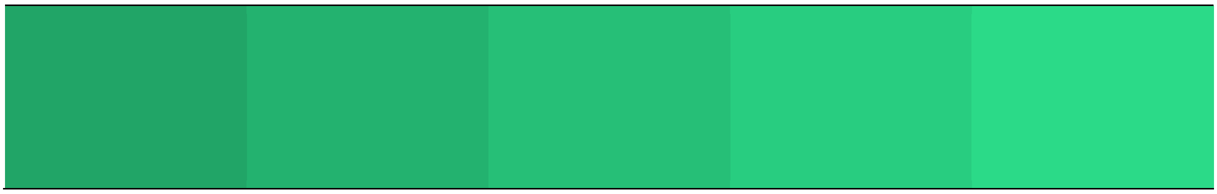

Regarding the train/test split, two folds are performed. These can be seen in Table 4.14. The first fold represents a traditional model evaluation, while the second evaluates the model performance in noisy environments. All classifiers presented in Section 3.6.1 are trained and tested in the first fold, while only the resulting best performing classifier is evaluated in the second fold. The same protocol presented by Sanhudo et al. [705] is used for training the different models. In summary, a nested cross-validation [706] with two training loops is applied. The inner loop is responsible for selecting the best performing hyperparameters for each of the tested models, while the outer loop is responsible for calculating each model's performance using the selected hyperparameters. Both loops consist of 5-fold cross-validations. Over 50 hyperparameters were tuned for all classifiers.

Table 4.14 – Performed folds for material classification with PCMat-30

Fold #	Training	Testing
1	1080 differently sized point clouds with brightness and random dropout levels of 0%	270 differently sized point clouds with brightness and random dropout levels of 0%
2	1080 differently sized point clouds with brightness and random dropout levels of 0%	5400 (i.e. 270×5×4) differently sized point clouds with brightness levels of -10%, -5%, 0%, 5%, 10% and random dropout levels of 0%, 5%, 10%, 15%

4.5.2. Results and discussion

Only quantitative results are presented for this experiment. These can be seen in Figure 4.26 and from Table 4.15 to Table 4.21.

Table 4.15 presents the results for all the tested classifiers in Fold 1. This fold did not contain any noise, meaning that a good performance was expected. Nevertheless, all classifiers except SVM and LR exceeded expectations, returning an $oAcc$ of over 96.51% and an $mAcc$ of over 94.94%, both values corresponding to MLP.

Focusing on SVM, no accuracies are presented for this classifier, given its extensive training and inference time with the available data. Attempts to accelerate this classifier through an assemble of SVMs (each trained on a smaller portion of the data) returned too low accuracies on preliminary tests: ~60%. Similarly, using a linear kernel for better time complexity (from quadratic complexity with polynomial, RBF, and sigmoid, to approximately linear) also returned subpar accuracies: ~25%.

Regarding the best performing classifiers, RF displayed the best performance in terms of $oAcc$, while GrB returned the best performance for $mAcc$. RF has a faster inference time between these two classifiers, thus being selected as the best performing classifier. Additionally, RF is recognized as working well with high-class datasets, which is essential given the desired dataset expansion in number of materials. Other classifiers such as KNN or DT were also strong candidates given their faster inference time, despite the slightly lower accuracy.

In what concern each independent material performance, Figure 4.26 presents the acquired Acc results for RF. By analysing this figure, it can be concluded that the selected classifier performs well in all materials, the worst being *Cobblestone 0*, *Leather 0*, *Metal 0* and *Brick 1* with approximately 92%, 91%, 91%, and 90% Acc, respectively.

Table 4.15 – PCMat-30 classification results for Fold 1. Overall accuracy ($oAcc$) and mean accuracy over classes ($mAcc$) for all proposed models

Model	oAcc (%)	mAcc (%)
Support Vector Machine	-	-
Logistic Regression	72.29	50.51
Multilayer Perceptron	96.51	94.94
k-Nearest Neighbours	97.75	96.67
Decision Tree	97.78	96.90
AdaBoost	98.16	97.39
Gradient Boosting	98.38	**97.81**
Voting	98.38	97.52
Extremely Randomized Forest	98.39	97.61
Random Forest	**98.42**	97.75

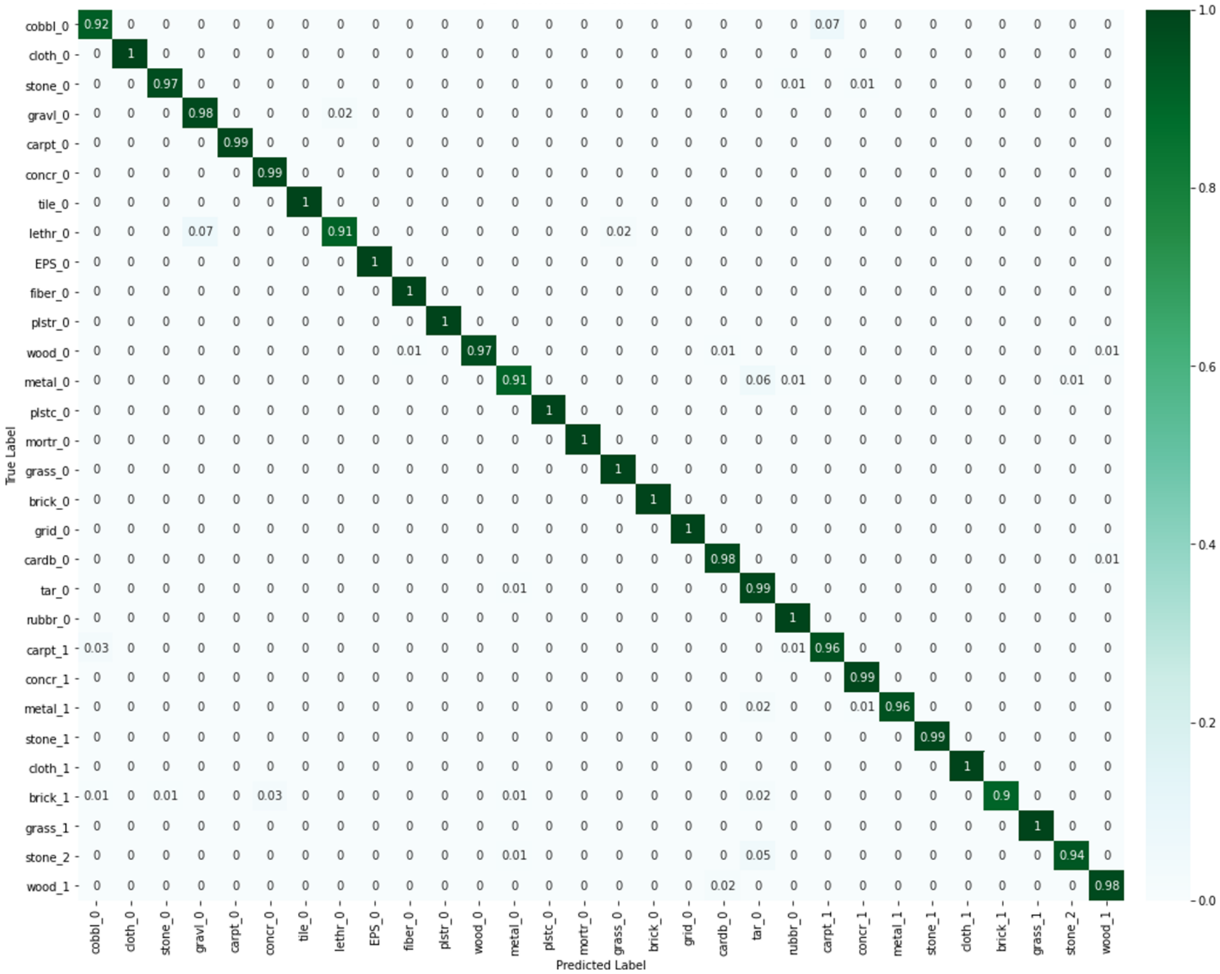

Figure 4.26 – PCMat-30 classification results for Fold 1. Per-class accuracy (Acc) for the RF classifier

With RF selected as the best performing classifier, Fold 2 was performed. Detailed results for each tested resolution, random dropout and brightness level combination can be seen in Table 4.16, Table 4.17, and Table 4.18. Results per resolution, random dropout and brightness level can be seen in Table 4.19, Table 4.20, and Table 4.21.

Table 4.16 – PCMat-30 classification results for resolution 3.1mm and Fold 2. Overall accuracy ($oAcc$) and mean accuracy over classes ($mAcc$) for the RF classifier

Resolution (mm)	Dropout (%)	Brightness (%)	oAcc (%)	mAcc (%)
3.1	0	-10	99.03	98.26
		-5	**99.04**	**98.30**
		0	99.02	98.28
		5	98.99	98.18
		10	99.02	98.25
	5	-10	98.99	98.20
		-5	98.99	98.23
		0	99.00	98.23
		5	98.97	98.22
		10	99.01	98.23
	10	-10	98.97	98.20
		-5	98.99	98.26
		0	98.98	98.28
		5	98.97	98.19
		10	98.97	98.22
	15	-10	98.95	98.17
		-5	98.95	98.18
		0	98.96	98.20
		5	98.95	98.18
		10	98.95	98.19

Once again, the acquired results exceeded expectations with RF returning a maximum accuracy of 99.04% and 98.30%, respectively, for $oAcc$ and $mAcc$. Strangely, these results correspond to a brightness level of -5%, with a resolution of 3.1mm and a random dropout of 0%. In fact, as seen in Table 4.21, the brightness levels do not seem to significantly interfere with the acquired accuracies, with the -5%, 0% and 10% levels all displaying an $oAcc$ of 98.47%. These results confirm the literature conclusions regarding the HSV colour scheme robustness to changes in illumination conditions [682], as stated in Section 3.4.3.2.3.

Table 4.17 – PCMat-30 classification results for resolution 6.3mm and Fold 2. Overall accuracy ($oAcc$) and mean accuracy over classes ($mAcc$) for the RF classifier

Resolution (mm)	Dropout (%)	Brightness (%)	oAcc (%)	mAcc (%)
6.3	0	-10	98.65	97.15
		-5	98.69	97.17
		0	98.68	97.16
		5	98.64	97.08
		10	98.70	97.28
	5	-10	98.64	96.99
		-5	98.57	96.92
		0	98.57	96.87
		5	98.61	97.04
		10	98.62	97.02
	10	-10	98.61	97.03
		-5	98.60	96.96
		0	98.64	97.08
		5	98.53	96.80
		10	98.57	96.90
	15	-10	98.54	96.87
		-5	98.57	97.04
		0	98.56	96.94
		5	98.56	96.90
		10	98.59	96.99

Regarding minimum accuracies, RF returns values of 97.60% and 94.08%, respectively, for $oAcc$ and $mAcc$. These correspond to a resolution of 12.5mm and random dropout of 10% while differing in their respective brightness levels: 5% and -10%. These results follow the visible trends in Table 4.19 and Table 4.20, which suggest a decline in accuracy with the decrease in resolution and increase in dropout.

Nevertheless, a decrease of only 1.44% $oAcc$ between the maximum and minimum results is more than acceptable, facing such dissimilar conditions as the ones presented.

Table 4.18 – PCMat-30 classification results for resolution 12.5mm and Fold 2. Overall accuracy ($oAcc$) and mean accuracy over classes ($mAcc$) for the RF classifier

Resolution (mm)	Dropout (%)	Brightness (%)	oAcc (%)	mAcc (%)
12.5	0	-10	97.98	94.94
		-5	97.84	94.85
		0	97.92	94.88
		5	97.87	94.55
		10	97.95	94.68
	5	-10	97.75	94.61
		-5	97.87	94.71
		0	97.83	94.84
		5	97.85	94.62
		10	97.87	94.84
	10	-10	97.65	94.08
		-5	97.70	94.49
		0	97.74	94.78
		5	97.60	94.09
		10	97.65	94.35
	15	-10	97.61	94.50
		-5	97.82	94.71
		0	97.70	94.39
		5	97.61	94.22
		10	97.73	94.55

Table 4.19 – PCMat-30 classification results per resolution for Fold 2. Overall accuracy ($oAcc$) and mean accuracy over classes ($mAcc$) for the RF classifier

Resolution (mm)	oAcc (%)	mAcc (%)
3,1	98.99	98.22
6,3	98.61	97.01
12,5	97.78	94.58

Table 4.20 – PCMat-30 classification results per random dropout percentage for Fold 2. Overall accuracy ($oAcc$) and mean accuracy over classes ($mAcc$) for the RF classifier

Random Dropout (%)	oAcc (%)	mAcc (%)
0	98.53	96.73
5	98.48	96.64
10	98.41	96.51
15	98.40	96.54

Table 4.21 – PCMat-30 classification results per brightness level for Fold 2. Overall accuracy ($oAcc$) and mean accuracy over classes ($mAcc$) for the RF classifier

Brightness Level (%)	oAcc (%)	mAcc (%)
-10	98.45	96.58
-5	98.47	96.65
0	98.47	96.66
+5	98.43	96.51
+10	98.47	96.63

4.6. Fifth Experiment

4.6.1. Experimental setting – Exportation to energy analysis software

The fifth experiment focused solely on validating the exportation of the generated BIM models to an energy analysis software.

To do this, initially, one of the generated BIM models was selected as an illustrative model to be exported. The selected BIM model was the hallway presented in Figure 4.5, also seen in Figure 4.27. This model was selected for its inherent difficulties in term of exportation, namely:

- the open room boundaries, at each end of the hallway;
- the three existing doors;
- the two curtain walls;
- and the non-linear geometry, with its small nook and corners.

Afterwards, the default families used by the developed software were manually exchanged by selected families. These can be seen in Figure 4.27. While exchanging families, the wrong dimensions of the curtain wall previously identified in the first experiment were corrected, equalling the second curtain wall. Apart from this element resize, no other modifications were performed.

With the model completed, its project and energy settings were modified to correspond to Stanford University's location and building type. Finally, the exportation to *DesignBuilder* was performed using the gbXML file option and the room/spaces volumes, as indicated in Section 3.6.3.

4.6.2. Results and discussion

Figure 4.28 displays the exported BIM model inside *DesignBuilder*. As in the hand modelled examples in Section 3.6.3, the generated BIM model also had its location, building type, operating schedule, and HVAC information failing the exportation process. The remaining information, namely, the building orientation, geometry, and construction solutions, were transferred correctly.

Regarding the geometric dimensions, as seen in Table 4.22, all element categories retained the same perimeter, area and volume, just as in the hand-modelled examples when using the gbXML file and room/space volumes. The perimeter and area values are presented per building element category but result from adding the acquired perimeter and area for each individual building element. As such, the dividing line between two consecutive elements is counted twice for the perimeter calculation.

Faced with these results, it can be concluded that the automatically generated BIM models can be exported to DesignBuilder without any additional obstacles than the manually modelled ones.

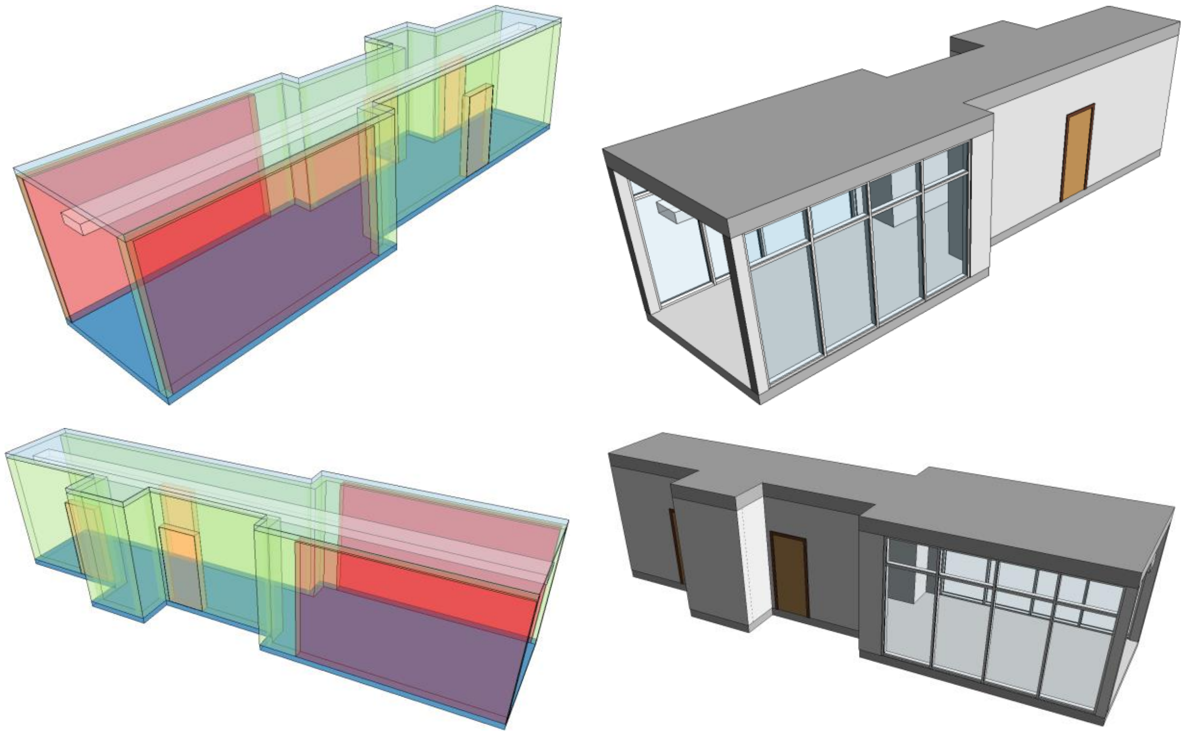

Figure 4.27 – Illustrative BIM model used during the fifth experiment. Manual exchange of the default families used by the modelling software with families selected by the author

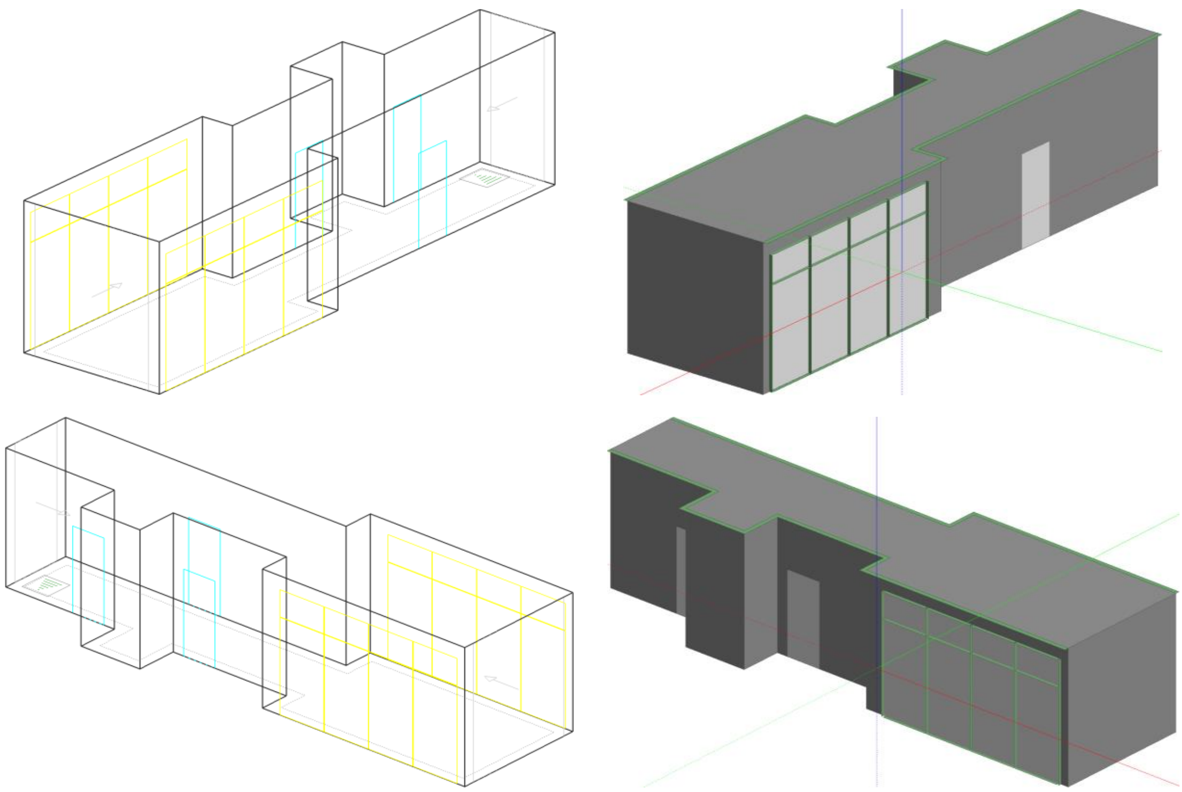

Figure 4.28 – Exported BIM model inside *DesignBuilder*

Table 4.22 – Perimeter, area, and volume for the exported BIM model in *Revit* and *DesignBuilder*

Building Element Category	Revit			DesignBuilder		
	Perimeter	Area	Volume	Perimeter	Area	Volume
Walls	157,136	128,376	–	157,136	128,376	–
Doors	18,294	5,857	–	18,294	5,857	–
Windows	33,056	31,925	–	33,056	31,925	–
Floor	37,636	39,623	–	37,636	39,623	–
Roof	37,636	39,623	–	37,636	39,623	–
Room	–	–	135,155	–	–	135,155

4.7. SUMMARY OF THE EXPERIMENTS

Five experiments were successfully carried out to validate the proposed methodology contributions. Throughout these experiments, it was possible to assess the developed AI models and BIM tools' performance in real case scenarios and compare the obtained results with other developed networks using the select publicly available datasets (i.e. S3DIS and ShapeNet).

All experiments originated positive results, with the author highlighting the following conclusions:

- from the first experiment it was possible to identify that the developed DL networks for point cloud semantic and instance segmentation performed well, with the proposed approach being classified third in the S3DIS dataset benchmark. Additionally, it was also concluded that the proposed BIM modelling tool performed a proper modelling of the identified elements, with any modelling errors deriving from mislabelings in the segmentation software or the lack of information in the surveyed point cloud;
- regarding the second experiment, the acquired results allowed for the validation of the developed artificial point cloud dataset, ArtBIM-PC, as an augmentation dataset. In fact, its use in augmenting the training of the *stairs* element enabled the DL networks to achieve accuracies that rival the best performing classes in the first experiment;
- focusing on the third experiment, the application of the developed DL network for part segmentation delivered above-average accuracies in the ShapeNet-Part dataset benchmark, validating its use. Although the dataset presents several classes that are not applicable in the scan-to-BIM process, its relevance in the current literature, coupled with the lack of a better-suited dataset, made it the appropriate dataset for validating the developed network. Furthermore, the acquired network knowledge from training he non-relevant classes is not pointless, since the network can generalized this knowledge to other classes – a frequent practice in research;
- regarding the fourth experiment, results acquired from the material classification in the developed PCMat-30 dataset allowed for the validation of Random Forest as a suitable classifier algorithm for identifying materials in point clouds. Facing dissimilar conditions of point cloud resolution, brightness, size, and dropout, RF achieved a minimum $oAcc$ and $mAcc$ of 97.60% and 94.08%, respectively;

- finally, the exportation of the automatically generated BIM model in the fifth experiment allowed for the understanding that the exportation process works as well for the generated models as for the manually modelled ones in Section 3.6.3. The findings further reinforced this section findings, with several portions of the analytical data failing exportation, while the geometric data was exchanged correctly.

5

CONCLUSIONS AND FUTURE WORKS

The present chapter marks the end of the thesis. The initially proposed objectives are revisited and answered, with the main contributions of the thesis being discussed. In addition, the author proposes several works to either improve the thesis' contributions and, by extension, the AIBEA workflow, or apply the acquired knowledge and technologies in other areas of the AEC industry.

5.1. CONCLUSIONS

The current thesis successfully developed and applied a methodology to enhance the AIBEA workflow.

This improvement to the AIBEA workflow was performed under the context of enabling an efficient energy retrofit of the existing building stock and the urgent achievement of its associated energy and sustainability goals. This retrofitting is currently being jeopardized by the disadvantages associated with existing methods which, although able to accomplish a building's energy retrofit, present several restrictions regarding its duration and cost-efficiency. By developing the proposed methodology and covering the entire process from contractual agreement to building energy analysis, this issue has been considerably mitigated, with most of the process being fully automated. Additionally, the author believes that the contributions presented in this work will help simplify current modelling practices associated with existing buildings, severely impacting the viability and efficiency of existing building-related projects, such as retrofitting, preservation, rehabilitation, restoration, reconstruction, and expansion.

Two approaches were followed to tackle the AIBEA workflow's improvement: (1) development of supporting documentation and tools for an accurate and swift AIBEA; and (2) integration and automation of the scan-to-BIM process. While the first approach tackled the problem from a broader perspective, through the development of standards and additional supporting tools, the second strictly focused on significantly improving and streamlining the current manual, time-consuming, labour-intensive, subjective, and error-prone modelling of existing buildings.

Initially, five key research areas were reviewed to properly develop these approaches and ground them in existing research, comprehensively covering its related topics, concepts, and nomenclature. These were: existing BIM standards and legislation; as-is building data acquisition; existing interoperability between BIM authoring and energy analysis tools; scan-to-BIM; and AI for point cloud segmentation and classification. All these areas are relevant to the AIBEA workflow, given that each presented different, yet vital, processes and approaches for the theoretical conceptualization of the proposed methodology, as well as its subsequent practical realization and assessment in case studies. For instance, laser scanning was essential in allowing an effective building data acquisition, while AI was critical in achieving the full automation of the scan-to-BIM process.

Given the high level of dissimilarity between these topics and their low level of overlap in research, the thesis' structure was also of vital importance to convey a clear understanding of the research problem's origin and impact, as well as the proposed solution's foundation and method of application. To accomplish this, the thesis was structured in two main parts, the literature review and the development of the proposed methodology. In both, the topics were initially approached from a wider point of view, either by examining a broader problem facing the AEC industry or by showcasing a complete overview of the methodology. Afterwards, both parts slowly narrowed their focus to a more concise topic, either by focusing on the scan-to-BIM problem or on the individual modules in which the methodology was divided. Both parts introduce the covered topics in the order by which they were applied in the proposed methodology.

Additionally, through the creation of secondary objectives, stated in Section 1.2, this thesis was also able to deliver several guidelines and tools that not only allowed for the delivery of the proposed methodology, but are also, by themselves, contributions to the research community. The following are some of the highlighted contributions:

- *Guidelines for the specification of information requirements in BIM energy-related projects* – these guidelines allow for the specification, during BIM contractual processes, of specific energy objectives, simulations, and required LODs for each design stage;
- *Guidelines for the acquisition of as-is building data, in particular, geometric data with laser scanning* – these guidelines cover a wide range of topics from laser scanner positioning and parameter selection, to point cloud treatment and registration;
- *Software tool for the simulation of a laser scanner inside a BIM environment and the generation of an artificial point cloud from a BIM model* – this software allowed, in conjunction with the following contribution, for the expansion of the acquired point cloud datasets and the training of the developed ML models, successfully circumventing the lengthy and laborious process of manually mass-producing labelled point clouds of existing buildings;
- *Software tool for the automated and optimized positioning of laser scanner stations within a BIM environment* – in addition to the previously indicated purpose, this software also enables the optimization of laser scanner surveys, as well as the optimization of monitoring tasks of ongoing construction works through laser scanning;
- *Two DL networks for the semantic, instance, and part segmentation of point clouds* – these networks are undoubtedly at the centre of the purposed methodology and allowed for its successful development and application. However, since their completion as standalone tools is still noteworthy, they are listed here as specific contributions;
- *ML framework for the extraction of relevant geometric features from the resulting point cloud segments* – this framework allowed for the removal of outlier points from the point cloud segments, as well as their ensuing clustering, plan segmentation and bounding box acquisition;
- *One traditional ML model for the identification of a building element surface's material and several of its associated characteristics, such as roughness, reflectance and colour* – this model

allowed for the implementation of automatic characterisation procedures within the proposed methodology, further enhancing its value. Additionally, it can be applied in numerous other AEC industry problems, such as controlling material storage in job sites;

- *Software tool for the automated BIM modelling of building point clouds* – using the geometric information extracted from the building point cloud, as well as the energy-related information from the building survey, this software tool allowed for the precise modelling of semantically enriched elements within an authoring BIM environment;
- *Two point cloud datasets, namely, ArtBIM-PC and PCMat-30* – these datasets provided additional training, testing and validation data for the developed AI models. Moreover, these datasets can be further expanded with additional point clouds and publicly stored online to assist other researchers in their studies.

By reviewing the above contributions, the author believes that the proposed secondary objectives were successfully completed, with the achieved results surpassing the initially planned by virtue of necessity and interest for the research problem.

Regarding the methodology assessment and validation, the performed experiments helped conclude that the methodology can be applied to most buildings with little effort and fully automatically, providing an accurate BIM model of the existing construction. In fact, based on the performed practical applications, it can be concluded that the tasks that may require any substantial effort are all linked with the data acquisition phase, in particular, the acquisition of non-geometric information through the use of traditional methods.

Additionally, it should be stated that in the carried experiments, a restricted number of construction elements were identified and modelled. These were: *walls*, *floors*, *ceilings*, *columns*, *beams*, *windows*, *doors*, *tables*, *chairs*, *sofas*, *bookcases*, *boards*, and *stairs*. Any other element present in the building was classified, by the developed models, as *clutter*. However, the thesis sought to generalize the idea that other elements can be easily included in the methodology, given enough data points and the models' additional training. In fact, this was the primary purpose behind the establishment of the original point cloud datasets, which are intended to be stored online, to crowdsource their development and thus allow for the training of additional classes.

In terms of the difficulties found throughout the multiple years of this thesis development, there were undoubtedly several obstacles. Among these difficulties, the coronavirus disease 2019 (COVID-19) pandemic is by far the most impactful, resulting in multiple delays of the ongoing activities. These delays were originated not only from the most obvious causes, such as the associated confinement periods, which restricted planned case studies, but also from less apparent issues, such as the constraints imposed on the *Google Colaboratory* platform's GPU usage. Apart from COVID-19, the additional difficulties are mostly associated with the intrinsic nature of a PhD. These range from clearly understanding the tackled problem and the multiple steps required to overcome it, to identifying and acquiring the necessary skills and resources to progress in the laid out steps.

5.2. Future Works

A natural extension of the current thesis' research would comprise the dissemination of its core findings and the refinement of the developed methodology. As such, the following bullet points indicate work efforts expected to be conducted in the near future. These are divided into short, medium and long-term efforts.

Short-term:

- Dissemination of the thesis’ scientific findings and contributions in national/international conferences/journals;
- Upload the developed point cloud databases to a publicly available website to crowdsource their growth. Alongside these databases, both the software for the artificial creation of building point clouds and the guidelines for material point clouds acquisition will also be made publicly available;

Medium-term:

- Expansion of the developed databases with the author’s own additional manual data acquisition efforts and further supplementation with newly created artificial point clouds. These efforts will include the surveying of new building elements and materials, with particular focus being given to the exterior of the building;
- Manual test and selection of new DBSCAN parameters for different classes and resolutions or automation of the process. The latter option could be achieved by applying a regression method using, as training data, the already tested and selected parameters, albeit, with further validation of the acquired results;
- Modification of the developed *Dynamo* routines (that still depend on its node system) into full *Python* script for further optimization. This modification can be achieved using *Python*’s code blocks within *Dynamo* or by completely rewriting the code in a full *Python* environment. Doing so will vastly decrease the current runtime of both developed *Dynamo* scripts, in particular, the runtime of the artificial point cloud generation software;
- Integration of new types of stair in the automated BIM modelling process. Further investigation of *Revit*’s API will have to be conducted to assess if this is currently feasible;
- Development of further automated characterisation procedures for the enrichment of the BIM model by leveraging existing data in post-occupancy databases;

Long-term:

- Adjustment of the developed AI models for incremental (also known as continual, continuous or lifelong) learning from the stream of data acquired from the publicly available databases – both for new and existing classes. This future work will require tackling and overcoming several existing problems associated with this type of learning, such as catastrophic forgetting (i.e. training a model with new information interferes with previously learned knowledge) [707];
- Improvement of the developed DL network performance by exchanging its current backbone network (i.e. PointNet) for an improved one. An early candidate would be Point Transformer, published online in mid-December 2020 (implementation code still not available), which relies on self-attention layers for 3D point cloud processing and has achieved remarkable evaluation metrics in S3DIS and ShapeNetPart [528], as identified in Chapter 4. However, backbone candidates will have to be evaluated in terms of efficiency, mainly in what concerns accuracy vs inference time. For instance, PointNet is quite efficient, while Point Transformer is already seen as memory expensive;

- Improvement of the developed DL network performance by integrating a joint instance semantic segmentation module [491], instead of performing these tasks separately. This module would try to take advantage of the fact that semantic and instance segmentation problems are related, in particular, points of the same instance belong to the same class, and points of different classes belong to different instances;
- Integration of thermography as a surveying technology within the workflow. This integration as two objectives: identification of further building elements, namely, hidden columns and beams; and the development of a new automated characterization procedure for the already identified elements. Initial tests will start by mapping thermal images onto the acquired point clouds, followed by the inclusion of the resulting point RGB values into the input vector of the developed DL network. Thus, the resulting input vector could be: $f_k = \{R_{photo}, G_{photo}, B_{photo}, N_x, N_y, N_z, I, R_{thermo}, G_{thermo}, B_{thermo}\}$;
- Adaptation and application of the proposed workflow to HBIM. Four main steps will need to be expanded upon to achieve this purpose: (1) training of the DL network for the segmentation and classification of detailed decorative features and finishes in historic buildings; (2) generation of a dense 3D geometry (i.e. triangle mesh) from the segmented points using surface reconstruction algorithms [708]; (3) establishment of a "container" relation between the typical building elements (e.g. wall, columns) and the decorative features and finishes (e.g. wall's cornice, column's chapiter); (4) development of families and parameters for these elements and their relationship with "container" elements in BIM authoring software.

Finally, it should be stated that a high volume of programming-related problems was tackled within the development of this thesis, both for the textual (*Python*) and visual (*Dynamo*) programming languages. These problems tended to revolve around the development of the proposed software tools, as well as its improvement in terms of accuracy, speed, efficiency, and ease of deployment. Given that these are non-traditional AEC industry problems, these were mostly kept from the final draft. However, the author intends to present and discuss these topics under a more suitable format, namely, within international/national journals/conference articles, thus contributing to the multiple cultural and technological challenges currently facing the AEC industry.

BIBLIOGRAPHY

[1] European Parliament and Council of the European Union, "Directive (EU) 2018/844 of the European Parliament and of the Council of 30 May 2018 amending Directive 2010/31/EU on the energy performance of buildings and Directive 2012/27/EU on energy efficiency (Text with EEA relevance)," *Official Journal of the European Union*, vol. L 156, pp. 75-91, 2018.

[2] European Parliament and Council of the European Union, "Directive (EU) 2018/2002 of the European Parliament and of the Council of 11 December 2018 amending Directive 2012/27/EU on energy efficiency," *Official Journal of the European Union*, vol. L 328, pp. 210-230, 2018.

[3] European Commission. (2021, 2021/14/02). *2030 climate & energy framework*. Available: https://ec.europa.eu/clima/policies/strategies/2030_en

[4] European Commission, "Communication from the Commission to the European Parliament, the Council, the European Economic and Social Committee and the Committee of the Regions. A policy framework for climate and energy in the period from 2020 up to 2030," *EUR-Lex*, no. 52014DC0015R(01), 2014.

[5] European Commission. (2019, 14 February). *Energy performance of buildings directive*. Available: https://ec.europa.eu/energy/en/topics/energy-efficiency/energy-performance-of-buildings/energy-performance-buildings-directive

[6] E. Miller and L. Buys, "Retrofitting commercial office buildings for sustainability: tenants' perspectives," *Journal of Property Investment & Finance*, vol. 26, no. 6, pp. 552-561, 2008/09/26/ 2008.

[7] Y. Ham and M. Golparvar-Fard, "EPAR: Energy Performance Augmented Reality models for identification of building energy performance deviations between actual measurements and simulation results," *Energy and Buildings*, vol. 63, pp. 15-28, 2013/08/01/ 2013.

[8] S.-M. Yu, Y. Tu, and C. Luo, "Green retrofitting costs and benefits: A new research agenda," *Institute Real Estate Studies Working Paper Series*, no. IRES2011-022, 2011.

[9] Z. Ma, P. Cooper, D. Daly, and L. Ledo, "Existing building retrofits: Methodology and state-of-the-art," *Energy and Buildings*, vol. 55, pp. 889-902, 2012/12/01/ 2012.

[10] Ö. Göçer, Y. Hua, and K. Göçer, "A BIM-GIS integrated pre-retrofit model for building data mapping," *Building Simulation*, vol. 9, no. 5, pp. 513-527, 2016/10/01 2016.

[11] European Commission. (2014, 14 February). *Financing renovations*. Available: https://ec.europa.eu/energy/en/topics/energy-efficiency/energy-performance-of-buildings/financing-renovations

[12] European Commission. (2019, 14 February). *Long-term renovation strategies*. Available: https://ec.europa.eu/energy/en/topics/energy-efficiency/energy-performance-of-buildings/long-term-renovation-strategies#long-term-renovation-strategies-2014-and-2017-

[13] G. V. Fracastoro and M. Serraino, "A methodology for assessing the energy performance of large scale building stocks and possible applications," *Energy and Buildings,* vol. 43, no. 4, pp. 844-852, 2011/04/01/ 2011.

[14] M. Cellura, A. Di Gangi, S. Longo, and A. Orioli, "An Italian input–output model for the assessment of energy and environmental benefits arising from retrofit actions of buildings," *Energy and Buildings,* vol. 62, pp. 97-106, 2013/07/01/ 2013.

[15] H. Ben and K. Steemers, "Energy retrofit and occupant behaviour in protected housing: A case study of the Brunswick Centre in London," *Energy and Buildings,* vol. 80, pp. 120-130, 2014/09/01/ 2014.

[16] G. M. D. Giuda, V. Villa, and P. Piantanida, "BIM and Energy Efficient Retrofitting in School Buildings," *Energy Procedia,* vol. 78, pp. 1045-1050, 2015/11/01/ 2015.

[17] J. Lee and Y. Ham, "Impact Analysis on the Variations of the Thermo-physical Property of Building Envelopes and Occupancy in Building Energy Performance Assessment," *Procedia Engineering,* vol. 145, pp. 556-564, 2016/01/01/ 2016.

[18] G. Gourlis and I. Kovacic, "A study on building performance analysis for energy retrofit of existing industrial facilities," *Applied Energy,* vol. 184, pp. 1389-1399, 2016/12/15/ 2016.

[19] M. Khaddaj and I. Srour, "Using BIM to Retrofit Existing Buildings," *Procedia Engineering,* vol. 145, pp. 1526-1533, 2016/01/01/ 2016.

[20] R. Santos, A. A. Costa, and A. Grilo, "Bibliometric analysis and review of Building Information Modelling literature published between 2005 and 2015," *Automation in Construction,* vol. 80, pp. 118-136, 2017/08/01/ 2017.

[21] S. Habibi, "The promise of BIM for improving building performance," *Energy and Buildings,* vol. 153, pp. 525-548, 2017/10/15/ 2017.

[22] L. Sanhudo *et al.*, "Building information modeling for energy retrofitting – A review," *Renewable and Sustainable Energy Reviews,* vol. 89, pp. 249-260, 2018/04/05/ 2018.

[23] P. Tang, D. Huber, B. Akinci, R. Lipman, and A. Lytle, "Automatic reconstruction of as-built building information models from laser-scanned point clouds: A review of related techniques," *Automation in construction,* vol. 19, no. 7, pp. 829-843, 2010/11/01/ 2010.

[24] D. Huber, B. Akinci, A. A. Oliver, E. Anil, B. E. Okorn, and X. Xiong, "Methods for automatically modeling and representing as-built building information models," in *Proceedings of the NSF CMMI Research Innovation Conference*, 2011, vol. 856558: NSF.

[25] J. B. Kim, W. Jeong, M. J. Clayton, J. S. Haberl, and W. Yan, "Developing a physical BIM library for building thermal energy simulation," *Automation in Construction,* vol. 50, pp. 16-28, 2015/02/01/ 2015.

[26] G. Gourlis and I. Kovacic, "Building Information Modelling for analysis of energy efficient industrial buildings – A case study," *Renewable and Sustainable Energy Reviews,* vol. 68, pp. 953-963, 2017/02/01/ 2017.

[27] H. Macher, T. Landes, and P. Grussenmeyer, "From Point Clouds to Building Information Models: 3D Semi-Automatic Reconstruction of Indoors of Existing Buildings," *Applied Sciences,* vol. 7, no. 10, p. 1030, 2017/10/12/ 2017.

[28] A. Rocha *et al.*, "A case study to improve the winter thermal comfort of an existing bus station," *Journal of Building Engineering,* vol. 29, p. 101123, 2019/12/01/ 2019.

[29] L. Sanhudo *et al.*, "A framework for in-situ geometric data acquisition using laser scanning for BIM modelling," *Journal of Building Engineering,* vol. 28, p. 101073, 2019/10/01/ 2019.

[30] F. M. Dinis, L. Sanhudo, J. P. Martins, and N. M. M. Ramos, "Improving project communication in the architecture, engineering and construction industry: Coupling virtual reality and laser scanning," *Journal of Building Engineering,* vol. 30, p. 101287, 2020/02/01/ 2020.

[31] N. Hichri, C. Stefani, L. De Luca, P. Veron, and G. Hamon, "From point cloud to BIM: a survey of existing approaches," in *International Archives of the Photogrammetry, Remote Sensing and Spatial Information Sciences - ISPRS Archives*, 2013, vol. XL-5/W2, pp. 343-348.

[32] L. Barazzetti, F. Banfi, R. Brumana, and M. Previtali, "Creation of Parametric BIM Objects from Point Clouds Using Nurbs," *The Photogrammetric Record,* vol. 30, no. 152, pp. 339-362, 2015/12/01 2015.

[33] L. Sanhudo, J. P. Martins, and N. M. M. Ramos, "An Initial Approach to Automatic Building Information Modelling," presented at the DCE19 - 3rd Doctoral Congress in Engineering, Porto, Portugal, 2019.

[34] R. J. Scherer and P. Katranuschkov, "BIMification: How to create and use BIM for retrofitting," *Advanced Engineering Informatics,* vol. 38, pp. 54-66, 2018/10/01/ 2018.

[35] L. Sanhudo *et al.*, "BIM framework for the specification of information requirements in energy-related projects," *Engineering, Construction and Architectural Management,* 2020/12/01/ 2020.

[36] L. Sanhudo *et al.*, "Técnicas de levantamento laser scanner - Aplicabilidade ao contexto dos edifícios," in *ptBIM - 2º congresso português de Building Information Modelling*, Lisbon, Portugal, 2018, pp. 611-620.

[37] L. Sanhudo, J. P. Martins, and N. M. M. Ramos, "Ferramentas para modelação automática scan-to-BIM," in *ptBIM - 3º congresso português de Building Information Modelling*, Porto, Portugal, 2020, pp. 669-679.

[38] P. Shaikh, F. Shaikh, A. Sahito, M. Uqaili, and Z. Umrani, "An Overview of the Challenges for Cost-Effective and Energy-Efficient Retrofits of the Existing Building Stock," in *Cost-Effective Energy Efficient Building Retrofitting*: Elsevier, 2017, pp. 257-278.

[39] S. Lagüela, L. Díaz-Vilariño, J. Martínez, and J. Armesto, "Automatic thermographic and RGB texture of as-built BIM for energy rehabilitation purposes," *Automation in Construction,* vol. 31, pp. 230-240, 2013/05/01/ 2013.

[40] É. Mata, J. Wanemark, V. M. Nik, and A. S. Kalagasidis, "Economic feasibility of building retrofitting mitigation potentials: Climate change uncertainties for Swedish cities," *Applied Energy,* vol. 242, pp. 1022-1035, 2019.

[41] M. Yalcinkaya and V. Singh, "Patterns and trends in building information modeling (BIM) research: A latent semantic analysis," *Automation in Construction,* vol. 59, pp. 68-80, 2015.

[42] X. Li, P. Wu, G. Q. Shen, X. Wang, and Y. Teng, "Mapping the knowledge domains of Building Information Modeling (BIM): A bibliometric approach," *Automation in Construction,* vol. 84, pp. 195-206, 2017.

[43] X. Zhao, "A scientometric review of global BIM research: Analysis and visualization," *Automation in Construction,* vol. 80, pp. 37-47, 2017.

[44] H.-Y. Chong, C.-Y. Lee, and X. Wang, "A mixed review of the adoption of Building Information Modelling (BIM) for sustainability," *Journal of Cleaner Production,* vol. 142, pp. 4114-4126, 2017/01/20/ 2017.

[45] Y. Arayici, "Towards building information modelling for existing structures," *Structural Survey,* vol. 26, no. 3, 2008/07/11/ 2008.

[46] R. Volk, J. Stengel, and F. Schultmann, "Building Information Modeling (BIM) for existing buildings — Literature review and future needs," *Automation in Construction,* vol. 38, pp. 109-127, 2014/03/01/ 2014.

[47] P. de Wilde, W. Tian, and G. Augenbroe, "Longitudinal prediction of the operational energy use of buildings," *Building and Environment,* vol. 46, no. 8, pp. 1670-1680, 2011/08/01/ 2011.

[48] Y. Heo and V. M. Zavala, "Gaussian process modeling for measurement and verification of building energy savings," *Energy and Buildings,* vol. 53, pp. 7-18, 2012/10/01/ 2012.

[49] K. Goldstein, M. Blasnik, M. Heaney, B. Polly, C. Christensen, and L. Norford, "Developing a pre-retrofit energy consumption metric to model post-retrofit energy savings: Phase one of a three-phase research initiative," *Energy and Buildings,* vol. 80, pp. 556-561, 2014/09/01/ 2014.

[50] R. A. Greta, C. Marta, S. Massimiliano, G. Laura, and D. Pietromaria, "Planning energy retrofit on historic building stocks: A score-driven decision support system," *Energy and Buildings,* vol. 224, p. 110066, 2020/10/01/ 2020.

[51] S. S. K. Kwok, R. K. K. Yuen, and E. W. M. Lee, "An intelligent approach to assessing the effect of building occupancy on building cooling load prediction," *Building and Environment,* vol. 46, no. 8, pp. 1681-1690, 2011/08/01/ 2011.

[52] L. G. Swan, V. I. Ugursal, and I. Beausoleil-Morrison, "Occupant related household energy consumption in Canada: Estimation using a bottom-up neural-network technique," *Energy and Buildings,* vol. 43, no. 2, pp. 326-337, 2011/02/01/ 2011.

[53] G. Mavromatidis, S. Acha, and N. Shah, "Diagnostic tools of energy performance for supermarkets using Artificial Neural Network algorithms," *Energy and Buildings,* vol. 62, pp. 304-314, 2013/07/01/ 2013.

[54] U. Ali *et al.*, "A data-driven approach to optimize urban scale energy retrofit decisions for residential buildings," *Applied Energy,* vol. 267, p. 114861, 2020/06/01/ 2020.

[55] B. Poel, G. van Cruchten, and C. A. Balaras, "Energy performance assessment of existing dwellings," *Energy and Buildings,* vol. 39, no. 4, pp. 393-403, 2007/04/01/ 2007.

[56] E. Asadi, M. G. da Silva, C. H. Antunes, and L. Dias, "Multi-objective optimization for building retrofit strategies: A model and an application," *Energy and Buildings*, vol. 44, pp. 81-87, 2012/01/01/ 2012.

[57] T. Mac Uidhir, F. Rogan, M. Collins, J. Curtis, and B. P. Ó. Gallachóir, "Improving energy savings from a residential retrofit policy: A new model to inform better retrofit decisions," *Energy and Buildings*, vol. 209, p. 109656, 2020/02/15/ 2020.

[58] F. Ascione, F. de Rossi, and G. P. Vanoli, "Energy retrofit of historical buildings: theoretical and experimental investigations for the modelling of reliable performance scenarios," *Energy and Buildings*, vol. 43, no. 8, pp. 1925-1936, 2011/08/01/ 2011.

[59] B. Güçyeter and H. M. Günaydın, "Optimization of an envelope retrofit strategy for an existing office building," *Energy and Buildings*, vol. 55, pp. 647-659, 2012/12/01/ 2012.

[60] F. Stazi, A. Vegliò, C. Di Perna, and P. Munafò, "Experimental comparison between 3 different traditional wall constructions and dynamic simulations to identify optimal thermal insulation strategies," *Energy and Buildings*, vol. 60, pp. 429-441, 2013/05/01/ 2013.

[61] M. Krarti, M. Aldubyan, and E. Williams, "Residential building stock model for evaluating energy retrofit programs in Saudi Arabia," *Energy*, vol. 195, p. 116980, 2020/03/15/ 2020.

[62] R. E. Edwards, E. Lou, A. Bataw, S. N. Kamaruzzaman, and C. Johnson, "Sustainability-led design: Feasibility of incorporating whole-life cycle energy assessment into BIM for refurbishment projects," *Journal of Building Engineering*, vol. 24, p. 100697, 2019/07/01/ 2019.

[63] T. Sartori and J. L. Calmon, "Analysis of the impacts of retrofit actions on the life cycle energy consumption of typical neighbourhood dwellings," *Journal of Building Engineering*, vol. 21, pp. 158-172, 2019/01/01/ 2019.

[64] V. J. L. Gan, M. Deng, Y. Tan, W. Chen, and J. C. P. Cheng, "BIM-based framework to analyze the effect of natural ventilation on thermal comfort and energy performance in buildings," *Energy Procedia*, vol. 158, pp. 3319-3324, 2019/02/01/ 2019.

[65] W. Ahmed and M. Asif, "BIM-based techno-economic assessment of energy retrofitting residential buildings in hot humid climate," *Energy and Buildings*, vol. 227, p. 110406, 2020/11/15/ 2020.

[66] F. Ascione *et al.*, "A real industrial building: Modeling, calibration and Pareto optimization of energy retrofit," *Journal of Building Engineering*, vol. 29, p. 101186, 2020/05/01/ 2020.

[67] J. d. S. Freitas, J. Cronemberger, R. M. Soares, and C. N. D. Amorim, "Modeling and assessing BIPV envelopes using parametric Rhinoceros plugins Grasshopper and Ladybug," *Renewable Energy*, vol. 160, pp. 1468-1479, 2020/11/01/ 2020.

[68] F. Zhang, Y. Ju, E. D. R. Santibanez Gonzalez, A. Wang, P. Dong, and M. Giannakis, "A new framework to select energy-efficient retrofit schemes of external walls: A case study," *Journal of Cleaner Production*, vol. 289, p. 125718, 2021/03/20/ 2021.

[69] S. Opricovic and G. H. Tzeng, "Multicriteria planning of post-earthquake sustainable reconstruction," *Computer-Aided Civil and Infrastructure Engineering*, Article vol. 17, no. 3, pp. 211-220, 2002/12/17/ 2002.

[70] C. Eastman, D. Fisher, G. Lafue, J. Lividini, D. Stoker, and C. Yessios, "An outline of the building description system," *Research Rep,* vol. 50, p. 1974, 1974.

[71] G. A. van Nederveen and F. P. Tolman, "Modelling multiple views on buildings," *Automation in Construction,* vol. 1, no. 3, pp. 215-224, 1992/12/01/ 1992.

[72] B. Autodesk, "Building information modelling," *Autodesk Inc. White Paper, San Rafael, CA,* 2002.

[73] N. Bui, C. Merschbrock, and B. E. Munkvold, "A Review of Building Information Modelling for Construction in Developing Countries," *Procedia Engineering,* vol. 164, pp. 487-494, 2016/01/01/ 2016.

[74] F. Mellado and E. C. W. Lou, "Building information modelling, lean and sustainability: An integration framework to promote performance improvements in the construction industry," *Sustainable Cities and Society,* vol. 61, p. 102355, 2020/10/01/ 2020.

[75] B. Abbasnejad, M. P. Nepal, A. Ahankoob, A. Nasirian, and R. Drogemuller, "Building Information Modelling (BIM) adoption and implementation enablers in AEC firms: a systematic literature review," *Architectural Engineering and Design Management,* pp. 1-23, 2020/07/16/ 2020.

[76] B. Succar, "Building information modelling framework: A research and delivery foundation for industry stakeholders," *Automation in construction,* vol. 18, no. 3, pp. 357-375, 2008/05/01/ 2009.

[77] C. Panteli, A. Kylili, and P. A. Fokaides, "Building information modelling applications in smart buildings: From design to commissioning and beyond A critical review," *Journal of Cleaner Production,* vol. 265, p. 121766, 2020/08/20/ 2020.

[78] C. M. Eastman, C. Eastman, P. Teicholz, R. Sacks, and K. Liston, *BIM handbook: A guide to building information modeling for owners, managers, designers, engineers and contractors*. John Wiley & Sons, 2011.

[79] W. Lu, A. Fung, Y. Peng, C. Liang, and S. Rowlinson, "Cost-benefit analysis of Building Information Modeling implementation in building projects through demystification of time-effort distribution curves," *Building and Environment,* vol. 82, pp. 317-327, 2014/12/01/ 2014.

[80] L. Sanhudo and J. P. Martins, "Building information modelling for an automated building sustainability assessment," *Civil Engineering and Environmental Systems,* vol. 35, no. 1-4, pp. 99-116, 2018/09/01/ 2018.

[81] Z. Liu, Y. Lu, and L. C. Peh, "A Review and Scientometric Analysis of Global Building Information Modeling (BIM) Research in the Architecture, Engineering and Construction (AEC) Industry," *Buildings,* vol. 9, no. 10, p. 210, 2019/09/26/ 2019.

[82] R. Charef, S. Emmitt, H. Alaka, and F. Fouchal, "Building Information Modelling adoption in the European Union: An overview," *Journal of Building Engineering,* vol. 25, p. 100777, 2019/09/01/ 2019.

[83] Z. Liu, Q. Wang, V. JL Gan, and L. Peh, "Envelope Thermal Performance Analysis Based on Building Information Model (BIM) Cloud Platform—Proposed Green Mark Collaboration Environment," *Energies*, vol. 13, no. 3, p. 586, 2020/01/27/ 2020.

[84] B. Succar, W. Sher, and A. Williams, "An integrated approach to BIM competency assessment, acquisition and application," *Automation in Construction*, vol. 35, pp. 174-189, 2013/11/01/ 2013.

[85] Y. Ham and M. Golparvar-Fard, "Mapping actual thermal properties to building elements in gbXML-based BIM for reliable building energy performance modeling," *Automation in Construction*, vol. 49, pp. 214-224, 2015/01/01/ 2015.

[86] S. Azhar, "Building information modeling (BIM): Trends, benefits, risks, and challenges for the AEC industry," *Leadership and management in engineering*, vol. 11, no. 3, pp. 241-252, 2011/07/01/ 2011.

[87] V. Singh, N. Gu, and X. Wang, "A theoretical framework of a BIM-based multi-disciplinary collaboration platform," *Automation in Construction*, vol. 20, no. 2, pp. 134-144, 2011/03/01/ 2011.

[88] V. Badenko *et al.*, "Scan-to-BIM methodology adapted for different application," in *International Archives of the Photogrammetry, Remote Sensing and Spatial Information Sciences - ISPRS Archives*, 2019, vol. 42, no. 5/W2.

[89] S. Azhar, M. Khalfan, and T. Maqsood, "Building information modelling (BIM): now and beyond," *Construction Economics and Building*, vol. 12, no. 4, pp. 15-28, 2015/10/15/ 2012.

[90] F. H. Abanda and L. Byers, "An investigation of the impact of building orientation on energy consumption in a domestic building using emerging BIM (Building Information Modelling)," *Energy*, vol. 97, pp. 517-527, 2016/02/15/ 2016.

[91] A. Kuriqi, A. N. Pinheiro, A. Sordo-Ward, and L. Garrote, "Influence of hydrologically based environmental flow methods on flow alteration and energy production in a run-of-river hydropower plant," *Journal of Cleaner Production*, vol. 232, pp. 1028-1042, 2019/09/20/ 2019.

[92] A. Andriamamonjy, D. Saelens, and R. Klein, "A combined scientometric and conventional literature review to grasp the entire BIM knowledge and its integration with energy simulation," *Journal of Building Engineering*, vol. 22, pp. 513-527, 2019/03/01/ 2019.

[93] S. T. Matarneh, M. Danso-Amoako, S. Al-Bizri, M. Gaterell, and R. Matarneh, "Building information modeling for facilities management: A literature review and future research directions," *Journal of Building Engineering*, vol. 24, p. 100755, 2019/07/01/ 2019.

[94] I. Othman, Y. Y. Al-Ashmori, Y. Rahmawati, Y. H. Mugahed Amran, and M. A. M. Al-Bared, "The level of Building Information Modelling (BIM) Implementation in Malaysia," *Ain Shams Engineering Journal*, 2020/06/11/ 2020.

[95] J. Li, K. Afsari, N. Li, J. Peng, Z. Wu, and H. Cui, "A review for presenting building information modeling education and research in China," *Journal of Cleaner Production*, vol. 259, p. 120885, 2020/06/20/ 2020.

[96] G. Rocha, L. Mateus, J. Fernández, and V. Ferreira, "A scan-to-BIM methodology applied to heritage buildings," *Heritage*, vol. 3, no. 1, pp. 47-67, 2020/02/06/ 2020.

[97] A. Ciribini, S. M. Ventura, and M. Paneroni, "Implementation of an interoperable process to optimise design and construction phases of a residential building: A BIM Pilot Project," *Automation in Construction*, vol. 71, pp. 62-73, 2016/11/01/ 2016.

[98] A. Ghaffarianhoseini *et al.*, "Building Information Modelling (BIM) uptake: Clear benefits, understanding its implementation, risks and challenges," *Renewable and Sustainable Energy Reviews*, vol. 75, pp. 1046-1053, 2017/08/01/ 2017.

[99] R. Charef, H. Alaka, and S. Emmitt, "Beyond the third dimension of BIM: A systematic review of literature and assessment of professional views," *Journal of Building Engineering*, vol. 19, pp. 242-257, 2018/09/01/ 2018.

[100] D. W. M. Chan, T. O. Olawumi, and A. M. L. Ho, "Perceived benefits of and barriers to Building Information Modelling (BIM) implementation in construction: The case of Hong Kong," *Journal of Building Engineering*, vol. 25, p. 100764, 2019/09/01/ 2019.

[101] K. Barlish and K. Sullivan, "How to measure the benefits of BIM — A case study approach," *Automation in Construction*, vol. 24, pp. 149-159, 2012/07/01/ 2012.

[102] D. Bryde, M. Broquetas, and J. M. Volm, "The project benefits of Building Information Modelling (BIM)," *International Journal of Project Management*, vol. 31, no. 7, pp. 971-980, 2013/10/01/ 2013.

[103] B. K. Giel and R. R. Issa, "Return on investment analysis of using building information modeling in construction," *Journal of Computing in Civil Engineering*, vol. 27, no. 5, pp. 511-521, 2013/09/01/ 2013.

[104] B. Ilhan and H. Yaman, "Meta-analysis of building information modeling literature in construction," *International Journal of Engineering and Innovative Technology (IJEIT)*, vol. 3, no. 4, pp. 373-379, 2013/10/01/ 2013.

[105] A. Costa, M. M. Keane, J. I. Torrens, and E. Corry, "Building operation and energy performance: Monitoring, analysis and optimisation toolkit," *Applied Energy*, vol. 101, pp. 310-316, 2013/01/01/ 2013.

[106] A. Cemesova, C. J. Hopfe, and R. S. McLeod, "PassivBIM: Enhancing interoperability between BIM and low energy design software," *Automation in Construction*, vol. 57, pp. 17-32, 2015/09/01/ 2015.

[107] D. Migilinskas, V. Popov, V. Juocevicius, and L. Ustinovichius, "The Benefits, Obstacles and Problems of Practical Bim Implementation," *Procedia Engineering*, vol. 57, pp. 767-774, 2013/01/01/ 2013.

[108] A. Haruna, N. Shafiq, and O. A. Montasir, "Building information modelling application for developing sustainable building (Multi criteria decision making approach)," *Ain Shams Engineering Journal*, 2020/07/30/ 2020.

[109] C. M. Eastman, *Building product models: computer environments, supporting design and construction*. CRC press, 1999.

[110] H. K. Biswas, "Automatic Planning for Scanning: Optimizing 3D Laser Scanning Operations Using BIM and TLS," *IAENG International Journal of Computer Science,* vol. 46, no. 3, 2020/10/01/ 2019.

[111] Y. Chen, H. Dib, and F. C. Robert, "A measurement model of building information modelling maturity," *Construction Innovation,* vol. 14, no. 2, pp. 186-209, 2014/04/01/ 2014.

[112] L. Sanhudo, "BIM for Building Sustainability assessment - Development of a software tool for Rainwater Runoff mitigation," MSc Thesis, Civil Engineering - Constructions, University of Porto, 2016.

[113] A. Ahankoob, K. Manley, and B. Abbasnejad, "The role of contractors' building information modelling (BIM) experience in realising the potential values of BIM," *International Journal of Construction Management,* pp. 1-12, 2019/07/11/ 2019.

[114] A. B. Saka and D. W. M. Chan, "Knowledge, skills and functionalities requirements for quantity surveyors in building information modelling (BIM) work environment: an international Delphi study," *Architectural Engineering and Design Management,* vol. 16, no. 3, pp. 227-246, 2020/05/03 2020.

[115] S. Azhar and J. Brown, "BIM for Sustainability Analyses," *International Journal of Construction Education and Research,* vol. 5, no. 4, pp. 276-292, 2009/11/25 2009.

[116] P. A. Fokaides, K. Polycarpou, and S. Kalogirou, "The impact of the implementation of the European Energy Performance of Buildings Directive on the European building stock: The case of the Cyprus Land Development Corporation," *Energy Policy,* vol. 111, pp. 1-8, 2017/12/01/ 2017.

[117] Y. Schwartz, R. Raslan, and D. Mumovic, "Implementing multi objective genetic algorithm for life cycle carbon footprint and life cycle cost minimisation: A building refurbishment case study," *Energy,* vol. 97, pp. 58-68, 2016/02/15/ 2016.

[118] H. Kim, Z. Shen, I. Kim, K. Kim, A. Stumpf, and J. Yu, "BIM IFC information mapping to building energy analysis (BEA) model with manually extended material information," *Automation in Construction,* vol. 68, pp. 183-193, 2016/08/01/ 2016.

[119] A. Schlueter and F. Thesseling, "Building information model based energy/exergy performance assessment in early design stages," *Automation in Construction,* vol. 18, no. 2, pp. 153-163, 2009/03/01/ 2009.

[120] R. Bull, N. Chang, and P. Fleming, "The use of building energy certificates to reduce energy consumption in European public buildings," *Energy and Buildings,* vol. 50, pp. 103-110, 2012/07/01/ 2012.

[121] E. Asadi, M. G. d. Silva, C. H. Antunes, L. Dias, and L. Glicksman, "Multi-objective optimization for building retrofit: A model using genetic algorithm and artificial neural network and an application," *Energy and Buildings,* vol. 81, pp. 444-456, 2014/10/01/ 2014.

[122] V. Cardoso *et al.*, "Thermal comfort evaluation in cruise terminals," *Building and Environment,* vol. 126, pp. 276-287, 2017/10 2017.

[123] C.-J. Chen, S.-y. Chen, S.-h. Li, and H.-t. Chiu, "Green BIM-based building energy performance analysis," *Computer-Aided Design and Applications,* vol. 14, no. 5, pp. 650-660, 2017/07/29 2017.

[124] J. Jeon, J. Lee, and Y. Ham, "Quantifying the impact of building envelope condition on energy use," *Building Research & Information,* vol. 47, no. 4, pp. 404-420, 2019/05/19 2019.

[125] H. Franconi, K. Tupper, B. Herrschaft, C. Schiller, and R. Hutchinson, "Building Energy Modeling for Owners and Managers," USA: Rocky Mountain Institute2013.

[126] Y. N. Bahar, C. Pere, J. Landrieu, and C. Nicolle, "A thermal simulation tool for building and its interoperability through the building information modeling (BIM) platform," *Buildings,* vol. 3, no. 2, pp. 380-398, 2013/05/22/ 2013.

[127] I. Motawa and K. Carter, "Sustainable BIM-based Evaluation of Buildings," *Procedia - Social and Behavioral Sciences,* vol. 74, pp. 419-428, 2013/03/29/ 2013.

[128] S. Eleftheriadis, D. Mumovic, and P. Greening, "Life cycle energy efficiency in building structures: A review of current developments and future outlooks based on BIM capabilities," *Renewable and Sustainable Energy Reviews,* vol. 67, pp. 811-825, 2017/01/01/ 2017.

[129] Y. Ham and M. Golparvar-Fard, "Updating R-Values of BIM Elements using 3D Thermography for Accurate Building Energy Performance Simulation," in *International Conference on Computing in Civil and Building Engineering*, Orlando, FL (United States), 2014, pp. 113-120.

[130] A. Schlueter and P. Geyer, "Linking BIM and Design of Experiments to balance architectural and technical design factors for energy performance," *Automation in Construction,* vol. 86, pp. 33-43, 2018/02/01/ 2018.

[131] R. Becker *et al.*, "Enabling BIM for property management of existing buildings based on automated as-is capturing," in *Proceedings of the International Symposium on Automation and Robotics in Construction (ISARC 2019)*, 2019, vol. 36, pp. 201-208: IAARC Publications.

[132] L. Yang, J. C. P. Cheng, and Q. Wang, "Semi-automated generation of parametric BIM for steel structures based on terrestrial laser scanning data," *Automation in Construction,* vol. 112, p. 103037, 2020/04/01/ 2020.

[133] Q. Lu, X. Xie, J. Heaton, A. K. Parlikad, and J. Schooling, "From BIM Towards Digital Twin: Strategy and Future Development for Smart Asset Management," in *International Workshop on Service Orientation in Holonic and Multi-Agent Manufacturing*, 2019, pp. 392-404: Springer.

[134] C. Boje, A. Guerriero, S. Kubicki, and Y. Rezgui, "Towards a semantic Construction Digital Twin: Directions for future research," *Automation in Construction,* vol. 114, p. 103179, 2020/06/01/ 2020.

[135] Hong Kong Institute of Building Information Modelling, "HKIBIM Specification Rev 3.0," *Hong Kong BIM Standard,* 2011.

[136] NATSPEC, "NATSPEC National BIM Guide," 2011.

[137] B. Finland, "COBIM - Common BIM Requirements 2012 Series 1-13," 2012.

[138] J. Messner *et al.*, "BIM Project Execution Planning Guide (v. 2.2)," 2019.

[139] *ISO 19650-1: 2018*, 2018.

[140] B. T. Group, "Employer's Information Requirements Core Content and Guidance Notes," 2013.

[141] A. Farzaneh, D. Monfet, and D. Forgues, "Review of using Building Information Modeling for building energy modeling during the design process," *Journal of Building Engineering,* vol. 23, pp. 127-135, 2019/05/01/ 2019.

[142] H. J. Moon, M. S. Choi, S. K. Kim, and S. H. Ryu, "Case studies for the evaluation of interoperability between a BIM based architectural model and building performance analysis programs," in *Proceedings of Building Simulation 2011: 12th Conference of International Building Performance Simulation Association*, Sidney, Australia, 2011, vol. 12, no. 5, pp. 326-328: International Building Performance Simulation Association (IBPSA).

[143] A. Osello *et al.*, "Architecture data and energy efficiency simulations: BIM and interoperability standards," in *Proceedings of Building Simulation 2011: 12th Conference of International Building Performance Simulation Association*, Sidney, Australia, 2011: International Building Performance Simulation Association (IBPSA).

[144] R. J. Hitchcock and J. Wong, "Transforming IFC architectural view BIMs for energy simulation," in *Proceedings of Building Simulation 2011: 12th Conference of International Building Performance Simulation Association*, Sidney, Australia, 2011, pp. 1089-1095: International Building Performance Simulation Association (IBPSA).

[145] J. O'Donnell, "SimModel: A domain data model for whole building energy simulation," in *Proceedings of Building Simulation 2011: 12th Conference of International Building Performance Simulation Association*, Sidney, Australia, 2012, vol. LBNL-5566E: International Building Performance Simulation Association (IBPSA).

[146] I. Kovacic, L. Oberwinter, C. Müller, and C. Achammer, "The "BIM-sustain" experiment – simulation of BIM-supported multi-disciplinary design," *Visualization in Engineering,* vol. 1, no. 1, p. 13, 2013/12/13 2013.

[147] M. Tobias, O. D. James, B. Vladimir, and R. Cody, "BIM - Geometry modelling guidelines for building energy performance simulation," in *Proceedings of Building Simulation 2013: 13th Conference of International Building Performance Simulation Association*, Chambery, France, 2013: International Building Performance Simulation Association (IBPSA).

[148] V. Nasyrov, S. Stratbücker, F. Ritter, A. Borrmann, S. Hua, and M. Lindauer, "Building information models as input for building energy performance simulation–the current state of industrial implementations," in *eWork and eBusiness in Architecture, Engineering and Construction : Proceedings of the 10th European Conference on Product and Process Modelling (ECPPM 2014)*, Vienna, Austria, 2014, pp. 479-488.

[149] K. Kim and J. Yu, "A process to divide curved walls in IFC-BIM into segmented straight walls for building energy analysis," *Journal of Civil Engineering and Management,* vol. 22, no. 3, pp. 333-345, 2016/04/02 2016.

[150] F. M. Ugliotti, M. Dellosta, and A. Osello, "BIM-based Energy Analysis Using Edilclima EC770 Plug-in, Case Study Archimede Library EEB Project," *Procedia Engineering,* vol. 161, pp. 3-8, 2016/01/01/ 2016.

[151] W. Jeong, J. B. Kim, M. J. Clayton, J. S. Haberl, and W. Yan, "A framework to integrate object-oriented physical modelling with building information modelling for building thermal simulation," *Journal of Building Performance Simulation,* vol. 9, no. 1, pp. 50-69, 2016/01/02 2016.

[152] Q. Wang, J. Guo, and M.-K. Kim, "An application oriented scan-to-BIM framework," *Remote sensing,* vol. 11, no. 3, p. 365, 2019/02/12/ 2019.

[153] J. Woo, J. Wilsmann, and D. Kang, "Use of as-built building information modeling," in *Construction Research Congress 2010: Innovation for Reshaping Construction Practice*, 2010, pp. 538-548.

[154] B. Hardin and D. McCool, *BIM and Construction Management: Proven Tools, Methods, and Workflows*. Indianapolis, IN (United States): Wiley Publishing Inc, 2009.

[155] B. Becerik-Gerber, F. Jazizadeh, N. Li, and G. Calis, "Application areas and data requirements for BIM-enabled facilities management," *Journal of Construction Engineering and Management,* vol. 138, no. 3, pp. 431-442, 2012/03/01/ 2012.

[156] P. Teicholz, *BIM for facility managers*. John Wiley & Sons, 2013.

[157] H. B. Cavka, S. Staub-French, and E. A. Poirier, "Developing owner information requirements for BIM-enabled project delivery and asset management," *Automation in Construction,* vol. 83, pp. 169-183, 2017/11/01/ 2017.

[158] C. Sun, S. Jiang, M. J. Skibniewski, Q. Man, and L. Shen, "A literature review of the factors limiting the application of BIM in the construction industry," *Technological and Economic Development of Economy,* vol. 23, no. 5, pp. 764-779, 2017/09/03 2017.

[159] Q. Lu and S. Lee, "Image-Based Technologies for Constructing As-Is Building Information Models for Existing Buildings," *Journal of Computing in Civil Engineering,* vol. 31, no. 4, p. 04017005, 2017/02/06/ 2017.

[160] H. Hamledari, E. Rezazadeh Azar, and B. McCabe, "IFC-Based Development of As-Built and As-Is BIMs Using Construction and Facility Inspection Data: Site-to-BIM Data Transfer Automation," *Journal of Computing in Civil Engineering,* vol. 32, no. 2, p. 04017075, 2017/11/22/ 2018.

[161] General Services Administration. (2021, 25/01/2021). *Level of Detail*. Available: https://www.gsa.gov/real-estate/design-construction/3d4d-building-information-modeling/guidelines-for-bim-software/document-guides/level-of-detail

[162] A. Boutle *et al.*, "Information Management according to BS EN ISO 19650 - Guidance Part 1: Concepts," vol. 2, 2019.

[163] W. Jeong and K. H. Kim, "A Performance Evaluation of the BIM-Based Object-Oriented Physical Modeling Technique for Building Thermal Simulations: A Comparative Case Study," *Sustainability,* vol. 8, no. 7, p. 648, 2016/07/01/ 2016.

[164] S. Beadle, "Employer's information requirements (EIR) - An overview of facilities management requirements," BIFM2017.

[165] BIMForum, "Level of Development Specification," 2020.

[166] E. Taskgroup, "Handbook for the introduction of building information modelling by the European public sector," *Pan-European collaboration of public sector organizations across*, vol. 21, 2017.

[167] M. N. Hamedani and R. E. Smith, "Evaluation of Performance Modelling: Optimizing Simulation Tools to Stages of Architectural Design," *Procedia Engineering*, vol. 118, pp. 774-780, 2015/01/01/ 2015.

[168] F. Shadram and J. Mukkavaara, "An integrated BIM-based framework for the optimization of the trade-off between embodied and operational energy," *Energy and Buildings*, vol. 158, pp. 1189-1205, 2018/01/01/ 2018.

[169] K. Lu *et al.*, "Development of a Carbon Emissions Analysis Framework Using Building Information Modeling and Life Cycle Assessment for the Construction of Hospital Projects," *Sustainability*, vol. 11, no. 22, p. 6274, 2019/11/08/ 2019.

[170] F. Shalabi and Y. Turkan, "BIM–energy simulation approach for detecting building spaces with faults and problematic behavior," *Journal of Information Technology in Construction*, vol. 25, no. 20, pp. 342-360, 2020/06/01/ 2020.

[171] R. Rezaei, T. K. Chiew, S. P. Lee, and Z. Shams Aliee, "Interoperability evaluation models: A systematic review," *Computers in Industry*, vol. 65, no. 1, pp. 1-23, 2014/01/01/ 2014.

[172] M. F. Muller, F. Esmanioto, N. Huber, E. R. Loures, and O. Canciglieri, "A systematic literature review of interoperability in the green Building Information Modeling lifecycle," *Journal of Cleaner Production*, vol. 223, pp. 397-412, 2019/06/20/ 2019.

[173] S. Kumar, *Interoperability between building information models (BIM) and energy analysis programs*. University of Southern California, 2008.

[174] P. W. Newton and S. Tucker, "Carbon Emissions From Domestic Built-In Appliances," *Environment Design Guide*, pp. 1-12, 2009/11/01/ 2009.

[175] E. Kurul, H. Abanda, J. Tah, and F. Cheung, "Rethinking the build process for BIM adoption," in *CIB World Building Congress Construction and Society. Australia*, 2013.

[176] F. H. Abanda, C. Vidalakis, A. H. Oti, and J. H. M. Tah, "A critical analysis of Building Information Modelling systems used in construction projects," *Advances in Engineering Software*, vol. 90, pp. 183-201, 2015/12/01/ 2015.

[177] NBS, "National BIM Report 2012," 2012, Available: https://www.thenbs.com/knowledge/nbs-national-bim-report-2012, Accessed on: November 9, 2020.

[178] NBS, "National BIM Report 2013," 2013, Available: https://www.thenbs.com/knowledge/nbs-national-bim-report-2013, Accessed on: November 9, 2020.

[179] NBS, "National BIM Report 2014," 2014, Available: https://www.thenbs.com/knowledge/nbs-national-bim-report-2014, Accessed on: November 9, 2020.

[180] NBS, "National BIM Report 2015," 2015, Available: https://www.thenbs.com/knowledge/nbs-national-bim-report-2015, Accessed on: November 9, 2020.

[181] NBS, "National BIM Report 2016," 2016, Available: https://www.thenbs.com/knowledge/nbs-national-bim-report-2016, Accessed on: November 9, 2020.

[182] NBS, "National BIM Report 2017," 2017, Available: https://www.thenbs.com/knowledge/nbs-national-bim-report-2017, Accessed on: November 9, 2020.

[183] NBS, "National BIM Report 2018," 2018, Available: https://www.thenbs.com/knowledge/the-national-bim-report-2018, Accessed on: November 9, 2020.

[184] NBS, "National BIM Report 2019," 2019, Available: https://www.thenbs.com/knowledge/the-national-bim-report-2019, Accessed on: November 9, 2020.

[185] NBS, "NBS' 10th National BIM Report," 2020, Available: https://www.thenbs.com/knowledge/the-national-bim-report-2020, Accessed on: November 9, 2020.

[186] C. Eastman, J.-m. Lee, Y.-s. Jeong, and J.-k. Lee, "Automatic rule-based checking of building designs," *Automation in Construction,* vol. 18, no. 8, pp. 1011-1033, 2009/12/01/ 2009.

[187] V. Bazjanac, "IFC BIM-Based Methodology for Semi-Automated Building Energy Performance Simulation," in *ICIT 2008*, Berkeley, CA (United States), 2008: Lawrence Berkeley National Lab. (LBNL).

[188] V. Bazjanac, "Implementation of semi-automated energy performance simulation: building geometry," in *CIB W*, 2009, vol. 78, pp. 595-602.

[189] United States Department of Energy. (2015, 06/08/2017). *Building Energy Software Tools Directory*. Available: https://www.buildingenergysoftwaretools.com/

[190] D. B. Crawley, J. W. Hand, M. Kummert, and B. T. Griffith, "Contrasting the capabilities of building energy performance simulation programs," *Building and Environment,* vol. 43, no. 4, pp. 661-673, 2008/04/01/ 2008.

[191] S. Attia, L. Beltrán, A. De Herde, and J. Hensen, "“Architect friendly”: A comparison of ten different building performance simulation tools," in *Proceedings of Building Simulation 2009: 11th International Building Performance Simulation Association Conference and Exhibition*, 2009: International Building Performance Simulation Association (IBPSA).

[192] S. Attia, "State of the Art of Existing Early Design Simulation Tools for Net Zero Energy Buildings: A Comparison of Ten Tools," Architecture et climat2011.

[193] Y. Lu, Z. Wu, R. Chang, and Y. Li, "Building Information Modeling (BIM) for green buildings: A critical review and future directions," *Automation in Construction,* vol. 83, pp. 134-148, 2017/11/01/ 2017.

[194] T. Maile, M. Fischer, and V. Bazjanac, "Building Energy Performance Simulation Tools - a Life-Cycle and Interoperable Perspective," *Center for Integrated Facility Engineering (CIFE),* no. WP107, pp. 1-49, 2017/06/02/ 2007.

[195] L. Wen and K. Hiyama, "A Review: Simple Tools for Evaluating the Energy Performance in Early Design Stages," *Procedia Engineering,* vol. 146, pp. 32-39, 2016/01/01/ 2016.

[196] M. Wetter, "Modelica-based modelling and simulation to support research and development in building energy and control systems," *Journal of Building Performance Simulation,* vol. 2, no. 2, pp. 143-161, 2009/06/01 2009.

[197] Alliance for Sustainable Energy. (2017, 01/04/2017). *OpenStudio Official Website*. Available: https://www.openstudio.net/

[198] D. Stundon, J. P. Spillane, J. P. Lim, P. Tansey, and M. Tracey, "Building information modelling energy performance assessment on domestic dwellings: a comparative study," presented at the Proceedings for 31stAnnual ARCOM Conference, 2015.

[199] R. Zmeureanu, "Assessment of the energy savings due to the building retrofit," *Building and Environment,* vol. 25, no. 2, pp. 95-103, 1990/01/01/ 1990.

[200] C. F. Reinhart and S. Herkel, "The simulation of annual daylight illuminance distributions — a state-of-the-art comparison of six RADIANCE-based methods," *Energy and Buildings,* vol. 32, no. 2, pp. 167-187, 2000/07/01/ 2000.

[201] T. R. Nielsen, "Simple tool to evaluate energy demand and indoor environment in the early stages of building design," *Solar Energy,* vol. 78, no. 1, pp. 73-83, 2005/01/01/ 2005.

[202] M. Santamouris *et al.*, "Investigating and analysing the energy and environmental performance of an experimental green roof system installed in a nursery school building in Athens, Greece," *Energy,* vol. 32, no. 9, pp. 1781-1788, 2007/09/01/ 2007.

[203] G. Ramos and E. Ghisi, "Analysis of daylight calculated using the EnergyPlus programme," *Renewable and Sustainable Energy Reviews,* vol. 14, no. 7, pp. 1948-1958, 2010/09/01/ 2010.

[204] E. Wang, Z. Shen, and C. Barryman, "A Building LCA Case Study Using Autodesk Ecotect and BIM Model," in *Proceedings of the 47th ASC Annual International Conference*, 2011.

[205] S. E. Chidiac, E. J. C. Catania, E. Morofsky, and S. Foo, "Effectiveness of single and multiple energy retrofit measures on the energy consumption of office buildings," *Energy,* vol. 36, no. 8, pp. 5037-5052, 2011/08/01/ 2011.

[206] X. Xu, D. Yuan, H. Sha, Y. Ji, and P. Xu, "Energy consumption simulation of the prototypical building for optimizing the orientation of building model in the simulated environment," in *Proceedings of ASim 2012: 13th Conference of International Building Performance Simulation Association*, 2012, vol. 30, pp. 0-42.

[207] J. T. Kim and M. S. Todorovic, "Tuning control of buildings glazing's transmittance dependence on the solar radiation wavelength to optimize daylighting and building's energy efficiency," *Energy and Buildings,* vol. 63, pp. 108-118, 2013/08/01/ 2013.

[208] F. Goia, M. Haase, and M. Perino, "Optimizing the configuration of a façade module for office buildings by means of integrated thermal and lighting simulations in a total energy perspective," *Applied Energy,* vol. 108, pp. 515-527, 2013/08/01/ 2013.

[209] S. Kota, J. S. Haberl, M. J. Clayton, and W. Yan, "Building Information Modeling (BIM)-based daylighting simulation and analysis," *Energy and Buildings,* vol. 81, pp. 391-403, 2014/10/01/ 2014.

[210] J. Alam and J. J. Ham, "Towards a BIM-based energy rating system," in *Proceedings of the 19th International Conference on Computer-Aided Architectural Design Research in Asia: Rethinking Comprehensive Design: Speculative Counterculture,* 2014, pp. 285-294: CAADRIA.

[211] I. G. Capeluto and C. E. Ochoa, "Simulation-based method to determine climatic energy strategies of an adaptable building retrofit façade system," *Energy,* vol. 76, pp. 375-384, 2014/11/01/ 2014.

[212] Z. Nagy, D. Rossi, C. Hersberger, S. D. Irigoyen, C. Miller, and A. Schlueter, "Balancing envelope and heating system parameters for zero emissions retrofit using building sensor data," *Applied Energy,* vol. 131, pp. 56-66, 2014/10/15/ 2014.

[213] R. Yao, Q. Luo, Z. Luo, L. Jiang, and Y. Yang, "An integrated study of urban microclimates in Chongqing, China: Historical weather data, transverse measurement and numerical simulation," *Sustainable Cities and Society,* vol. 14, pp. 187-199, 2015/02/01/ 2015.

[214] S. Liu, X. Meng, and C. Tam, "Building information modeling based building design optimization for sustainability," *Energy and Buildings,* vol. 105, pp. 139-153, 2015/10/15/ 2015.

[215] Z. Lin, M. Courbariaux, R. Memisevic, and Y. Bengio, "Neural networks with few multiplications," *arXiv preprint arXiv:1510.03009,* 2015.

[216] R. Evins, "Multi-level optimization of building design, energy system sizing and operation," *Energy,* vol. 90, pp. 1775-1789, 2015/10/01/ 2015.

[217] T. Méndez Echenagucia, A. Capozzoli, Y. Cascone, and M. Sassone, "The early design stage of a building envelope: Multi-objective search through heating, cooling and lighting energy performance analysis," *Applied Energy,* vol. 154, pp. 577-591, 2015/09/15/ 2015.

[218] M. V. Shoubi, M. V. Shoubi, A. Bagchi, and A. S. Barough, "Reducing the operational energy demand in buildings using building information modeling tools and sustainability approaches," *Ain Shams Engineering Journal,* vol. 6, no. 1, pp. 41-55, 2015/03/01/ 2015.

[219] N. L. Harmati, R. J. Folić, and Z. Magyar, "Energy Performance Modelling and Heat Recovery Unit Efficiency Assessment of an Office Building," *Thermal science,* vol. 19, no. 3, pp. 865-880, 2015/01/01/ 2015.

[220] R. M. S. F. Almeida, N. M. M. Ramos, and S. Manuel, "Towards a methodology to include building energy simulation uncertainty in the Life Cycle Cost analysis of rehabilitation alternatives," *Journal of Building Engineering,* vol. 2, pp. 44-51, 2015/06/01/ 2015.

[221] A. H. Oti, E. Kurul, F. Cheung, and J. H. M. Tah, "A framework for the utilization of Building Management System data in building information models for building design and operation," *Automation in Construction,* vol. 72, pp. 195-210, 2016/12/01/ 2016.

[222] H.-J. Kuo, S.-H. Hsieh, R.-C. Guo, and C.-C. Chan, "A verification study for energy analysis of BIPV buildings with BIM," *Energy and Buildings,* vol. 130, pp. 676-691, 2016/10/15/ 2016.

[223] N. Harmathy, Z. Magyar, and R. Folić, "Multi-criterion optimization of building envelope in the function of indoor illumination quality towards overall energy performance improvement," *Energy,* vol. 114, pp. 302-317, 2016/11/01/ 2016.

[224] A. Krstić-Furundžić and T. Kosić, "Assessment of energy and environmental performance of office building models: A case study," *Energy and Buildings*, vol. 115, pp. 11-22, 2016/03/01/ 2016.

[225] X. Xie, O. Sahin, Z. Luo, and R. Yao, "Impact of neighbourhood-scale climate characteristics on building heating demand and night ventilation cooling potential," *Renewable Energy*, vol. 150, pp. 943-956, 2020/05/01/ 2020.

[226] F. Haller, "ARMILLA-ein Installationsmodell," *Institut fur Industrielle Bauproduktion, Universit at Karlsruhe*, 1985.

[227] G. Augenbroe, "Integrated building performance evaluation in the early design stages," *Building and Environment*, vol. 27, no. 2, pp. 149-161, 1992/04/01/ 1992.

[228] S. J. Fenves, U. Flemming, C. Hendrickson, M. L. Maher, and G. Schmitt, "Integrated software environment for building design and construction," *Computer-Aided Design*, vol. 22, no. 1, pp. 27-36, 1990/01/01/ 1990.

[229] L. Myers and J. Pohl, "ICADS expert design advisor: an aid to reflective thinking," *Knowledge-Based Systems*, vol. 5, no. 1, pp. 41-54, 1992/03/01/ 1992.

[230] H. Mason, "ISO 10303-1 overview and fundamentals principles of STEP," Technical Report TC184/SC4/PMAG, EU1992.

[231] J. R. Bedell and N. Kohler, "A hierarchical model for building applications," presented at the CAAD Futures, 1993.

[232] B. Dong, K. Lam, Y. Huang, and G. Dobbs, "A comparative study of the IFC and gbXML informational infrastructures for data exchange in computational design support environments," in *Proceedings: Building Simulation 2007*, 2007.

[233] V. Bazjanac and D. B. Crawley, "Industry foundation classes and interoperable commercial software in support of design of energy-efficient buildings," in *Proceedings of Building Simulation'99*, 1999, vol. 2, pp. 661-667.

[234] V. Bazjanac and D. B. Crawley, "The implementation of industry foundation classes in simulation tools for the building industry," presented at the Proceedings of Building Simulation '97, Prague, Czech Republic, 1997.

[235] A. Cemesova, C. Hopfe, and Y. Rezgui, "An approach to facilitating data exchange between BIM environments and a low energy design tool," in *Proceedings of Building Simulation 2013: 13th Conference of International Building Performance Simulation Association*, Chambery, France, 2013, pp. 25-30: International Building Performance Simulation Association (IBPSA).

[236] S. Lagüela, L. Díaz-Vilariño, J. Armesto, and P. Arias, "Non-destructive approach for the generation and thermal characterization of an as-built BIM," *Construction and Building Materials*, vol. 51, pp. 55-61, 2014/01/31/ 2014.

[237] E. El Asmi, S. Robert, B. Haas, and K. Zreik, "A standardized approach to BIM and energy simulation connection," *International Journal of Design Sciences and Technology*, vol. Volume 21, pp. 59-82, 01/01 2015.

[238] S. Roth, *Open Green Building XML Schema: A Building Information Modeling Solution for Our Green World, gbXML Schema (5.12)*. 2014.

[239] I. Sokolov and J. Crosby, "Utilizing gbXML with AECOsim building designer and speedikon," in "Building Performance Analysis Using Bentley Products," Bentley2011.

[240] M. Horvat and M.-C. Dubois, "Tools and Methods for Solar Design–An Overview of IEA SHC Task 41, Subtask B," *Energy Procedia,* vol. 30, pp. 1120-1130, 2012/01/01/ 2012.

[241] Integrated Environmental Solutions. (2015, 07/04/2017). *Virtual Environment Official Website*. Available: https://www.iesve.com/

[242] S. Chen, R. Jin, and M. Alam, "Investigation of interoperability between building information modelling (BIM) and building energy simulation (BES)," (in English), *International Review of Applied Sciences and Engineering IRASE,* vol. 9, no. 2, pp. 137-144, 2018/12/01/ 2018.

[243] D. Utkucu and H. Sözer, "Interoperability and data exchange within BIM platform to evaluate building energy performance and indoor comfort," *Automation in Construction,* vol. 116, p. 103225, 2020/08/01/ 2020.

[244] C. Rodríguez-Moreno, J. Reinoso-Gordo, E. Rivas-López, A. Gómez-Blanco, F. Ariza-López, and I. Ariza-López, "From point cloud to BIM: An integrated workflow for documentation, research and modelling of architectural heritage," *Survey Review,* vol. 50, no. 360, pp. 212-231, 2016/12/01/ 2016.

[245] A. Fryskowska and J. Stachelek, "A no-reference method of geometric content quality analysis of 3D models generated from laser scanning point clouds for hBIM," *Journal of Cultural Heritage,* vol. 34, pp. 95-108, 2018/11/01/ 2018.

[246] P. Arias, C. Ordóñez, H. Lorenzo, and J. Herraez, "Methods for documenting historical agro-industrial buildings: a comparative study and a simple photogrammetric method," *Journal of Cultural Heritage,* vol. 7, no. 4, pp. 350-354, 2006/10/01/ 2006.

[247] Z. Zhu and I. Brilakis, "Comparison of Optical Sensor-Based Spatial Data Collection Techniques for Civil Infrastructure Modeling," *Journal of Computing in Civil Engineering,* vol. 23, no. 3, pp. 170-177, 2009/05/01/ 2009.

[248] M. Golparvar-Fard, J. Bohn, J. Teizer, S. Savarese, and F. Peña-Mora, "Evaluation of image-based modeling and laser scanning accuracy for emerging automated performance monitoring techniques," *Automation in Construction,* vol. 20, no. 8, pp. 1143-1155, 2011/12/01/ 2011.

[249] A. Bhatla, S. Y. Choe, O. Fierro, and F. Leite, "Evaluation of accuracy of as-built 3D modeling from photos taken by handheld digital cameras," *Automation in Construction,* vol. 28, pp. 116-127, 2012/12/01/ 2012.

[250] F. Dai, A. Rashidi, I. Brilakis, and P. Vela, "Comparison of Image-Based and Time-of-Flight-Based Technologies for Three-Dimensional Reconstruction of Infrastructure," *Journal of construction engineering and management,* vol. 139, no. 1, pp. 929-939, 2013/01/01/ 2013.

[251] T. Omar and M. L. Nehdi, "Data acquisition technologies for construction progress tracking," *Automation in Construction,* vol. 70, pp. 143-155, 2016/10/01/ 2016.

[252] C. Fröhlich and M. Mettenleiter, "Terrestrial Laser Scanning - New Perspectives in 3D Surveying," in *International Archives of the Photogrammetry, Remote Sensing and Spatial Information Sciences - ISPRS Archives*, 2004, vol. 36, no. Part 8, p. W2.

[253] P. Henry, M. Krainin, E. Herbst, X. Ren, and D. Fox, "RGB-D Mapping: Using Depth Cameras for Dense 3D Modeling of Indoor Environments," in *Experimental Robotics: The 12th International Symposium on Experimental Robotics*, O. Khatib, V. Kumar, and G. Sukhatme, Eds. Berlin, Heidelberg: Springer Berlin Heidelberg, 2014, pp. 477-491.

[254] C. Boardman and P. Bryan, "3D Laser Scanning for Heritage. Advice and Guidance on the Use of Laser Scanning in Archaeology and Architecture," *Historic England*, p. 119, 2018/02/08/ 2018.

[255] R. Brumana, P. Condoleo, A. Grimoldi, F. Banfi, A. G. Landi, and M. Previtali, "HR LOD based HBIM to detect influences on geometry and shape by stereotomic construction techniques of brick vaults," *Applied Geomatics*, vol. 10, no. 4, pp. 529-543, 2018/12/01 2018.

[256] C. Philo, *International Encyclopedia of Human Geography*. Elsevier, 2009.

[257] J. Walstra, N. Dixon, and J. H. Chandler, "Historical aerial photographs for landslide assessment: two case histories," *Quarterly Journal of Engineering Geology and Hydrogeology*, vol. 40, no. 4, pp. 315-332, 2007/11/01/ 2007.

[258] J. S. Aber, I. Marzolff, J. Ries, and S. E. W. Aber, *Small-format aerial photography and UAS imagery: Principles, techniques and geoscience applications*. Academic Press, 2019.

[259] A. Florina, "D Spatial Data Acquisition and Modeling of Anghel Saligny Monument using Terrestrial Laser Scanning JOCEA," 2012.

[260] Y. Ham and M. Golparvar-Fard, "An automated vision-based method for rapid 3D energy performance modeling of existing buildings using thermal and digital imagery," *Advanced Engineering Informatics*, vol. 27, no. 3, pp. 395-409, 2013/08/01/ 2013.

[261] Z. Ma and S. Liu, "A review of 3D reconstruction techniques in civil engineering and their applications," *Advanced Engineering Informatics*, vol. 37, pp. 163-174, 2018/08/01/ 2018.

[262] G. Yu and J.-M. Morel, "ASIFT: An algorithm for fully affine invariant comparison," *Image Processing On Line*, vol. 1, pp. 11-38, 2011/02/24/ 2011.

[263] S. Wassim, T. Joliveau, and E. Favier, "Buildings Recognition and Camera Localization Using Image Texture Description," in *25th International Cartographic Conference (Sageo)*, Paris, France, 2011: ENISE.

[264] P. Waldhäusl and C. Ogleby, "3 x 3 rules for simple photogrammetric documentation of architecture," *International Archives of Photogrammetry and Remote Sensing*, vol. 30, pp. 426-429, 1994/01/01/ 1994.

[265] F. Kern, "Supplementing laser scanner geometric data with photogrammetric images for modeling," *International Society for Photogrammetry and Remote Sensing*, vol. 34, 2011/11/30/ 2001.

[266] J. A. Beraldin, "Integration of Laser Scanning and Close-Range Photogrammetry - The Last Decade and Beyond," in *Proceedings of the XXth ISPRS Congress*, ed, 2004.

[267] P. Rönnholm, E. Honkavaara, P. Litkey, H. Hyyppä, and J. Hyyppä, "Integration of Laser Scanning and Photogrammetry," in *International Archives of the Photogrammetry, Remote Sensing and Spatial Information Sciences - ISPRS Archives*, 2006, vol. 36.

[268] S. El-Omari and O. Moselhi, "Integrating 3D laser scanning and photogrammetry for progress measurement of construction work," *Automation in Construction,* vol. 18, no. 1, pp. 1-9, 2008/12/01/ 2008.

[269] Y. M. Ibrahim, T. C. Lukins, X. Zhang, E. Trucco, and A. P. Kaka, "Towards automated progress assessment of workpackage components in construction projects using computer vision," *Advanced Engineering Informatics,* vol. 23, no. 1, pp. 93-103, 2009/01/01/ 2009.

[270] J. L. Lerma, S. Navarro, M. Cabrelles, and V. Villaverde, "Terrestrial laser scanning and close range photogrammetry for 3D archaeological documentation: the Upper Palaeolithic Cave of Parpalló as a case study," *Journal of Archaeological Science,* vol. 37, no. 3, pp. 499-507, 2010/03/01/ 2010.

[271] A. Khaloo and D. Lattanzi, "Hierarchical dense structure-from-motion reconstructions for infrastructure condition assessment," *Journal of Computing in Civil Engineering,* vol. 31, no. 1, p. 04016047, 2017/01/01/ 2017.

[272] Y. Furukawa, B. Curless, S. M. Seitz, and R. Szeliski, "Reconstructing building interiors from images," in *Proceedings of the IEEE International Conference on Computer Vision (ICCV 2009)*, Kyoto, Japan, 2009, pp. 80-87: IEEE.

[273] F. Dai and M. Lu, "Assessing the Accuracy of Applying Photogrammetry to Take Geometric Measurements on Building Products," *Journal of Construction Engineering and Management,* vol. 136, no. 2, pp. 242-250, 2010/02/01 2010.

[274] S. El-Omari and O. Moselhi, "Data acquisition from construction sites for tracking purposes," *Engineering, Construction and Architectural Management,* vol. 16, no. 5, pp. 490-503, 2009/09/04/ 2009.

[275] I. S. Lee, J. O. Lee, H. J. Park, and K. H. Bae, "Investigations into the influence of object characteristics on the quality of terrestrial laser scanner data," *KSCE Journal of Civil Engineering,* vol. 14, no. 6, pp. 905-913, 2010/11/01 2010.

[276] Y. Arayici, "An approach for real world data modelling with the 3D terrestrial laser scanner for built environment," *Automation in Construction,* vol. 16, no. 6, pp. 816-829, 2007/09/01/ 2007.

[277] Leica Geosystems, "Leica ScanStation P30/P40 product specifications," Hexagon AB, Heerbrugg, Switzerland2016.

[278] D. Rebolj, Z. Pučko, N. Č. Babič, M. Bizjak, and D. Mongus, "Point cloud quality requirements for Scan-vs-BIM based automated construction progress monitoring," *Automation in Construction,* vol. 84, pp. 323-334, 2017/12/01/ 2017.

[279] B. Giel and R. R. A. Issa, "Using Laser Scanning to Access the Accuracy of As-Built BIM," in *International Workshop on Computing in Civil Engineering (2011)*, 2011, pp. 665-672.

[280] J. H. Garrett, "Constructing As-Is BIMs from Progressive Scan Data," presented at the Proceedings of the International Symposium on Automation and Robotics in Construction (ISARC 2012), Eindhoven, Netherlands, 2012/06/29, 2012.

[281] D. Barber, J. Mills, and S. Smith-Voysey, "Geometric validation of a ground-based mobile laser scanning system," *ISPRS Journal of Photogrammetry and Remote Sensing,* vol. 63, no. 1, pp. 128-141, 2008/01/01/ 2008.

[282] K. Williams, M. Olsen, G. Roe, and C. Glennie, "Synthesis of transportation applications of mobile LiDAR," *Remote Sensing,* vol. 5, no. 9, pp. 4652-4692, 2013/09/18/ 2013.

[283] H. Lauterbach, D. Borrmann, R. Heß, D. Eck, K. Schilling, and A. Nüchter, "Evaluation of a backpack-mounted 3D mobile scanning system," *Remote Sensing,* vol. 7, no. 10, pp. 13753-13781, 2015/10/21/ 2015.

[284] H. Cui, X. Ren, Q. Mao, Q. Hu, and W. Wang, "Shield subway tunnel deformation detection based on mobile laser scanning," *Automation in Construction,* vol. 106, p. 102889, 2019/10/01/ 2019.

[285] C. Zhang and D. Arditi, "Automated progress control using laser scanning technology," *Automation in Construction,* vol. 36, pp. 108-116, 2013/12/01/ 2013.

[286] C. Kim, H. Son, and C. Kim, "Automated construction progress measurement using a 4D building information model and 3D data," *Automation in Construction,* vol. 31, pp. 75-82, 2013/05/01/ 2013.

[287] F. Bosché, A. Guillemet, Y. Turkan, C. T. Haas, and R. Haas, "Tracking the built status of MEP works: Assessing the value of a Scan-vs-BIM system," *Journal of Computing in Civil Engineering,* vol. 28, no. 4, p. 05014004, 2013/07/01/ 2013.

[288] F. Bosché, M. Ahmed, Y. Turkan, C. T. Haas, and R. Haas, "The value of integrating Scan-to-BIM and Scan-vs-BIM techniques for construction monitoring using laser scanning and BIM: The case of cylindrical MEP components," *Automation in Construction,* vol. 49, pp. 201-213, 2015/01/01/ 2015.

[289] Z. Pučko, N. Šuman, and D. Rebolj, "Automated continuous construction progress monitoring using multiple workplace real time 3D scans," *Advanced Engineering Informatics,* vol. 38, pp. 27-40, 2018/10/01/ 2018.

[290] F. Bosché, "Automated recognition of 3D CAD model objects in laser scans and calculation of as-built dimensions for dimensional compliance control in construction," *Advanced Engineering Informatics,* vol. 24, no. 1, pp. 107-118, 2010/01/01/ 2010.

[291] F. Bosché and E. Guenet, "Controlling Slab Flatness Automatically using Laser Scanning and BIM," in *Proceedings of the International Symposium on Automation and Robotics in Construction and Mining (ISARC 2014),* Sydney, Australia, 2014: Curran Associates.

[292] M.-K. Kim, J. C. Cheng, H. Sohn, and C.-C. Chang, "A framework for dimensional and surface quality assessment of precast concrete elements using BIM and 3D laser scanning," *Automation in Construction,* vol. 49, pp. 225-238, 2015/01/01/ 2015.

[293] T. S. Kalyan, P. A. Zadeh, S. Staub-French, and T. M. Froese, "Construction Quality Assessment Using 3D as-built Models Generated with Project Tango," *Procedia Engineering,* vol. 145, pp. 1416-1423, 2016/01/01/ 2016.

[294] M.-K. Kim, Q. Wang, J.-W. Park, J. C. Cheng, H. Sohn, and C.-C. Chang, "Automated dimensional quality assurance of full-scale precast concrete elements using laser scanning and BIM," *Automation in Construction,* vol. 72, pp. 102-114, 2016/12/01/ 2016.

[295] J. Valença, I. Puente, E. Júlio, H. González-Jorge, and P. Arias-Sánchez, "Assessment of cracks on concrete bridges using image processing supported by laser scanning survey," *Construction and Building Materials,* vol. 146, pp. 668-678, 2017/08/15/ 2017.

[296] J. Guo, Q. Wang, and J.-H. Park, "Geometric quality inspection of prefabricated MEP modules with 3D laser scanning," *Automation in Construction,* vol. 111, p. 103053, 2020/03/01/ 2020.

[297] C. Panteli, A. Kylili, L. Stasiuliene, L. Seduikyte, and P. A. Fokaides, "A framework for building overhang design using Building Information Modeling and Life Cycle Assessment," *Journal of Building Engineering,* vol. 20, pp. 248-255, 2018/11/01/ 2018.

[298] M. Bassier, B. Van Genechten, and M. Vergauwen, "Classification of sensor independent point cloud data of building objects using random forests," *Journal of Building Engineering,* vol. 21, pp. 468-477, 2019/01/01/ 2019.

[299] J. O'Donnell, L. Truong-Hong, N. Boyle, E. Corry, J. Cao, and D. F. Laefer, "LiDAR point-cloud mapping of building façades for building energy performance simulation," *Automation in Construction,* vol. 107, p. 102905, 2019/11/01/ 2019.

[300] S. Pu and G. Vosselman, "Knowledge based reconstruction of building models from terrestrial laser scanning data," *ISPRS Journal of Photogrammetry and Remote Sensing,* vol. 64, no. 6, pp. 575-584, 2009/11/01/ 2009.

[301] I. Brilakis *et al.*, "Toward automated generation of parametric BIMs based on hybrid video and laser scanning data," *Advanced Engineering Informatics,* vol. 24, no. 4, pp. 456-465, 2010/11/01/ 2010.

[302] A. Adan and D. Huber, "3D Reconstruction of Interior Wall Surfaces under Occlusion and Clutter," in *2011 International Conference on 3D Imaging, Modeling, Processing, Visualization and Transmission*, 2011, pp. 275-281.

[303] X. Xiong, A. Adan, B. Akinci, and D. Huber, "Automatic creation of semantically rich 3D building models from laser scanner data," *Automation in Construction,* vol. 31, pp. 325-337, 2013/05/01/ 2013.

[304] H. Son, C. Kim, and C. Kim, "Fully automated as-built 3D pipeline segmentation based on curvature computation from laser-scanned data," in *International Workshop on Computing in Civil Engineering (2013)*, 2013, pp. 765-772.

[305] C. Thomson and J. Boehm, "Automatic geometry generation from point clouds for BIM," *Remote Sensing,* vol. 7, no. 9, pp. 11753-11775, 2015/09/14/ 2015.

[306] V. Pătrăucean, I. Armeni, M. Nahangi, J. Yeung, I. Brilakis, and C. Haas, "State of research in automatic as-built modelling," *Advanced Engineering Informatics*, vol. 29, no. 2, pp. 162-171, 2015/04/01/ 2015.

[307] I. Anagnostopoulos, V. Pătrăucean, I. Brilakis, and P. Vela, "Detection of walls, floors, and ceilings in point cloud data," in *Construction Research Congress 2016: Old and New Construction Technologies Converge in Historic San Juan*, 2016, pp. 2302-2311.

[308] S. Ochmann, R. Vock, R. Wessel, and R. Klein, "Automatic reconstruction of parametric building models from indoor point clouds," *Computers & Graphics*, vol. 54, pp. 94-103, 2016/02/01/ 2016.

[309] J. Jung, C. Stachniss, S. Ju, and J. Heo, "Automated 3D volumetric reconstruction of multiple-room building interiors for as-built BIM," *Advanced Engineering Informatics*, vol. 38, pp. 811-825, 2018/10/01/ 2018.

[310] A. C. Menezes, A. Cripps, D. Bouchlaghem, and R. Buswell, "Predicted vs. actual energy performance of non-domestic buildings: Using post-occupancy evaluation data to reduce the performance gap," *Applied Energy*, vol. 97, pp. 355-364, 2012/09/01/ 2012.

[311] P. de Wilde, "The gap between predicted and measured energy performance of buildings: A framework for investigation," *Automation in Construction*, vol. 41, pp. 40-49, 2014/05/01/ 2014.

[312] C. van Dronkelaar, M. Dowson, E. Burman, C. Spataru, and D. Mumovic, "A Review of the Energy Performance Gap and Its Underlying Causes in Non-Domestic Buildings," *Frontiers in Mechanical Engineering*, 10.3389/fmech.2015.00017 vol. 1, p. 17, 2016/01/13/ 2016.

[313] A. Marshall *et al.*, "Domestic building fabric performance: Closing the gap between the in situ measured and modelled performance," *Energy and Buildings*, vol. 150, pp. 307-317, 2017/09/01/ 2017.

[314] G. Bauwens and S. Roels, "Co-heating test: A state-of-the-art," *Energy and Buildings*, vol. 82, pp. 163-172, 2014/10/01/ 2014.

[315] A. Law and J. P. C. Wong, "Application of the Co-heating test in Australian climates," *Energy and Buildings*, vol. 224, p. 110153, 2020/10/01/ 2020.

[316] D. Johnston, D. Miles-Shenton, J. Wingfield, D. Farmer, and M. Bell, "Whole House Heat Loss Test Method (Coheating)," in *Environmental Science*, 2012.

[317] S. F. Stamp, "Assessing uncertainty in co-heating tests: Calibrating a whole building steady state heat loss measurement method," MSc Thesis, Civil Engineering, UCL - University College London, 2016.

[318] M. Modera, "Electric co-heating: A method for evaluating seasonal heating efficiencies and heat loss rates in dwellings," in *CIB Symposium on Energy Conservation in the Built Environment*, Copenhagen, Denmark, 1979, no. LBL-8949.

[319] A. Shea, M. Lawrence, and P. Walker, "Hygrothermal performance of an experimental hemp–lime building," *Construction and Building Materials*, vol. 36, pp. 270-275, 2012/11/01/ 2012.

[320] A. Stafford, D. Johnston, D. Miles-Shenton, D. Farmer, M. Brooke-Peat, and C. Gorse, "Adding value and meaning to coheating tests," *Structural Survey,* vol. 32, no. 4, pp. 331-342, 2014/08/05/ 2014.

[321] P. W. Francisco, J. Siegel, L. Palmiter, and B. Davis, "Measuring residential duct efficiency with the short-term coheat test methodology," *Energy and Buildings,* vol. 38, no. 9, pp. 1076-1083, 2006/09/01/ 2006.

[322] J. Hopper *et al.*, "Assessing the execution of retrofitted external wall insulation for pre-1919 dwellings in Swansea (UK)," *Structural Survey,* vol. 30, no. 3, pp. 245-266, 2012.

[323] O. Guerra-Santin, C. Tweed, H. Jenkins, and S. Jiang, "Monitoring the performance of low energy dwellings: Two UK case studies," *Energy and Buildings,* vol. 64, pp. 32-40, 2013/09/01/ 2013.

[324] E. Latif, M. Lawrence, A. Shea, and P. Walker, "In situ assessment of the fabric and energy performance of five conventional and non-conventional wall systems using comparative coheating tests," *Building and Environment,* vol. 109, pp. 68-81, 2016/11/15/ 2016.

[325] Leica Geosystems, "Leica BLK360 image scanner product specifications," ed, 2016.

[326] F. Asdrubali, G. Baldinelli, and F. Bianchi, "A quantitative methodology to evaluate thermal bridges in buildings," *Applied Energy,* vol. 97, pp. 365-373, 2012/09/01/ 2012.

[327] E. Grinzato, V. Vavilov, and T. Kauppinen, "Quantitative infrared thermography in buildings," *Energy and Buildings,* vol. 29, no. 1, pp. 1-9, 1998/12/01/ 1998.

[328] C. A. Balaras and A. A. Argiriou, "Infrared thermography for building diagnostics," *Energy and Buildings,* vol. 34, no. 2, pp. 171-183, 2002/02/01/ 2002.

[329] E. Barreira, R. M. S. F. Almeida, and M. Moreira, "An infrared thermography passive approach to assess the effect of leakage points in buildings," *Energy and Buildings,* vol. 140, pp. 224-235, 2017/04/01/ 2017.

[330] Y. El Masri and T. Rakha, "A scoping review of non-destructive testing (NDT) techniques in building performance diagnostic inspections," *Construction and Building Materials,* vol. 265, p. 120542, 2020/12/30/ 2020.

[331] E. Barreira and V. P. de Freitas, "Evaluation of building materials using infrared thermography," *Construction and Building Materials,* vol. 21, no. 1, pp. 218-224, 2007/01/01/ 2007.

[332] E. Barreira and R. M. Almeida, *Infrared Thermography for Building Moisture Inspection*. Springer, 2019.

[333] S. Martín Ocaña, I. Cañas Guerrero, and I. González Requena, "Thermographic survey of two rural buildings in Spain," *Energy and Buildings,* vol. 36, no. 6, pp. 515-523, 2004/06/01/ 2004.

[334] R. Madding, "Finding R-values of stud frame constructed houses with IR thermography," *Proc., InfraMation 2008,* pp. 261-277, 2008.

[335] R. Albatici and A. M. Tonelli, "Infrared thermovision technique for the assessment of thermal transmittance value of opaque building elements on site," *Energy and Buildings,* vol. 42, no. 11, pp. 2177-2183, 2010/11/01/ 2010.

[336] P. A. Fokaides and S. A. Kalogirou, "Application of infrared thermography for the determination of the overall heat transfer coefficient (U-Value) in building envelopes," *Applied Energy*, vol. 88, no. 12, pp. 4358-4365, 2011/12/01/ 2011.

[337] M. I. Alba, L. Barazzetti, M. Scaioni, E. Rosina, and M. Previtali, "Mapping Infrared Data on Terrestrial Laser Scanning 3D Models of Buildings," *Remote Sensing*, vol. 3, no. 9, 2011/08/25/ 2011.

[338] S. Lagüela, J. Martínez, J. Armesto, and P. Arias, "Energy efficiency studies through 3D laser scanning and thermographic technologies," *Energy and Buildings*, vol. 43, no. 6, pp. 1216-1221, 2011/06/01/ 2011.

[339] D. González-Aguilera, P. Rodriguez-Gonzalvez, J. Armesto, and S. Lagüela, "Novel approach to 3D thermography and energy efficiency evaluation," *Energy and Buildings*, vol. 54, pp. 436-443, 2012/11/01/ 2012.

[340] H. J. Im, M. Gai, C. Wang, and Y. Cho, "Hybrid Approach to Visualize Building Energy Information Model in Geospatial Application Programs," in *Construction Research Congress 2012: Construction Challenges in a Flat World*, 2012, pp. 1262-1270.

[341] D. Borrmann *et al.*, "The Project ThermalMapper – Thermal 3D Mapping of Indoor Environments for Saving Energy," *IFAC Proceedings Volumes*, vol. 45, no. 22, pp. 31-38, 2012/01/01/ 2012.

[342] X. Zhang, M. Pipattanasomporn, T. Chen, and S. Rahman, "An IoT-Based Thermal Model Learning Framework for Smart Buildings," *IEEE Internet of Things Journal*, vol. 7, no. 1, pp. 518-527, 2020.

[343] J. Gubbi, R. Buyya, S. Marusic, and M. Palaniswami, "Internet of Things (IoT): A vision, architectural elements, and future directions," *Future Generation Computer Systems*, vol. 29, no. 7, pp. 1645-1660, 2013/09/01/ 2013.

[344] I. Khajenasiri, A. Estebsari, M. Verhelst, and G. Gielen, "A Review on Internet of Things Solutions for Intelligent Energy Control in Buildings for Smart City Applications," *Energy Procedia*, vol. 111, pp. 770-779, 2017/03/01/ 2017.

[345] W. Yaïci, K. Krishnamurthy, E. Entchev, and M. Longo, "Survey of Internet of Things (IoT) Infrastructures for Building Energy Systems," in *2020 Global Internet of Things Summit (GIoTS)*, 2020, pp. 1-6.

[346] X. J. Luo, L. O. Oyedele, A. O. Ajayi, C. G. Monyei, O. O. Akinade, and L. A. Akanbi, "Development of an IoT-based big data platform for day-ahead prediction of building heating and cooling demands," *Advanced Engineering Informatics*, vol. 41, p. 100926, 2019/08/01/ 2019.

[347] C. K. Metallidou, K. E. Psannis, and E. A. Egyptiadou, "Energy Efficiency in Smart Buildings: IoT Approaches," *IEEE Access*, vol. 8, pp. 63679-63699, 2020.

[348] P. P. Ray, "A survey on Internet of Things architectures," *Journal of King Saud University - Computer and Information Sciences*, vol. 30, no. 3, pp. 291-319, 2018/07/01/ 2018.

[349] L. Sanhudo, J. Rodrigues, and Ê. V. Filho, "Multivariate time series clustering and forecasting for building energy analysis: Application to weather data quality control," *Journal of Building Engineering*, vol. 35, p. 101996, 2020/11/01/ 2020.

[350] A. Kumar, A. Kumar, and A. Singh, "Energy efficient and low cost air quality sensor for smart buildings," in *2017 3rd International Conference on Computational Intelligence & Communication Technology (CICT)*, 2017, pp. 1-4.

[351] M. Sophocleous, P. Savva, M. F. Petrou, J. K. Atkinson, and J. Georgiou, "A Durable, Screen-Printed Sensor for In Situ and Real-Time Monitoring of Concrete's Electrical Resistivity Suitable for Smart Buildings/Cities and IoT," *IEEE Sensors Letters*, vol. 2, no. 4, pp. 1-4, 2018.

[352] H. N. Rafsanjani, C. R. Ahn, and J. Chen, "Linking building energy consumption with occupants' energy-consuming behaviors in commercial buildings: Non-intrusive occupant load monitoring (NIOLM)," *Energy and Buildings*, vol. 172, pp. 317-327, 2018/08/01/ 2018.

[353] L. Zimmermann, R. Weigel, and G. Fischer, "Fusion of Nonintrusive Environmental Sensors for Occupancy Detection in Smart Homes," *IEEE Internet of Things Journal*, vol. 5, no. 4, pp. 2343-2352, 2018.

[354] J. Yang, H. Zou, H. Jiang, and L. Xie, "Device-Free Occupant Activity Sensing Using WiFi-Enabled IoT Devices for Smart Homes," *IEEE Internet of Things Journal*, vol. 5, no. 5, pp. 3991-4002, 2018.

[355] H. N. Rafsanjani and A. Ghahramani, "Extracting occupants' energy-use patterns from Wi-Fi networks in office buildings," *Journal of Building Engineering*, vol. 26, p. 100864, 2019/11/01/ 2019.

[356] K. McGlinn, B. Yuce, H. Wicaksono, S. Howell, and Y. Rezgui, "Usability evaluation of a web-based tool for supporting holistic building energy management," *Automation in Construction*, vol. 84, pp. 154-165, 2017/12/01/ 2017.

[357] M. H. Y. Moghaddam and A. Leon-Garcia, "A fog-based internet of energy architecture for transactive energy management systems," *IEEE Internet of Things Journal*, vol. 5, no. 2, pp. 1055-1069, 2018.

[358] W. Li, T. Logenthiran, V. Phan, and W. L. Woo, "Implemented IoT-Based Self-Learning Home Management System (SHMS) for Singapore," *IEEE Internet of Things Journal*, vol. 5, no. 3, pp. 2212-2219, 2018.

[359] S. Habibi, "Micro-climatization and real-time digitalization effects on energy efficiency based on user behavior," *Building and Environment*, vol. 114, pp. 410-428, 2017/03/01/ 2017.

[360] X. Zhang, M. Cai, M. Pipattanasomporn, and S. Rahman, "A Power Disaggregation Approach to Identify Power-Temperature Models of HVAC Units," in *2018 IEEE International Smart Cities Conference (ISC2)*, 2018, pp. 1-6.

[361] A. Rajith, S. Soki, and M. Hiroshi, "Real-time optimized HVAC control system on top of an IoT framework," in *Proceedings of the 3rd International Conference on Fog and Mobile Edge Computing (FMEC 2018)*, 2018, pp. 181-186.

[362] G. Alsuhli and A. Khattab, "A Fog-based IoT Platform for Smart Buildings," in *2019 International Conference on Innovative Trends in Computer Engineering (ITCE)*, 2019, pp. 174-179.

[363] A. Zakharov, A. Romazanov, A. Shirokikh, and I. Zakharova, "Intellectual Data Analysis System of Building Temperature Mode Monitoring," in *2019 International Russian Automation Conference (RusAutoCon)*, 2019, pp. 1-6.

[364] A. Pandharipande, M. Zhao, and E. Frimout, "Connected Indoor Lighting Based Applications in a Building IoT Ecosystem," *IEEE Internet of Things Magazine*, vol. 2, no. 1, pp. 22-26, 2019.

[365] T. Sonnekalb and S. Lucia, "Smart Hot Water Control with Learned Human Behavior for Minimal Energy Consumption," in *2019 IEEE 5th World Forum on Internet of Things (WF-IoT)*, 2019, pp. 572-577.

[366] P. D. Leo, F. Spertino, S. Fichera, G. Malgaroli, and A. Ratclif, "Improvement of Self-Sufficiency for an Innovative Nearly Zero Energy Building by Photovoltaic Generators," in *2019 IEEE Milan PowerTech*, 2019, pp. 1-6.

[367] M. Cai, M. Pipattanasomporn, and S. Rahman, "Day-ahead building-level load forecasts using deep learning vs. traditional time-series techniques," *Applied Energy*, vol. 236, pp. 1078-1088, 2019/02/15/ 2019.

[368] J.-H. Woo, M. A. Peterson, and B. Gleason, "Developing a virtual campus model in an interactive game-engine environment for building energy benchmarking," *Journal of Computing in Civil Engineering*, vol. 30, no. 5, p. C4016005, 2016/05/11/ 2016.

[369] T. Gerrish, K. Ruikar, M. Cook, M. Johnson, M. Phillip, and C. Lowry, "BIM application to building energy performance visualisation and management: Challenges and potential," *Energy and Buildings*, vol. 144, pp. 218-228, 2017/06/01/ 2017.

[370] S. Tang, D. R. Shelden, C. M. Eastman, P. Pishdad-Bozorgi, and X. Gao, "A review of building information modeling (BIM) and the internet of things (IoT) devices integration: Present status and future trends," *Automation in Construction*, vol. 101, pp. 127-139, 2019/05/01/ 2019.

[371] L. Bottaccioli *et al.*, "Building Energy Modelling and Monitoring by Integration of IoT Devices and Building Information Models," in *2017 IEEE 41st Annual Computer Software and Applications Conference (COMPSAC)*, 2017, vol. 1, pp. 914-922.

[372] D. F. Huber and M. Hebert, "Fully automatic registration of multiple 3D data sets," *Image and Vision Computing*, vol. 21, no. 7, pp. 637-650, 2003/07/01/ 2003.

[373] F. Bosché and E. Guenet, "Automating surface flatness control using terrestrial laser scanning and building information models," *Automation in Construction*, vol. 44, pp. 212-226, 2014/08/01/ 2014.

[374] Q. Wang, M.-K. Kim, J. C. P. Cheng, and H. Sohn, "Automated quality assessment of precast concrete elements with geometry irregularities using terrestrial laser scanning," *Automation in Construction*, vol. 68, pp. 170-182, 2016/08/01/ 2016.

[375] K. K. Han, D. Cline, and M. Golparvar-Fard, "Formalized knowledge of construction sequencing for visual monitoring of work-in-progress via incomplete point clouds and low-LoD 4D BIMs," *Advanced Engineering Informatics,* vol. 29, no. 4, pp. 889-901, 2015/10/01/ 2015.

[376] C. Rausch, M. Nahangi, C. Haas, and J. West, "Kinematics chain based dimensional variation analysis of construction assemblies using building information models and 3D point clouds," *Automation in Construction,* vol. 75, pp. 33-44, 2017/03/01/ 2017.

[377] J. Balado, L. Díaz-Vilariño, P. Arias, and M. Soilán, "Automatic building accessibility diagnosis from point clouds," *Automation in Construction,* vol. 82, pp. 103-111, 2017/10/01/ 2017.

[378] C. Wang, Y. K. Cho, and C. Kim, "Automatic BIM component extraction from point clouds of existing buildings for sustainability applications," *Automation in Construction,* vol. 56, pp. 1-13, 2015/08/01/ 2015.

[379] C. Wang and Y. K. Cho, "Performance evaluation of automatically generated BIM from laser scanner data for sustainability analyses," *Procedia Engineering,* vol. 118, pp. 918-925, 2015/12/01/ 2015.

[380] A. Adán, B. Quintana, S. A. Prieto, and F. Bosché, "Scan-to-BIM for 'secondary' building components," *Advanced Engineering Informatics,* vol. 37, pp. 119-138, 2018/08/01/ 2018.

[381] L. M. Khodeir, D. Aly, and S. Tarek, "Integrating HBIM (Heritage Building Information Modeling) tools in the application of sustainable retrofitting of heritage buildings in Egypt," *Procedia Environmental Sciences,* vol. 34, pp. 258-270, 2016/05/07/ 2016.

[382] C. Dore and M. Murphy, "Current state of the art historic building information modelling," *International Archives of the Photogrammetry, Remote Sensing & Spatial Information Sciences,* vol. 42, no. 2/W5, pp. 185–192, 2017/08/18/ 2017.

[383] S. Bruno, M. De Fino, and F. Fatiguso, "Historic Building Information Modelling: performance assessment for diagnosis-aided information modelling and management," *Automation in Construction,* vol. 86, pp. 256-276, 2018/02/01/ 2018.

[384] D. P. Pocobelli, J. Boehm, P. Bryan, J. Still, and J. Grau-Bové, "Building information models for monitoring and simulation data in heritage buildings," in *International Archives of the Photogrammetry, Remote Sensing and Spatial Information Sciences - ISPRS Archives*, 2018, vol. 42, no. 2, pp. 909-916.

[385] M. Bassier and M. Vergauwen, "Unsupervised reconstruction of Building Information Modeling wall objects from point cloud data," *Automation in Construction,* vol. 120, p. 103338, 2020/12/01/ 2020.

[386] Q. Wang, Y. Tan, and Z. Mei, "Computational Methods of Acquisition and Processing of 3D Point Cloud Data for Construction Applications," *Archives of Computational Methods in Engineering,* vol. 27, no. 2, pp. 479-499, 2020/04/01 2020.

[387] D. Jakhar and I. Kaur, "Artificial intelligence, machine learning and deep learning: definitions and differences," *Clinical and Experimental Dermatology,* vol. 45, no. 1, pp. 131-132, 2020/01/01/ 2020.

[388] E. Alpaydin, *Introduction to Machine Learning*. The MIT Press, 2010.

[389] S. Das, A. dey, A. Pal, and N. Roy, "Applications of Artificial Intelligence in Machine Learning: Review and Prospect," *International Journal of Computer Applications*, vol. 115, pp. 31-41, 2015/04/22/ 2015.

[390] C. M. Bishop, *Pattern recognition and machine learning*. Springer, 2006.

[391] T. M. Mitchell, *Machine Learning*. McGraw-Hill, Inc., 1997.

[392] D. Aiger, N. J. Mitra, and D. Cohen-Or, "4-points congruent sets for robust pairwise surface registration," presented at the Proceedings of SIGGRAPH '08: Special Interest Group on Computer Graphics and Interactive Techniques, Los Angeles, CA (United States), 2008.

[393] R. B. Rusu, N. Blodow, Z. C. Marton, and M. Beetz, "Aligning point cloud views using persistent feature histograms," in *Proceedings of the International Conference on Intelligent Robots and Systems (IROS 2008)*, Nice, France, 2008, pp. 3384-3391: IEEE.

[394] R. B. Rusu, N. Blodow, and M. Beetz, "Fast Point Feature Histograms (FPFH) for 3D registration," in *2009 IEEE International Conference on Robotics and Automation*, 2009, pp. 3212-3217.

[395] J. B. Paul and D. M. Neil, "Method for registration of 3-D shapes," in *Proceedings of SPIE*, 1992, vol. 1611.

[396] Y. Chen and G. Medioni, "Object modelling by registration of multiple range images," *Image and Vision Computing*, vol. 10, no. 3, pp. 145-155, 1992/04/01/ 1992.

[397] E. Turner and A. Zakhor, "Automatic indoor 3D surface reconstruction with segmented building and object elements," in *Proceedings of the International Conference on 3D Vision (3DV 2015)*, Lyon, France, 2015, pp. 362-370: IEEE.

[398] K. Ishida, N. Kano, and K. Kimoto, "Shape recognition with point clouds in rebars," in *Proceedings of the International Symposium on Automation and Robotics in Construction (ISARC 2012)*, 2012, vol. 29: Vilnius Gediminas Technical University, Department of Construction Economics.

[399] M. A. Fischler and R. C. Bolles, "Random sample consensus: a paradigm for model fitting with applications to image analysis and automated cartography," in *Communications of the ACM*, 1981, vol. 24, no. 6, pp. 381–395.

[400] D. H. Ballard, "Generalizing the Hough transform to detect arbitrary shapes," *Pattern Recognition*, vol. 13, no. 2, pp. 111-122, 1981/01/01/ 1981.

[401] R. Raguram, J.-M. Frahm, and M. Pollefeys, "A Comparative Analysis of RANSAC Techniques Leading to Adaptive Real-Time Random Sample Consensus," in *Proceedings of the 10th European Conference on Computer Vision (ECCV 2008)*, Marseille, France, 2008, pp. 500-513: Springer.

[402] S. Choi, T. Kim, and W. Yu, "Performance evaluation of RANSAC family," in *Proceedings of the British Machine Vision Conference (BMVC 2009)*, 2009, vol. 24.

[403] R. Raguram, O. Chum, M. Pollefeys, J. Matas, and J. Frahm, "USAC: A Universal Framework for Random Sample Consensus," *IEEE Transactions on Pattern Analysis and Machine Intelligence,* vol. 35, no. 8, pp. 2022-2038, 2013.

[404] D. Borrmann, J. Elseberg, K. Lingemann, and A. Nüchter, "The 3D Hough Transform for plane detection in point clouds: A review and a new accumulator design," *3D Research,* vol. 2, no. 2, p. 3, 2011/11/03/ 2011.

[405] F. A. Limberger and M. M. Oliveira, "Real-time detection of planar regions in unorganized point clouds," *Pattern Recognition*, vol. 48, no. 6, pp. 2043-2053, 2015/06/01/ 2015.

[406] A. Kaiser, J. A. Ybanez Zepeda, and T. Boubekeur, "A Survey of Simple Geometric Primitives Detection Methods for Captured 3D Data," *Computer Graphics Forum*, vol. 38, no. 1, pp. 167-196, 2019/02/01/ 2019.

[407] Y. Xie, J. Tian, and X. X. Zhu, "Linking Points With Labels in 3D: A Review of Point Cloud Semantic Segmentation," *IEEE Geoscience and Remote Sensing Magazine,* vol. 8, no. 4, pp. 38-59, 2020.

[408] N. Hidaka, T. Michikawa, A. Motamedi, N. Yabuki, and T. Fukuda, "Polygonization of point clouds of repetitive components in civil infrastructure based on geometric similarities," *Automation in Construction*, vol. 86, pp. 99-117, 2018/02/01/ 2018.

[409] A. Dimitrov and M. Golparvar-Fard, "Segmentation of building point cloud models including detailed architectural/structural features and MEP systems," *Automation in Construction*, vol. 51, pp. 32-45, 2015/03/01/ 2015.

[410] T. Czerniawski, M. Nahangi, C. Haas, and S. Walbridge, "Pipe spool recognition in cluttered point clouds using a curvature-based shape descriptor," *Automation in Construction*, vol. 71, pp. 346-358, 2016/11/01/ 2016.

[411] A. K. Patil, P. Holi, S. K. Lee, and Y. H. Chai, "An adaptive approach for the reconstruction and modeling of as-built 3D pipelines from point clouds," *Automation in Construction*, vol. 75, pp. 65-78, 2017/03/01/ 2017.

[412] H. Boulaassal, T. Landes, P. Grussenmeyer, and F. Tarsha-Kurdi, "Automatic segmentation of building facades using Terrestrial Laser Data," in *International Archives of the Photogrammetry, Remote Sensing and Spatial Information Sciences - ISPRS Archives*, 2012, vol. 36.

[413] D. Chen, L. Zhang, P. T. Mathiopoulos, and X. Huang, "A Methodology for Automated Segmentation and Reconstruction of Urban 3-D Buildings from ALS Point Clouds," *IEEE Journal of Selected Topics in Applied Earth Observations and Remote Sensing,* vol. 7, no. 10, pp. 4199-4217, 2014.

[414] A. Adam, E. Chatzilari, S. Nikolopoulos, and I. Kompatsiaris, "H-RANSAC: A Hybrid Point Cloud Segmentation Combining 2D and 3D Data," in *International Archives of the Photogrammetry, Remote Sensing and Spatial Information Sciences - ISPRS Archives*, 2018, vol. IV-2, pp. 1-8.

[415] R. Schnabel, R. Wahl, and R. Klein, "Efficient RANSAC for Point-Cloud Shape Detection," *Computer Graphics Forum*, vol. 26, no. 2, pp. 214-226, 2007/06/01/ 2007.

[416] Y. Perez-Perez, M. Golparvar-Fard, and K. El-Rayes, "Segmentation of point clouds via joint semantic and geometric features for 3D modeling of the built environment," *Automation in Construction*, vol. 125, p. 103584, 2021/05/01/ 2021.

[417] A.-V. Vo, L. Truong-Hong, D. F. Laefer, and M. Bertolotto, "Octree-based region growing for point cloud segmentation," *ISPRS Journal of Photogrammetry and Remote Sensing*, vol. 104, pp. 88-100, 2015/06/01/ 2015.

[418] Y. Liu and Y. Xiong, "Automatic segmentation of unorganized noisy point clouds based on the Gaussian map," *Computer-Aided Design*, vol. 40, no. 5, pp. 576-594, 2008/05/01/ 2008.

[419] E. Valero, A. Adán, and C. Cerrada, "Automatic Method for Building Indoor Boundary Models from Dense Point Clouds Collected by Laser Scanners," *Sensors*, vol. 12, no. 12, pp. 16099-16115, 2012/11/22/ 2012.

[420] S. Z. Li, "Markov random field models in computer vision," in *Proceedings of the 3rd European Conference on Computer Vision (ECCV '94)*, Stockholm, Sweden, 1994, pp. 361-370: Springer Berlin Heidelberg.

[421] P. J. Besl and R. C. Jain, "Segmentation through variable-order surface fitting," *IEEE Transactions on Pattern Analysis and Machine Intelligence*, vol. 10, no. 2, pp. 167-192, 1988.

[422] X. Ning, X. Zhang, Y. Wang, and M. Jaeger, "Segmentation of architecture shape information from 3D point cloud," in *Proceedings of the 8th International Conference on Virtual Reality Continuum and its Applications in Industry*, 2009, pp. 127-132: ACM.

[423] Q. Zhan, Y. Liang, and Y. Xiao, "Color-based segmentation of point clouds," *Laser Scanning*, vol. 38, no. 3, pp. 155-161, 2009/07/01/ 2009.

[424] M. Ester, H.-P. Kriegel, J. Sander, and X. Xu, "A density-based algorithm for discovering clusters in large spatial databases with noise," in *Kdd*, 1996, vol. 96, no. 34, pp. 226-231.

[425] T. Czerniawski, B. Sankaran, M. Nahangi, C. Haas, and F. Leite, "6D DBSCAN-based segmentation of building point clouds for planar object classification," *Automation in Construction*, vol. 88, pp. 44-58, 2018/04/01/ 2018.

[426] J. Zhao *et al.*, "An Automatic Density Clustering Segmentation Method for Laser Scanning Point Cloud Data of Buildings," *Mathematical Problems in Engineering*, vol. 2019, p. 3026758, 2019/07/07/ 2019.

[427] M.-K. Kim, J. P. P. Thedja, H.-L. Chi, and D.-E. Lee, "Automated rebar diameter classification using point cloud data based machine learning," *Automation in Construction*, vol. 122, p. 103476, 2021/02/01/ 2021.

[428] H. Son, C. Kim, and C. Kim, "3D reconstruction of as-built industrial instrumentation models from laser-scan data and a 3D CAD database based on prior knowledge," *Automation in Construction*, vol. 49, pp. 193-200, 2015/01/01/ 2015.

[429] V. Sanchez and A. Zakhor, "Planar 3D modeling of building interiors from point cloud data," in *2012 19th IEEE International Conference on Image Processing*, 2012, pp. 1777-1780.

[430] B. Quintana, S. A. Prieto, A. Adán, and F. Bosché, "Door detection in 3D coloured point clouds of indoor environments," *Automation in Construction,* vol. 85, pp. 146-166, 2018/01/01/ 2018.

[431] F. Hamid-Lakzaeian, "Structural-based point cloud segmentation of highly ornate building façades for computational modelling," *Automation in Construction,* vol. 108, p. 102892, 2019/12/01/ 2019.

[432] M. Weinmann, A. Schmidt, C. Mallet, S. Hinz, F. Rottensteiner, and B. Jutzi, "Contextual classification of point cloud data by exploiting individual 3D neigbourhoods," *ISPRS Annals of Photogrammetry, Remote Sensing and Spatial Information Sciences*, vol. II-3, no. W4, pp. 271-278, 2015/03/11/ 2015.

[433] M. Weinmann, B. Jutzi, S. Hinz, and C. Mallet, "Semantic point cloud interpretation based on optimal neighborhoods, relevant features and efficient classifiers," *ISPRS Journal of Photogrammetry and Remote Sensing,* vol. 105, pp. 286-304, 2015/07/01/ 2015.

[434] L. Breiman, "Random forests," *Machine learning,* vol. 45, no. 1, pp. 5-32, 2001/10/01/ 2001.

[435] J. Niemeyer, F. Rottensteiner, and U. Soergel, "Contextual classification of lidar data and building object detection in urban areas," *ISPRS Journal of Photogrammetry and Remote Sensing,* vol. 87, pp. 152-165, 2014/01/01/ 2014.

[436] G. Vosselman, M. Coenen, and F. Rottensteiner, "Contextual segment-based classification of airborne laser scanner data," *ISPRS Journal of Photogrammetry and Remote Sensing,* vol. 128, pp. 354-371, 2017/06/01/ 2017.

[437] P.-H. Hsu and Z.-Y. Zhuang, "Incorporating Handcrafted Features into Deep Learning for Point Cloud Classification," *Remote Sensing,* vol. 12, no. 22, 2020/11/12/ 2020.

[438] N. Chehata, L. Guo, and C. Mallet, "Airborne LiDAR Feature Selection for Urban Classification Using Random Forests," in *Laser Scanning*, Paris, France, 2009.

[439] J. Zhang, X. Lin, and X. Ning, "SVM-Based Classification of Segmented Airborne LiDAR Point Clouds in Urban Areas," *Remote Sensing,* vol. 5, no. 8, 2013/07/31/ 2013.

[440] Z. Wang *et al.,* "A Multiscale and Hierarchical Feature Extraction Method for Terrestrial Laser Scanning Point Cloud Classification," *IEEE Transactions on Geoscience and Remote Sensing,* vol. 53, no. 5, pp. 2409-2425, 2015.

[441] Y. Lu and C. Rasmussen, "Simplified markov random fields for efficient semantic labeling of 3D point clouds," in *Proceedings of the International Conference on Intelligent Robots and Systems (IROS 2012),* Vilamoura, Algarve, 2012, pp. 2690-2697: IEEE.

[442] J. Niemeyer, F. Rottensteiner, and U. Soergel, "Conditional random fields for lidar point cloud classification in complex urban areas," *ISPRS Annals of Photogrammetry, Remote Sensing and Spatial Information Sciences,* vol. I-3, 2012/07/20/ 2012.

[443] E. H. Lim and D. Suter, "3D terrestrial LIDAR classifications with super-voxels and multi-scale Conditional Random Fields," *Computer-Aided Design*, vol. 41, no. 10, pp. 701-710, 2009/10/01/ 2009.

[444] J. F. Lalonde, R. Unnikrishnan, N. Vandapel, and M. Hebert, "Scale selection for classification of point-sampled 3D surfaces," in *Fifth International Conference on 3-D Digital Imaging and Modeling (3DIM'05)*, 2005, pp. 285-292.

[445] D. Munoz, J. A. Bagnell, N. Vandapel, and M. Hebert, "Contextual classification with functional Max-Margin Markov Networks," in *Proceedings of the 2009 IEEE Conference on Computer Vision and Pattern Recognition (CVPR 2009)*, Miami Beach, FL (United States), 2009, pp. 975-982: IEEE.

[446] M. Najafi, S. Taghavi Namin, M. Salzmann, and L. Petersson, "Non-associative Higher-Order Markov Networks for Point Cloud Classification," in *Proceedings of the 13th European Conference on Computer Vision (ECCV 2014)*, Zurich, Switzerland, 2014, pp. 500-515: Springer International Publishing.

[447] Q. Wang, J. C. P. Cheng, and H. Sohn, "Automated Estimation of Reinforced Precast Concrete Rebar Positions Using Colored Laser Scan Data," *Computer-Aided Civil and Infrastructure Engineering*, vol. 32, no. 9, pp. 787-802, 2017/09/01/ 2017.

[448] Y. Xu, S. Tuttas, L. Hoegner, and U. Stilla, "Reconstruction of scaffolds from a photogrammetric point cloud of construction sites using a novel 3D local feature descriptor," *Automation in Construction*, vol. 85, pp. 76-95, 2018/01/01/ 2018.

[449] J.-F. Lalonde, N. Vandapel, D. F. Huber, and M. Hebert, "Natural terrain classification using three-dimensional ladar data for ground robot mobility," *Journal of Field Robotics*, vol. 23, no. 10, pp. 839-861, 2006/10/01/ 2006.

[450] B. G. Baumgart, "Winged edge polyhedron representation," Stanford University, Stanford, CA, United States1972.

[451] W.-C. Lin and T.-W. Chen, "CSG-based object recognition using range images," in *9th International Conference on Pattern Recognition*, 1988, pp. 99-103: IEEE.

[452] L. De Luca, P. Véron, and M. Florenzano, "Reverse engineering of architectural buildings based on a hybrid modeling approach," *Computers & Graphics*, vol. 30, no. 2, pp. 160-176, 2006/04/01/ 2006.

[453] S. Nikoohemat, A. A. Diakité, S. Zlatanova, and G. Vosselman, "Indoor 3D reconstruction from point clouds for optimal routing in complex buildings to support disaster management," *Automation in Construction*, vol. 113, p. 103109, 2020/05/01/ 2020.

[454] B. Wang, C. Yin, H. Luo, J. C. P. Cheng, and Q. Wang, "Fully automated generation of parametric BIM for MEP scenes based on terrestrial laser scanning data," *Automation in Construction*, vol. 125, p. 103615, 2021/05/01/ 2021.

[455] T. Kang, S. Patil, K. Kang, D. Koo, and J. Kim, "Rule-Based Scan-to-BIM Mapping Pipeline in the Plumbing System," *Applied Sciences*, vol. 10, no. 21, 2020/10/22/ 2020.

[456] F. Xue, W. Lu, K. Chen, and C. J. Webster, "BIM reconstruction from 3D point clouds: A semantic registration approach based on multimodal optimization and architectural design knowledge," *Advanced Engineering Informatics,* vol. 42, p. 100965, 2019/10/01/ 2019.

[457] M. Bassier, R. Klein, B. Van Genechten, and M. Vergauwen, "IFC Wall reconstruction from unstructured point clouds," in *Annals of the photogrammetry remote sensing and spatial information sciences*, 2018.

[458] X. X. Zhu *et al.*, "Deep Learning in Remote Sensing: A Comprehensive Review and List of Resources," *IEEE Geoscience and Remote Sensing Magazine,* vol. 5, no. 4, pp. 8-36, 2017.

[459] A. Shrestha and A. Mahmood, "Review of Deep Learning Algorithms and Architectures," *IEEE Access,* vol. 7, pp. 53040-53065, 2019.

[460] Y. LeCun, Y. Bengio, and G. Hinton, "Deep learning," *Nature,* vol. 521, no. 7553, pp. 436-444, 2015/05/01/ 2015.

[461] A. F. Agarap, "Deep Learning using Rectified Linear Units (ReLU)," *arXiv preprint arXiv:1803.08375,* 2018.

[462] S. Sharma. (2017, 2021/01/14/). *Activation Functions in Neural Networks*. Available: https://towardsdatascience.com/activation-functions-neural-networks-1cbd9f8d91d6

[463] G. Cybenko, "Approximation by superpositions of a sigmoidal function," *Mathematics of control, signals and systems,* vol. 2, no. 4, pp. 303-314, 1989/01/01/ 1989.

[464] K. Hornik, "Approximation capabilities of multilayer feedforward networks," *Neural Networks,* vol. 4, no. 2, pp. 251-257, 1991/01/01/ 1991.

[465] Y. Guo, H. Wang, Q. Hu, H. Liu, L. Liu, and M. Bennamoun, "Deep Learning for 3D Point Clouds: A Survey," *IEEE Transactions on Pattern Analysis and Machine Intelligence,* pp. 1-1, 2020.

[466] X. Song *et al.*, "ApolloCar3D: A Large 3D Car Instance Understanding Benchmark for Autonomous Driving," in *Proceedings of the IEEE Conference on Computer Vision and Pattern Recognition (CVPR 2019),* Long Beach, CA (United States), 2019, pp. 5447-5457: IEEE.

[467] Z. Wu *et al.*, "3D ShapeNets: A deep representation for volumetric shapes," in *Proceedings of the IEEE Conference on Computer Vision and Pattern Recognition (CVPR 2015)*, Boston, MA (United States), 2015, pp. 1912-1920: IEEE.

[468] N. Silberman, D. Hoiem, P. Kohli, and R. Fergus, "Indoor Segmentation and Support Inference from RGBD Images," in *Proceedings of the 12th European Conference on Computer Vision (ECCV 2012),* Florence, Italy, 2012, pp. 746-760: Springer Berlin Heidelberg.

[469] X. Roynard, J.-E. Deschaud, and F. Goulette, "Paris-Lille-3D: A large and high-quality ground-truth urban point cloud dataset for automatic segmentation and classification," *The International Journal of Robotics Research,* vol. 37, no. 6, pp. 545-557, 2018/05/01/ 2018.

[470] K. Mo *et al.*, "PartNet: A Large-scale Benchmark for Fine-grained and Hierarchical Part-level 3D Object Understanding," in *Proceedings of the IEEE Conference on Computer Vision and Pattern Recognition (CVPR 2019),* Long Beach, CA (United States), 2019: IEEE.

[471] I. Armeni *et al.*, "3d semantic parsing of large-scale indoor spaces," in *Proceedings of the IEEE Conference on Computer Vision and Pattern Recognition (CVPR 2016)*, Las Vegas, NV (United States), 2016, pp. 1534-1543: IEEE.

[472] A. Dai, A. X. Chang, M. Savva, M. Halber, T. Funkhouser, and M. Nießner, "ScanNet: Richly-Annotated 3D Reconstructions of Indoor Scenes," in *Proceedings of the IEEE Conference on Computer Vision and Pattern Recognition (CVPR 2017)*, Honolulu, HI (United States), 2017, pp. 2432-2443: IEEE.

[473] M. A. Uy, Q. Pham, B. Hua, T. Nguyen, and S. Yeung, "Revisiting Point Cloud Classification: A New Benchmark Dataset and Classification Model on Real-World Data," in *Proceedings of the IEEE International Conference on Computer Vision (ICCV 2019) - Workshop*, Seul, Korea, 2019, pp. 1588-1597: IEEE.

[474] B. Hua, Q. Pham, D. T. Nguyen, M. Tran, L. Yu, and S. Yeung, "SceneNN: A Scene Meshes Dataset with aNNotations," in *Proceedings of the 4th International Conference on 3D Vision (3DV 2016)*, Stanford, CA (United States), 2016, pp. 92-101: IEEE.

[475] T. Hackel, N. Savinov, L. Ladicky, J. D. Wegner, K. Schindler, and M. Pollefeys, "SEMANTIC3D.NET: A New Large-Scale Point Cloud Classification Benchmark," *ISPRS Annals of Photogrammetry, Remote Sensing and Spatial Information Sciences,* vol. IV-1/W1, pp. 91-98, 2017.

[476] A. Geiger, P. Lenz, and R. Urtasun, "Are we ready for autonomous driving? The KITTI vision benchmark suite," in *Proceedings of the 2012 IEEE Conference on Computer Vision and Pattern Recognition (CVPR 2012)*, Providence, RI (United States), 2012, pp. 3354-3361: IEEE.

[477] J. Behley *et al.*, "SemanticKITTI: A Dataset for Semantic Scene Understanding of LiDAR Sequences," in *Proceedings of the IEEE International Conference on Computer Vision (ICCV 2019)*, Seul, Korea, 2019, pp. 9296-9306: IEEE.

[478] A. Chang *et al.*, "ShapeNet: An Information-Rich 3D Model Repository," *arXiv preprint arXiv:1512.03012*, 2015.

[479] F. Rottensteiner *et al.*, "The ISPRS benchmark on urban object classification and 3D building reconstruction," in *ISPRS Annals of Photogrammetry, Remote Sensing and Spatial Information Sciences*, 2012, vol. I-3.

[480] Y. Aoki, H. Goforth, R. A. Srivatsan, and S. Lucey, "PointNetLK: Robust & Efficient Point Cloud Registration Using PointNet," in *Proceedings of the IEEE Conference on Computer Vision and Pattern Recognition (CVPR 2019)*, Long Beach, CA (United States), 2019, pp. 7156-7165: IEEE.

[481] X. Liu, C. R. Qi, and L. J. Guibas, "FlowNet3D: Learning Scene Flow in 3D Point Clouds," in *Proceedings of the IEEE Conference on Computer Vision and Pattern Recognition (CVPR 2019)*, Long Beach, CA (United States), 2019, pp. 529-537: IEEE.

[482] L. Ge, Y. Cai, J. Weng, and J. Yuan, "Hand PointNet: 3D Hand Pose Estimation Using Point Sets," in *Proceedings of the IEEE Conference on Computer Vision and Pattern Recognition (CVPR 2018)*, Salt Lake City, UT (United States), 2018, pp. 8417-8426: IEEE.

[483] J. R. Pinto *et al.*, "Audiovisual Classification of Group Emotion Valence Using Activity Recognition Networks," in *Proceedings of the IEEE 4th International Conference on Image Processing, Applications and Systems (IPAS 2020)*, 2020, pp. 114-119.

[484] X. F. Han, H. Laga, and M. Bennamoun, "Image-Based 3D Object Reconstruction: State-of-the-Art and Trends in the Deep Learning Era," *IEEE Transactions on Pattern Analysis and Machine Intelligence,* vol. 43, no. 5, pp. 1578-1604, 2021.

[485] A. Ioannidou, E. Chatzilari, S. Nikolopoulos, and I. Kompatsiaris, "Deep Learning Advances in Computer Vision with 3D Data: A Survey," *ACM Computing Surveys (CSUR),* vol. 50, no. 2, p. Article 20, 2017.

[486] E. Ahmed *et al.*, "Deep Learning Advances on Different 3D Data Representations: A Survey," *arXiv preprint arXiv:1808.01462,* 2018.

[487] E. Arnold, O. Y. Al-Jarrah, M. Dianati, S. Fallah, D. Oxtoby, and A. Mouzakitis, "A Survey on 3D Object Detection Methods for Autonomous Driving Applications," *IEEE Transactions on Intelligent Transportation Systems,* vol. 20, no. 10, pp. 3782-3795, 2019.

[488] A. Nguyen and B. Le, "3D point cloud segmentation: A survey," in *Proceedings of the IEEE 6th Conference on Robotics, Automation and Mechatronics (RAM 2013)*, Manila, Philippines, 2013, pp. 225-230.

[489] E. Grilli, F. Menna, and F. Remondino, "A Review of Point Clouds Segmentation and Classification Algorithms," in *International Archives of the Photogrammetry, Remote Sensing and Spatial Information Sciences - ISPRS Archives*, 2017, vol. XLII-2/W3, pp. 339-344.

[490] B. Yang *et al.*, "Learning object bounding boxes for 3d instance segmentation on point clouds," *arXiv preprint arXiv:1906.01140,* 2019.

[491] Q.-H. Pham, T. Nguyen, B.-S. Hua, G. Roig, and S.-K. Yeung, "Jsis3d: Joint semantic-instance segmentation of 3d point clouds with multi-task pointwise networks and multi-value conditional random fields," in *Proceedings of the IEEE Conference on Computer Vision and Pattern Recognition (CVPR 2019)*, Long Beach, CA (United States), 2019, pp. 8827-8836: IEEE.

[492] F. Engelmann, M. Bokeloh, A. Fathi, B. Leibe, and M. NieBner, "3D-MPA: Multi-Proposal Aggregation for 3D Semantic Instance Segmentation," presented at the Proceedings of the IEEE Conference on Computer Vision and Pattern Recognition (CVPR 2020), 2020.

[493] C. R. Qi, L. Yi, H. Su, and L. J. Guibas, "Pointnet++: Deep hierarchical feature learning on point sets in a metric space," *arXiv preprint arXiv:1706.02413,* 2017.

[494] H. Thomas, C. R. Qi, J.-E. Deschaud, B. Marcotegui, F. Goulette, and L. J. Guibas, "KPConv: Flexible and deformable convolution for point clouds," in *Proceedings of the 2019 IEEE International Conference on Computer Vision*, Seul, Korea, 2019, pp. 6411-6420: IEEE.

[495] S. Saha. (2018). *A Comprehensive Guide to Convolutional Neural Networks — the ELI5 way*. Available: https://towardsdatascience.com/a-comprehensive-guide-to-convolutional-neural-networks-the-eli5-way-3bd2b1164a53

[496] M. Mishra. (2020). *Convolutional Neural Networks, Explained*. Available: https://towardsdatascience.com/convolutional-neural-networks-explained-9cc5188c4939

[497] H. Habibi Aghdam and E. Jahani Heravi, "Convolutional Neural Networks," in *Guide to Convolutional Neural Networks: A Practical Application to Traffic-Sign Detection and Classification*: Springer International Publishing, 2017, pp. 85-130.

[498] S. Albawi, T. A. Mohammed, and S. Al-Zawi, "Understanding of a convolutional neural network," in *International Conference on Engineering and Technology (ICET 2017)*, Antalya, Turkey, 2017, pp. 1-6.

[499] Z. J. Wang *et al.*, "CNN Explainer: Learning Convolutional Neural Networks with Interactive Visualization," *IEEE Transactions on Visualization and Computer Graphics*, vol. 27, no. 2, pp. 1396-1406, 2021.

[500] A. W. Harley, "An Interactive Node-Link Visualization of Convolutional Neural Networks," in *Advances in Visual Computing*, 2015, pp. 867-877: Springer International Publishing.

[501] H. Su, S. Maji, E. Kalogerakis, and E. Learned-Miller, "Multi-view Convolutional Neural Networks for 3D Shape Recognition," in *Proceedings of the IEEE International Conference on Computer Vision (ICCV 2015)*, Santiago, Chile, 2015, pp. 945-953: IEEE.

[502] J. Schmidhuber, "Deep learning in neural networks: An overview," *Neural Networks*, vol. 61, pp. 85-117, 2015/01/01/ 2015.

[503] T. Yu, J. Meng, and J. Yuan, "Multi-view Harmonized Bilinear Network for 3D Object Recognition," in *Proceedings of the IEEE Conference on Computer Vision and Pattern Recognition (CVPR 2018)*, Salt Lake City, UT (United States), 2018, pp. 186-194: IEEE.

[504] Z. Yang and L. Wang, "Learning Relationships for Multi-View 3D Object Recognition," in *Proceedings of the IEEE International Conference on Computer Vision (ICCV 2019)*, Seul, Korea, 2019, pp. 7504-7513: IEEE.

[505] F. J. Lawin, M. Danelljan, P. Tosteberg, G. Bhat, F. S. Khan, and M. Felsberg, "Deep Projective 3D Semantic Segmentation," in *Proceedings of the International Conference on Computer Analysis of Images and Patterns (CAIP 2017)*, Ystad, Sweden, 2017, pp. 95-107: Springer International Publishing.

[506] A. Boulch, B. L. Saux, and N. Audebert, "Unstructured point cloud semantic labeling using deep segmentation networks," in *Proceedings of the Workshop on 3D Object Retrieval*, Lyon, France, 2017, pp. 17–24: Eurographics Association.

[507] A. Boulch, J. Guerry, B. Le Saux, and N. Audebert, "SnapNet: 3D point cloud semantic labeling with 2D deep segmentation networks," *Computers & Graphics*, vol. 71, pp. 189-198, 2018/04/01/ 2018.

[508] N. Audebert, B. Le Saux, and S. Lefèvre, "Semantic Segmentation of Earth Observation Data Using Multimodal and Multi-scale Deep Networks," in *Proceddings of the 13th Asian Conference on Computer Vision (ACCV 2016)*, Taipei, Taiwan, 2017, pp. 180-196: Springer International Publishing.

[509] M. Tatarchenko, J. Park, V. Koltun, and Q. Zhou, "Tangent Convolutions for Dense Prediction in 3D," in *Proceedings of the IEEE Conference on Computer Vision and Pattern Recognition (CVPR 2018)*, Salt Lake City, UT (United States), 2018, pp. 3887-3896: IEEE.

[510] Y. Feng, Z. Zhang, X. Zhao, R. Ji, and Y. Gao, "GVCNN: Group-View Convolutional Neural Networks for 3D Shape Recognition," in *Proceedings of the IEEE Conference on Computer Vision and Pattern Recognition (CVPR 2018),* Salt Lake City, UT (United States), 2018, pp. 264-272: IEEE.

[511] X. Chen, H. Ma, J. Wan, B. Li, and T. Xia, "Multi-view 3D Object Detection Network for Autonomous Driving," in *Proceedings of the IEEE Conference on Computer Vision and Pattern Recognition (CVPR 2017),* Honolulu, HI (United States), 2017, pp. 6526-6534: IEEE.

[512] A. Kanezaki, Y. Matsushita, and Y. Nishida, "RotationNet for Joint Object Categorization and Unsupervised Pose Estimation from Multi-View Images," *IEEE Transactions on Pattern Analysis and Machine Intelligence,* vol. 43, no. 1, pp. 269-283, 2021.

[513] V. Vineet *et al.*, "Incremental dense semantic stereo fusion for large-scale semantic scene reconstruction," in *Proceedings of the IEEE International Conference on Robotics and Automation (ICRA 2015),* Seattle, WA (United States), 2015, pp. 75-82: IEEE.

[514] G. Pang and U. Neumann, "3D point cloud object detection with multi-view convolutional neural network," in *Proceedings of the 23rd International Conference on Pattern Recognition (ICPR 2016),* Cancun, Mexico, 2016, pp. 585-590: IEEE.

[515] B. Li, T. Zhang, and T. Xia, "Vehicle Detection from 3D Lidar Using Fully Convolutional Network," in *Robotics: Science and Systems (RSS 2016),* Cambridge, MA (United States), 2016: University of Michigan.

[516] C. Wang, M. Pelillo, and K. Siddiqi, "Dominant Set Clustering and Pooling for Multi-View 3D Object Recognition," in *Proceedings of the British Machine Vision Conference,* London, England, 2017.

[517] C. Ma, Y. Guo, J. Yang, and W. An, "Learning Multi-View Representation With LSTM for 3-D Shape Recognition and Retrieval," *IEEE Transactions on Multimedia,* vol. 21, no. 5, pp. 1169-1182, 2019.

[518] J. Huang and S. You, "Vehicle detection in urban point clouds with orthogonal-view convolutional neural network," in *Proceedings of the IEEE International Conference on Image Processing (ICIP 2016),* Phoenix, AZ (United States), 2016, pp. 2593-2597: IEEE

[519] A. H. Lang, S. Vora, H. Caesar, L. Zhou, J. Yang, and O. Beijbom, "PointPillars: Fast Encoders for Object Detection From Point Clouds," in *Proceedings of the IEEE Conference on Computer Vision and Pattern Recognition (CVPR 2019),* Long Beach, CA (United States), 2019, pp. 12689-12697: IEEE.

[520] B. Wu, A. Wan, X. Yue, and K. Keutzer, "SqueezeSeg: Convolutional Neural Nets with Recurrent CRF for Real-Time Road-Object Segmentation from 3D LiDAR Point Cloud," in *Proceedings of the IEEE International Conference on Robotics and Automation (ICRA 2018),* Brisbane, Australia, 2018, pp. 1887-1893: IEEE.

[521] F. N. Iandola, S. Han, M. W. Moskewicz, K. Ashraf, W. J. Dally, and K. Keutzer, "SqueezeNet: AlexNet-level accuracy with 50x fewer parameters and< 0.5 MB model size," *arXiv preprint arXiv:1602.07360,* 2016.

[522] B. Wu, X. Zhou, S. Zhao, X. Yue, and K. Keutzer, "SqueezeSegV2: Improved Model Structure and Unsupervised Domain Adaptation for Road-Object Segmentation from a LiDAR Point Cloud," in *Proceedings of the IEEE International Conference on Robotics and Automation (ICRA 2019),* Montreal, Canada, 2019, pp. 4376-4382: IEEE.

[523] A. Milioto, I. Vizzo, J. Behley, and C. Stachniss, "RangeNet ++: Fast and Accurate LiDAR Semantic Segmentation," in *Proceedings of the International Conference on Intelligent Robots and Systems (IROS 2019),* Macau, China, 2019, pp. 4213-4220: IEEE.

[524] Y. Wang, T. Shi, P. Yun, L. Tai, and M. Liu, "PointSeg: Real-Time Semantic Segmentation Based on 3D LiDAR Point Cloud," *arXiv preprint arXiv:1807.06288,* 2018.

[525] Y. Wang, Y. Yu, and M. Liu, "PointIT: A Fast Tracking Framework Based on 3D Instance Segmentation," *arXiv preprint arXiv:1902.06379,* 2019.

[526] H. Zhao, L. Jiang, C.-W. Fu, and J. Jia, "Pointweb: Enhancing local neighborhood features for point cloud processing," in *Proceedings of the IEEE Conference on Computer Vision and Pattern Recognition (CVPR 2019)*, Long Beach, CA (United States), 2019, pp. 5565-5573: IEEE.

[527] L. Landrieu and M. Simonovsky, "Large-scale point cloud semantic segmentation with superpoint graphs," in *Proceedings of the IEEE Conference on Computer Vision and Pattern Recognition (CVPR 2018)*, Salt Lake City, UT (United States), 2018, pp. 4558-4567: IEEE.

[528] H. Zhao, L. Jiang, J. Jia, P. Torr, and V. Koltun, "Point transformer," *arXiv preprint arXiv:2012.09164*, 2020.

[529] D. Maturana and S. Scherer, "VoxNet: A 3D Convolutional Neural Network for real-time object recognition," in *Proceedings of the International Conference on Intelligent Robots and Systems (IROS 2015)*, Hamburg, Germany, 2015, pp. 922-928: IEEE.

[530] D. T. Nguyen, B. Hua, M. Tran, Q. Pham, and S. Yeung, "A Field Model for Repairing 3D Shapes," in *Proceedings of the IEEE Conference on Computer Vision and Pattern Recognition (CVPR 2016),* Las Vegas, NV (United States), 2016, pp. 5676-5684: IEEE.

[531] S. Song, F. Yu, A. Zeng, A. X. Chang, M. Savva, and T. Funkhouser, "Semantic Scene Completion from a Single Depth Image," in *Proceedings of the IEEE Conference on Computer Vision and Pattern Recognition (CVPR 2017)*, Honolulu, HI (United States), 2017, pp. 190-198: IEEE.

[532] Y. Ben-Shabat, M. Lindenbaum, and A. Fischer, "3DmFV: Three-Dimensional Point Cloud Classification in Real-Time Using Convolutional Neural Networks," *IEEE Robotics and Automation Letters,* vol. 3, no. 4, pp. 3145-3152, 2018.

[533] B. Lecigne, S. Delagrange, and C. Messier, "Exploring trees in three dimensions: VoxR, a novel voxel-based R package dedicated to analysing the complex arrangement of tree crowns," *Annals of Botany,* vol. 121, no. 4, pp. 589-601, 2017/09/07/ 2018.

[534] H. Jing and Y. Suya, "Point cloud labeling using 3D Convolutional Neural Network," in *Proceedings of the 23rd International Conference on Pattern Recognition (ICPR 2016)*, Cancun, Mexico, 2016, pp. 2670-2675: IEEE.

[535] C. R. Qi, H. Su, M. Nießner, A. Dai, M. Yan, and L. J. Guibas, "Volumetric and Multi-view CNNs for Object Classification on 3D Data," in *Proceedings of the IEEE Conference on Computer Vision and Pattern Recognition (CVPR 2016)*, Las Vegas, NV (United States), 2016, pp. 5648-5656: IEEE.

[536] L. Tchapmi, C. Choy, I. Armeni, J. Gwak, and S. Savarese, "Segcloud: Semantic segmentation of 3d point clouds," in *Proceedings of the International Conference on 3D vision (3DV 2017)*, Qingdao, China, 2017, pp. 537-547: IEEE.

[537] J. Long, E. Shelhamer, and T. Darrell, "Fully convolutional networks for semantic segmentation," in *Proceedings of the IEEE Conference on Computer Vision and Pattern Recognition (CVPR 2015)*, Boston, MA (United States), 2015, pp. 3431-3440: IEEE.

[538] D. Rethage, J. Wald, J. Sturm, N. Navab, and F. Tombari, "Fully-Convolutional Point Networks for Large-Scale Point Clouds," presented at the Proceedings of the 15th European Conference on Computer Vision (ECCV 2018), Munich, Germany, 2018.

[539] A. Dai, D. Ritchie, M. Bokeloh, S. Reed, J. Sturm, and M. Nießner, "ScanComplete: Large-Scale Scene Completion and Semantic Segmentation for 3D Scans," in *Proceedings of the IEEE Conference on Computer Vision and Pattern Recognition (CVPR 2018)*, Salt Lake City, UT (United States), 2018, pp. 4578-4587: IEEE.

[540] H. Meng, L. Gao, Y. Lai, and D. Manocha, "VV-Net: Voxel VAE Net With Group Convolutions for Point Cloud Segmentation," in *Proceedings of the IEEE International Conference on Computer Vision (ICCV 2019)*, Seul, Korea, 2019, pp. 8499-8507: IEEE.

[541] Y. Ben-Shabat, M. Lindenbaum, and A. Fischer, "3D Point Cloud Classification and Segmentation using 3D Modified Fisher Vector Representation for Convolutional Neural Networks," *arXiv preprint arXiv:1711.08241*, 11/22 2017.

[542] Z. Liu, H. Tang, Y. Lin, and S. Han, "Point-voxel cnn for efficient 3d deep learning," *arXiv preprint arXiv:1907.03739*, 2019.

[543] G. Riegler, A. O. Ulusoy, and A. Geiger, "OctNet: Learning Deep 3D Representations at High Resolutions," in *Proceedings of the IEEE Conference on Computer Vision and Pattern Recognition (CVPR 2017)*, Honolulu, HI (United States), 2017, pp. 6620-6629: IEEE.

[544] P.-S. Wang, Y. Liu, Y.-X. Guo, C.-Y. Sun, and X. Tong, "O-CNN: octree-based convolutional neural networks for 3D shape analysis," *ACM Transactions on Graphics (ToG)*, vol. 36, no. 4, p. Article 72, 2017.

[545] A. Miller, V. Jain, and J. L. Mundy, "Real-time rendering and dynamic updating of 3-d volumetric data," presented at the Proceedings of the 4th Workshop on General Purpose Processing on Graphics Processing Units, Newport Beach, CA (United States), 2011.

[546] Y. Li, S. Pirk, H. Su, C. Ruizhongtai Qi, and L. Guibas, "FPNN: Field Probing Neural Networks for 3D Data," *Advances in Neural Information Processing Systems*, vol. 29, pp. 307-315, 2016/05/20/ 2016.

[547] T. Shao, Y. Yang, Y. Weng, Q. Hou, and K. Zhou, "H-CNN: Spatial Hashing Based CNN for 3D Shape Analysis," *IEEE Transactions on Visualization and Computer Graphics,* vol. 26, no. 7, pp. 2403-2416, 2020.

[548] R. Klokov and V. Lempitsky, "Escape from cells: Deep kd-networks for the recognition of 3d point cloud models," in *Proceedings of the IEEE International Conference on Computer Vision (ICCV 2017)*, Venice, Italy, 2017, pp. 863-872: IEEE.

[549] R. Rosu, P. Schütt, J. Quenzel, and S. Behnke, "LatticeNet: Fast Point Cloud Segmentation Using Permutohedral Lattices," in *Proceedings of Robotics: Science and Systems (RSS 2020)*, Corvalis, OR (United States), 2020.

[550] C. Choy, J. Gwak, and S. Savarese, "4D Spatio-Temporal ConvNets: Minkowski Convolutional Neural Networks," in *Proceedings of the IEEE Conference on Computer Vision and Pattern Recognition (CVPR 2019)*, Long Beach, CA (United States), 2019, pp. 3070-3079: IEEE.

[551] T. Le and Y. Duan, "PointGrid: A Deep Network for 3D Shape Understanding," in *Proceedings of the IEEE Conference on Computer Vision and Pattern Recognition (CVPR 2018),* Salt Lake City, UT (United States), 2018, pp. 9204-9214: IEEE.

[552] Y. Yan, Y. Mao, and B. Li, "SECOND: Sparsely Embedded Convolutional Detection," *Sensors,* vol. 18, no. 10, p. 3337, 2018/10/06/ 2018.

[553] B. Graham, "Sparse 3D convolutional neural networks," *arXiv preprint arXiv:1505.02890,* 2015/05/12/ 2015.

[554] H. Su *et al.*, "SPLATNet: Sparse Lattice Networks for Point Cloud Processing," in *Proceedings of the IEEE Conference on Computer Vision and Pattern Recognition (CVPR 2018),* Salt Lake City, UT (United States), 2018, pp. 2530-2539: IEEE.

[555] B. Graham, M. Engelcke, and L. Van Der Maaten, "3d semantic segmentation with submanifold sparse convolutional networks," in *Proceedings of the IEEE Conference on Computer Vision and Pattern Recognition (CVPR 2018)*, Salt Lake City, UT (United States), 2018, pp. 9224-9232: IEEE.

[556] C. R. Qi, H. Su, K. Mo, and L. J. Guibas, "Pointnet: Deep learning on point sets for 3d classification and segmentation," in *Proceedings of the IEEE Conference on Computer Vision and Pattern Recognition (CVPR 2017),* Honolulu, HI (United States), 2017, pp. 652-660: IEEE.

[557] M. Lin, Q. Chen, and S. Yan, "Network in network," *arXiv preprint arXiv:1312.4400,* 2014.

[558] T. Suzuki, K. Ozawa, and Y. Sekikawa, "Rethinking PointNet Embedding for Faster and Compact Model," *arXiv preprint arXiv:2007.15855,* 2020.

[559] M. Zaheer, S. Kottur, S. Ravanbakhsh, B. Poczos, R. Salakhutdinov, and A. Smola, "Deep sets," *arXiv preprint arXiv:1703.06114,* 2017.

[560] M. Joseph-Rivlin, A. Zvirin, and R. Kimmel, "Momen^et: Flavor the Moments in Learning to Classify Shapes," in *Proceedings of the IEEE International Conference on Computer Vision (ICCV 2019) - Workshop*, Seul, Korea, 2019, pp. 4085-4094: IEEE.

[561] Y. Duan, Y. Zheng, J. Lu, J. Zhou, and Q. Tian, "Structural Relational Reasoning of Point Clouds," in *Proceedings of the IEEE Conference on Computer Vision and Pattern Recognition (CVPR 2019)*, Long Beach, CA (United States), 2019, pp. 949-958: IEEE.

[562] H. Lin, Z. Xiao, Y. Tan, H. Chao, and S. Ding, "Justlookup: One Millisecond Deep Feature Extraction for Point Clouds By Lookup Tables," in *Proceedings of the IEEE International Conference on Multimedia and Expo (ICME 2019)*, Shanghai, China, 2019, pp. 326-331: IEEE.

[563] W. Wang, R. Yu, Q. Huang, and U. Neumann, "Sgpn: Similarity group proposal network for 3d point cloud instance segmentation," in *Proceedings of the IEEE Conference on Computer Vision and Pattern Recognition (CVPR 2018)*, Salt Lake City, UT (United States), 2018, pp. 2569-2578: IEEE.

[564] X. Yan, C. Zheng, Z. Li, S. Wang, and S. Cui, "PointASNL: Robust Point Clouds Processing Using Nonlocal Neural Networks With Adaptive Sampling," in *Proceedings of the IEEE Conference on Computer Vision and Pattern Recognition (CVPR 2020)*, 2020, pp. 5589-5598: IEEE.

[565] Y. Eldar, M. Lindenbaum, M. Porat, and Y. Y. Zeevi, "The farthest point strategy for progressive image sampling," *IEEE Transactions on Image Processing*, vol. 6, no. 9, pp. 1305-1315, 1997.

[566] R. Li, X. Li, P. A. Heng, and C. W. Fu, "PointAugment: An Auto-Augmentation Framework for Point Cloud Classification," in *Proceedings of the IEEE Conference on Computer Vision and Pattern Recognition (CVPR 2020)*, 2020, pp. 6377-6386: IEEE.

[567] C. Qin, H. You, L. Wang, C.-C. J. Kuo, and Y. Fu, "PointDAN: A Multi-Scale 3D Domain Adaption Network for Point Cloud Representation," *arXiv preprint arXiv:1911.02744*, 2019.

[568] O. Dovrat, I. Lang, and S. Avidan, "Learning to sample," in *Proceedings of the IEEE Conference on Computer Vision and Pattern Recognition (CVPR 2019)*, Long Beach, CA (United States), 2019, pp. 2760-2769: IEEE.

[569] X. Sun, Z. Lian, and J. Xiao, "SRINet: Learning Strictly Rotation-Invariant Representations for Point Cloud Classification and Segmentation," presented at the Proceedings of the 27th ACM International Conference on Multimedia, Nice, France, 2019.

[570] M. Jiang, Y. Wu, and C. Lu, "PointSIFT: A SIFT-like Network Module for 3D Point Cloud Semantic Segmentation," *arXiv preprint arXiv:1807.00652*, 2018.

[571] D. G. Lowe, "Distinctive Image Features from Scale-Invariant Keypoints," *International Journal of Computer Vision*, vol. 60, no. 2, pp. 91-110, 2004/11/01/ 2004.

[572] F. Engelmann, T. Kontogianni, J. Schult, and B. Leibe, "Know What Your Neighbors Do: 3D Semantic Segmentation of Point Clouds," in *Computer Vision – ECCV 2018 Workshops*, Munich, Germany, 2019, pp. 395-409: Springer International Publishing.

[573] Q. Hu *et al.*, "Randla-net: Efficient semantic segmentation of large-scale point clouds," in *Proceedings of the IEEE Conference on Computer Vision and Pattern Recognition (CVPR 2020)*, 2020, pp. 11108-11117: IEEE.

[574] W. Zeng and T. Gevers, "3DContextNet: K-d Tree Guided Hierarchical Learning of Point Clouds Using Local and Global Contextual Cues," in *Computer Vision – ECCV 2018 Workshops*, Munich, Germany, 2019, pp. 314-330: Springer International Publishing.

[575] J. L. Bentley, "Multidimensional binary search trees used for associative searching," *Communications of the ACM*, vol. 18, no. 9, pp. 509–517, 1975/09/01/ 1975.

[576] Y. Zhao, T. Birdal, H. Deng, and F. Tombari, "3D Point Capsule Networks," in *Proceedings of the IEEE Conference on Computer Vision and Pattern Recognition (CVPR 2019)*, Long Beach, CA (United States), 2019, pp. 1009-1018: IEEE.

[577] C. Zhao, W. Zhou, L. Lu, and Q. Zhao, "Pooling Scores of Neighboring Points for Improved 3D Point Cloud Segmentation," in *Proceedings of the IEEE International Conference on Image Processing (ICIP 2019)*, Taipei, Taiwan, 2019, pp. 1475-1479: IEEE.

[578] L.-Z. Chen, X.-y. Li, D.-P. Fan, M.-M. Cheng, K. Wang, and S.-P. Lu, "LSANet: Feature Learning on Point Sets by Local Spatial Attention," *arXiv preprint arXiv:1905.05442*, 2019.

[579] J. Yang *et al.*, "Modeling Point Clouds With Self-Attention and Gumbel Subset Sampling," in *Proceedings of the IEEE Conference on Computer Vision and Pattern Recognition (CVPR 2019)*, Long Beach, CA (United States), 2019, pp. 3318-3327: IEEE.

[580] N. Zhao, T. S. Chua, and G. H. Lee, "PS2-Net: A Locally and Globally Aware Network for Point-Based Semantic Segmentation," in *Proceedings of the 25th International Conference on Pattern Recognition (ICPR 2020)*, Milan, Italy, 2021, pp. 723-730: IEEE.

[581] Z. Zhang, B. Hua, and S. Yeung, "ShellNet: Efficient Point Cloud Convolutional Neural Networks Using Concentric Shells Statistics," in *Proceedings of the IEEE International Conference on Computer Vision (ICCV 2019)*, Seul, Korea, 2019, pp. 1607-1616: IEEE.

[582] J. Li, B. M. Chen, and G. H. Lee, "So-net: Self-organizing network for point cloud analysis," in *Proceedings of the IEEE Conference on Computer Vision and Pattern Recognition (CVPR 2018)*, Salt Lake City, UT (United States), 2018, pp. 9397-9406: IEEE.

[583] S. Wang, S. Suo, W. Ma, A. Pokrovsky, and R. Urtasun, "Deep Parametric Continuous Convolutional Neural Networks," in *Proceedings of the IEEE Conference on Computer Vision and Pattern Recognition (CVPR 2018)*, Salt Lake City, UT (United States), 2018, pp. 2589-2597: IEEE.

[584] A. Poulenard, M. Rakotosaona, Y. Ponty, and M. Ovsjanikov, "Effective Rotation-Invariant Point CNN with Spherical Harmonics Kernels," in *Proceedings of the International Conference on 3D Vision (3DV 2019)*, Québec City, Canada, 2019, pp. 47-56: IEEE.

[585] A. Boulch, "ConvPoint: Continuous convolutions for point cloud processing," *Computers & Graphics*, vol. 88, pp. 24-34, 2020/02/26/ 2020.

[586] W. Wu, Z. Qi, and L. Fuxin, "Pointconv: Deep convolutional networks on 3d point clouds," in *Proceedings of the IEEE Conference on Computer Vision and Pattern Recognition (CVPR 2019)*, Long Beach, CA (United States), 2019, pp. 9621-9630: IEEE.

[587] P. Hermosilla, T. Ritschel, P.-P. Vázquez, À. Vinacua, and T. Ropinski, "Monte Carlo convolution for learning on non-uniformly sampled point clouds," *ACM Transactions on Graphics (ToG)*, vol. 37, no. 6, p. 235, 2018.

[588] C. Esteves, C. Allen-Blanchette, A. Makadia, and K. Daniilidis, "Learning SO(3) Equivariant Representations with Spherical CNNs," *International Journal of Computer Vision*, vol. 128, no. 3, pp. 588-600, 2020/03/01/ 2020.

[589] Y. Liu, B. Fan, G. Meng, J. Lu, S. Xiang, and C. Pan, "DensePoint: Learning Densely Contextual Representation for Efficient Point Cloud Processing," in *Proceedings of the IEEE International Conference on Computer Vision (ICCV 2019)*, Seul, Korea, 2019, pp. 5238-5247: IEEE.

[590] F. Groh, P. Wieschollek, and H. P. A. Lensch, "Flex-Convolution," in *Proceddings of the 14th Asian Conference on Computer Vision (ACCV 2018)*, Perth, Australia, 2019, pp. 105-122: Springer International Publishing.

[591] M. Atzmon, H. Maron, and Y. Lipman, "Point convolutional neural networks by extension operators," *ACM Transactions on Graphics (ToG)*, vol. 37, no. 4, p. 71, 2018.

[592] Y. Liu, B. Fan, S. Xiang, and C. Pan, "Relation-shape convolutional neural network for point cloud analysis," in *Proceedings of the IEEE Conference on Computer Vision and Pattern Recognition (CVPR 2019)*, Long Beach, CA (United States), 2019, pp. 8895-8904: IEEE.

[593] T. Cohen, M. Geiger, J. Köhler, and M. Welling, "Spherical CNNs," *arXiv preprint arXiv:1801.10130v1*, 2018.

[594] Y. Xu, T. Fan, M. Xu, L. Zeng, and Y. Qiao, "SpiderCNN: Deep learning on point sets with parameterized convolutional filters," in *Proceedings of the 15th European Conference on Computer Vision (ECCV 2018)*, Munich, Germany, 2018, pp. 87-102: Springer International Publishing.

[595] N. Thomas *et al.*, "Tensor field networks: Rotation-and translation-equivariant neural networks for 3d point clouds," *arXiv preprint arXiv:1802.08219*, 2018.

[596] B.-S. Hua, M.-K. Tran, and S.-K. Yeung, "Pointwise convolutional neural networks," in *Proceedings of the IEEE Conference on Computer Vision and Pattern Recognition (CVPR 2018)*, Salt Lake City, UT (United States), 2018, pp. 984-993: IEEE.

[597] H. Lei, N. Akhtar, and A. Mian, "Octree Guided CNN With Spherical Kernels for 3D Point Clouds," in *Proceedings of the IEEE Conference on Computer Vision and Pattern Recognition (CVPR 2019)*, Long Beach, CA (United States), 2019, pp. 9623-9632: IEEE.

[598] Y. Li, R. Bu, M. Sun, W. Wu, X. Di, and B. Chen, "PointCNN: Convolution on χ-transformed points," in *Proceedings of the 32nd International Conference on Neural Information Processing Systems (NeurIPS 2018)*, Montréal, Canada, 2018, vol. 31, pp. 828-838.

[599] A. Komarichev, Z. Zhong, and J. Hua, "A-CNN: Annularly Convolutional Neural Networks on Point Clouds," in *Proceedings of the IEEE Conference on Computer Vision and Pattern Recognition (CVPR 2019)*, Long Beach, CA (United States), 2019, pp. 7413-7422: IEEE.

[600] F. Engelmann, T. Kontogianni, and B. Leibe, "Dilated Point Convolutions: On the Receptive Field Size of Point Convolutions on 3D Point Clouds," in *Proceedings of the IEEE International Conference on Robotics and Automation (ICRA 2020)*, 2020, pp. 9463-9469: IEEE.

[601] S. Lan, R. Yu, G. Yu, and L. S. Davis, "Modeling Local Geometric Structure of 3D Point Clouds Using Geo-CNN," in *Proceedings of the IEEE Conference on Computer Vision and Pattern Recognition (CVPR 2019)*, Long Beach, CA (United States), 2019, pp. 998-1008: IEEE.

[602] J. Mao, X. Wang, and H. Li, "Interpolated Convolutional Networks for 3D Point Cloud Understanding," in *Proceedings of the IEEE International Conference on Computer Vision (ICCV 2019)*, Seul, Korea, 2019, pp. 1578-1587: IEEE.

[603] S. Kumawat and S. Raman, "LP-3DCNN: Unveiling Local Phase in 3D Convolutional Neural Networks," in *Proceedings of the IEEE Conference on Computer Vision and Pattern Recognition (CVPR 2019)*, Long Beach, CA (United States), 2019, pp. 4898-4907: IEEE.

[604] Z. Zhang, B. Hua, D. W. Rosen, and S. Yeung, "Rotation Invariant Convolutions for 3D Point Clouds Deep Learning," in *Proceedings of the International Conference on 3D Vision (3DV 2019)*, Québec City, Canada, 2019, pp. 204-213: IEEE.

[605] Y. Rao, J. Lu, and J. Zhou, "Spherical Fractal Convolutional Neural Networks for Point Cloud Recognition," in *Proceedings of the IEEE Conference on Computer Vision and Pattern Recognition (CVPR 2019)*, Long Beach, CA (United States), 2019, pp. 452-460: IEEE.

[606] M. Simonovsky and N. Komodakis, "Dynamic edge-conditioned filters in convolutional neural networks on graphs," in *Proceedings of the IEEE Conference on Computer Vision and Pattern Recognition (CVPR 2017)*, Honolulu, HI (United States), 2017, pp. 3693-3702: IEEE.

[607] J. Zhou *et al.*, "Graph neural networks: A review of methods and applications," *AI Open*, vol. 1, pp. 57-81, 2020/01/01/ 2020.

[608] Z. Wu, S. Pan, F. Chen, G. Long, C. Zhang, and P. S. Yu, "A Comprehensive Survey on Graph Neural Networks," *IEEE Transactions on Neural Networks and Learning Systems*, vol. 32, no. 1, pp. 4-24, 2021.

[609] Y. Wang, Y. Sun, Z. Liu, S. E. Sarma, M. M. Bronstein, and J. M. Solomon, "Dynamic Graph CNN for Learning on Point Clouds," *ACM Transactions on Graphics (ToG)*, vol. 38, no. 5, p. Article 146, 2019.

[610] L. Wang, Y. Huang, Y. Hou, S. Zhang, and J. Shan, "Graph Attention Convolution for Point Cloud Semantic Segmentation," in *Proceedings of the IEEE Conference on Computer Vision and Pattern Recognition (CVPR 2019)*, Long Beach, CA (United States), 2019, pp. 10288-10297: IEEE.

[611] K. Zhang, M. Hao, J. Wang, C. D. Silva, and C. Fu, "Linked Dynamic Graph CNN: Learning on Point Cloud via Linking Hierarchical Features," *arXiv preprint arXiv:1904.10014*, 2019.

[612] Z. Kang and L. Ning, "PyramNet: Point Cloud Pyramid Attention Network and Graph Embedding Module for Classification and Segmentation," *arXiv preprint arXiv:1906.03299*, 2019.

[613] J. Wei, G. Lin, K. H. Yap, T. Y. Hung, and L. Xie, "Multi-Path Region Mining for Weakly Supervised 3D Semantic Segmentation on Point Clouds," in *Proceedings of the IEEE Conference on Computer Vision and Pattern Recognition (CVPR 2020)*, 2020, pp. 4383-4392: IEEE.

[614] X. Xu and G. H. Lee, "Weakly supervised semantic point cloud segmentation: Towards 10x fewer labels," in *Proceedings of the IEEE Conference on Computer Vision and Pattern Recognition (CVPR 2020)*, 2020, pp. 13706-13715: IEEE.

[615] G. Pan, J. Wang, R. Ying, and P. Liu, "3DTI-Net: Learn Inner Transform Invariant 3D Geometry Features using Dynamic GCN," *arXiv preprint arXiv:1812.06254*, 2018.

[616] R. Li, S. Wang, F. Zhu, and J. Huang, "Adaptive Graph Convolutional Neural Networks," *ArXiv*, vol. abs/1801.03226, 2018.

[617] C. Chen, G. Li, R. Xu, T. Chen, M. Wang, and L. Lin, "ClusterNet: Deep Hierarchical Cluster Network With Rigorously Rotation-Invariant Representation for Point Cloud Analysis," in *Proceedings of the IEEE Conference on Computer Vision and Pattern Recognition (CVPR 2019)*, Long Beach, CA (United States), 2019, pp. 4989-4997: IEEE.

[618] G. Li, M. Muller, A. Thabet, and B. Ghanem, "Deepgcns: Can gcns go as deep as cnns?," in *Proceedings of the 2019 IEEE International Conference on Computer Vision*, Seul, Korea, 2019, pp. 9267-9276: IEEE.

[619] J. Liu, B. Ni, C. Li, J. Yang, and Q. Tian, "Dynamic Points Agglomeration for Hierarchical Point Sets Learning," in *Proceedings of the IEEE International Conference on Computer Vision (ICCV 2019)*, Seul, Korea, 2019, pp. 7545-7554: IEEE.

[620] M. Dominguez, R. Dhamdhere, A. Petkar, S. Jain, S. Sah, and R. Ptucha, "General-Purpose Deep Point Cloud Feature Extractor," in *Proceedings of the IEEE Winter Conference on Applications of Computer Vision (WACV 2018)*, 2018, pp. 1972-1981.

[621] J. Masci, D. Boscaini, M. M. Bronstein, and P. Vandergheynst, "Geodesic Convolutional Neural Networks on Riemannian Manifolds," in *Proceedings of the IEEE International Conference on Computer Vision (ICCV 2015) - Workshop*, Santiago, Chile, 2015, pp. 832-840: IEEE.

[622] Q. Xu, X. Sun, C. Y. Wu, P. Wang, and U. Neumann, "Grid-GCN for Fast and Scalable Point Cloud Learning," in *Proceedings of the IEEE Conference on Computer Vision and Pattern Recognition (CVPR 2020)*, 2020, pp. 5660-5669: IEEE.

[623] Y. Feng, H. You, Z. Zhang, R. Ji, and Y. Gao, "Hypergraph Neural Networks," in *Proceedings of the AAAI Conference on Artificial Intelligence*, Honolulu, HI (United States), 2019, vol. 33, no. 01, pp. 3558-3565: AAAI.

[624] Y. Shen, C. Feng, Y. Yang, and D. Tian, "Mining Point Cloud Local Structures by Kernel Correlation and Graph Pooling," in *Proceedings of the IEEE Conference on Computer Vision and Pattern Recognition (CVPR 2018)*, Salt Lake City, UT (United States), 2018, pp. 4548-4557: IEEE.

[625] C. Wang, B. Samari, and K. Siddiqi, "Local Spectral Graph Convolution for Point Set Feature Learning," in *Proceedings of the 15th European Conference on Computer Vision (ECCV 2018)*, Munich, Germany, 2018, pp. 56-71: Springer International Publishing.

[626] F. Monti, D. Boscaini, J. Masci, E. Rodolà, J. Svoboda, and M. M. Bronstein, "Geometric Deep Learning on Graphs and Manifolds Using Mixture Model CNNs," in *Proceedings of the IEEE Conference on Computer Vision and Pattern Recognition (CVPR 2017)*, Honolulu, HI (United States), 2017, pp. 5425-5434: IEEE.

[627] Y. Ma, Y. Guo, H. Liu, Y. Lei, and G. Wen, "Global Context Reasoning for Semantic Segmentation of 3D Point Clouds," in *Proceedings of the 2020 IEEE Winter Conference on Applications of Computer Vision (WACV 2020)*, 2020, pp. 2920-2929.

[628] G. Te, W. Hu, Z. Guo, and A. Zheng, "RGCNN: Regularized Graph CNN for Point Cloud Segmentation," in *Proceedings of the 26th ACM international conference on Multimedia*, 2018.

[629] L. Landrieu and M. Boussaha, "Point Cloud Oversegmentation With Graph-Structured Deep Metric Learning," in *Proceedings of the IEEE Conference on Computer Vision and Pattern Recognition (CVPR 2019)*, Long Beach, CA (United States), 2019, pp. 7432-7441: IEEE.

[630] O. I. Abiodun *et al.*, "Comprehensive Review of Artificial Neural Network Applications to Pattern Recognition," *IEEE Access,* vol. 7, pp. 158820-158846, 2019.

[631] X. Ye, J. Li, H. Huang, L. Du, and X. Zhang, "3D Recurrent Neural Networks with Context Fusion for Point Cloud Semantic Segmentation," in *Proceedings of the 15th European Conference on Computer Vision (ECCV 2018)*, Munich, Germany, 2018, pp. 415-430: Springer International Publishing.

[632] Z. Zhao, M. Liu, and K. Ramani, "DAR-Net: Dynamic Aggregation Network for Semantic Scene Segmentation," *arXiv preprint arXiv:1907.12022,* 2019.

[633] Q. Huang, W. Wang, and U. Neumann, "Recurrent slice networks for 3d segmentation of point clouds," in *Proceedings of the IEEE Conference on Computer Vision and Pattern Recognition (CVPR 2018)*, Salt Lake City, UT (United States), 2018, pp. 2626-2635: IEEE.

[634] X. Liu, Z. Han, Y.-S. Liu, and M. Zwicker, "Point2sequence: Learning the shape representation of 3d point clouds with an attention-based sequence to sequence network," in *Proceedings of the AAAI Conference on Artificial Intelligence*, 2019, vol. 33, no. 01, pp. 8778-8785.

[635] F. Liu *et al.*, "3DCNN-DQN-RNN: A Deep Reinforcement Learning Framework for Semantic Parsing of Large-Scale 3D Point Clouds," in *Proceedings of the IEEE International Conference on Computer Vision (ICCV 2017)*, Venice, Italy, 2017, pp. 5679-5688: IEEE.

[636] P. Wu, C. Chen, J. Yi, and D. Metaxas, "Point Cloud Processing via Recurrent Set Encoding," *Proceedings of the AAAI Conference on Artificial Intelligence,* vol. 33, no. 01, pp. 5441-5449, 07/17 2019.

[637] F. Engelmann, T. Kontogianni, A. Hermans, and B. Leibe, "Exploring Spatial Context for 3D Semantic Segmentation of Point Clouds," in *Proceedings of the IEEE International Conference on Computer Vision (ICCV 2017) - Workshop,* Venice, Italy, 2017, pp. 716-724: IEEE.

[638] A. Dai and M. Nießner, "3DMV: Joint 3D-Multi-view Prediction for 3D Semantic Scene Segmentation," in *Proceedings of the 15th European Conference on Computer Vision (ECCV 2018)*, Munich, Germany, 2018, pp. 458-474: Springer International Publishing.

[639] C. R. Qi, W. Liu, C. Wu, H. Su, and L. J. Guibas, "Frustum PointNets for 3D Object Detection from RGB-D Data," in *Proceedings of the IEEE Conference on Computer Vision and Pattern Recognition (CVPR 2018)*, Salt Lake City, UT (United States), 2018, pp. 918-927: IEEE.

[640] J. Ku, M. Mozifian, J. Lee, A. Harakeh, and S. L. Waslander, "Joint 3D Proposal Generation and Object Detection from View Aggregation," in *Proceedings of the International Conference on Intelligent Robots and Systems (IROS 2018)*, Madrid, Spain, 2018, pp. 1-8: IEEE.

[641] S. Peng, Y. Liu, Q. Huang, X. Zhou, and H. Bao, "PVNet: Pixel-Wise Voting Network for 6DoF Pose Estimation," in *Proceedings of the IEEE Conference on Computer Vision and Pattern Recognition (CVPR 2019)*, Long Beach, CA (United States), 2019, pp. 4556-4565: IEEE.

[642] H. You, Y. Feng, X. Zhao, C. Zou, R. Ji, and Y. Gao, "PVRNet: Point-View Relation Neural Network for 3D Shape Recognition," in *Proceedings of the AAAI Conference on Artificial Intelligence*, 2019, vol. 33, no. 01, pp. 9119-9126: AAAI.

[643] M. Jaritz, J. Gu, and H. Su, "Multi-View PointNet for 3D Scene Understanding," in *Proceedings of the IEEE International Conference on Computer Vision (ICCV 2019) - Workshop*, Seul, Korea, 2019, pp. 3995-4003: IEEE.

[644] H. Chiang, Y. Lin, Y. Liu, and W. H. Hsu, "A Unified Point-Based Framework for 3D Segmentation," in *Proceedings of the International Conference on 3D Vision (3DV 2019)*, Québec City, Canada, 2019, pp. 155-163: IEEE.

[645] J. Hou, A. Dai, and M. Nießner, "3D-SIS: 3D Semantic Instance Segmentation of RGB-D Scans," in *Proceedings of the IEEE Conference on Computer Vision and Pattern Recognition (CVPR 2019)*, Long Beach, CA (United States), 2019, pp. 4416-4425: IEEE.

[646] Y. Zhou and O. Tuzel, "VoxelNet: End-to-End Learning for Point Cloud Based 3D Object Detection," in *Proceedings of the IEEE Conference on Computer Vision and Pattern Recognition (CVPR 2018)*, Salt Lake City, UT (United States), 2018, pp. 4490-4499: IEEE.

[647] GSA, "GSA BIM guide for 3D imaging," *US General Services Administration, Washington, DC*, 2009.

[648] ASHRAE, "ANSI/ASHRAE Standard 209-2018 - Energy Simulation Aided Design for Buildings except Low Rise Residential Buildings," 2018.

[649] BIMForum, "Level of Development Specification Guide," 2017.

[650] BIMForum, "Level of Development Specification - Part I," 2017.

[651] A. Rocha *et al.*, "Technical Report on the Application of Digital Tools to Innovative Management Solutions - Part 1 and 2," Interreg Sudoe Stop CO22019.

[652] FARO, "FARO Laser Scanner User Manual," 2018.

[653] Zoller+Fröhlich, "Z+F LaserControl® Scout - Z+F IMAGER® 5010 C," 2015.

[654] A. K. Roy Choudhury, "3 - Colour-difference assessment," in *Principles of Colour and Appearance Measurement*, A. K. Roy Choudhury, Ed. Oxford: Woodhead Publishing, 2015, pp. 55-116.

[655] L. Shapiro and G. Stockman, "Computer Vision," ed: ISBN-1O, 2000.

[656] L. Sanhudo, F. M. Dinis, J. P. Martins, and N. M. M. Ramos, "Técnicas de Laser Scanning e Realidade Virtual para melhoria da comunicação entre equipas de projeto e obra," presented at the Construção 2018 - Reabilitar e Construir de Forma Sustentável, Porto, Portugal, 2018.

[657] Leica Geosystems, "Leica ScanStation P20 - System Field Manual v. 2.0," 2021.

[658] L. Sanhudo, J. P. Martins, and N. M. M. Ramos, "BIM methodology for an automated and accurate as-built energy performance assessment," presented at the Construct Day 2017, Porto, Portugal, 2017.

[659] L. Yuan, J. Guo, and Q. Wang, "Automatic classification of common building materials from 3D terrestrial laser scan data," *Automation in Construction,* vol. 110, p. 103017, 2020/02/01/ 2020.

[660] H. Balta, J. Velagic, W. Bosschaerts, G. De Cubber, and B. Siciliano, "Fast Statistical Outlier Removal Based Method for Large 3D Point Clouds of Outdoor Environments," *IFAC-PapersOnLine,* vol. 51, no. 22, pp. 348-353, 2018/01/01/ 2018.

[661] M. Corsini, P. Cignoni, and R. Scopigno, "Efficient and Flexible Sampling with Blue Noise Properties of Triangular Meshes," *IEEE Transactions on Visualization and Computer Graphics,* vol. 18, no. 6, pp. 914-924, 2012.

[662] N. Charron, S. Phillips, and S. L. Waslander, "De-noising of Lidar Point Clouds Corrupted by Snowfall," in *Proceedings of the 15th Conference on Computer and Robot Vision (CRV 2018)*, 2018, pp. 254-261.

[663] Point Cloud Library. (2020, 20/01/2021). *Removing outliers using a StatisticalOutlierRemoval filter*. Available: https://pcl-tutorials.readthedocs.io/en/latest/statistical_outlier.html

[664] C. Sungjoon, Q. Zhou, and V. Koltun, "Robust reconstruction of indoor scenes," in *Proceedings of the IEEE Conference on Computer Vision and Pattern Recognition (CVPR 2015)*, Boston, MA (United States), 2015, pp. 5556-5565: IEEE.

[665] S. Rusinkiewicz and M. Levoy, "Efficient variants of the ICP algorithm," in *Proceedings Third International Conference on 3-D Digital Imaging and Modeling*, 2001, pp. 145-152.

[666] S. Ioffe and C. Szegedy, "Batch normalization: Accelerating deep network training by reducing internal covariate shift," *arXiv preprint arXiv:1502.03167,* 2015.

[667] A. K. Dubey and V. Jain, "Comparative Study of Convolution Neural Network's Relu and Leaky-Relu Activation Functions," in *Applications of Computing, Automation and Wireless Systems in Electrical Engineering*, Singapore, 2019, pp. 873-880: Springer Singapore.

[668] D. R. Canelhas, T. Stoyanov, and A. J. Lilienthal, "A Survey of Voxel Interpolation Methods and an Evaluation of Their Impact on Volumetric Map-Based Visual Odometry," in

Proceedings of the IEEE International Conference on Robotics and Automation (ICRA 2018), Brisbane, Australia, 2018, pp. 3637-3643: IEEE.

[669] N. Srivastava, G. Hinton, A. Krizhevsky, I. Sutskever, and R. Salakhutdinov, "Dropout: A Simple Way to Prevent Neural Networks from Overfitting," *Journal of Machine Learning Research*, vol. 15, pp. 1929-1958, 2014/06/01/ 2014.

[670] B. De Brabandere, D. Neven, and L. Van Gool, "Semantic instance segmentation with a discriminative loss function," *arXiv preprint arXiv:1708.02551*, 2017.

[671] L. Sanhudo, "BIM Methodology for an Automated and Accurate As-Built Energy Performance Assessment," Research Thesis Project, Civil Engineering - Constructions, University of Porto, 2019.

[672] E. Schubert, J. Sander, M. Ester, H. P. Kriegel, and X. Xu, "DBSCAN Revisited, Revisited: Why and How You Should (Still) Use DBSCAN," *ACM Transactions on Database Systems (TODS)*, vol. 42, no. 3, p. 19, 2017.

[673] B. Wang, C. Zhang, L. Song, L. Zhao, Y. Dou, and Z. Yu, "Design and optimization of DBSCAN Algorithm based on CUDA," *arXiv preprint arXiv:1506.02226*, 2015.

[674] Q.-Y. Zhou, J. Park, and V. Koltun, "Open3D: A modern library for 3D data processing," *arXiv preprint arXiv:1801.09847*, 2018.

[675] E. Valero, A. Forster, F. Bosché, E. Hyslop, L. Wilson, and A. Turmel, "Automated defect detection and classification in ashlar masonry walls using machine learning," *Automation in Construction*, vol. 106, p. 102846, 2019/10/01/ 2019.

[676] M. Franceschi, G. Teza, N. Preto, A. Pesci, A. Galgaro, and S. Girardi, "Discrimination between marls and limestones using intensity data from terrestrial laser scanner," *ISPRS Journal of Photogrammetry and Remote Sensing*, vol. 64, no. 6, pp. 522-528, 2009/11/26/ 2009.

[677] K. Tan and X. Cheng, "Surface reflectance retrieval from the intensity data of a terrestrial laser scanner," *Journal of the Optical Society of America A*, vol. 33, no. 4, pp. 771-778, 2016/04/01/ 2016.

[678] O. Svelto and D. C. Hanna, *Principles of lasers*. Springer, 2010.

[679] B. Höfle and N. Pfeifer, "Correction of laser scanning intensity data: Data and model-driven approaches," *ISPRS Journal of Photogrammetry and Remote Sensing*, vol. 62, no. 6, pp. 415-433, 2007/12/01/ 2007.

[680] S. Kaasalainen, A. Jaakkola, M. Kaasalainen, A. Krooks, and A. Kukko, "Analysis of Incidence Angle and Distance Effects on Terrestrial Laser Scanner Intensity: Search for Correction Methods," *Remote Sensing*, vol. 3, no. 10, pp. 2207-2221, 2011/10/20/ 2011.

[681] W. Fang, X. Huang, F. Zhang, and D. Li, "Intensity Correction of Terrestrial Laser Scanning Data by Estimating Laser Transmission Function," *IEEE Transactions on Geoscience and Remote Sensing*, vol. 53, no. 2, pp. 942-951, 2015.

[682] H. Liu, S.-H. Lee, and J. S. Chahl, "Transformation of a high-dimensional color space for material classification," *Journal of the Optical Society of America A,* vol. 34, no. 4, pp. 523-532, 2017/04/01/ 2017.

[683] J.-D. Chang, S.-S. Yu, H.-H. Chen, and C. Tsai, "HSV-based Color Texture Image Classification using Wavelet Transform and Motif Patterns," *Journal of Computers,* vol. 20, no. 4, 2010/01/09/ 2010.

[684] L. Yi *et al.*, "A scalable active framework for region annotation in 3d shape collections," *ACM Transactions on Graphics (ToG),* vol. 35, no. 6, pp. 1-12, 2016.

[685] M. Hittmeir, A. Ekelhart, and R. Mayer, "On the utility of synthetic data: an empirical evaluation on machine learning tasks," in *Proceedings of the 14th International Conference on Availability, Reliability and Security*, 2019, pp. 1-6.

[686] S. I. Nikolenko, "Synthetic data for deep learning," *arXiv preprint arXiv:1909.11512,* 2019.

[687] T. Bloch and R. Sacks, "Comparing machine learning and rule-based inferencing for semantic enrichment of BIM models," *Automation in Construction,* vol. 91, pp. 256-272, 2018/07/01/ 2018.

[688] N. M. Nasrabadi, "Pattern Recognition and Machine Learning," *Journal of Electronic Imaging,* vol. 16, no. 4, p. 049901, 2007/10/01/ 2007.

[689] N. S. Altman, "An introduction to kernel and nearest-neighbor nonparametric regression," *The American Statistician,* vol. 46, no. 3, pp. 175-185, 1992/08/01/ 1992.

[690] J. Friedman, T. Hastie, and R. Tibshirani, *The elements of statistical learning* (no. 10). Springer, 2001.

[691] M. H. Hassoun, *Fundamentals of artificial neural networks*. MIT press, 1995.

[692] J. A. Suykens and J. Vandewalle, "Least squares support vector machine classifiers," *Neural Processing Letters,* vol. 9, no. 3, pp. 293-300, 1999/06/01/ 1999.

[693] Y. Freund and R. E. Schapire, "Schapire R: Experiments with a new boosting algorithm," in *Proceedings of the 13th International Conference on Machine Learning (ICML '96),* Murray Hill, NJ (United States), 1996, pp. 148–156: Citeseer.

[694] P. Geurts, D. Ernst, and L. Wehenkel, "Extremely randomized trees," *Machine Learning,* vol. 63, no. 1, pp. 3-42, 2006/03/02/ 2006.

[695] J. H. Friedman, "Greedy function approximation: A gradient boosting machine," *Annals of statistics,* vol. 29, no. 5, pp. 1189-1232, 2001/10/01/ 2001.

[696] J. H. Friedman, "Stochastic gradient boosting," *Computational Statistics & Data Analysis,* vol. 38, no. 4, pp. 367-378, 2002/02/28/ 2002.

[697] T. G. Dietterich, "Ensemble methods in machine learning," in *Proceedings of the International Workshop on Multiple Classifier Systems (MCS 2000)*, Cagliari, Italy, 2000, pp. 1-15: Springer.

[698] Y. Ham and M. Golparvar-Fard, "Updating R-Values of BIM Elements using 3D Thermography for Accurate Building Energy Performance Simulation," in *Computing in Civil and Building Engineering (2014)*, 2014, pp. 113-120.

[699] A. Chong, W. Xu, S. Chao, and N.-T. Ngo, "Continuous-time Bayesian calibration of energy models using BIM and energy data," *Energy and Buildings,* vol. 194, pp. 177-190, 2019/07/01/ 2019.

[700] Matterport. (2021, 05/03/2021). *Matterport 3d models of interior spaces*. Available: https://matterport.com/

[701] X. Wang, S. Liu, X. Shen, C. Shen, and J. Jia, "Associatively segmenting instances and semantics in point clouds," in *Proceedings of the IEEE Conference on Computer Vision and Pattern Recognition (CVPR 2019)*, Long Beach, CA (United States), 2019, pp. 4096-4105: IEEE.

[702] J. Tan, L. Chen, K. Wang, J. Peng, J. Li, and X. Zhang, "SASO: Joint 3D Semantic-Instance Segmentation via Multi-scale Semantic Association and Salient Point Clustering Optimization," *arXiv preprint arXiv:2006.15015,* 2020.

[703] L. Zhao and W. Tao, "Jsnet: Joint instance and semantic segmentation of 3d point clouds," in *Proceedings of the AAAI Conference on Artificial Intelligence*, 2020, vol. 34, no. 07, pp. 12951-12958.

[704] L. Yi, H. Su, X. Guo, and L. J. Guibas, "Syncspeccnn: Synchronized spectral cnn for 3d shape segmentation," in *Proceedings of the IEEE Conference on Computer Vision and Pattern Recognition (CVPR 2017)*, Honolulu, HI (United States), 2017, pp. 2282-2290: IEEE.

[705] L. Sanhudo *et al.*, "Activity Classification using Accelerometers and Machine Learning for Complex Construction Worker Activities," *Journal of Building Engineering,* vol. 35, p. 102001, 2020/11/01/ 2020.

[706] G. C. Cawley and N. L. Talbot, "On over-fitting in model selection and subsequent selection bias in performance evaluation," *The Journal of Machine Learning Research,* vol. 11, no. 70, pp. 2079-2107, 2010/07/10/ 2010.

[707] G. I. Parisi, R. Kemker, J. L. Part, C. Kanan, and S. Wermter, "Continual lifelong learning with neural networks: A review," *Neural Networks,* vol. 113, pp. 54-71, 2019/05/01/ 2019.

[708] M. Kazhdan and H. Hoppe, "Screened poisson surface reconstruction," *ACM Transactions on Graphics (ToG),* vol. 32, no. 3, pp. 1-13, 2013.